

NEURAL NETWORKS FOR SMART FIRE DETECTION

James A. Milke and Thomas J. McAvoy

**Department of Fire Protection Engineering
and Chemical Engineering
University of Maryland
College Park, MD**

December 1996



**U.S. Department of Commerce
Michael Kantor, *Secretary*
Technology Administration
Mary L. Good, *Under Secretary for Technology*
National Institute of Standards and Technology
Arati Prabhakar, *Director***

Notice

This report was prepared for the Building and Fire Research Laboratory of the National Institute of Standards and Technology under grant number 60NANB2D1300. The statement and conclusions contained in this report are those of the authors and do not necessarily reflect the views of the National Institute of Standards and Technology or the Building and Fire Research Laboratory.

NEURAL NETWORKS FOR SMART FIRE DETECTION
FINAL REPORT

submitted to

Building and Fire Research Laboratory
National Institute of Standards and Technology
Grant 60NANB2D1300

by

James A. Milke and Thomas J. McAvoy
Departments of Fire Protection Engineering and Chemical Engineering
University of Maryland at College Park



June 28, 1996

ABSTRACT

Research was conducted using multiple sensors with an algorithm to detect fires more quickly than currently available smoke detectors while also decreasing the susceptibility to unnecessary alarms. The effort involved the production of signatures from three types of sources: flaming fires, non-flaming fires and non-fire, nuisance sources, followed by analysis to recognize signature patterns for the three types of sources. The first phase of research consisted of establishing the feasibility of distinguishing between signatures from fire and non-fire sources using a small-scale apparatus. The second phase consisted of introducing the signatures in a 12 ft square room with a height of 8 ft. Measurements included CO, CO₂, and O₂ concentrations, presence of oxidizable gases, light obscuration and temperature. The signatures measured could be associated with the three types of sources. Using a multivariate statistical analysis, the response time of a prototype detector was appreciably less than that of commercially available detectors, with a significant reduction in unnecessary alarm susceptibility. In the third phase, pairs of sources were provided simultaneously to determine if a nuisance source could mask the signature from a fire source and if two nuisance sources provide a signature similar to that from a fire. Results indicate that the ratio of the CO to CO₂ concentrations is representative of flaming fire sources and to a limited extent for non-flaming fire sources, independent of the presence of a nuisance source.

I. Background

Since 1992, research has been conducted at the University of Maryland to investigate the use of multiple sensors with an algorithm to detect fires more quickly than currently available smoke detectors while also decreasing the susceptibility to unnecessary alarms. This work, supported by the Building and Fire Research Laboratory of the National Institute of Standards and Technology, has been conducted in three phases. The research was conducted by an interdisciplinary team from the Departments of Fire Protection Engineering and Chemical Engineering. The team within the Department of Fire Protection Engineering was responsible for conducting the experimental work involving the production of signatures from three types of sources: flaming fires, non-flaming fires and products representing nuisance sources (non-fire). This included selection of the sources, formulation of a protocol for generation of the signatures, selection of sensors and data collection. The Chemical Engineering team was responsible for data analysis to recognize signature patterns for the three types of sources.

The first phase of research consisted of establishing the feasibility of distinguishing between signatures from fire and non-fire sources using a small-scale apparatus. The second phase of research consisted of introducing the signatures from the sources in a 12 ft square room with a height of 8 ft. A total of 87 large-scale tests were conducted involving a variety of mechanisms to produce the signature, depending upon the characteristics of the source. For example, flaming fires were generally initiated via a flaming ignition of the sample, while signatures from smoldering fires were produced by placing the source on a hot plate. Non-fire sources were introduced using aerosol cans, hot plates, and small kitchen appliances. Sensors included measurements of CO, CO₂, and O₂ concentrations, presence of oxidizable gases, light obscuration and temperature.

In the second phase, each of the sources were introduced alone in the tests. In the third phase of research, pairs of sources were provided. Combinations included either a flaming or a non-flaming fire source with a nuisance source or two nuisance sources. The purposes of the third phase were to determine if the presence of a nuisance source could mask the signature from a fire source and if two nuisance sources could provide a signature similar to that from a fire.

As a result of the second phase of research, the signatures measured by the array of sensors could be associated with the three types of sources. Using a multivariate statistical analysis as the basis of the intelligence algorithm, the response time of a prototype detector was appreciably less than that of the commercially available detectors, with a significant reduction in unnecessary alarm susceptibility. Results from the third phase indicate that the ratio of the CO to CO₂ concentrations is especially representative of a particular flaming fire source and to a limited extent for a non-flaming fire source, independent of the presence of a nuisance source.

The final report is divided into the following three sections:

- overview of experiments to document signatures of fire and non-fire sources
- overview of methods to process sensor data for smart fire detection
- publications associated with the project

Acknowledgements

The direction of Dr. William Grosshandler, technical monitor for the grant is greatly appreciated. The efforts of all of the graduate and undergraduate students who contributed to this project are recognized, including research assistants Mr. Samuel A. Denny, Mr. Bjarne C. Hagen, Mr. Mark Hopkins, Mr. Dongling Pan, and Mr. Tekin A. Kunt and undergraduate research assistants Mr. Douglas A. Ingerson and Ms. Sarina L. Luft.

TABLE OF CONTENTS

Abstract		i
Background		ii
Section 1	Overview of Experiments to Document Signatures of Fire and Non-Fire Sources	1
Chapter 1	INTROUDCTION	1
1.1	Problem Statement	1
1.2	Project Motivation	9
1.3	Scope and Limitations	10
Chapter 2	DETECTION PRINCIPLES	12
2.1	Compartment Fires	12
2.2	Fire Signatures	19
2.3	Previous Research Involving Tin Oxide Sensors	31
2.4	Using Multivariate Statistical Methods to Detect Fires	47
2.5	Artificial Intelligence TechniquesPrevious for Fire Detection	56
Chapter 3	EXPERIMENTAL APPARATUS	70
3.1	Design Considerations	70
3.2	Instrumentation and Sensors	70
3.1	Location of Equipment	77
Chapter 4	EXPERIMENTATION	79
4.1	Test Sources	79
4.2	Experimental Procedures	79
Chapter 5	DATA ANALYSIS	87
5.1	Introduction	87
5.2	Theory and Method of Analysis	87
5.3	Analyysis	97
Chapter 6	DATA ANALYSIS	110
6.1	Discussion of Results	110
6.2	Conclusions	112
6.3	Considerations for Future Research	113
Appendix A	Comparison of Detection Times for Conventional Detectors and PCA	115
Appendix B	Calibration Curves	119

5. Hamburger (approximately 70 grams)

Three sets of procedures were followed for the nuisance sources because of the inherent characteristics of each source. At the completion of monitoring the ambient conditions for 2 minutes, each source was applied. One procedure was used for the disinfectant, glass cleaner and hairspray experiments. The application of these sources consisted of vigorously spraying the sample throughout the space for 90 seconds, allowing diffusion to transport the sources closer to the sensors and analyzers.

The next procedure was for the boiling water. A metal container holding 500 ml of water was placed on a hot plate outside of the test room and covered. The water was brought to a boil and then carefully transported into the test room and the cover removed. The water was boiled for approximately 10 minutes. The power source for the hotplate was then shut off. At the completion of the each test, the remaining water was measured. Indicating that an average of 150 ml was introduced into the test room.

The final procedure was for the hamburger experiments. At the completion of the ambient period, a hot plate, at approximately 350°C, was placed on the load cell, the hamburger was then placed on the hot plate with a

Section I

Overview of Experiments to Document Signatures of Fire and Non-Fire Sources

A STUDY OF GASEOUS SIGNATURES IN LARGE-SCALE TESTS
WITH MULTIPLE SOURCE SCENARIOS

by

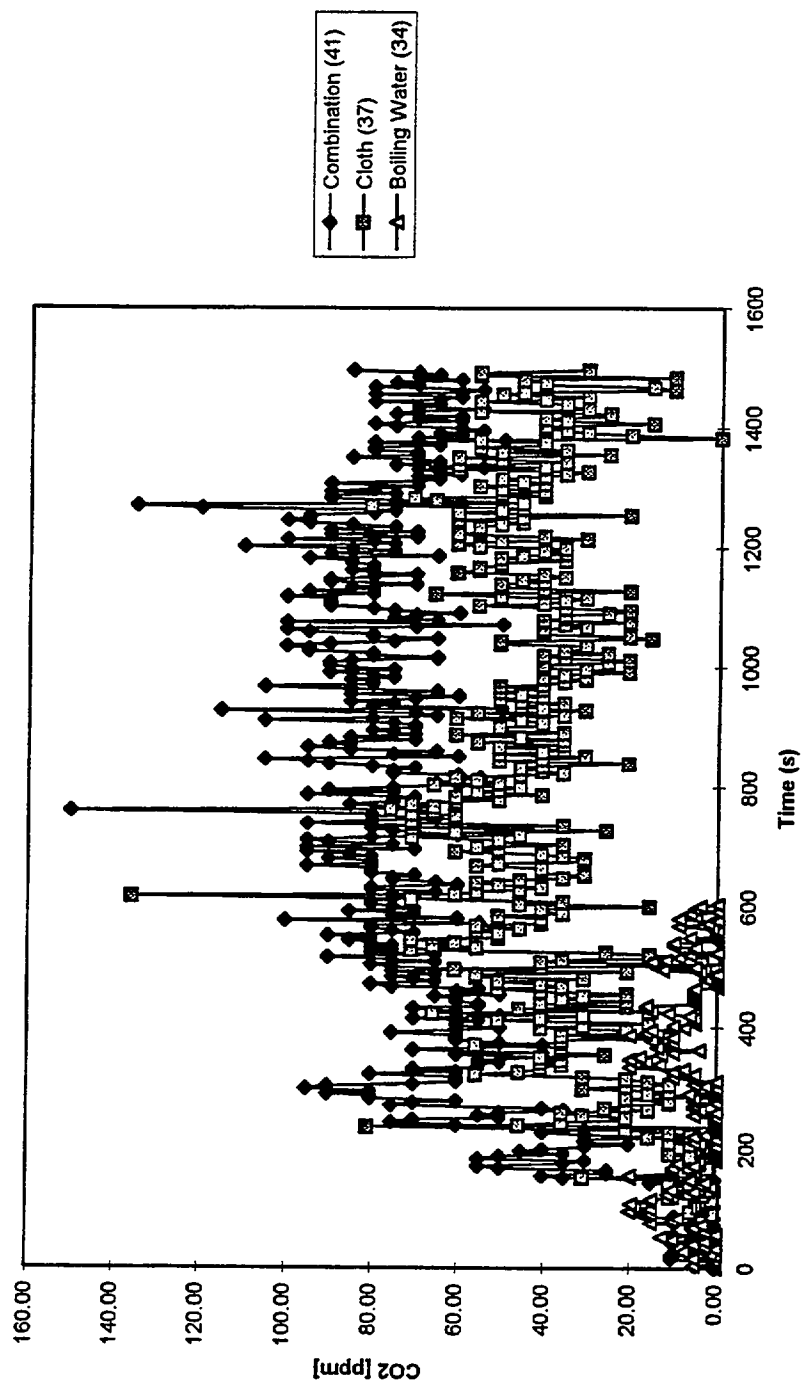
Mark Hopkins

Thesis submitted to the Faculty of the Graduate School of the
University of Maryland at College Park in partial fulfillment
of the requirements of the degree of
Master of Science
1996

Advisory Committee:

Assistant Professor James A. Milke, Chairman/Advisor
Professor James G. Quintiere
Professor Steven M. Spivak

CO2 Concentration vs. Time



A series of large-scale tests were conducted in a 3.6 x 3.6 x 2.44 m test facility. The test scenario involved 8 sources tested both individually and in combinations, resulting in 24 scenarios. The instrumentation for this study consisted of CO, CO₂, and O₂ analyzers, two Taguchi gas sensors, thermocouples and a photocell.

The results indicate that additional sensors are required to correctly discriminate between fire and nuisance signatures in tests with multiple sources. The use of CO and CO₂ signatures the CO/CO₂ are effective for discriminating between flaming and pyrolysing solid sources.

ACKNOWLEDGMENTS

This research was supported by a grant from the National Institute for Standards and Technology (NIST) Division of Exploratory Fire Technologies, grant number 60NANB2D1300. Special thanks are extended to Dr. William L. Grosshandler of NIST for his support of this effort and for serving as the Technical Monitor of this project.

Guidance and direction of this project was provided by Dr. James A. Milke, Dr. James G. Quintiere and Dr. Steven M. Spivak of the Department of Fire Protection Engineering and Dr. Thomas J. McAvoy of the Department of Chemical Engineering at the University of Maryland. Additional guidance was provided by Mr. Tekin A. Kunt of the Department of Chemical Engineering for the arrangement of data required for the PCA analysis. Consultation was also provided by Mr. Bjarne C. Hagen.

Assistance in the experimental set up and experimentation was provided by Mr. Brian Grove, Mr. Stephen Hill, Mr. John Kraweic, Mr. Dave Peterson, Mr. Daniel Szepesi, Mr. Scott Panowitz and Ms. Stacy Niedhart.

Thanks to Mr. Gerry Back of Hughes Associates, for the use of his neutral density filters. Thanks to Mr. Kazumi Unno of Figaro USA, Inc. for the donation

of adapters required for extension wires for the remote location of the TGS sensors and also the prompt expedition of the same. Thanks to the Maryland Fire and Rescue Institute Training Academy at the University of Maryland for the use of the test facilities. And special thanks to Mr. John Fisher and Mr. Lenny Johnson for making special arrangements to allow testing during the weekends, when the facility is usually closed. Thanks to Ms. Cindy Gilbert and Ms. Susan Williams and the rest of the faculty and staff of the Department of Fire Protection Engineering for their patience and help throughout this project.

TABLE OF CONTENTS

List of Tables		vi
List of Figures		viii
Chapter 1	INTRODUCTION	1
1.1	Problem Statement	1
1.2	Project Motivation	9
1.3	Scope and Limitations	10
Chapter 2	DETECTION PRINCIPLES	12
2.1	Compartment Fires	12
2.2	Fire Signatures	19
2.2.1	Aerosol (Smoke) Signatures	19
2.2.2	Energy Signatures	22
2.2.2.1	Radiant Energy Signature	22
2.2.2.2	Convective (Thermal) Energy Signature	23
2.2.3	Gas (Species) Signatures	24
2.3	Previous Research Involving Tin Dioxide Gas Sensors	31
2.4	Using Multivariate Statistical Methods to Detect Fires	47
2.5	Artificial Intelligence Techniques for Fire Detection	56
Chapter 3	EXPERIMENTAL APPARATUS	70
3.1	Design Considerations	70
3.2	Instrumentation and Sensors	70
3.3	Location of Equipment	77
Chapter 4	EXPERIMENTATION	79
4.1	Test Sources	79
4.2	Experimental Procedures	79
4.2.1	Flaming Liquid (heptane)	82
4.2.2	Flaming Solid (paper)	83
4.2.3	Pyrolysing Solid (cloth)	84
4.2.4	Nuisance Sources	84

TABLE OF CONTENTS CONTINUED

	4.2.5 Test with Multiple Sources	86
	4.2.6 Termination of Tests	86
Chapter 5	DATA ANALYSIS	87
5.1	Introduction	87
5.2	Theory and Method of Analysis	87
5.3	Analysis	97
Chapter 6	DISCUSSION AND CONCLUSIONS	110
6.1	Discussion of Results	110
6.2	Conclusions	112
6.3	Considerations for Future Research	113
Appendix A	Comparison of Detection Times for Conventional Detectors and PCA	115
Appendix B	Calibration Curves	119
Appendix C	Data Summaries	122
Appendix D	Representative Sensor Data	124
Appendix E	Example Calculations Used in Analysis	221
References		226

LIST OF TABLES

Table 1.1	Detector Performance in Home Fires, 1989-1991	4
Table 1.2	Percentage of Home Smoke Detectors That Are Operational	5
Table 1.3	Causes of Smoke Detector Failure (Hawkins)	6
Table 1.4	Causes of Smoke Detector Failure (CSPC)	7
Table 2.1	CO/CO ₂ in Small-Scale Tests	29
Table 2.2	CO/CO ₂ in Large-Scale Tests	30
Table 2.3	Test Descriptions	33
Table 2.4	Test Results	34
Table 2.5	Candidate Test Sources (Denny)	37
Table 2.6	Test Sources (Hagen)	40
Table 2.7	Threshold Values for Combination A	43
Table 2.8	Evaluation of Threshold Value Systems (Hagen)	45
Table 2.9	Detection Rate for Smoke Detectors (Hagen)	46
Table 2.10	Percent Variance Captured by PCA Model	50
Table 2.11	Classification by PCA	53
Table 2.12	Time to Detection	54
Table 2.13	Sensor Data for Fire and non-Fire Sources	61
Table 3.1	Summary of Instrumentation	73

LIST OF TABLES CONTINUED

Table 3.2	Thermocouple Locations and Elevations	78
Table 4.1	Test Sources	80
Table 4.2	Test Matrix of Single and Combined Sources	81
Table 5.1	Calculated Heat Release Rates	97
Table 5.2	Calculated Virtual Origins	99
Table 5.3	Calculated Maximum Temperature Rise at Plume Centerline	100
Table 5.4	Calculated Plume Radii	101
Table 5.5	Calculated Maximum Velocity in Plume	102
Table 5.6	Calculated Maximum Temperature Rise in Ceiling Jet	102
Table 5.7	Calculated Maximum Velocity in Ceiling Jet	103
Table 5.8	Calculated Lag Times	104
Table 5.9	Comparison of Estimated and Reported CO Yields	106
Table 5.10	Comparison of Estimated and Reported CO ₂ Yields	107
Table 5.11	Comparison of Average CO/CO ₂ Ratios	109

LIST OF FIGURES

Figure 1.1	Growth in Home Smoke Detector Usage 1970-1993	2
Figure 2.1	The Stages of a Compartment Fire Represented by the Average Gas Temperature as a Function of Time	14
Figure 2.2	The Four Stages of Compartment Fires	15
Figure 2.3	CO and CO ₂ Yield Data	27
Figure 2.4	SnO ₂ Output Traces	35
Figure 2.5	Expert System - Fire Data Classification Rules	39
Figure 2.6	Test Room Layout and Instrumentation	42
Figure 2.7	Classification for Combination A	44
Figure 2.8	Projection of Scores for Nuisance and non-Flaming Experiments onto t ₁ -t ₂ Plane	51
Figure 2.9	Thin Film Gas Sensor	55
Figure 2.10	Preliminary Neural Network Structure	58
Figure 2.11	Developed Neural Network Structure	60
Figure 2.12	Fire Detection System Using a Neural Network with a Delay Circuit	63
Figure 2.13	Structure of Fuzzy Logic Algorithm	66
Figure 3.1	Test Room Layout	71

LIST OF FIGURES CONTINUED

Figure 5.1	Mass Loss History of Flaming Heptane	89
Figure 5.2	Comparison of CO/CO ₂ Ratios	108

CHAPTER I - INTRODUCTION

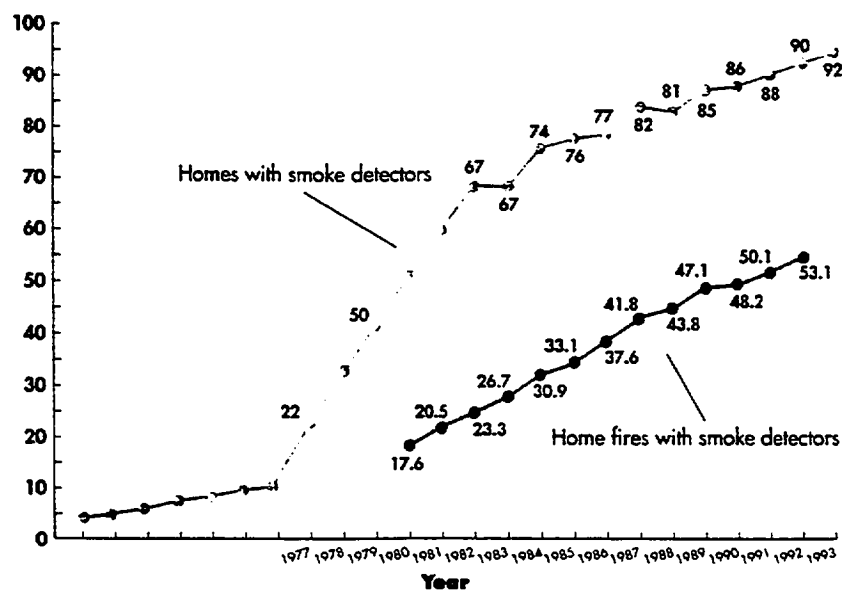
1.1 Problem Statement

The use of smoke detectors in the residential environment was established in the United States (U.S.), in the early 1970's, as an effort to reduce the loss of life due to fires in the home. Approximately 6000 lives have been lost each year, for the past 10 years, in the U.S. as a result of fires, with an outstanding 79% contribution due to residential fires (Hall, 1991). The Consumer Product Safety Commission (CPSC, 1995) has indicated that almost 4,000 deaths and over 21,000 injuries are caused by residential structure fires annually. Initially, the use of residential smoke detectors resulted in a reduction in the number of deaths and property losses caused by residential fires (Hall, 1991).

Smoke detector usage has continued to increase in the U.S. since 1975. The most significant increase of 10% to 74% occurred from 1975 to 1984 (Hall, 1994). Since then, the usage has continued to increase to approximately 92% in 1993. This increase in usage is observed in Figure 1.1 (Hall, 1994).

The National Smoke Detector Project, a multi-phase national survey conducted by the U.S. Consumer Product Safety Commission (CPSC) has indicated that 32% of home smoke detectors, failed to operate in the event of a

Figure 1.1
Growth in Home Smoke Detector Usage
1970-1993 (Hall)



Sources for homes with smoke detectors: 1977, 1980, 1982 estimates from sample surveys by the U.S. Fire Administration; 1983-1993 estimates from Louis Harris surveys for *Prevention Magazine*.

fire. However, the overall use of smoke detectors has been significant in saving lives.

“Smoke detectors are very effective in saving lives. The death rate in fires where they have been present and operated was nearly half the rate in fires where they were present but did not operate (CPSC, 1995).”

The performance of smoke detectors in home fires is presented in Table 1.1 (CPSC, 1995). Additionally, Hall (1994) listed results of several studies indicating the percentage of home smoke detectors that are operational, see Table 1.2.

In a 1983 study by Hawkins, 92% of the nonoperational smoke detectors could be attributed to the lack of knowledge, neglect or misapplication by the end user of these devices. The most significant finding was that 69 % of the failures could be attributed to power source related problems. See Table 1.3 for a listing of the results found in that study (Hall, 1994). The National Smoke Detector Project (CPSC,1995) found that the classification of nonoperational detectors (detectors with power source failures) could be subdivided further. The study consisted of 273 cases that involved detectors that failed to activate (CPSC,1995). In this study, 59 % of the failures could be attributed to power source related problems. See Table 1.4 for the results of this study (CPSC,1995).

Table 1.1
Detector Performance in Home Fires
Average Annual Estimates, 1989-1991(CPC)

a) Detector Presence, Excludes Incidents Where Detector Presence Was Not Required

Presence	Fires		Deaths		Injuries	
	Estimated	Percent	Estimated	Percent	Estimated	Percent
Total	321,400	100	2,590	100	15,200	100
No Detector	152,700	48	1,550	60	6,700	44
Detector Present	168,700	52	1,040	40	8,500	56

b) Detector Operation, Excludes Incidents Where It was Likely that Smoke Did Not Reach the Detector¹

Operation	Fires		Deaths		Injuries	
	Estimated	Percent	Estimated	Percent	Estimated	Percent
Total	83,400	100	880	100	6,500	100
Operated	57,100	68	480	55	4,200	65
Did Not Operate	26,300	32	400	45	2,300	35

¹ If the detector was in the room of origin, only incidents with smoke damage beyond part of the room were included. If the detector was outside the room of origin, only incidents with smoke damage beyond the room the origin were included.

Source: Estimates were derived by applying proportions observed in the U.S. Fire Administration's National Fire Incident Reporting System (NFIRS), to aggregate national estimates from annual surveys conducted by the National Fire Protection Association (NFPA).

Table 1.2
Percentage of Home Smoke Detectors
That Are Operational (Hall)

Results of Several Studies

1. Twelve communities* (principally Montgomery County, Maryland), 1978-1979	92%
2. Santa Barbara, California, 1983**	64%
3. Oregon, 1984**	75%
4. DeKalb County, Georgia, 1985***	70%
5. Inference from two national studies****	83%
6. Unreported fires study (fires with smoke spread beyond room of origin)*****	68%
7. National Smoke Detector Project Survey *****	80%

* Raymond E. Hawkins. *An Evaluation of Residential Smoke Detectors Under Field Conditions: Final Phase*. Washington, D.C.: International Association of Fire Chiefs Foundation, March 1983. p. xiii.

** Leon Cooper. "Why We Need to Test Smoke Detectors," *Fire Journal*, November 1986, pp. 43-45.

*** Centers for Disease Control. U.S. Department of Health and Human Services, *Morbidity and Mortality Weekly Report*, July 18, 1986.

**** "The Prevention Index '87," *Prevention Magazine*, 33 East Minor Street, Emmaus, Pennsylvania 18098, 1987, and R.E. Hoffman. "Tracking 1990 Objectives for Injury Prevention With 1985 NHIS Findings," *Public Health Report #101*, November-December 1986, pp. 581-586. The former estimated 76% of homes had at least one detector in 1985, and the latter estimated 63.3% of homes had at least one functioning detector in 1985, which would mean an 83% rate of operability.

***** Audits & Surveys, Inc., *1984 National Simple Survey of Unreported Residential Fires*, Final Technical Report, Contract C-83-1239, for the U.S. Consumer Product Safety Commission, June 13, 1985.

***** Charles L. Smith. *Smoke Detector Operability Survey—Report on Findings*, Bethesda, Md.: U.S. Consumer Product Safety Commission, November 1993, p. ii.

Table 1.3
Causes of Smoke Detector Failures (Hawkins)

69%	Dead or battery, disconnected AC power supply, disconnected smoke detector, etc. *
12%	Incorrect installation of detector *
11%	Incorrect location of detector *
8%	Other (unidentified)
100%	Total

*Note: 92 % of the failures can be attributed to
lack of knowledge, neglect and misapplication

Results are based on Hawkins study in 1983 (Hall, 1994)

Table 1.4
Causes of Smoke Detector Failures (CPSC)

Condition	No.	Percent of Detectors
Power Disconnected	162	59
Missing Battery	102	37
Disconnected Battery	41	15
Disconnected AC	19	7
Other	180	
Heat Deformed	41	15
Missing Cover	36	13
Clogged with dust/dirt	23	8
Insect Infestation	14	5
Failure of AC Power Supply	6	2
Located in dead air space	5	2
Other	55	20

Note: It was possible to specify multiple conditions for a detector. Therefore, number of conditions is greater than 273 and the percent of detectors adds to more than 100. The conditions cited under "Power Disconnected" do not overlap each other, but could overlap conditions in the "Other" section.

Source: U.S. Consumer Product Safety Commission/EPHA
Data from 15 fire departments

The National Smoke Detector Project (CPSC,1995) also indicated that the leading reason for the nonoperational smoke detectors was directly related to nuisance alarms. This was consistent with the reportings of Denny (1993) in his review. The main causes of nuisance alarms were cooking fumes and continuous response when powered. The next largest group consisted of alarms with unspecified reasons and the third group cited was reaction to humidity and steam. The results of the study indicated that nuisance alarms could be reduced by decreasing the sensitivity of detectors, however, it was cautioned because this would reduce the ability for the detectors to adequately respond to fire conditions (CPSC,1995) (Hall, 1994).

This project involves the improvement of detector technologies in an effort to decrease the nuisance alarm problems currently existing with residential smoke detectors, without sacrificing the ability of the detectors to respond to fire conditions. This will be done by combining the current technology of gas sensors and an artificial intelligence technique to reduce detection times and improve the ability of residential smoke detectors in distinguishing between fire and non-fire signatures. Currently, the ionization and photocell detectors used in the residential setting can only accomplish one of these objectives, at an acceptable level, at a single time. False alarms can be reduced by decreasing the sensitivity

of the detector, however, this usually results in longer response times for the detector. Conversely, by increasing the sensitivity the response times will be shorter, but this usually results in an increase in nuisance alarms.

1.2 Project Motivation

The goal of this project is to develop a detector that has short response times, the ability to detect a wide variety of fire scenarios and the capability of discriminating between fire and non-fire sources. As the third and final stage of a multi-year project to investigate the feasibility of combining gas sensors with a neural network, an evaluation will need to be made.

The first phase consisted of a series of small scale experiments conducted by Denny (1993) in a modified U.L. 217 smoke box (U.L. 217, 1985). The success of this testing led to a series of large scale experiments in phase 2 conducted by Hagen (1994). The success of this phase and the limited scope of previous research involving large scale testing of gas sensors for use as fire detectors has led to this phase of the project.

There have been indications that tin dioxide gas sensors may be inadequate for use as smoke or fire detectors. The use of a single gas sensor as a smoke or fire detector has resulted in both high levels of false alarms and/or lack of detection. However, the combined use with other sensors has been

demonstrated to yield better detection (Bukowski and Bright, 1975) (Hagen, 1994) . Algorithms like principle component analysis (PCA), expert system analysis and fuzzy logic can be used to detect changes in multiple variables, however, there is a problem in the classification of such changes. Further investigation of the combined effects may result in a method of classification that would yield more accurate detection. Milke (1995) suggests that additional experiments are required to determine if there is a potential for flaming and smoldering sources to be masked by a nuisance source.

The purpose of this phase of the research project is to continue the large scale testing, in an effort to further understand the behavior of gas sensors and to evaluate the potential use of these gas sensors as detectors in the residential setting. This study will evaluate the ability of these sensors to differentiate between a nuisance source and a fire source for multiple source scenarios.

1.3 Scope and Objectives

The scope of this paper is to evaluate the use of gas sensors for applications with the Principle Component Analysis (PCA) for the detection of fires. This study will identify fire signatures and compartment fire dynamics that are relevant to the development of a protocol fire detector. A review of previous

research will be conducted to establish what is already known about the use of gas sensors for fire detection. The potential use will then be evaluated.

The results of these experiments will be used to evaluate the potential use of gas sensors as part of a prototype fire detector, based on the ability of the detector to identify a fire signature in a masked environment and the ability of the detector to reclassify an event. The issues of spacing and coverage area have not yet been addressed. This is an area that will need to be evaluated as part of future research projects. These issues can not be addressed at this time, since the size of the test room is not large enough to make a comprehensive evaluation.

The overall objective of this paper is to study signatures of combined sources. In addition, signatures best suited for use with PCA are identified. The lack of testing with similar scenarios presents a challenging problem in evaluating the results of these tests with combined sources.

CHAPTER II - DETECTION PRINCIPLES

2.1 Compartment Fires

In order to correctly describe the principles associated with detection, it is important to understand fire behavior within a compartment. A fire will affect its surrounding environment in several ways; it will add energy both in the forms of heat and electromagnetic radiation, it will induce flows within the compartment, it will produce a variety of gases and will consume oxygen. Additionally, the characteristics of the compartment will affect the extent of these changes in the environmental conditions. The ventilation of the compartment will affect the combustion process associated with the fire and the movement of smoke. The characteristics of the boundaries of the compartment will affect both the fire induced flows and the net energy increase to the environment.

The behavior of a fire within a compartment has been extensively studied, providing a variety of information. There have been ways of describing the entire process or phenomenon from very simplistic models describing the global effects, to extremely complex models taking into account a wide variety of variables such as mixing correlations and turbulence.

Drysdale (1985) described compartment fires in three stages , the growth or pre-flashover stage, the fully developed or post-flashover stage and the decay

stage. In this description the temperature signature is used to describe the phenomenon. Figure 2.1 shows the stages of a compartment fire as a function of the average gas temperature described by Drysdale (1985). The growth stage is described as the initial period of a fire, with low average temperatures and localized burning in the area of the fire origin, leading to the onset of flashover. The fully-developed stage is described as the post flashover period involving most or all combustibles in the enclosure, resulting in peak heat release rate and temperature for the fire. The decay stage is described as the period after the temperature has fallen to 80 % of its peak value.

Milke and Mowrer (1993) have described a compartment (enclosure) fire in four stages, the plume and ceiling jet stage, the unventilated filling stage, the pre-flashover vented stage and the post-flashover vented stage. See Fig 2.2 for the four stages described. In this description, the most significant variables for the compartment fire are; heat release rate, enclosure construction, enclosure ventilation rate and enclosure size.

Milke and Mowrer (1993) compiled a comprehensive review of the effects of air entrainment in fire plumes. Most of the entrainment models discussed are based on the weak point source plume theory developed by

Figure 2.1
The Stages of a Compartment Fire
Represented by the Average Gas Temperature
As a Function of Time (Drysdales)

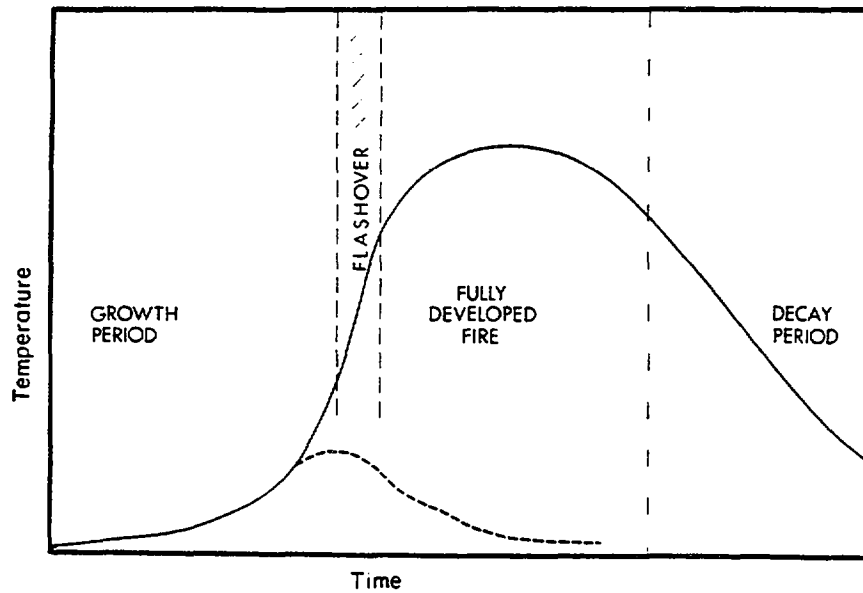
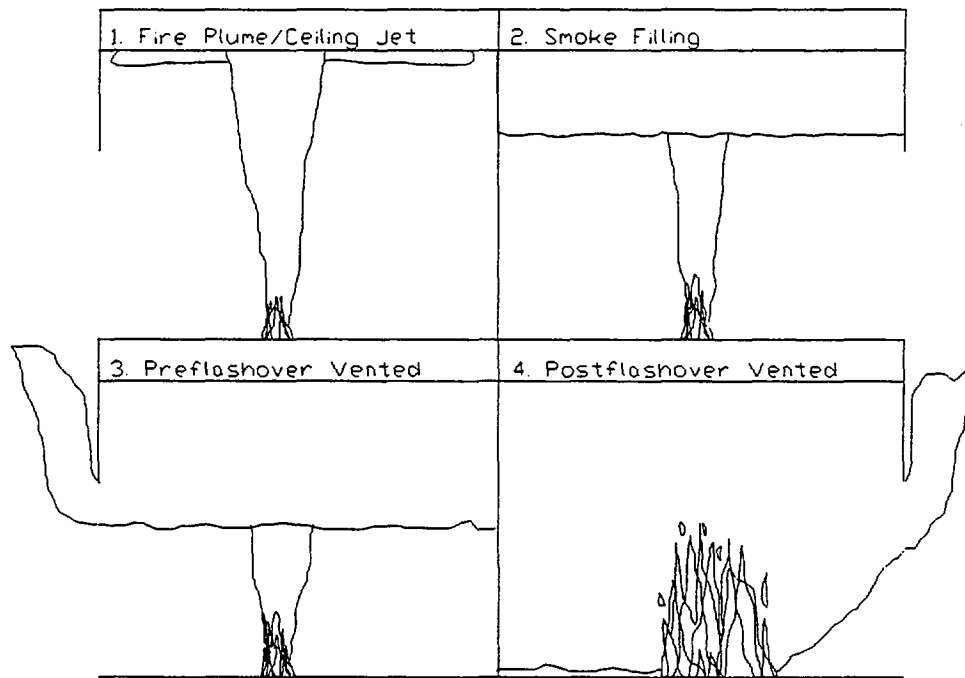


Figure 2.2
The Four Stages of Compartment Fires
(Milke and Mowrer)



Morton, Taylor and Turner (1956) for axisymmetric fire plumes. This model assumes that all of the energy is released at a point and that density variations between the plume and ambient fluid are small. The model also assumes that the plume is located in the open with minimal aerodynamic disturbances caused by wind or mechanical ventilation effects. This theory is known as a far field model and is valid for regions located away from the combustion zone. For the purposes of this paper the model developed by Heskestad (1995) shall be utilized.

For enclosure fires, there may be a second region of interest established as a result of the boundary imposed by a ceiling preventing the plume from rising to its maximum height based the effects of buoyancy. This region is known as the ceiling jet region which is observed as the radial flow along the ceiling, resulting from the excess buoyant effect in the smoke above the plume. From a detection standpoint, this is the region of concern, since it is essential in the recognition of a fire signature in the incipient or early stages of fire development. There is a transport time lag associated with the ignition of a fuel and the time at which the smoke reaches a detector with a sufficient change in some signature quantity to cause an alarm (Milke and Mowrer, 1993).

For the purposes of this paper, the model prepared by Alpert (1971) and the modified equations of Evans (1995) shall be used. This theory is in

agreement with the point source theory to be used for calculations of the plume region. All variables will be represented as a function of the radial distance from the center-line of the plume.

“These empirically determined relations for gas temperature and similar types of relations for gas velocity are in good agreement with the previous theoretical analysis for a “small” fire” (Alpert, 1972).

The filling stage, described by Cooper (1995) is next in the chain of events, which begins when the ceiling jet extends radially to the extent of the walls of the enclosure. There may be a transitional effect at the wall and ceiling interface, known as the wall jet, which results from substantial velocities remaining in the ceiling jet at the interface.

The momentum effects driving the wall jet downward are countered by the effects of buoyancy remaining in the hot wall jet layer and there is a point where the wall jet is halted and the effects of buoyancy drive the smoke back up. There are additional frictional and heat loss effects which will decrease the time for this transition resulting from momentum losses. There is some mixing that occurs at this transition, however, the result is the formation of a quiescent hot gas layer beneath the ceiling jet. Eventually this layer becomes uniform in thickness and fills at a steady rate. The formation of the upper gas layer is

usually treated as a homogeneous mixture of uniform temperature and gas concentrations (Cooper, 1995).

The filling stage in compartments with insignificant ventilation will continue until the smoke layer descends to the floor or there is an insufficient quantity of oxygen or fuel to allow burning to continue. For enclosures with openings and/or mechanical ventilation, the filling period will continue until a quasi-steady mass flow is created for the mass flow into and out of the enclosure (Milke and Mowrer, 1993). The preflashover vented period begins at the onset of this flow. There is a potential for mixing at the interface of the ventilation openings, which would effect the temperature and composition of the smoke layer (Milke and Mowrer, 1993).

The postflashover vented period is the final stage for compartment fires and is the most hazardous. This period begins when there is sufficient oxygen available to allow all or most combustibles within the compartment to ignite. This provides the peak heat release rate for the burning, although it is limited by the ventilation flow rate into the compartment (Milke and Mowrer, 1993).

2.2 Fire Signatures

To effectively detect a fire it is important to understand that fires can be recognized on the basis of common trends or patterns that occur among similar fire scenarios.

“From the moment of its initiation, fire produces a variety of changes in the surrounding environment. Any of these changes in the ambient conditions is referred to as a “fire signature” and can be monitored by a detection system. The production of smoke, for example, will result in a decrease in visibility that can be detected. To be useful, however, a fire signature should generate a measurable change in some ambient condition and magnitude of that change (the “signal”) must be greater than the normal background variations (the “noise”) for the condition.” (Bukowski and O’Laughlin, 1994)

In essence, two fires of the same size and fuel, in the same mode of burning and with similar environmental conditions, should produce similar quantities of energy and combustion products and consume similar quantities of oxygen. The fire signatures of concern include aerosol concentration, species production, oxygen consumption and energy increase.

2.2.1 Aerosol (Smoke) Signatures

The term aerosol is used to define the liquid and solid particles found in smoke from fire generated sources. It was determined that materials burning in

the flaming mode tend to produce a large number of small particulates, while, the smoldering mode of combustion tends to produce fewer particles that are typically larger in size (Lee and Mulholland, 1977). Additionally, particulates can be classified as visible or invisible, with visible particles typically ranging in size from 4 to 5 microns (Bryan, 1993). Visible particulates are usually unconsumed carbon and carbon-rich compounds. Invisible particles may consist of various gases and ions, that may be seen as a light haze, when a significant quantity is present (Bryan, 1993).

“The process of combustion releases very large numbers of solid and liquid particles into the atmosphere. The size of the particles ranges from 5×10^{-4} micrometers to 10 micrometers. These particles suspended in air are called aerosols and when produced by fire, usually called smoke.” (Bukowski and O’Laughlin, 1994)

The particle size, quantity of particles and size distribution affect the ability for detection. Lee and Mulholland (1977) specified that the most significant variable is the size distribution of aerosol particles. Smoke does not consist of uniformly sized particles, but rather a range of particles from 0.005 to 5 μm , with a peak concentration at a specific size. Bukowski and O’Laughlin (1994) suggest that condensation nuclei (cloud chamber) type detection should be used to detect invisible aerosol signatures and the ion chamber and photoelectric types should be used for larger aerosol signatures.

The size distribution of particles changes as the smoke ages. The particles increase in size as a result of coagulation due to Brownian collisions. The effect is observed as a reduction in the number of particles. The volumes of the particles remains constant, however, indicating an increase in particle diameters. The rate of coagulation was observed to increase at higher concentrations, in agreement with coagulation theory (Lee and Mulholland, 1977).

A recent study conducted by Aggarwal and Motevalli (1995) investigated smoke properties for non-flaming fuels. Nine fuels were tested in a 2.4 m x 1.8 m x 1.8 m high enclosure for the smoke properties used for ionization and photoelectric detection principles. The fuels tested consisted of seven conventional fuels; wood (douglas fir and particle board), paper, nylon, wool, polyurethane, PMMA and two non-conventional fuels, cooking oil and bread. Smoke properties that were measured were the following; scattered light intensity, response of Measuring Ionization Chamber (MIC), obscuration, smoke particle density and fuel mass loss. The fuels were ranked by both ionization (MIC) and light scattering (Mie) reference detector responses. There was consistency in the ranking of the materials, although, the ranking was in the reverse order for the two methods used. It was determined that the classification of fuels based on a simplified Mie theory, a model used to calculate the intensity

of light scattered by smoke particles, was fuel dependent and may not be practical without more precise measurement techniques. Coagulation was identified as contributing to variations in particle diameter, which was an assumption needed for this analysis. Aggarwal and Motevalli (1995) found that the cellulosic materials have higher smoke generation per unit mass than the synthetic materials tested.

2.2.2 Energy Signatures

A fire can be defined as an oxidation-reduction reaction accompanied by heat and light. The energy introduced to the environment in all stages of a fire is observed through the release of radiative and convective energy. The radiative energy fraction can be approximately 25 to 40 % of the total energy output of the fire, where the total energy is considered to be the sum of the radiative and convective fractions. (Milke and Mowrer, 1993)

2.2.2.1 Radiant Energy Signature

The radiative energy signatures produced by a fire, typically the infrared (IR) and the ultraviolet (UV) signatures, are the earliest energy signatures to detect. The IR noise levels produced by solar and man-made sources can create a challenging design problem. Yet, the IR detector can be used to detect both

the carbon dioxide (CO₂) - water vapor (H₂O) and flicker signatures with an excellent signal-to-noise ratio. The UV signatures are observed as emissions and often have signal-to-noise ratios which are less than IR signatures. (Bukowski and O'Laughlin, 1994)

2.2.2.2 Convective (Thermal) Energy Signature

The convective energy, 60 to 75% of the total, is primarily responsible for the temperature increase in the environmental surroundings and the movement of smoke. In compartment fires, 60 to 90% of the energy is lost to the surrounding environment as a result of the conduction of heat through the compartment boundaries.

“Heskestad (1991) has suggested that for relatively small fires in large spaces the heat loss factor is less than in small spaces because the temperature difference driving the heat loss is smaller in large spaces. For very large spaces, Heskestad suggests a reasonably conservative value for the heat loss factor would be $(1 - \chi_R)$, where χ_R is the radiative fraction” (Milke and Mowrer, 1993).

Additionally, the smoke layer becomes diluted by the entrainment of air in the plume and ceiling jet regions resulting in a decrease in temperature in the smoke layer. For detection purposes, thermal signature can be utilized on an absolute value or a rate basis. The time required to cause a sufficient

temperature increase for detection can range from less than a minute to several hours based on the scenario of the fire (Bukowski and O’Laughlin, 1994). This signature is most effective for fires with fast growth rates, providing a large initial energy increase. Typically, detection based on the use of the thermal signature is slower than detection by other signatures.

2.2.3 Gas (Species) Signatures

Fires produce many species which are not normally present in high concentrations during ambient environmental conditions. Most organic fires produce carbon dioxide (CO_2) and water vapor (H_2O) under ideal conditions. Usually, conditions are not ideal and many other species are produced as a result, for example, carbon monoxide (CO) and solid carbon (C) particulates are produced in oxygen (O_2) limited reactions. For some materials, there are additional reactions that occur, resulting in the production of species such as: hydrogen chloride (HCl), ammonia (NH_3), hydrogen fluoride (HF), hydrogen cyanide (HCN), nitrogen oxides (NO_x), acids, etc.

A study conducted by Jackson and Robins (1993) investigated the potential use of carbon monoxide, hydrogen, humidity and oxygen signatures for use in detecting fires. In their findings it was determined that carbon monoxide was the best suited candidate for use, since it exists in ambient conditions in low

concentrations and any increase would be significant. However, Jackson and Robins (1993) recommended that careful judgment be used in determining the alarm threshold limits, since there are many nuisance sources that could cause false alarms. Jackson and Robins (1993) suggest that a 20 ppm alarm level would have led to the detection of five of the six large scale fire tests that were conducted.

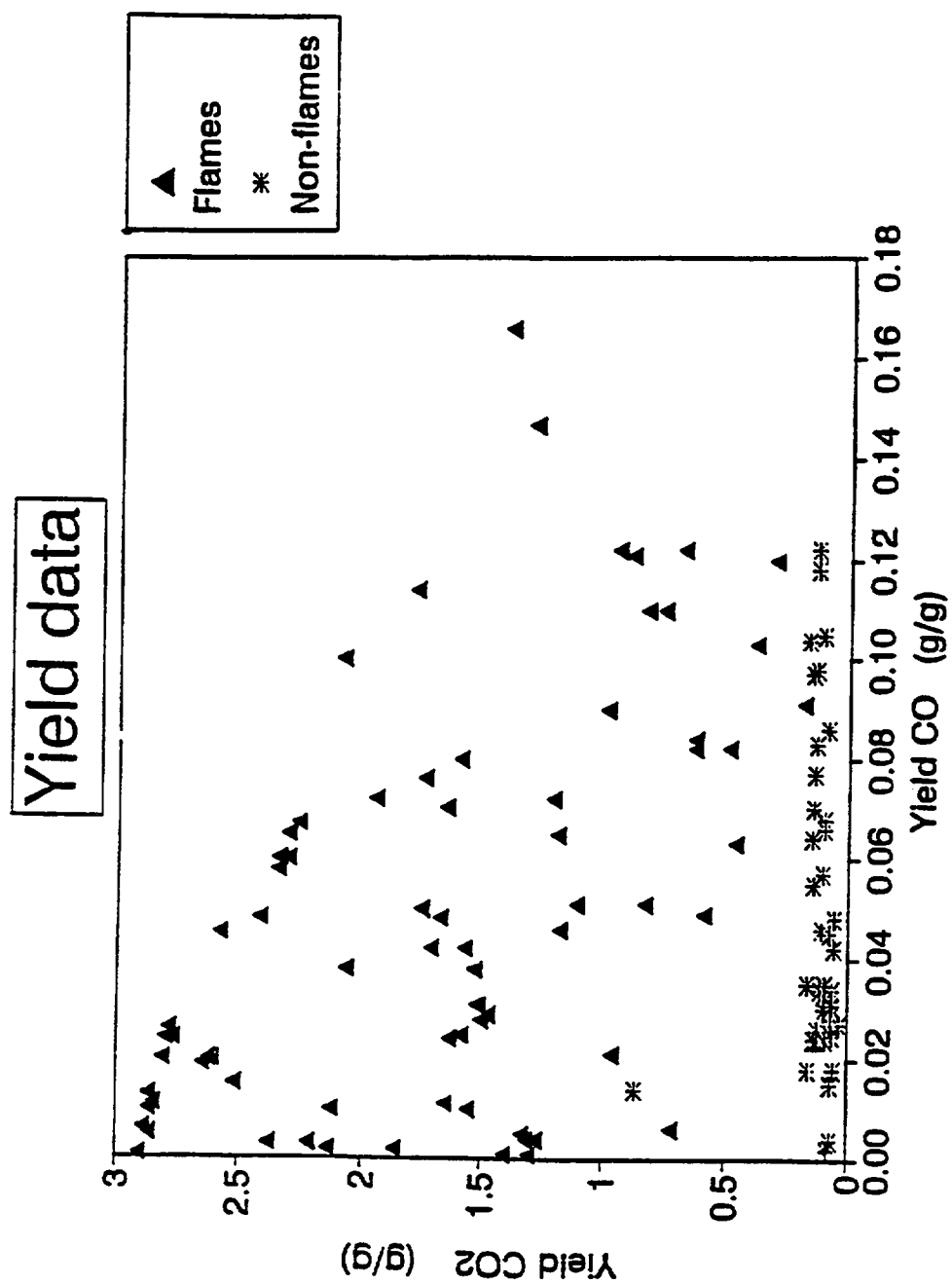
Gottuk et al (1992) investigated the relationship of species yields and the equivalence ratio for compartment fires. A series of tests were conducted using hexane, polymethylmethacrylate (PMMA), spruce and polyurethane. The measurements consisted of carbon monoxide, carbon dioxide and oxygen concentrations, temperature, fuel volatilization rate and air entrainment rate. The production of carbon monoxide was reported as having a strong dependence on the compartment flow dynamics and upper layer temperature and a less sensitive dependence on fuel type. The generation of carbon dioxide and consumption of oxygen were reported as having a dependence on the equivalence ratio, temperature and fuel type.

The combustion of most organic compounds results in the production of carbon monoxide and carbon dioxide. The generation rates of these compounds vary as a function of the chemical bonds of the material, the ventilation rate and the mode of combustion (Tewarson, 1995). Several trends were noted on the

dependence of the ventilation rate, the generation of carbon dioxide and the depletion of oxygen increase with an increase in the ventilation rate, while conversely, the generation of carbon monoxide will decrease with an increase in the ventilation rate. Tewarson has studied the yield fraction for a variety of fuels in both the flaming and non-flaming modes. The ratio of carbon monoxide and carbon dioxide concentrations can thus be used as an indicator of the combustion mode. See Figure 2.3, for a plot of the carbon monoxide and carbon dioxide yields presented by Tewarson (1995).

Tsuchiya (1994) has conducted experiments on CO/CO₂ ratios via the use of the cone calorimeter. The concentrations of these gases were measured under normal ventilation conditions for the cone calorimeter. It was noted that the CO/CO₂ ratio was nearly constant for the complete combustion of each fuel tested. The tests were conducted for a variety of materials in the three stages of combustion, oxidative pyrolysis, flaming (and non-flaming) and glowing. The generation of carbon monoxide and the CO/CO₂ ratios were noted as being the highest among the tests in the oxidative pyrolysis mode, followed by the glowing tests. For the combustion of flaming liquids and non-charforming plastics, the CO/CO₂ values ranged from 0.0002 to 0.056. The three modes of combustion of wood had representative values of 0.90 for pyrolysis, 0.25 for glowing and 0.0035 for flaming. The CO/CO₂ ratios for the oxidative pyrolysis

Figure 2.3
CO and CO₂ Yield Data (Tewarson)



of polymers were reported in the range of .09 to 0.9. The combustion of charforming polymers had CO/CO₂ ratios ranging from 0.01 to 0.37 in the flaming mode and 0.11 to 2.2 in the glowing mode. Tsuchiya (1994) has also reported CO/CO₂ ratios for a number of other researchers, both for small-scale and large-scale experiments, these results are presented in Tables 2.1 and 2.2, respectively.

Roby and Beyler (1990) indicated that although fire dynamics has been studied for decades, little has been done in the areas of combustion efficiency and toxic gas production rates. The scope of that study included species generation rates, major toxic and smoke generation rates and the effects of external flames in destroying toxic gases for oxygen limited fires. The study indicated that oxygen depletion and temperature effects are dominant over carbon monoxide production in open (flaming) combustion.

In the early stages of fire development, the depletion of oxygen is usually considered to be important in the immediate fire area. The mode of burning and the generation rates of other species are dependent on the oxygen consumption rate of a fire as identified by Gottuk et al (1992) and Tewarson (1995). For later times in the fire development, the depletion of oxygen may be observed as a global effect throughout the compartment. For ventilated spaces the oxygen

Table 2.1
CO/CO₂ in Small-Scale Tests (Tsuchiya)

Apparatus	Fuel	Mode	CO/CO ₂	Reference
NBS Test	6 materials	Flaming	0.047±0.017	Hirschler[9]
NBS Cup	Douglas fir	Flaming	0.092	Purser[10]
DIN Tube	Fibres	Flaming and non-flaming	0.17 - 0.6	Kallonen[11]
DIN Tube	Wood	Flaming and non-flaming	0.01 - 0.6	Prager[12]
Heated tube	PU	Pyrolysis	2.8, 18	Woolley & Wadley[13]
HRR apparatus	Various	Combustion	0.004-0.11	Tewarson[14]
Cone calorimeter	Various	Combustion	0.007- 0.05	Paul[15]
OSU apparatus	Plywood	Flaming and non-flaming	0.01 - 0.53	Tsuchiya, Mathieu[16]
UPITT	4 materials	Combustion	0.05 - 0.4	Grand[17]
Small chamber	4 liquids	Combustion	0.05 - 0.5	Morikawa[18]
Small chamber	Methanol	Combustion	0.09 - 0.9	Kim et al[19]
Fluidized bed	Peat	Pyrolysis	0.2 - 4	Arpiainen, Lappi[20]

Table 2.2
CO/CO₂ in Large-Scale Tests (Tsuchiya)

Fire Type	Fuel	CO/CO ₂	O ₂ %	Reference
18 room fires	Fibreboard cribs	0.37±0.19		Gross,Robertson[21]
37 room fires	Wood cribs	0.35±0.19		Tewarson[22]
16 room fires	Cribs, panels etc.	0.03-0.63	19.5-3	Budnick[23]
Low-vent. fire	Wood	0.36	3.6	Woolley & Fardel[7]
A room fire	Wood	0.13	0.01	Portier et al[6]
A room fire	Wood, low & high ventilation	0.33, 0.07	4, 9	Purser[10]
A room fire	PU	0.07	5.8	Alpert et al[24]
1/2 scale house	Fuel oil	0.01-0.037	14-12	Kaya & Itaya[25]
Dormitory room	Furniture	0.05	9-6	Kim[26]
Two bldg.fires	Furniture	0.33, 0.53	3.1, 2.8	Morikawa et al[27]

concentration within the space may eventually reach a steady state condition where there is a strong dependence on the ventilation capacity of the space. For unventilated spaces, however, the only available oxygen is that which is initially present within the space and that which enters through leaky construction, indicating that the depletion of oxygen can become important throughout a compartment.

Oxygen is consumed in the combustion zone, resulting in the formation of oxidized compounds. Inefficiencies in burning, result in oxidizable compounds and unburned fuel remaining the smoke. The use of tin dioxide gas sensors has demonstrated the ability to monitor increases in such compounds. The operating principles of these devices are discussed in detail by Ihokura and Watson (1994), Bright and Bukowski (1975), Mandelis and Christofides (1993), and Denny (1993). The oxygen signature can also be used as an indicator of the rate of combustion, which is a key feature in oxygen calorimetry.

2.3 Previous Research Involving Tin Dioxide Gas Sensors

The idea of using Taguchi (TGS, tin dioxide) gas sensors for detecting fires is not a new one, but recent studies demonstrated that there may be some potential for their use. Bukowski and Bright (1975) indicated that the use of TGS sensors as fire detectors provided little merit. The study involved 26 test

fires including shredded paper, wood cribs, gasoline, polystyrene, polyurethane and cotton. See Table 2.3 for the description of these tests. All of the fires were in the flaming mode except for the cotton which was in the smoldering mode.

The test fires were conducted at NIST (formerly NBS) in a large room about 55,000 cubic feet (1,557 cubic meters) in volume. Ten smoke detectors were installed in the space approximately 21 feet from the center of the fire. The TGS sensor detected 1 of 26 fires and indicated a trouble signal for 1 of 26 fires. This response was poor in comparison to the photoelectric and ionization detectors also used in the tests. See Table 2.4 for the performance of these detectors. Bukowski et al (1975) also expressed concerns of long-term stability and false alarm problems and a lack of confidence in the use of these gas sensors in detecting fires.

In a small scale study conducted by Okayama (1991) two tin dioxide (SnO_2) sensors of differing tin dioxide layer thickness were evaluated for use with a neural network. The tests were performed by introducing various smoldering and nuisance source odors into a 1.8 liter glass jar containing the two sensors. The sensor output for the two sensors were plotted against one another for the 18 tests conducted, see Figure 2.4 (Okayama, 1991). The majority of the tests demonstrated trends capable of distinguishing between the smoldering

Table 2.3
Test Descriptions
(Bukowski and Bright)

Test Nos.	Types of Test Fires
1,2,3,10	Eight ounces (250g) of shredded paper in hardware cloth basket. Match ignited in bottom center.
4,5	Class A wood brand ignited by 100 cc of ethyl alcohol.
6	100 cc of motor gasoline, match ignition.
7	200 cc of motor gasoline, match ignition.
8,9,27	Two ounces (57g) of polystyrene packing material, ignited by 50 cc of ethyl alcohol.
11,12	Two Class A wood brands ignited by 100 cc of ethyl alcohol.
13,14,21	Two Class A wood brands ignited by 25 cc of ethyl alcohol.
15	Class A wood brand on 1000-watt hot plate. Immediate ignition, flaming fire.
16	Two 12"x12"x3" (30x30x8cm) pieces of flexible polyurethane foam ignited by 10 cc of ethyl alcohol.
17A	Three 12"x12"x3" (30x30x8cm) pieces of flexible polyurethane foam ignited by 10 cc of ethyl alcohol.
19,24	Three 12"x12"x3" (30x30x8cm) pieces of flexible polyurethane foam ignited by 10 cc of ethyl alcohol.
20	Raw cotton, 2 pounds (900g), in pan on 1000-watt hot plate.
22,23	One Class A wood brand ignited by 10 cc of ethyl alcohol.
25,26	One 12"x12"x3" (30x30x8cm) piece of flexible polyurethane foam ignited by 10 cc of ethyl alcohol.

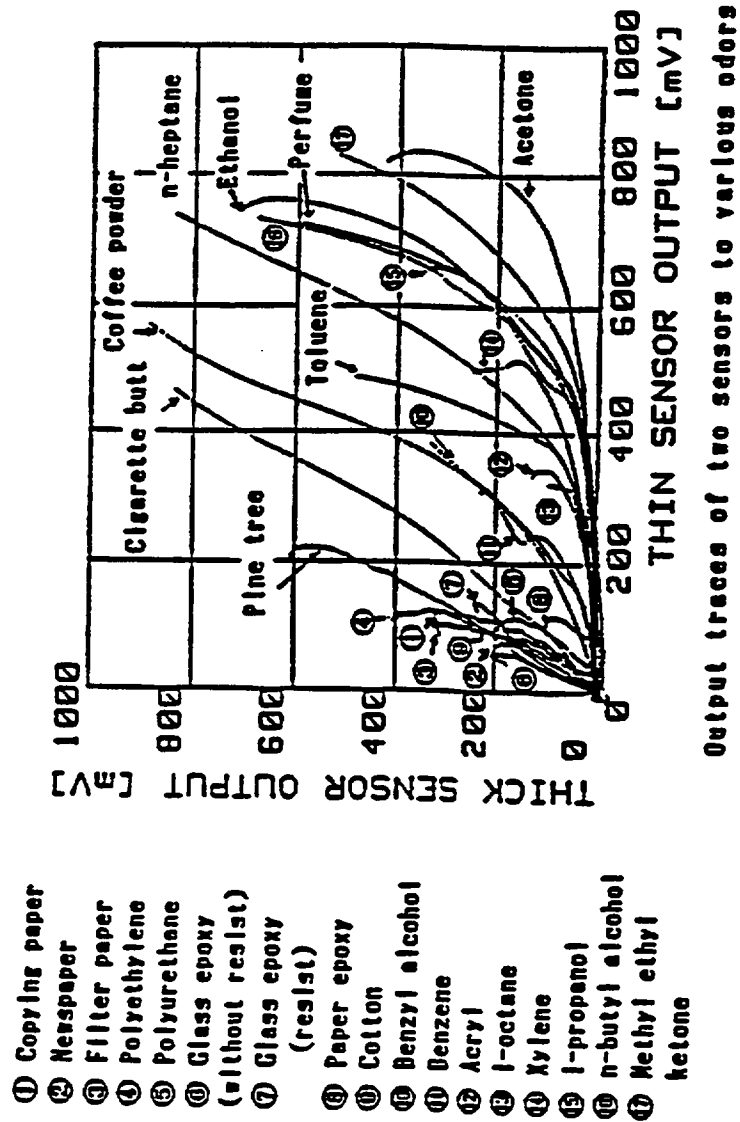
Table 2.4
Test Results
(Bukowski and Bright)

Detector Alarm Response - In Seconds

Test No.	A Photoelectric	J Photoelectric	H Ion Chamber	B Photoelectric	C Photoelectric	D Photoelectric	E Photoelectric	G Photoelectric	F Photoelectric	I Ion Chamber	K TCS Semiconductor
1	30	56	33	46	27	29	28	34	36	30	36
2	---	---	32	29	---	---	---	---	---	27	---
3	28	---	30	30	26	28	27	31	32	27	---
4	---	---	45	45	---	---	---	---	---	38	---
5	---	---	45	42	---	---	---	---	41	35	---
6	62	---	44	52	55	72	58	107	57	39	---
7	63	---	46	55	76	76	59	132	64	NR	---
8	44	---	42	52	42	46	42	41	44	31	---
9	34	---	32	30	31	36	30	34	41	NR	---
10	28	---	30	28	27	28	28	31	34	28	---
11	49	---	52	51	53	58	58	---	49	43	---
12	48	---	49	56	49	55	---	46	51	47	---
13	49	---	47	49	54	119*	52	70	47	44	---
14	47	---	53	53	88	*	63	45	49	46	---
15	---	---	139	---	---	*	---	---	---	113	---
16	156	---	90	103	162	*	138	---	134	107	---
17A	154	---	85	108	163	*	138	---	170	108	---
19	123	---	97	102	124	*	124	---	119	109	---
20	1,656	---	---	1,582	---	1,754	1,762	1,690	1,632	1,654	IND
21	74	160	72	67	76	103	111	74	74	73	---
22	103	---	106	97	103	130	118	103	102	110	---
23	96	---	102	92	101	124	102	95	100	101	---
24	138	---	92	111	141	134	136	---	138	114	---
25	134	---	104	109	145	134	132	---	141	120	---
26	127	---	118	137	138	131	133	---	134	113	---
27	51	---	50	51	52	55	54	---	58	48	---

Notes: --- No alarm or indication
IND Indication but no alarm
* Clock Timer malfunction
NR Not resettable

Figure 2.4
Tin Dioxide Sensor Output Traces
(Okayama)



odors and the organic compound odors. The sensors were also compared by ranging the heater voltages. Two distinct trends were noted, a decrease in heater voltage increases the sensitivity of the sensor in detecting smoldering odors and decreases the sensitivity to organic compound odors. Okayama (1991) concluded that there may be some potential for the use of tin dioxide gas sensors as fire detectors.

The ability to detect slow burning fires was studied by Kohl et al. (1995) using a three metal oxide gas sensor array. The sensors were designed for the detection of carbon monoxide, hydrogen (H_2) and nitrogen oxides (NO_x) gases for the detection of smoldering lignite fires. The signals for the detectors were used to develop eight conditions which would discriminate between smoldering fires and nuisance sources. The system was capable of detecting low quantities of gases, representative of very small or smoldering fires, however, the detection times were on the order of hours.

A study conducted by Denny (1993) at The University of Maryland addressed the possibility of using tin dioxide gas sensors in an algorithm, the expert system, capable of distinguishing between fire and non-fire sources. The study consisted of 31 small scale tests in a modified U.L. 217 smoke box (U.L., 1985). The test sources consisted of flaming and boiling liquids, flaming and pyrolysing solids and nuisance odors. See Table 2.5 for the list of candidate

Table 2.5
Candidate Test Sources (Denny)

Boiling Liquids	Flaming Liquids	Pyrolyzing Solids	Flaming Solids	Environmental Sources
Heptane		Newsprint		Nail Polish Remover
Kerosene		Cheesecloth		Furniture Polish
Paint Thinner		Polystyrene		Hairspray
70% Isopropyl Alcohol		Hot Dogs		Boiling Water (Humidity)
Vegetable Oil		Toast		Ammonia Based Window Cleaner
				Cooking Spray

sources used for these tests. The expert system developed used the maximum output values for carbon monoxide, carbon dioxide and Taguchi (Figaro TGS 822) sensors. The system is shown in Figure 2.5 (Denny, 1993). The system classifies flaming fires based on the carbon dioxide concentration and differentiates between smoldering and nuisance sources based on threshold values for both the TGS 822 sensor output and carbon monoxide concentration. The performance of the expert system was such that all of the flaming fires and nuisance sources were correctly classified and 60% of the non-flaming fires were correctly classified. The main drawback in the concept of this system is that the high threshold limits established may result in high detection times. While somewhat crude, this algorithm demonstrated the ability of tin dioxide gas sensors to be used for the discrimination between fire and non-fire sources. The results of this project were significant enough to warrant a second phase of the project.

The study was continued by Hagen (1994) in a test facility at The Maryland Fire and Rescue Institute at The University of Maryland. A series of large scale tests were conducted to determine the feasibility of using gas sensors to detect fires. A 3.6 x 3.6 x 2.44 ft room was used for the conduction of the 87 tests. The test sources consisted of flaming and boiling liquids, flaming and pyrolysing solids, flaming gas and nuisance odors. See Table 2.6 for a complete

Figure 2.5
Expert System -
Fire Data Classification Rules (Denny)

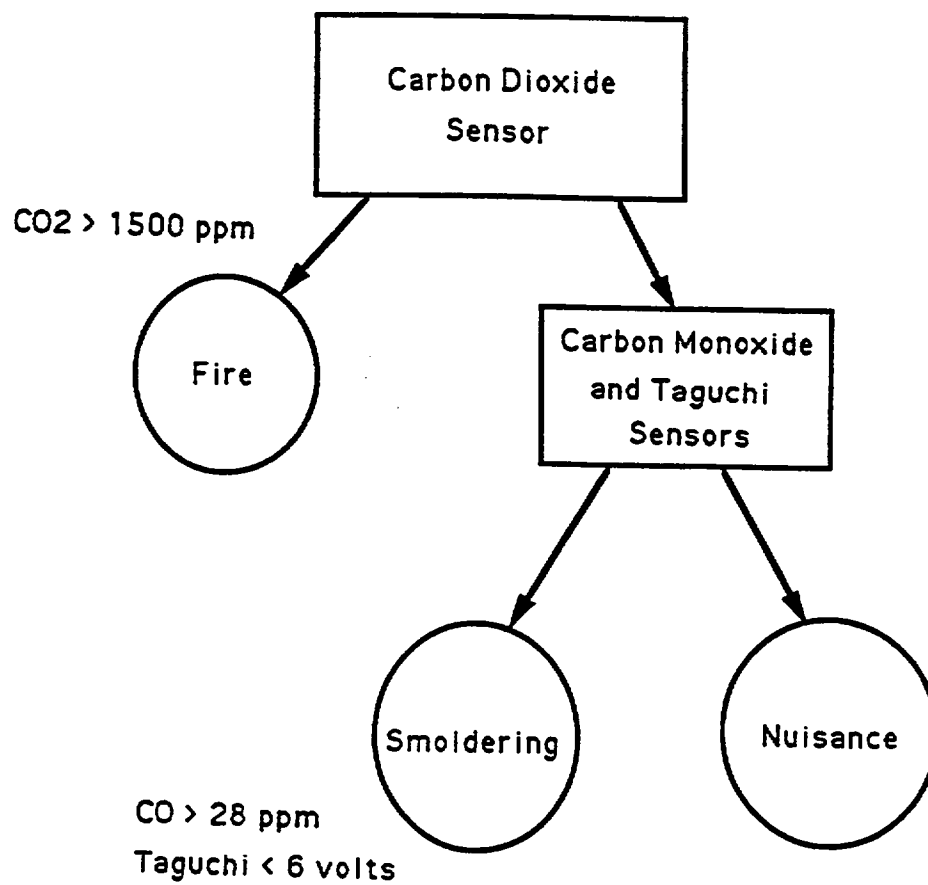


Table 2.6
Test Sources (Hagen)

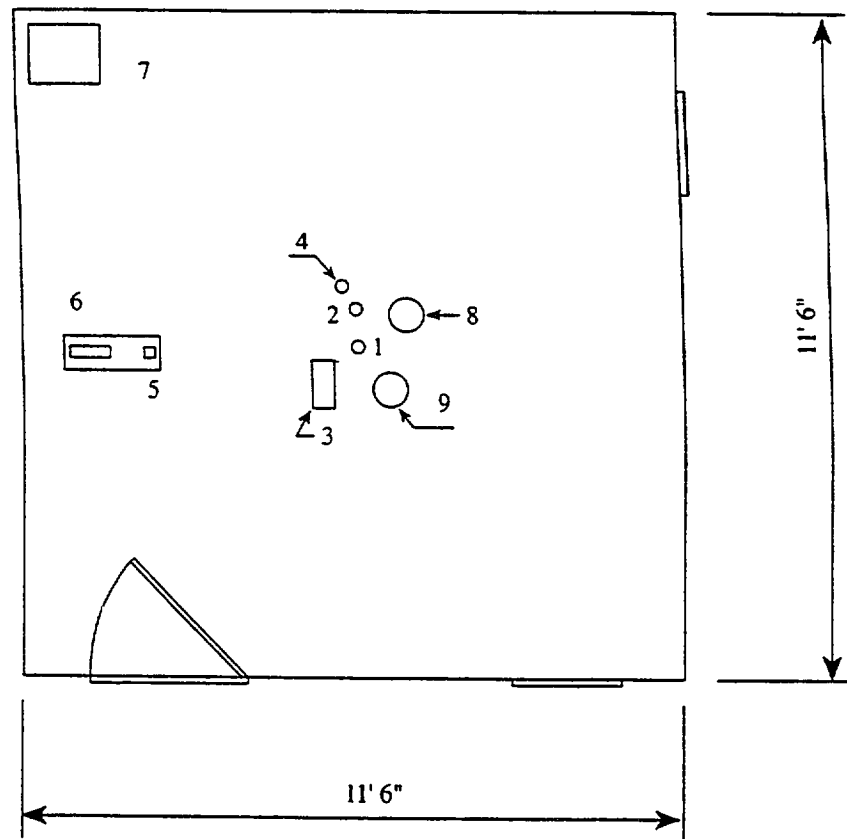
Flaming Liquid	Boiling Liquid	Flaming Solids	Pyrolysing Solids	Flaming Gas	Environmental Sources
	Vegetable Oil		Toast	Propane	Coffee
	Heptane	Paper			Ammonia based window cleaner
	1-Propanol		Paper Towel		Hair spray
	Methanol	Cotton			Nail polish remover
	Toluene	Cotton Cloth			Cooking spray
		Polystyrene			Furniture polish
		Pine wood			Lysol
		Cardboard			Water mist
		Cheesecloth			Boiling water
		Polyethylene			Toast in toaster
					Bleach
					Cigarette smoke

list of test sources. The instrumentation used for the development of an expert system based on this series of tests consisted of carbon monoxide, carbon dioxide, and oxygen analyzers, two Taguchi sensors and thermocouples. See Figure 2.6 for the locations of these devices.

Hagen (1994) evaluated four combinations of threshold value systems, A - D, which led to the development of a new expert system. Combination A was identified as the best suited candidate for use and is shown in Table 2.7 and graphically in Figure 2.7 (Hagen, 1994). The evaluation of all four systems are shown in Table 2.8 (Hagen, 1994). He noted that Combination D was more prone to false alarms than Combination A, which disqualified the selection of that system, even though the results were 87% effective for both systems. He demonstrated that threshold limits can be established for a set of sensors and analyzers capable of discriminating between flaming fires, non-flaming fires and nuisance sources.

Hagen (1994) provided the detection rate for the smoke detectors used for comparison in the study, see Table 2.9, and concluded that the new expert system was 11 % more effective than commercially available detectors.

Figure 2.6
Test Room Layout and Instrumentation (Hagen)



- | | |
|-------------------------------|---------------------------------|
| 1. Thermocouple tree | 6. Helium-neon laser |
| 2. Taguchi sensor (TGS 822) | 7. Load cell |
| 3. Taguchi sensor (TGS 880) | 8. Ionization smoke detector |
| 4. 3/16" copper sampling tube | 9. Photoelectric smoke detector |
| 5. Photocell | |

Table 2.7
Threshold Values for Combination A (Hagen)

Combination A	Flaming Fire	Nuisance Source	Smoldering Fire
Tag 822		> 0.9 V	> 0.270 V
Tag 880		> 0.15 V	
CO			> 17 ppm
CO₂	> 210 ppm		> 22 ppm
Temperature	> 105 °F		

Figure 2.7
Classification for Combination A (Hagen)

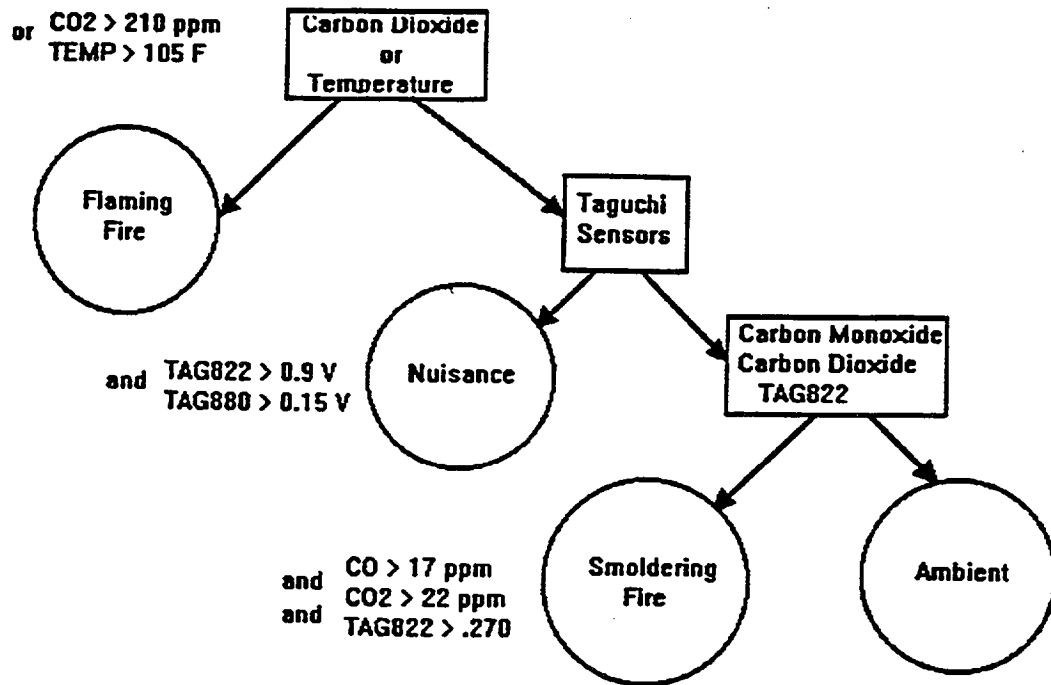


Table 2.8
Evaluation of Threshold Value Systems (Hagen)

Combination A	FL	SM	NU/AM	Total	Total Incorrect	% Wrong
Flaming Fire	34	0	0	34	0	0
Smoldering Fire	0	10	6	16	6	38
Nuisance/Ambient	0	5	32	37	5	13
Total				87	11	13
Combination B						
Flaming Fire	34	0	0	34	0	0
Soldering Fire	0	13	3	16	3	19
Nuisance/Ambient	0	15	22	37	15	40
Total				87	18	21
Combination C						
Flaming Fire	34	0	0	34	0	0
Smoldering Fire	0	8	8	16	8	50
Nuisance/Ambient	0	5	32	37	5	13
Total				87	13	15
Combination D						
Flaming Fire	34	0	0	34	0	0
Smoldering Fire	0	10	6	16	6	38
Nuisance/Ambient	0	5	32	37	5	13
Total				87	11	13

FL: Flaming, SM = Smoldering, NU/AM = Nuisance/Ambient

Table 2.9
Detection Rate for Smoke Detectors (Hagen)

Smoke detectors	FL	SM	AM	Total	Total Incorrect	% Wrong
Flaming Fire	26	0	8	34	8	24
Smoldering Fire	0	8	8	16	8	50
Nuisance source	0	4	33	37	4	11
Total				87	20	23

FL: Flaming, SM = Smoldering, NU/AM = Nuisance/Ambient

2.4 Using Multivariate Statistical Methods to Detect Fires

As part of this research project, the Departments of Fire Protection Engineering and Chemical Engineering at the University of Maryland have been collaborating to develop a discriminating fire detector. The key characteristics for such a protocol detector are that it should be capable of discriminating between fire and non-fire sources, detect a wide variety of fire scenarios and have short response times. The research efforts in the first two phases led to the development of a Principle Component Analysis (PCA) technique providing the desired qualities for a protocol detector. The efforts of the fire protection engineering team focused on identifying signatures from fire and non-fire sources. The chemical engineering team concentrated on processing analysis techniques to investigate sensor response patterns and the capability for discrimination between fire and non-fire sources (McAvoy et al., 1996).

McAvoy et al. (1996) indicated that in chemical process industries the collection of data for hundreds or thousands of variables in real time is required for control systems. This vast number of variables required to be processed, can be overwhelming and difficult to analyze. The development of multivariate statistical methods have been effectively employed to assist operators in detecting abnormal conditions. The coupling of these multivariate statistical methods with

sensor technology looks promising for detecting fires more accurately than the current technology available at this time (McAvoy et al., 1996).

As part of the first two phases, the development of the expert system described in section 2.3, was employed as a preliminary analysis to the PCA method. This system correctly classified all 34 flaming fires, however, it misclassified 12 of 53 non-flaming and nuisance sources. This suggests that further discrimination is required for the correct classification of these events. Also, the discrimination between these sources is inherently difficult. For example, when is burning toast classified as a nuisance source and when is it classified as a smoldering source?

The application of the PCA makes use of a set of experimental measurements arranged in a data matrix, X (McAvoy et al., 1996). The rows of the matrix, X , are the sets of data measurements for all m of the x_i variables recorded at each time step throughout the experiment. Where, m is the total number of steps and x_i is the number of sensor outputs recorded. The number of rows in X is equal to the total number of time steps taken throughout the experiment. PCA finds linear combinations of the raw measurements to describe variations in the raw data. The linear combinations are referred to as scores, t_i . The number of scores used is typically much smaller than the number of measurements taken. The scores are used to detect abnormal variations and can

be used to reconstruct the raw sensor measurements. The difference between the raw sensor values and the reconstructed values is termed the squared prediction error (SPE). The SPE is also used for the determination of abnormal situations. The combination of the scores and the SPE represent all of the sensor measurements. Sensor fusion and data compression are required to construct both the scores and SPE.

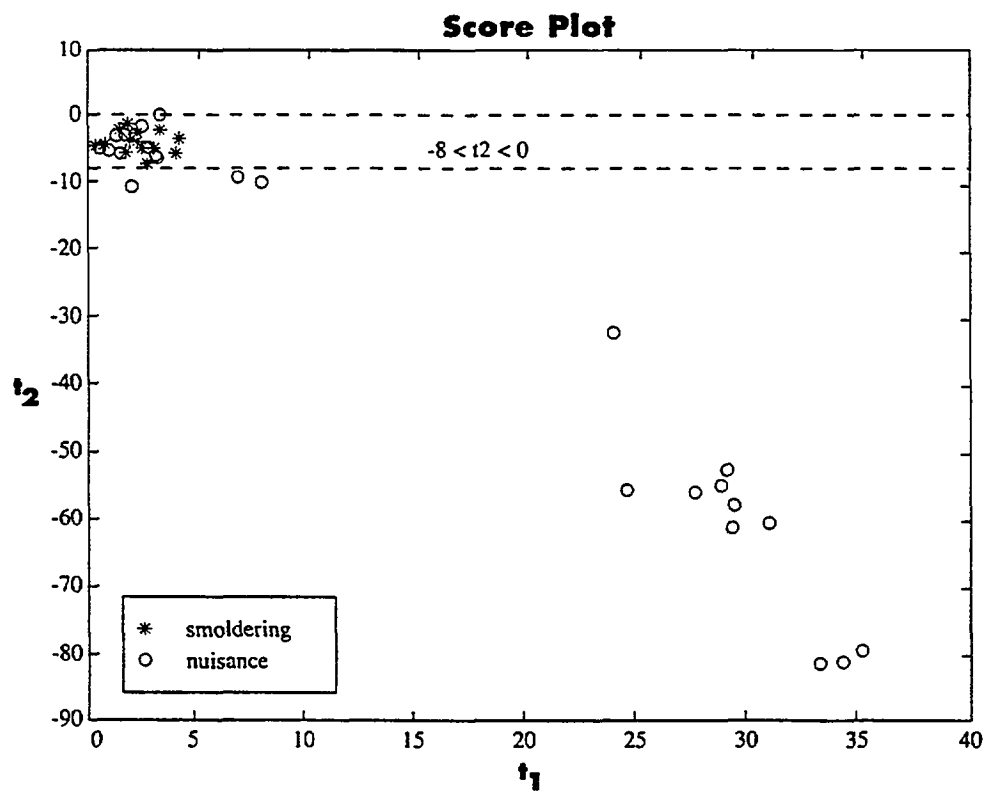
For the analysis of the large-scale fire tests conducted in phase 2, the PCA model was constructed using six sensor signals. The sensors consisted of two Taguchi sensors (TGS 822 and TGS 880), carbon monoxide, carbon dioxide, temperature and light obscuration. The data was scaled to zero mean and unit variance for each sensor. The results of the PCA model constructed are presented as Table 2.10 (McAvoy et al., 1996).

The SPE declares an abnormal situation if the data is beyond the 99.5 % confidence limit of normal data. The SPE requires three successive violations to identify abnormal situations. An examination of the scores was required to distinguish between flaming fires, non-flaming fires and nuisance cases. See Figure 2.8 (McAvoy et al., 1996) for the projection of scores for nuisance and non- flaming sources. This led to the development of the following rules for the PCA to classify sources by determining the scores associated with a signature:

Table 2.10
Percent Variance Captured by PCA Model (McAvoy et al., 1996)

Percent Variance Captured by PCA Model			
Principal Component	Eigenvalue	% Variance	Cumulative % Variance
1	1.8700	31.1660	31.1660
2	1.4766	24.6096	55.7756
3	1.2086	20.1427	75.9183
4	0.6578	10.9630	86.8813
5	0.4678	7.7963	94.6776
6	0.3193	5.3224	100.0000

Figure 2.8
Projection of Scores for Nuisance and non-Flaming
Experiments onto t1-t2 Plane (McAvoy et al., 1996)



If $t_3 > 5$, then there is a flaming fire,
if $-8 < t_2 < 0$ there is a non-flaming fire,
or else there is nuisance.

This scheme led to the successful classification of all 34 flaming cases, 14 of 16 non-flaming cases, but only 27 of 37 nuisance cases. See Table 2.11 for the classifications by PCA (McAvoy et al., 1996). The results are analogous to 10 nuisance alarms and 2 undetected non-flaming fires.

The PCA system was able to reduce detection times from those attained using conventional detectors, by an average of 45 seconds for flaming fires and 245 seconds for non-flaming fires, the results are presented in Table 2.12 (McAvoy et al., 1996). A comparison of detection times for conventional detectors and PCA is presented in Appendix A (McAvoy et al., 1996). In order to improve the performance of this technique, additional sensors are required. The determination of the sensors should be such that there is a separation in the scores, which allow for the distinction between non-flaming fires and nuisance sources (McAvoy et al., 1996). Figure 2.9 represents a detector capable of providing the required number of variables to effectively implement the use of PCA (McAvoy et al., 1996, Cavicchi et al., 1994). This device contains a large

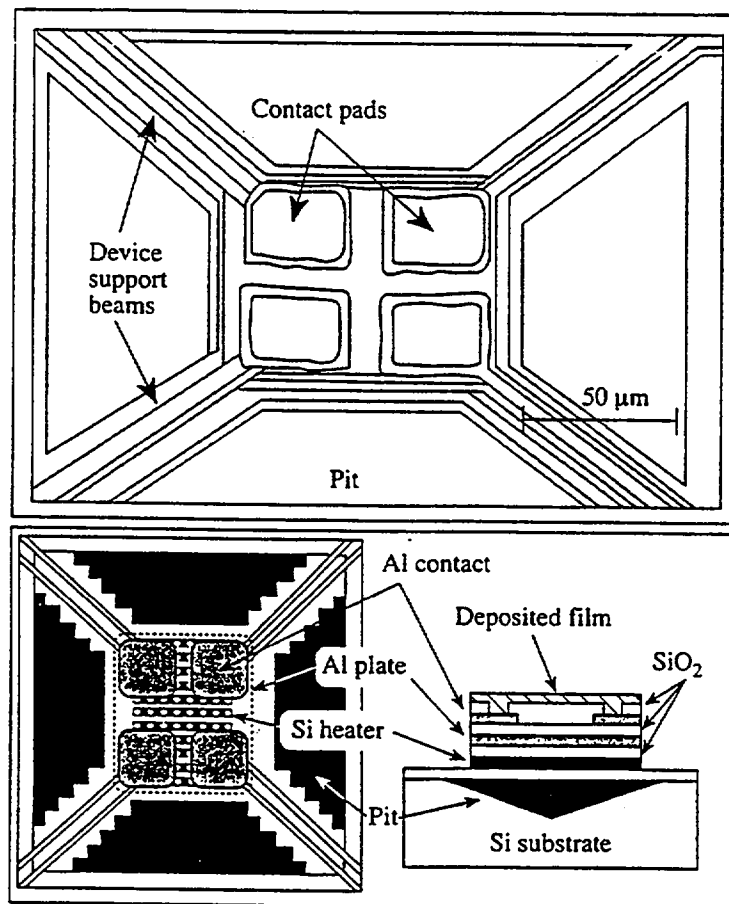
Table 2.11
Classification by PCA (McAvoy et al., 1996)

	Flaming Fire	Non-flaming Fire	Nuisance	Total
Flaming Source	34			34
Non-flaming Source		14	2	16
Nuisance Source		10	27	37
Total	34	24	29	87

Table 2.12
Time to Detection (McAvoy et al., 1996)

	Flaming Fires	Smoldering Fires
Total	34	16
Number of fires undetected—commercial	8	8
Number of fires undetected—PCA	0	2
Average reduction in detection time (s)	45 (57%)	245 (30%)
Range of reduction in detection time (s)	6–244 (41–94%)	182–332 (20–40%)

Figure 2.9
Thin Film Gas Sensor
(McAvoy et al., 1996, Cavicchi et al., 1994)



array of micro-machined, silicon-based sensors which can be produced to respond to low concentrations of different gas mixtures (Grosshandler,1995,NISTIR 5555) (Cavicchi et al., 1994) (McAvoy et al., 1996) (Grosshandler,1995, NISTIR 5700).

The key conclusions of this study are that prompt detection is obtainable using the PCA approach. The classification of various sources into the following categories is possible: flaming, non-flaming and nuisance. Variations in ambient conditions can also be accounted for (McAvoy et al., 1996).

Continuation of this study by Chemical Engineering will be conducted for combination source scenarios using the measurements obtained as part of this phase of the project. The results of this analysis have not yet been developed and will be included as part of another paper.

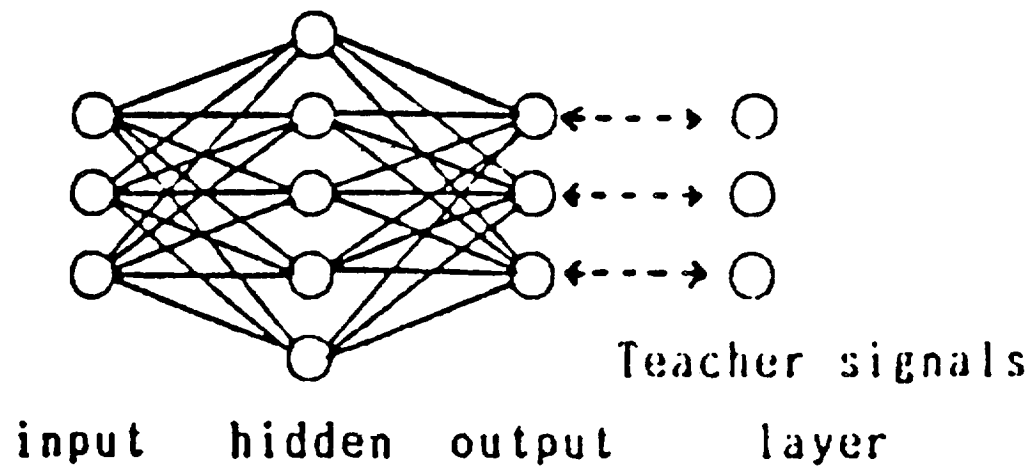
2.5 Artificial Intelligence Techniques for Fire Detection

In 1991 Okayama proposed the use of an artificial intelligence technique known as back-propagation to be used with addressable sensors for use as a neural network for fire detection. It was identified that back-propagation could be used for pattern-matching, but, more significantly that it is capable of coping with changes in definitions.

Okayama (1991) identified four features that are required for the development of such a system. First, the neural network structure would consist of three layers, an input layer, a hidden layer and an output layer, with the accuracy of the system having the highest dependence on the characteristics of the hidden layer. The neural network is the series of strings used to connect the layers as a signal processing network. See Figure 2.10 for the structure of a neural network. Second, signals are given to the input and output layers of the structure to teach it. The strength of the strings between the layers adapt to the definitions and can continue to learn based on the frequency of the inputs. Next, it was identified that the result of introducing a variety of signals leads to the development of a set of simple equations, thus, a neural network would not require an algorithm. Finally, the relationship of the input and output depends on the strength of the strings between layers.

Okayama (1991) established a primitive neural network to obtain fire probability, fire risk and smoldering probability by using smoke, temperature and gas sensors. He used four cases to develop the definitions required to teach the network and provide strength in the strings between the three layers. He indicated that if the definitions are carefully formulated that a neural network

Figure 2.10
Preliminary Neural Network Structure (Okayama)



system could potentially be developed that would be somewhat representative of the human senses and has potential use in fire detection.

Okayama (1991) continued his research with neural networks by testing two tin dioxide sensors of different thickness, subjecting them to a variety of odors previously discussed in section 2.3. Output signals from these devices were used to train a neural network. The results revealed that tin dioxide gas sensors and a neural network could be used to differentiate between the odors of smoldering fires and the odors of organic compounds. He identified that this type of system would have the capability of quickly and effectively identifying abnormal environmental conditions required to detect fire in its very early stages.

An evaluation of the developed neural network was then conducted using "real sensor data" (Okayama, 1994). The neural network that was eventually developed is presented in Figure 2.11. The input and output layers for this structure consist of four neurons each. The fire probability was characterized using sensor data above a fire source at a distance of 3 m from the center of the source. The neural network was trained using the data sets which resulted in sixteen definition patterns, presented in Table 2.13.

Figure 2.11
Developed Neural Network Structure (Okayama)

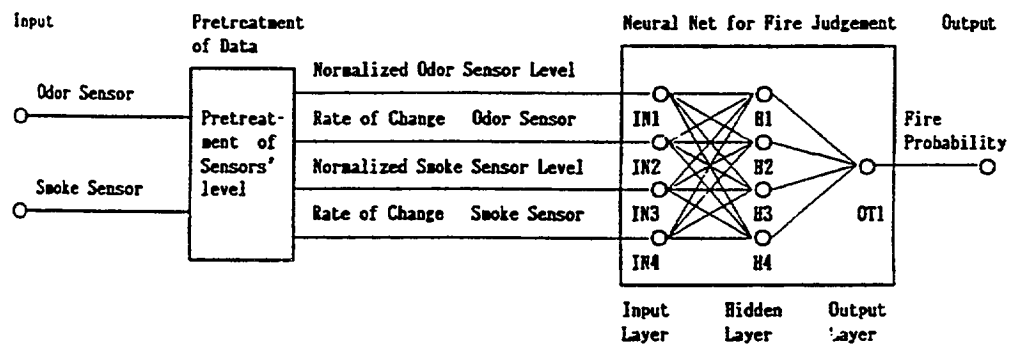


Table 2.13
Sensor Data for Fire and non-Fire (Okayama)

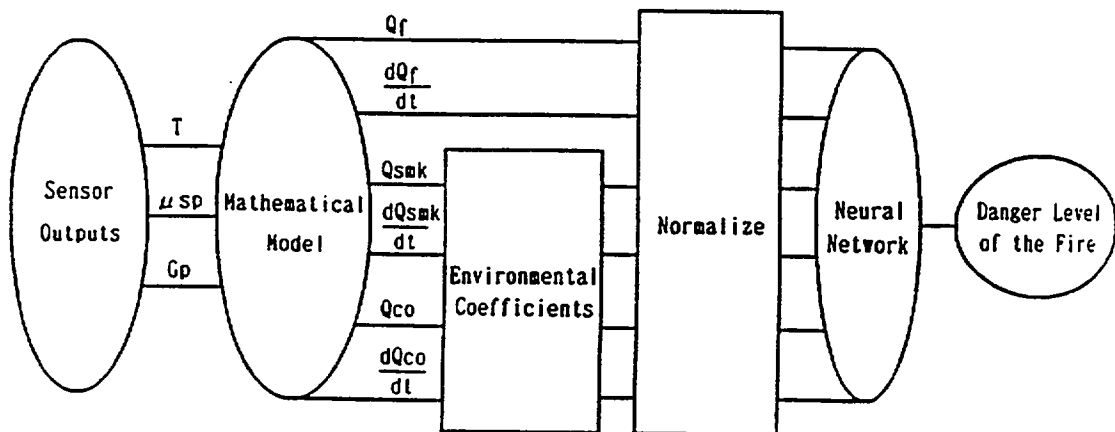
Conditon	Normalized Data		Rate of Change		Fire Probability	
	Odor Sensor	Smoke Sensor	Odor Sensor	Smoke Sensor	Defined	Caluculated
<i>Unmanned</i>	0.037	0.080	0.015	0.009	0.000	0.039
<i>Unmanned</i>	0.027	0.080	0.006	0.012	0.000	0.035
<i>Non-fire</i>	0.255	0.150	0.079	0.039	0.050	0.090
<i>Non-fire</i>	0.388	0.184	0.122	0.094	0.200	0.271
<i>Non-fire</i>	0.167	0.652	0.146	0.603	0.250	0.248
<i>Non-fire</i>	0.193	0.167	0.058	0.096	0.100	0.048
<i>Non-fire</i>	0.538	0.295	0.090	0.305	0.250	0.255
<i>Non-fire</i>	0.744	0.066	0.586	0.008	0.100	0.067
<i>Non-fire</i>	0.170	0.100	-0.100	0.000	0.150	0.161
<i>Fire Test</i>	0.465	0.211	0.077	0.131	0.750	0.697
<i>Fire Test</i>	0.442	1.000	0.405	1.000	0.750	0.745
<i>Fire Test</i>	0.956	1.000	0.786	1.000	0.990	0.994
<i>Fire Test</i>	0.702	0.506	0.160	0.230	0.900	0.937
<i>Fire Test</i>	0.904	1.000	0.535	1.000	0.950	0.980
<i>Fire Test</i>	0.965	1.000	0.898	1.000	0.950	0.987
<i>Fire Test</i>	0.956	1.000	0.786	1.000	0.990	0.994

The evaluation of the neural network consisted of using six experimental data sets, four environmental data sets and two fire data sets. The environmental data sets consisted of normal environmental data, cooking (no further explanation), coffee aroma, and cigarette smoke. The two fire data sets were both for smoldering beechwood chips.

The key conclusion of this evaluation was that the neural network made fire decisions that were quite reasonable. Although, the fire decisions in fluctuating environments were not as reliable as the decisions in stable environments, because the sensor output was nearly the same as fire phenomena.

Ishii et al. (1994) developed a fire detection system which uses a neural network structure, similar to the one developed by Okayama, and a delay circuit to incorporate a concept of time. The fire detection system is represented in Figure 2.12. The neural network was developed using output signals for three sensors, a chromel-alumel thermocouple, a smoke density meter and a tin dioxide gas sensor sensitive to carbon monoxide. The mathematical model used in the system is ASET-B, which is used to calculate the heat release rate, smoke generation rate and gas generation rate. The calculated values are normalized and used as input for the neural network. Finally, the output of the neural network is representative of the danger level of the fire (Ishii et al., 1994).

Figure 2.12
Fire Detection System Using a Neural Network
with a Delay Circuit(Ishii et al.)



The neural network was trained using a variety of fire and environmental sources. The flaming fire sources used were: heptane, ethanol, wood, curtains and fusumas (Japanese papered sliding doors). Additionally, smoldering wood was used. The environmental sources were: cigarettes, grilled fish and chicken, a kerosene heater and a gas heater.

The test room was 6.26 m in length, 10.12 m in width and 3 m high. Three sensors were mounted on the ceiling at one meter from the center of the room. All of the sources were tested at the center of the room.

Ishii et al. (1994) concluded that this system can be used to make highly reliable judgments for fire and non-fire situations. The neural network structure used with a delay circuit can reduce false alarms caused by transient variations of output of a single sensor.

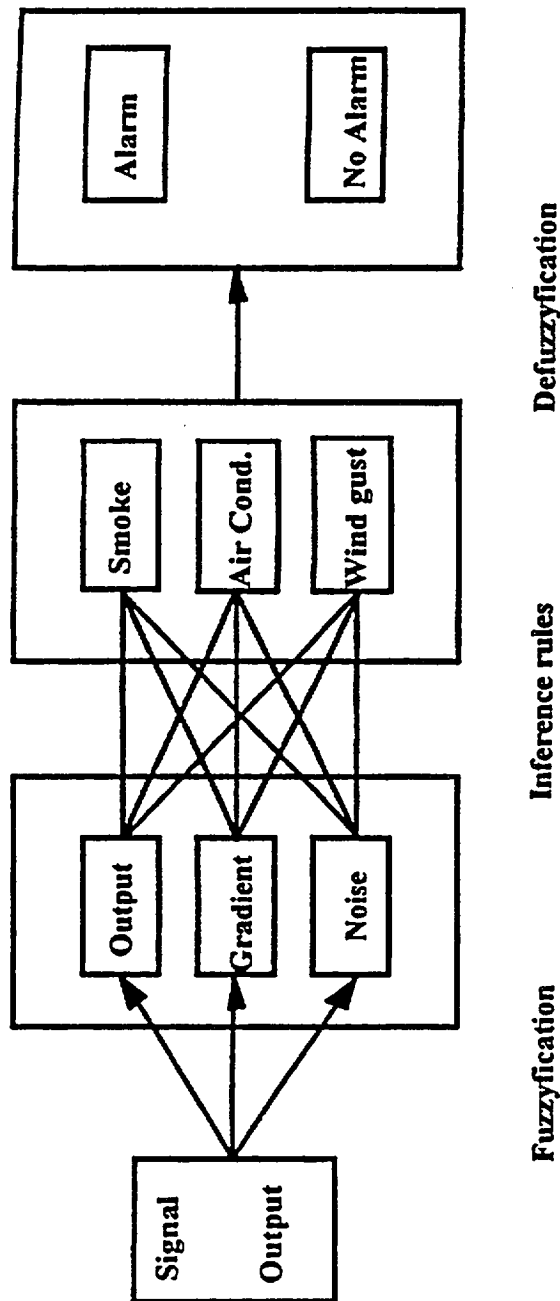
Thuillard applied a fuzzy logic algorithm with an ionization detector (1992) and a linear optical beam detector (1996) to reduce the potential for false alarms associated with these types of detectors. The term fuzzy logic refers to a method of logic which is less rigid than classical logic and allows for the combination of several signal processing algorithms. Thuillard (1992) indicated that the term fuzzy logic may be misleading, suggesting that the results are unpredictable, however, very often the results are more accurate than those attained using classical logic algorithms. The structure of the fuzzy logic

algorithm is presented in Figure 2.13. A double information method was implemented to distinguish between environmental conditions, perturbations and fire conditions. Thuillard (1992) concluded that the use of fuzzy logic can be applied to a wide range of problems and can be used to prevent false alarms.

Thuillard (1996) continued his research with fuzzy logic and combined it with neural network technology, into a single method NeuroFuzzy, which combines the advantages of both techniques. The use of NeuroFuzzy method requires the trainer to closely observe each step of the learning process, termed man-machine interface. Thuillard (1996) concluded that NeuroFuzzy can be a powerful tool in the development of reliable algorithms for smoke detectors. The man-machine interface provides many feedback mechanisms, which allow the user to establish a list of goals, priorities and validation criteria.

Nakanishi et al. (1996) also implemented a neuro-fuzzy technique to develop a fuzzy intelligent fire alarm system. The system uses a combination smoke, heat and carbon monoxide sensor and a fuzzy reasoning technique to determine fire and non-fire conditions. The application of the neural network is to allow the system to continually develop as more test data are introduced. The system redefines the classification rules as often as it is trained. Nakanishi et al.

Figure 2.13
Structure of Fuzzy Logic Algorithm (Thuillard)



(1996) suggest that this research will result in the development of a reliable low cost fire alarm system.

Meacham (1994) identified that the main historical reason for false alarms, is the susceptibility of a single sensor using a threshold value to reach an alarm level when exposed to a nuisance source. The cross-correlation method, developed by Heskestad and Newman (1992), uses a time-averaged product of two or more sensor signals. The use of multiple sensors reduces the signal-to-noise problem associated with single sensor detection. The reliability of this technique increases as the time-averaging period is increased. Meacham (1994) suggests that the use of artificial intelligence techniques, such as neural networks, fuzzy logic and signal cross correlation using multi-sensor arrays will eventually result in more accurate fire detection. Additionally, Meacham (1994) suggests that this technology can be used with fire simulation programs to evaluate fire detectors for design purposes.

Grosshandler (1995, AUBE '95) proposed the concept of a universal fire emulator/detector evaluator (FE/DE). The objective of the emulator is to eliminate the unavoidable variations in full-scale tests that have been observed in repeat runs of the same test scenario (Grosshandler, 1995, NISTIR 5555). Computational fluid dynamic (CFD) models are then recommended to insert fire sources into a space to be protected as a guide for detector placement and to

estimate the system performance under a set of realistic conditions

(Grosshandler, 1995, AUBE '95).

Fischer and Luck (1994) developed a vector autoregressive modeling technique to assist in the development of detection algorithms. The model uses a cross correlation technique of single sensors and is aided by simulation techniques. The applicability of the model was evaluated using simulation results for signals of a ionization chamber, an optical scattered light smoke sensor and a temperature sensor used for fire detection measurements in the field. Fischer and Luck (1994) have concluded that the results for detection times and the capability for discrimination using this method are comparable to other techniques using multi-sensor arrays.

Fischer and Muller (1995) propose a simulation technique to aid the design of multi-sensor detection principles using previously recorded sensor data and statistical modeling. The sensor data is compiled into a statistical data base of representative fire and non-fire conditions. The statistical model provides the capability of expanding recorded signal data to the desired simulation times. A detection algorithm was constructed using a fuzzy expert system based on four input variables, a rule base containing five rules and one output variable.

The model was applied to both fire and non-fire scenarios. The data sets *contained measurements of an optical light scattering sensor and a temperature*

sensor. The results demonstrate that the model is capable of discriminating between fire and non-fire conditions. The output variable is scaled within the range of 0 to 31, where a value of 15 indicates a fire condition. The output decision is provided at each time step accounting for variations in the output of the two sensors and indicating that the model is capable of reclassifying an event. Fischer and Muller (1995) suggest that the statistical modeling and computer simulation technique can be used to study detector behavior and provide quantitative estimates for detector parameters.

CHAPTER III - EXPERIMENTAL APPARATUS

3.1 Design Considerations

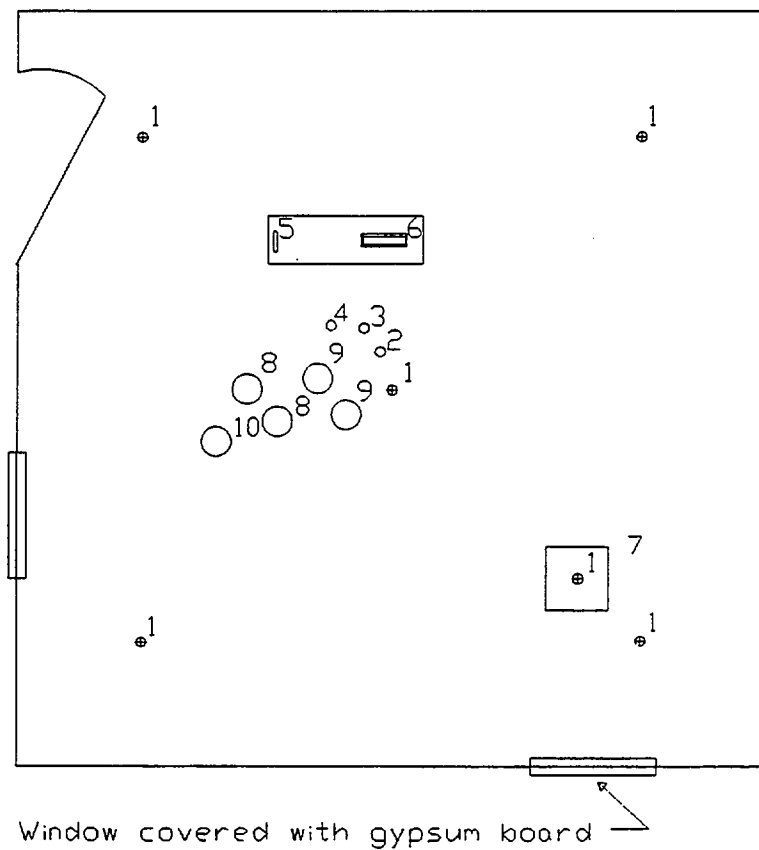
The experiments were conducted in a room of the following dimensions, 3.6 x 3.6 x 2.44 m in height. The test room walls and ceiling were composed of gypsum board in all areas except for the locations of the two windows and the door. See Figure 3.1 for layout of this test room and the location of instrumentation. The test room was located in a test building at The Maryland Fire and Rescue Institute Training Academy at the University of Maryland, College Park.

The test scenarios were based on the selection of phase 2 test materials, presented in Table 2.6, that were readily available. This phase of the research attempts to evaluate the ability of the gas sensors in detecting a fire in an atmosphere masked by a nuisance source, and to avoid detection in an atmosphere with multiple nuisance sources.

3.2 Instrumentation and Sensors

The selection of equipment used to perform these experiments was based on availability and cost. A variety of instruments were used to measure carbon monoxide, carbon dioxide and oxygen concentrations, smoke obscuration, mass

Figure 3.1
Test Room Layout



The legend for this figure is as follows:

1. Thermocouple or thermocouple tree
2. Taguchi gas sensor, TGS 822
3. Taguchi gas sensor, TGS 880
4. Gas analyzer sampling tube, 3/16" OD (1/4" ID)
5. Photocell
6. Helium-neon laser
7. Load cell (fire)
8. Ionization smoke detector
9. Photoelectric smoke detector
10. Residential spot type smoke detector

loss, temperature and the presence of oxidizable and volatile gases. The instrumentation is summarized in Table 3.1.

Carbon monoxide and carbon dioxide concentrations were measured using two Horiba PIR-2000 gas analyzers. These analyzers use the infrared absorption principle of measurement. The sample gases are introduced into a sample cell where infrared radiation is emitted by a light source. The presence of the sample gas will absorb a portion of the infrared light which is received by a detector cell. The measurement is compared to a sealed reference cell containing nitrogen. The difference between the two cells is produced as an electrical output proportional to the concentration of the sample gas (Horiba Manual No. 09652).

Oxygen concentration is measured by a Servomex 540A gas analyzer. This analyzer uses the principle of paramagnetic susceptibility developed by Faraday. The paramagnetic susceptibility of oxygen is much larger than for most other common gases, which means that there is a stronger attraction to a magnetic field. Most other gases are diamagnetic, which means that the gases are repelled by a magnetic field. The analyzer consists of three main components, the oxygen cell, a light source and two photocells. The oxygen cell contains a magneto with a mirror mounted at its fulcrum point. The

Table 3.1
Summary of Instrumentation

Manufacturer	Model	Measurement	Range
Servomex	540A	O ₂	0-1% 0-2.5% 0-5% 0-25% 0-100% by volume
Horiba	PIR-2000	CO ₂	0-5% 0-15% 0-25% by volume
Horiba	PIR-2000	CO	0-1% 0-3% 0-5% by volume
Figaro Engineering	TGS 822	Oxidizable gases	Varies by gases
Figaro Engineering	TGS 880	Volatile gases	Varies by gases
Centronic	OSD100-5T-BNC	Smoke obscuration	0-9 V
Automatic Timing and Controls	6005	Weight	0-0.172.6 N
Fyrnetics - Life Saver	photoelectric sensor	smoke obscuration	1.26%/ft ± 0.38%/ft
Notifier	SDX-751A photoelectric smoke sensor	smoke obscuration	threshold value 1.5% obscuration per foot
Notifier	CPX-551 ionization sensor	smoke particles	threshold value high sensitivity
FCI	ASD-P photoelectric smoke sensor	smoke obscuration	threshold value 2.0% obscuration per foot
FCI	ASD-I ionization sensor	smoke particles	threshold value low sensitivity

light source projects a beam at this mirror which reflects the light to the photocell. Oxygen is introduced into the cell, creating a magnetic attraction with the magneto which causes a change in the angle of the light traveling to the photocells. This results in a change in the electrical output of the photocells which is proportional to the concentration of oxygen (Servomex Manual 00540/001A/0).

These gases were continuously sampled from the test room via a sampling tube located approximately 4 inches down from the ceiling. A pump (compressor) was used to transport the sample gases from the test room to the gas analyzers. The sample gases were passed through an ice bath, a kao-wool filter and a drie-rite filter to cool the sample gases, remove large solid particulates and water vapor respectively. This process is required to prevent damaging the gas analyzers. There was a time lag of approximately 22 seconds associated with this configuration and was taken into account in the data analysis.

The smoke obscuration was measured by using a helium-neon laser and photocell arrangement. The laser provided a light source of approximately 0.015 W, which provided photocell readings ranging from 0 to 9.5 V, when the photocell was covered and with the test room door open respectively. The tests were conducted with the test room door closed providing a range of output for the photocell of 0 to 4V. There was some noise associated with light entering

the test room through the windows and the photocell was positioned to minimize the effects. The photocell was calibrated using a set of neutral density filters with optical densities ranging from 1 ft⁻¹ to 4 ft⁻¹.

The calibration curve for this instrument is provided in Appendix B. The output of this device was considered to be suspicious as a result of interference due to the ambient light entering through the test room windows. The following relationship has been correlated for the optical density from the calibration curve:

$$OD = -1.75 \cdot \log_{10}(x) + 0.85 \quad (3.1)$$

The mass loss was determined by measuring the rate of change detected by a load cell as a function of time. The load cell uses a loading platform mounted on a precision spring and a linear variable differential transformer (LVDT) to measure the changes. Vertical displacement of the platform is proportional to the weight applied, following Hooke's Law, and is measured by the LVDT. The tare weight and zero adjust were calibrated to provide a linear output voltage proportional to the input weight. The calibration curve for this instrument is provided in Appendix B.

The following relationship has been correlated for the mass loss from the calibration curve.

$$\dot{m} = 5621.6 \cdot x - 15837 \quad (3.2)$$

The temperature was measured at various locations within the enclosure to provide a horizontal and vertical profile of the space and along the center-line of the plume. The space was provided with 24 type K thermocouples monitored by a LabVIEW system. The LabVIEW program was configured to monitor temperatures of 0 to 1370° C, following the polynomial equations provided by NIST Monograph 175 (LabView Program Book, 1993). The program was configured to measure temperatures at 4 second intervals, providing a graphical display of the output of all 24 thermocouples throughout the tests.

The presence of oxidizable and volatile gases were measured by using the Taguchi 822 and Taguchi 880 stannic oxide gas sensors respectively.

Several smoke detectors were installed in the test room for comparative purposes. The test facility is provided with two fire alarm panels, a Notifier AFP 200 panel, and a FCI.7200 panel. Each of these panels monitored one photoelectric sensor and one ionization sensor. Additionally, a single spot type detector, used for residential occupancies, was installed, see Table 3.1 for details. The operating principles for these types of detectors will not be discussed as part of this paper, however, the interested reader may find information in the following sources, Bryan (1993), Bukowski and O'Laughlin (1994) and Denny (1993).

3.3 Location of Equipment


The locations selected for instrumentation were determined to provide a lag time associated with the transport of combustion products and to minimize the effects of boundary effects of the compartment walls. This was done by balancing the requirements for maintaining an axisymmetric plume and maximizing the distance to the sensors. The size of the room confined the majority of the instrumentation to be located within the center of the room. The location of the fire was then selected to provide an axisymmetric plume to simplify the assumptions required in the analysis of the results.

The configuration of the test room is similar to the phase 2 tests conducted by Hagen (1994). The major differences being the location of the fire and the addition of thermocouples, to provide a wider range of measurements across the horizontal and vertical profiles of the test room. The thermocouple locations and elevations are summarized in Table 3.2. The locations of the thermocouples and other instrumentation are represented in Figure 3.1.

Table 3.2
Thermocouple Locations and Elevations

Thermocouple Reference No.	Thermocouple Elevation and Location
1	Outside ambient temperature or hot plate
2	0.2 m above floor, center of the room
3	0.4 m above floor, center of the room
4	0.6 m above floor, center of the room
5	0.8 m above floor, center of the room
6	1.0 m above floor, center of the room
7	1.2 m above floor, center of the room
8	1.4 m above floor, center of the room
9	1.6 m above floor, center of the room
10	1.8 m above floor, center of the room
11	2.0 m above floor, center of the room
12	2.2 m above floor, center of the room
13	2.3 m above floor, center of the room
14	0.2 m above floor, center of the fire
15	0.6 m above floor, center of the fire
16	1.0 m above floor, center of the fire
17	1.4 m above floor, center of the fire
18	1.8 m above floor, center of the fire
19	2.2 m above floor, center of the fire
20	2.3 m above floor, corner 1
21	2.3 m above floor, corner 2
22	2.3 m above floor, corner 3
23	2.3 m above floor, corner 4
24	ambient

 Indicates thermocouple tree # 1

 Indicates thermocouple tree # 2

CHAPTER IV - EXPERIMENTATION

4.1 Test Sources

The test sources were selected to cover a range of fire and nuisance signatures. The phase 2 work of Hagen (1994) prepared a somewhat comprehensive list of test sources, of which several sources were selected for comparative purposes. The sources can be separated into three categories: flaming, non-flaming and environmental. Table 4.1 identifies the sources selected for these tests. The flaming and non-flaming sources were selected from the list prepared as part of phase 2 of this project, providing a range of fire sources. The first four environmental sources were selected for two reasons, the results could be compared to the phase 2 tests and the sources were identified as creating significant false alarm problems for home smoke detectors. The fifth environmental source, hamburger, was selected as being representative of a typical cooking odor produced in a residential atmosphere, which, was identified as being one of the two leading causes for nonoperational smoke detectors.


4.2 Experimental Procedures

Each source was tested individually to create a set of control cases. Next, 16 combinations of multiple sources were tested. Table 4.2 is a test matrix

Table 4.1
Test Sources

Flaming Solid	Flaming Liquid	Pyrolysing Solid	Environmental Sources
paper	heptane	cloth	disinfectant glass cleaner hair spray boiling water hamburger

Table 4.2
Test Matrix of Single and Combine Sources

	None	Disinfectant	Window Cleaner	Hairspray	Boiling Water
None		test 33	test 35	test 36	test 34
Heptane	test 32	test 4	test 5	test 6	test 7
Paper	test 9	test 10	test 11	test 12	test 13
Cloth	test 37	test 38	test 39	test 40	test 41
Hamburger	test 42	test 43	test 44	test 45	test 46

identifying the selected combinations and the test identification numbers for each of these combinations. The combinations including either a flaming or non-flaming source and an environmental source were selected to evaluate the ability of the protocol detector to identify a fire in a masked environment. This may require the ability of the detector to continuously reclassify the environmental conditions. The combinations of environmental sources were selected to evaluate the possibility of misclassification of multiple environmental sources as a flaming or non-flaming fire source. A more comprehensive list identifying the specific details of each test scenario is provided in Appendix C.

Several sets of procedures were required to produce the desired signatures for each of the sources and/or combination of sources tested.

4.2.1 Flaming Liquid (heptane)

The heptane was burned in a 15x 15 x 1.2 cm high, square metal pan in an attempt to maintain consistency with the phase 2 research. Hagen (1994) conducted experiments with flaming liquids using four different size and shape containers. Hagen (1994) has indicated that the majority of the tests that were conducted in phase 2 used this container.

The test procedure was initiated by starting the data acquisition system and allowing it to monitor the ambient conditions for approximately 2 minutes.

The next step involved pouring the, 50 ml, of heptane into the container and igniting the heptane using a propane torch. The effect of the propane torch was characterized by Hagen (1994), with the carbon dioxide concentration being the only signature that was affected. The time of ignition and all smoke detector responses were recorded.

4.2.2 Flaming Solid (paper)

The amount, size and arrangement of paper was based on the results obtained by Hagen (1994). The phase 2 experiments were conducted using 2, 8, 10 and 20 sheets of 25% cotton, 20 lb. weight stock paper. Ten sheets of paper were used in this phase, based on the observation by Hagen (1994) that this quantity provided sufficient vapors for detection. In each case, the 10 sheets of paper were shredded into slivers ranging from approximately 6.5 to 9.5 mm in width and 50 mm in length. The paper was placed into a metal container and was placed on the load cell. The experiment was initiated by starting the data acquisition system and allowing 2 minutes of ambient data to be collected. The paper was then ignited, in four locations, using a disposable lighter, at the center of each edge of the container. The effects of the lighter were considered to be negligible.

4.2.3 Pyrolysing Solid (cloth)

A 50% polyester / 50% cotton blend cloth was cut into sections and folded twice, resulting in an exposed surface area of 10.2 x 14 cm for heating. This arrangement was initially used by Hagen (1994). The tests were again initiated by the start of the data acquisition system, which monitored the ambient conditions for a 2 minute period. Prior to the test, a hot plate was turned on and allowed to stabilize at approximately 350°C. At the completion of the ambient period, the hot plate was placed on the load cell, the cloth on the hot plate, a small weight placed on top of the cloth and a thermocouple placed at the center between the cloth and the surface of the hot plate. The weight was used to keep the cloth and thermocouple in place throughout the test. The thermocouple was used to observe any noticeable changes in heating.

4.2.4 Nuisance Sources

The following five nuisance sources were used in this series of tests:

1. Disinfectant (79 % ethanol, 20.9 % inert ingredients, 0.1% Alkyl (50% C₁₄, 40% C₁₂, 10% C₁₆))
2. Glass cleaner (Ammonia D, no further description provided)
3. Hairspray (SD Alcohol, Butane, Propane, Vinyl Acetate, Crotonic Acid/Vinyl Neodecanoate Copolymer, Aminomethyl Propanol, Fragrance, and possibly Isobutane)
4. Boiling water (approximately 150 ml)

5. Hamburger (approximately 70 grams)

Three sets of procedures were followed for the nuisance sources because of the inherent characteristics of each source. At the completion of monitoring the ambient conditions for 2 minutes, each source was applied. One procedure was used for the disinfectant, glass cleaner and hairspray experiments. The application of these sources consisted of vigorously spraying the sample throughout the space for 90 seconds, allowing diffusion to transport the sources closer to the sensors and analyzers.

The next procedure was for the boiling water. A metal container holding 500 ml of water was placed on a hot plate outside of the test room and covered. The water was brought to a boil and then carefully transported into the test room and the cover removed. The water was boiled for approximately 10 minutes. The power source for the hotplate was then shut off. At the completion of the each test, the remaining water was measured. Indicating that an average of 150 ml was introduced into the test room.

The final procedure was for the hamburger experiments. At the completion of the ambient period, a hot plate, at approximately 350°C, was placed on the load cell, the hamburger was then placed on the hot plate with a

thermocouple placed between the two surfaces. The thermocouple was used to observe any significant changes in heating.

4.2.5 Tests with Multiple Sources

The tests involving multiple sources followed the same procedure for the nuisance source involved in the test scenario. The fire or second nuisance source was then implemented at the completion of 90 seconds after the end of the ambient data collection. The procedures were the same as those prescribed above.

4.2.6 Termination of Tests

Several criteria were used to decide when to terminate each test, however, data was collected for a minimum of 10 minutes. The termination criteria are as follows:

1. The fuel was consumed and the sensor outputs were passed the peak values and descending continuously.
2. All five smoke detectors were in the alarm mode.
3. The test duration reached 25 minutes.

CHAPTER V - DATA ANALYSIS

5.1 Introduction

The capability of using tin dioxide gas sensors as part of a protocol detector has been established as part of the first two phases of this project. This analysis will include estimations of gas concentrations, velocities and temperatures within the fire plume, ceiling jet and smoke layer. These estimations will be compared to the test data collected as part of this research phase. Characteristic signals will then be developed for the sensors used to make these measurements.

5.2 Theory and Method of Analysis

The theory to be used in this analysis has been established for flaming fires, the theory for non-flaming fires and nuisance sources has not, thus, this analysis will be primarily focused on the flaming fires. The non-flaming fires and nuisance source scenarios will be addressed where possible. As an example, the calculations for test 32 will be provided in section 5.3.

This analysis will use the temperature profile within the compartment to calculate gas concentrations in the fire plume, ceiling jet and smoke layer. The gas concentrations will be considered to be proportional to the temperature at

each location. In order to make predictions on the temperatures and gas concentrations, the heat release rate of the fire must first be calculated.

The mass loss rate was measured using a load cell, as described in Chapter 3. The mass loss rate will be used to calculate the heat release rate of each fire using one of the following relationships described by Drysdale (1985):

$$\dot{Q} = \frac{m \cdot \Delta H_c}{t} \quad (5.1a)$$

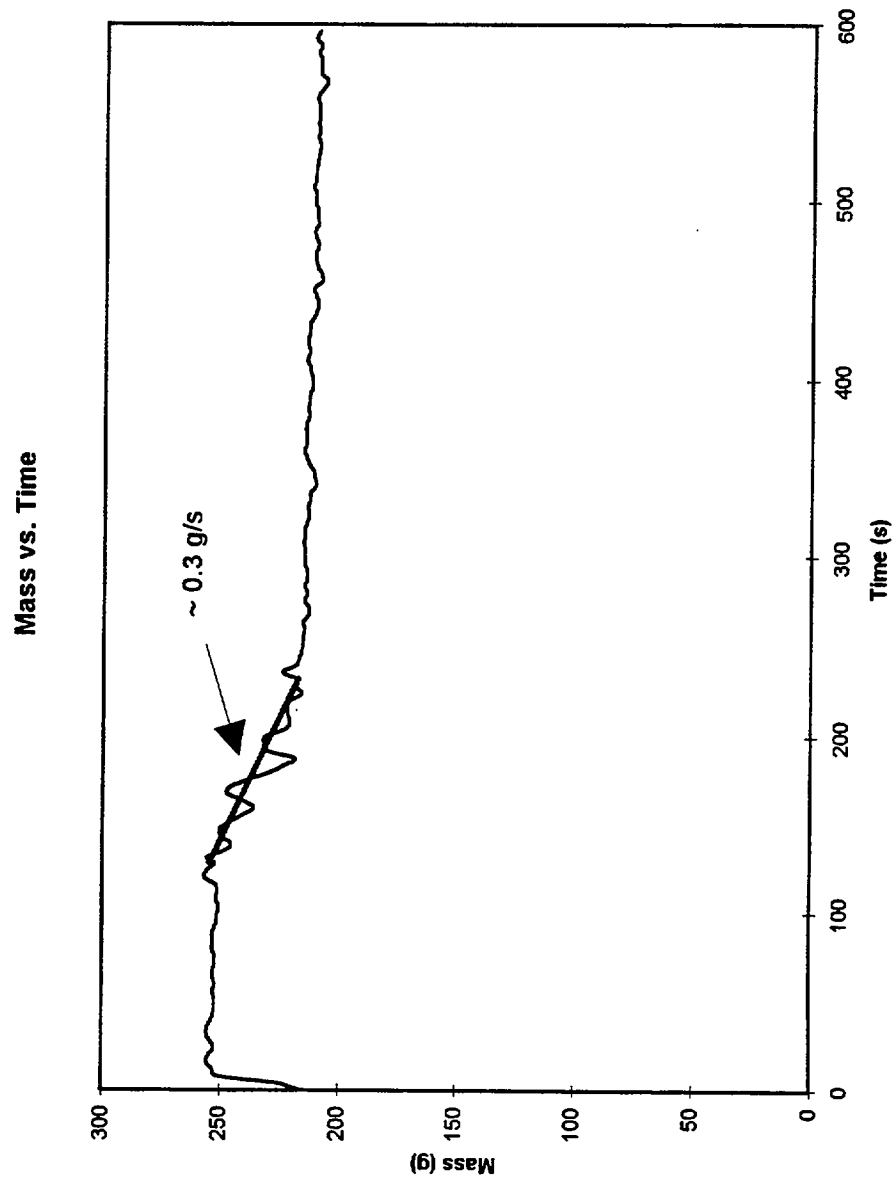
or

$$\dot{Q} = \dot{m}'' \cdot \Delta H_c \cdot A \quad (5.1b)$$

In these equations, \dot{Q} is the heat release rate (kW), m is the total mass loss of fuel (g), \dot{m}'' is the mass loss rate per unit area (g/m²/s), ΔH_c is the heat of combustion (kJ/g), A is the exposed surface area of the fuel (m²) and t is the test duration (s). The mass loss rate was observed to be nearly constant as represented by the constant slope in the mass loss history graphs. Therefore, equation (5.1a) will be used to represent an average heat release rate. A representative mass loss history plot for flaming heptane is provided in Figure 5.1.

The heat release rate can be used to estimate the temperature rise in the fire plume, ΔT , the plume velocity, u_0 , and the plume radius, $b_{\Delta T}$. Heskestad (1995) indicated that the relationships developed for these quantities based on

Figure 5.1
Mass Loss History for Flaming Heptane



the Morton, Taylor and Turner (1956) weak-plume theory have been supported by measurements in fire plumes. The equations are as follows:

$$\Delta T_0 = 9.1 [T_\infty / (g c_p^2 \rho_\infty^2)]^{1/3} Q_c^{2/3} (z - z_0)^{-5/3} \quad (5.2)$$

$$u_0 = 3.4 [g / (c_p \rho_\infty T_\infty)]^{1/3} Q_c^{1/3} (z - z_0)^{-1/3} \quad (5.3)$$

$$b_{\Delta T} = 0.12 (T_0 / T_\infty)^{1/2} (z - z_0) \quad (5.4)$$

In these equations, ΔT_0 (K) is the plume centerline temperature increase, T_∞ (K) is the ambient temperature, g (m^2/s) is gravity, c_p is the specific heat ($J / kg \cdot K$), ρ_∞ is the ambient density, Q_c is the convective heat release rate, $(z - z_0)$ is the elevation above the virtual origin and $b_{\Delta T}$ is the point where the temperature has declined to $0.5 \Delta T_0$.

The virtual origin is used to approximate the location of the point source of energy assumed in this theoretical approach. Heskestad (1995) provides several correlations that have been developed to locate the virtual origin. Two methods will be used for comparative purposes. The method developed by Cetegen et al. (1984) and the method developed by Heskestad (1983).

The calculation of the virtual origin by the method of Cetegen et al. (1984), requires the calculation of a nondimensional parameter Q^* . This parameter is calculated by the following equation:

$$Q^* = \frac{Q_c}{\rho_\infty c_p T_\infty g^{1/2} D^{5/2}} \quad (5.5)$$

Correlations for the virtual origin have been developed for burners flush with the floor and for burners located above the floor. These correlations are as follows:

$$z_0 / D = c + 1.09 \cdot Q^{*2/5}, \quad Q^* > 1 \quad (5.6a)$$

and

$$z_0 / D = c + 1.09 \cdot Q^{*2/3}, \quad Q^* \leq 1 \quad (5.6b)$$

Where $c = -0.50$ for burners flush to the floor and $c = -0.80$ for burners above the floor. For this study, the value of $c = -0.80$ is used with these equations, because the load cell elevated the fire above floor level.

The correlation developed by Heskestad (1983) is as follows:

$$z_0 / D = -1.02 + F \cdot Q^{2/5} / D \quad (5.7)$$

where F is a complex dimensional function that was observed to behave as a constant, $F = 0.083 \text{ m kW}^{-2/5}$.

Equation (5.2) will be used with equations (5.6) and (5.7) to compare the estimated temperature increase to the measured value attained at the elevation of thermocouple 19. Equation (5.4) will then be used to verify the axisymmetric plume assumption used in this analysis by comparing the estimated plume radius to the distance between the centerline of the fire and the compartment walls.

Equation (5.3) will be used to estimate the centerline velocity of the fluid in the plume at the ceiling elevation.

Next, the volumetric air entrainment rate will be calculated for the fire plume. This information will be used to determine the amount of dilution that will occur in the plume as a result of entrainment. This is required to estimate the gas concentrations at the location of the sensors. Again, the correlations developed for the air entrainment into the fire plume are based on the point source theory developed by Morton et al. (1956). The mass entrainment relationship deduced by Morton et al. (1956), is as follows:

$$\dot{m} = k_m \dot{Q}^{1/3} z^{5/3} \quad (5.8)$$

Milke and Mowrer (1993) presented several correlations developed for calculating the mass entrainment based on the point source plume theory. Again, two models have been selected for comparative purposes, the model developed by Zukoski et al. (1981) and the model developed by Heskestad (1983).

The model developed by Zukoski et al. (1981) utilizes the virtual origin correlation presented as equation (5.6). The correlation for the mass entrainment in the fire plume is as follows:

$$\dot{m}_e = 0.076 \cdot \dot{Q}^{1/3} (z - z_0)^{5/3} \quad (5.9)$$

As a comparison, the model developed by Heskestad (1983) will be used.

This correlation is expressed as:

$$\dot{m}_e = 0.0054 \cdot \dot{Q}_c z / z_{fl} \quad \text{for } z < z_{fl} \quad (5.10a)$$

and

$$\dot{m}_e = 0.071 \cdot \dot{Q}_c^{1/3} (z - z_0)^{5/3} + 0.002 \cdot \dot{Q}_c \quad \text{for } z < z_{fl} \quad (5.10b)$$

where z_{fl} , the limiting elevation, corresponds to the mean flame height, where the plume centerline temperature rise, $\Delta T_0 = 500$ K. The correlation is as follows:

$$z_{fl} = z_0 + 0.166 \cdot \dot{Q}_c^{2/5} \quad (5.11)$$

where z_0 is calculated using equation (5.7).

If the radiative fraction χ_R is assumed to be 0.3, then $\dot{Q}_c \approx 0.7\dot{Q}$ and

assuming the second term in equation (5.10b) to be negligible, then equation (5.10b) can be rewritten in terms of the total heat release rate (Milke and Mowrer., 1993), as follows:

$$\dot{m}_e \approx 0.063 \dot{Q}^{1/3} (z - z_0)^{5/3} \quad (5.12)$$

The volumetric flow rate can now be calculated using equations (5.9) and (5.12) and an ambient density of 1.2 kg/m^3 for air at a room temperature of 20°C .

The volumetric entrainment rate using the Zukoski method is as follows:

$$\dot{V}_e \approx 0.0633 \cdot Q^{1/3} (z - z_0)^{5/3} \quad (5.13)$$

and the volumetric entrainment rate using the Heskestad method is as follows:

$$\dot{V}_e \approx 0.0525 \cdot Q^{1/3} (z - z_0)^{5/3} \quad (5.14)$$

These equations do not take into account the transport time lag for the plume to reach the ceiling. This can be estimated using the correlation presented by Newman (1988) and Mowrer (1990):

$$t_{pl} = \frac{2 \cdot H^{4/3}}{3 \cdot \dot{Q}_f^{1/3}} \quad (5.15)$$

The maximum temperature and velocity in the ceiling jet was calculated using the correlations developed by Alpert (1971, 1972) and modified by Evans (1995). The equations for the maximum temperature increase are as follows:

$$T - T_\infty = \frac{16.9 Q^{2/3}}{H^{5/3}} \quad \text{for } r/H \leq 0.18 \quad (5.16a)$$

and

$$T - T_\infty = \frac{5.83(Q/r)^{2/3}}{H} \quad \text{for } r/H > 0.18 \quad (5.16b)$$

The equations for the maximum velocity are as follows:

$$U = 0.96 \left(\frac{Q}{H} \right)^{1/3} \quad \text{for } r/H \leq 0.15 \quad (5.17a)$$

and

$$U = \frac{0.195 Q^{1/3} H^{1/2}}{r^{5/6}} \quad \text{for } r/H > 0.15 \quad (5.17b)$$

where $T(^{\circ}C)$ is temperature, $U(m/s)$ is velocity, $Q(kW)$ is the total energy release rate, $r(m)$ is radial position and $H(m)$ is ceiling height.

The two sets of equations apply to the region, close to the plume impingement on the ceiling, where there is a transitional effect as the flow of gases changes from vertical movement to horizontal movement beneath the ceiling and the region where there is only horizontal movement. The region of impingement is usually termed the turning region.

The location of the maximum temperature in the ceiling jet has been observed at locations within a couple of inches from the ceiling. The temperature approaches room temperature at approximately 5.5 to 12.5 % of the total ceiling height.

As with the plume correlations, the transport lag time is not considered. This can be estimated using the correlation presented by Newman (1988) and Mowrer (1990):

$$t_{cj} = \frac{H^{4/3}}{1.2 \dot{Q}_f^{1/3}} \cdot \frac{[(r/H) - 0.2]^2}{[(r/H)^{1/6} - 0.2^{1/6}]} \quad (5.18)$$

The layer descent due to entrainment only can be expressed for the case of constant cross-sectional area as (Milke and Mowrer, 1993):

$$\frac{dz_u}{dt} = \frac{\dot{V}_e}{A_n} = \frac{k_v \dot{Q}^{1/3} (H - z_u)^{5/3}}{[A_u - 0.04\pi (H - z_u)^2]} \quad (5.19)$$

Making use of the measured gas concentrations and temperature and the ideal gas law, the number of moles can be calculated for each gas specie. The quantity of fuel consumed is known, thus, the yield factor for each material can be estimated. The specie yield is proportional to the measured gas concentration by the following relationship.

$$C_i \propto \left(\frac{\dot{m}_f}{\dot{m}_o} \right) Y_i \quad (5.20)$$

The concentration of each specie, C_i , is related to the related yield, Y_i , mass loss rate, \dot{m}_f , and the mass flow rate past each sensor. The species yield will be calculated for the two entrainment models using equations (5.14) and (5.15) to calculate the volumetric air entrainment rates and equation (5.19) to calculate the layer descent rate. Using the ideal gas law, the molecular weight of each specie and the mass of fuel burned, the specie yield can then be calculated. These values will then be compared to literature values.

5.3 Analysis

As previously discussed in section 5.2, the first parameter to calculate is the heat release rate. Two methods were provided as equations (5.1a) and (5.1b), for this example both equations will be utilized, to demonstrate the similarity in results using each equation.

$$\dot{Q} = \frac{(38g) \cdot (44.6kJ / g)}{(110s)} = 15.41kW \quad (5.1a)$$

$$\dot{Q} = (14.87 \frac{g}{m^2 \cdot s}) \cdot (44.6kJ / g) \cdot (.0232m^2) = 15.39kW \quad (5.1b)$$

The results of the five heptane combination tests are provided in Table 5.1.

Table 5.1 Calculation of Heat Release Rate for Heptane Fires

$\Delta H_c(kJ/g)$: 44.6		Mass (g): 38.0	
Test #	Diameter	Duration (s)	$Q_{test}(kW)$
4	0.172	134	12.7
5	0.172	125	13.6
6	0.172	127	13.3
7	0.172	128	13.3
32	0.172	110	15.4

Next, equation (5.5) was used to calculate the nondimensional parameter Q^* , so that the virtual origin could be calculated using equation (5.6b). The

convective fraction of the heat release rate was assumed to be 0.7, such that

$$\dot{Q}_c \approx 0.7\dot{Q}.$$

$$Q^* = \frac{0.7 \cdot (15.41 kW)}{\left(1.2 \frac{kg}{m^3}\right) \cdot \left(1.0 \frac{kJ}{kg \cdot ^\circ K}\right) \cdot (305^\circ K) \cdot \left(9.81 \frac{m}{s^2}\right)^{1/2} \cdot (0.172m)^{5/2}} = 0.7668 \quad (5.5)$$

The virtual origin was then calculated using the method described by Cetegen et al. (1984), in equation (5.6b).

$$z_0 / D = -0.80 + 1.09 \cdot (0.7668)^{2/3} = 0.1132 \quad (5.6b)$$

or

$$z_0 = 0.1132 \cdot (0.172m) = 0.01946$$

The virtual origin was then calculated using the method described by Heskestad (1983), in equation (5.7).

$$z_0 / D = -1.02 + (0.083 m kW^{-2/5}) \cdot (15.41)^{2/5} / (0.172m) = 0.4210 \quad (5.7)$$

or

$$z_0 = 0.4210 \cdot (0.172m) = 0.07242$$

The results of the five heptane combination tests are provided in the following table.

Table 5.2 Calculation of Virtual Origin for Heptane Fires

Test #	Q*	z _{o,2} (m)	z _{o,1} (m)
4	0.655	0.004	0.054
5	0.702	0.011	0.060
6	0.691	0.009	0.059
7	0.686	0.008	0.058
32	0.798	0.024	0.072
	Cetegen	Cetegen	Heskestad

Using the calculated virtual origin offsets with equation (5.2), an estimate can be made for the maximum temperature rise at the plume centerline, at the elevation of thermocouple 19, so that, a comparison can be made. The calculation will be made using the virtual offsets attained using the method described by Heskestad.

$$\Delta T_0 = 9.1 \left[\frac{305K}{\left(\left(981 \frac{m}{s^2} \right) \cdot (1)^2 \cdot \left(12 \frac{kg}{m^3} \right)^2 \right)} \right]^{1/3} \cdot (0.7 \cdot 1541 kW)^{2/3} (1.7284 - 0.0237)^{-5/3} = 5085^\circ K \quad (5.2)$$

The results for the two methods are presented in the following table.

Table 5.3 Calculation of Maximum Temperature Rise at Plume Centerline

Test #	$\Delta T_{0,TC 19,est}$	$\Delta T_{0,TC 19,est}$	$T_{0,TC 19,meas} (k)$	$T_{0,TC 19,est}(k)$	$T_{0,TC 19,est}(k)$
4	39	41	339	344	346
5	42	45	334	349	352
6	42	44	335	348	350
7	41	43	342	344	346
32	48	51	352	353	356
	Cetegen	Heskestad		Cetegen	Heskestad

The calculated temperatures are in good agreement with the measured values, suggesting that the axisymmetric plume assumption is correct.

Additionally, this suggests that the placement of the thermocouple tree is at or close to the plume centerline.

The plume radius was calculated for both methods using equation (5.4). The calculation will be made using the virtual offsets attained using the method described by Cetegen.

$$b_{\Delta T} = 0.12 \left(\frac{344.5^\circ K}{305^\circ K} \right)^{1/2} (1.835m - 0.0237m) = 0.2310m \quad (5.4)$$

The results for the two methods are presented in the following table.

Table 5.4 Calculation of Plume Radius

Test #	b _{ΔT,ceiling} (m)	b _{ΔT,ceiling} (m)	Distance (m)
4	0.24	0.23	0.86
5	0.24	0.22	0.86
6	0.24	0.23	0.86
7	0.24	0.23	0.86
32	0.23	0.22	0.86
	Cetegen	Heskestad	

The calculated values for the plume radius are significantly lower than the minimum distance from the center of the fire to the wall, again, suggesting that the assumption of an axisymmetric plume is correct.

Similarly, the maximum velocity in the ceiling jet was calculated using equation (5.3). The calculation will be made using the virtual offsets attained using the method described by Cetegen.

$$u_0 = 34 \left[\frac{981 \frac{m}{s^2}}{\left((10 kJ / kg \cdot K) (12 kg / m^3) (305 K) \right)} \right]^{1/3} \cdot (0.7 \cdot 1541 kW)^{1/3} \cdot (1.835 m - 0.0237 m)^{-1/3} = 184 \frac{m}{s} \quad (5.3)$$

The results for the two methods are presented in the following table.

Table 5.5 Calculation of Maximum Velocity in Plume

Test #	$u_{0,est}$ (m/s)	$u_{0,est}$ (m/s)
4	1.70	1.74
5	1.74	1.78
6	1.74	1.76
7	1.74	1.78
32	1.84	1.89
	Cetegen	Heskestad

Next, the ceiling jet region was analyzed, for the maximum temperature rise and maximum velocity. The maximum temperature in the ceiling jet was calculated using equation (5.16b).

$$T - T_{\infty} = \frac{5.83(15.41kW / 1.21m)^{2/3}}{1.7622m} = 18.04^{\circ} K \quad (5.16b)$$

The calculations are at the height of thermocouple 13, the results are presented in the following table.

Table 5.6 Calculation of Maximum Temperature Rise in the Ceiling Jet

Test #	$\Delta T_{0,TC 13,est}$	$T_{0,TC 13,est}$	$T_{0,TC 13,meas}$
4	15	320	326
5	16	323	322
6	16	322	322
7	16	318	315
32	18	323	329

The calculation of the maximum temperature within the ceiling jet is again in good agreement with the measured values attained at thermocouple 13, suggesting that the placement of the equipment was in the ceiling jet region.

The maximum velocity was then calculated for the ceiling jet region, using equation (5.17b).

$$U = \frac{0.195(15.41kW)^{1/3}(1.7622m)^{1/2}}{(1.21m)^{5/6}} = 0.5495m/s \quad (5.17b)$$

The results are presented in the following table.

Table 5.7 Calculation of Maximum Velocity in Ceiling Jet

Test #	Umax
4	0.52
5	0.53
6	0.53
7	0.53
32	0.55

The maximum velocities calculated for the center of the room are considerably lower than the estimated values for the plume centerline, as expected, due to the air entrainment and heat transfer losses.

Next, equations (5.15) and (5.18) were used to calculate the transport lag times associated with the plume and ceiling jet regions. The addition of the two

lag times is representative for the total lag time for the products leaving the combustion zone to reach the location of the sensors.

$$t_{pl} = \frac{2 \cdot (1.7622m)^{4/3}}{3 \cdot (15.41kW)^{1/3}} \approx 0.5703s \quad (5.15)$$

$$t_{ej} = \frac{(1.7622m)^{4/3}}{12(15.41kW)^{1/3}} \cdot \frac{[(1.21m / 1.7622m) - 0.2]^2}{[(1.21m / 1.7622m)^{1/6} - 0.2^{1/6}]} \approx 0.9672s \quad (5.18)$$

Indicating a total lag time of 1.54s, which is reasonable, given the location of the fire and the location of the devices. The results are presented in the following table.

Table 5.8 Calculation of Lag Times

Test #	t_p (s)	t_{cl} (s)	t_{tot}
4	0.64	1.01	1.65
5	0.61	1.00	1.61
6	0.62	1.00	1.62
7	0.62	1.00	1.62
32	0.57	0.97	1.54

A spreadsheet model was developed to calculate the volumetric air entrainment into the plume, the layer descent rate and the species yields. The calculations are presented in Appendix E.

The calculated yields for carbon monoxide and carbon dioxide are presented in Table 5.9 and Table 5.10, respectively. The calculated yields for carbon monoxide and carbon dioxide were compared to the values measured by Tewarson (1995). The estimated yields for carbon monoxide over-predicted the values reported by Tewarson (1995), conversely, the estimated yields for carbon dioxide were under-predicted.

The CO/CO₂ ratios were compared to the reported value of 0.01 by Tsuchiya. See Figure 5.1 for the comparative plot. The values were compared for the period after the fires had achieved a steady burning rate to the end of the test. The results are in relative agreement with the reported value of 0.01.

A comparison of the average CO/CO₂ ratios for the various fire source combinations, indicates that there is approximately one order of magnitude difference in the values for the flaming fires and the pyrolysing solids. The average values were calculated for the steady period of burning/heating to the end of the test. The average CO/CO₂ ratios are presented in Table 5.11.

Table 5.9
Comparison of Estimated and Reported CO Yields

Test Number	Mass Loss g/s	Average Measured Concentration CO ppm	Estimated Yield Factor g/g	Published Yield Factor g/g	Estimated Yield Factor g/g
4	0.3	80	0.03	0.01	0.02
5	0.3	55	0.02	0.01	0.01
6	0.3	72	0.02	0.01	0.02
7	0.3	38	0.01	0.01	0.01
32	0.3	53	0.02	0.01	0.01

Cetegen/Zukoski Tewarson Heskestad

Table 5.10
Comparison of Estimated and Reported CO₂ Yields

Test Number	Mass Loss g/s	Maximum Measured Concentration CO ₂ ppm	Estimated Yield Factor g/g	Published Yield Factor g/g	Estimated Yield Factor g/g
4	0.3	5202	2.7	2.9	2.1
5	0.3	4720	1.6	2.9	1.3
6	0.3	4941	1.8	2.9	1.5
7	0.3	5352	2.0	2.9	1.7
32	0.3	5082	2.1	2.9	1.7

Cetegen/Zukoski Tewarson Heskestad

Figure 5.2
Comparison of CO/CO₂ Ratios

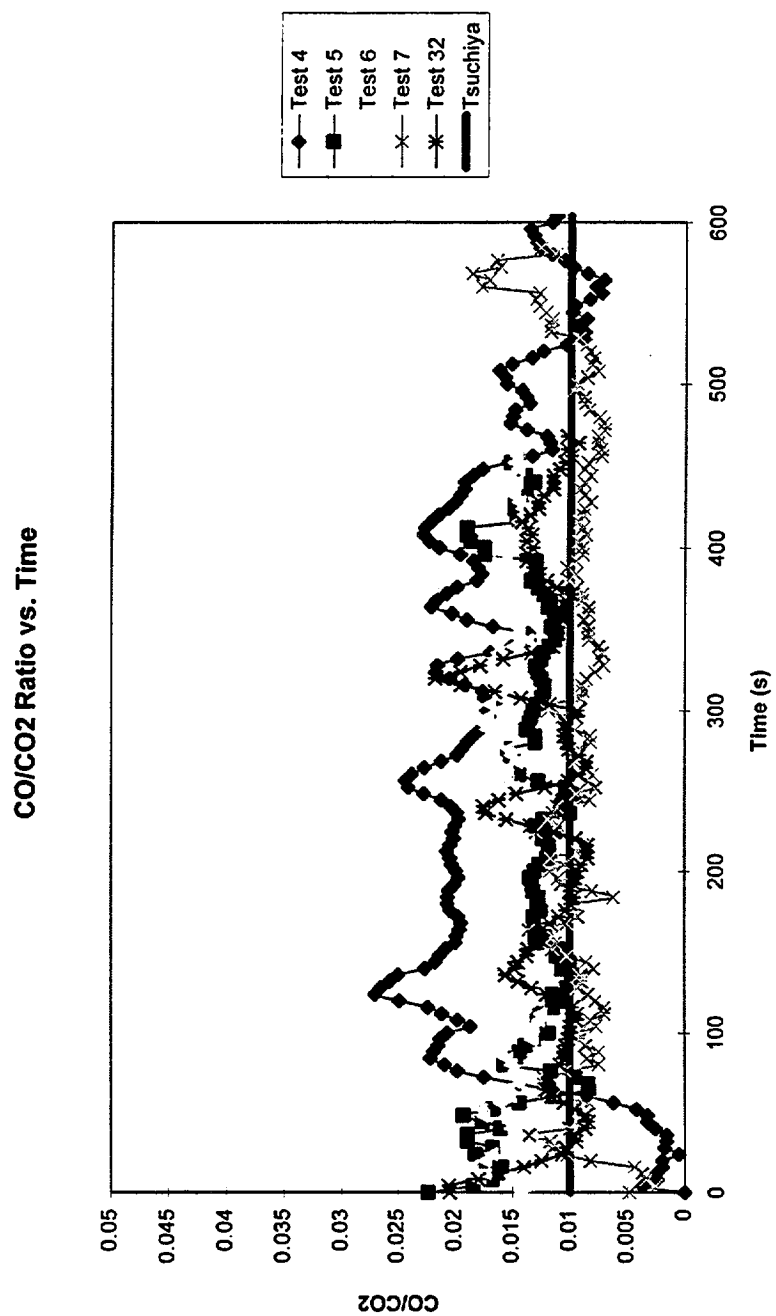


Table 5.11
Comparison of Average CO/CO₂ Ratios

Flaming Heptane Combinations					
Test #	4	5	6	7	32
CO/CO ₂	0.02	0.01	0.02	0.01	0.01
Flaming Paper Combinations					
Test #	9	10	11	12	13
CO/CO ₂	0.11	0.09	0.08	0.14	0.06
Pyrolysing Cloth Combinations					
Test #	37	38	39	40	41
CO/CO ₂	0.85	0.24	0.49	0.29	0.23

CHAPTER VI - DISCUSSION AND CONCLUSIONS

6.1 Discussion of Results

It was observed from the experiments with combined sources that the expert system, developed by Hagen (1994) in phase 2 of this project, would require modifications. However, such modifications are beyond the scope of this paper. It is anticipated that a system based on maximum values would result in the misclassification of the majority of the experiments conducted with combined sources. The dependence of the expert system on the response of the TGS 822 and TGS 880 sensors for discriminating between nuisance and smoldering/pyrolysing sources would not be sufficient.

It was observed in the experiments with combined sources that the signatures provided by the TGS 822 sensor were representative of nuisance sources. In most cases, the TGS 822 sensor was not observed to have any significant change in output when the fire source was introduced, and the sensor would follow similar patterns to the tests with single nuisance sources. The TGS 880 sensor would also follow the similar pattern of the tests with single nuisance sources, however, the sensor output was observed to have a tendency to decrease when the fire source was introduced. The output was observed to approach the magnitude of the output achieved in the tests of a single fire

source, in an asymptotic manner. The tendency of the TGS 880 sensor output to decrease as the fire was introduced would render the expert system ineffective based on the maximum value output. The maximum level achieved is rather a measure of the nuisance source and not the fire source.

The trends observed for the carbon monoxide and carbon dioxide concentrations, in the tests with combined sources, were similar to those observed in the tests with single fire sources. The test combinations with the disinfectant seem to have additional effects, because the measured carbon monoxide concentrations were significantly higher than those measured in the tests with single sources. This effect seems to be more than a simple additive effect, possibly synergistic, but the determination of this effect is beyond the scope of this paper.

The use of the carbon monoxide and carbon dioxide signatures provide a good indication of the source present, however, this would not be sufficient to provide the level of discrimination required. The expert system developed as part of phase 2 required additional sensors to achieve the correct classification of 87% of the sources tested as part of that phase.

The behavior of the photocell was sporadic, possibly due to the effects of light entering the test room through the window. This behavior was also observed in the phase 2 testing. It was anticipated that the change in orientation

of the laser and photocell arrangement from the phase 2 testing would have more of an impact in reducing outside effects.

Additionally, the procedures followed in this set of experiments may not have provided sufficient signatures for better response by the TGS 822 and TGS 880 sensors. Without a more accurate description by the manufacturer of the sensitivity of the TGS 822 sensor and the TGS 880 sensor, it is not possible to determine if there are unseen effects occurring as a result of drift in sensor output or surface contamination. The procedures followed for the nuisance sources may have resulted in concentrations that were higher than expected.

It was anticipated that the combination of a nuisance source and a fire source would result in more distinct changes than were observed. The TGS 822 and TGS 880 signature were less effective in discriminating sources than were anticipated when the experiments were planned. This may be partially attributed to the selection of combinations based on the single sources experiments conducted as part of phase 2.

6.2 Conclusions

In order to provide an adequate level of discrimination for tests with multiple sources, additional sensors are required. It is more difficult to discriminate between signatures in tests with multiple sources than in tests with

single sources. The use of carbon dioxide and carbon dioxide concentrations and CO/CO₂ ratios were effective in discriminating between flaming and pyrolysing sources for these experiments. The development of an expert system based on the maximum sensor output levels would not be effective, based on the results attained by these tests.

6.3 Considerations for Future Research

The number and type of sensors could be increased to provide a more diverse profile for testing. This would allow for a higher level of discrimination than can be attained with the limited number of sensors used for these experiments. The inability of the TGS 822 and TGS 880 sensors to discriminate between combustion effects and nuisance effects, suggests that sensors with a higher level of selectivity should be used. Tin dioxide sensors can be manufactured to have a sensitivity to a specific type of gas, such as hydrogen, carbon monoxide, hydro-carbons, etc. (Ihokura and Watson, 1994). Additionally, Cavivicci et al. (1994) demonstrated that a thin film gas sensor can be manufactured to provide a large array of micro-machined, silicon-based sensors. It is suggested that a set of more selective sensors be used for future testing.

Sensor drift may have resulted in unseen effects associated with the output of these devices, which could be reduced or eliminated by the design of a delay circuit for these devices (Ihokura and Watson, 1994). Additionally, there may have been effects associated with sensor contamination, which would also effect the sensor output readings. This can be reduced by cycling the heater voltage between a high level and a low level. The low level would allow for a higher level of sensitivity in detecting gas concentrations and the higher level would be used for decreasing the effects of contamination (Ihokura and Watson, 1994).

It would be useful to measure the velocity profiles in the ceiling jet. This would allow for better estimates of carbon monoxide and carbon dioxide yields, because the mass flow rate could be more accurately characterized at the location of the sensors.

Additional combinations can be tested to further evaluate the effects of the interaction of nuisance sources and fire sources. This set of experiments does not represent a complete range of sources that can be tested in multiple source combinations. The procedures could be modified to more accurately represent a nuisance environment.

Appendix A: Comparison of Detection Times for Conventional Detectors and PCA

		Detection Time (min)		Scores		
File	Type ^a	Detector	PCA Model	t ₁	t ₂	t ₃
72904	s	11:31	11:58	1.82	-1.37	1.44
72906	s	14:06	9:36	3.27	-2.35	1.84
72702	s	13:40	11:54	2.21	-2.67	1.11
72505	s	13:46	8:14	0.35	-4.74	0.05
72507	s	12:38	9:20	2.70	-7.32	1.72
80102	s	13:58	10:48	3.00	-5.70	1.49
80806	s	15:24	12:22	3.98	-5.63	1.70
80905	s	14:24	11:18	2.26	-4.04	1.58
72902	s	—	12:40	4.13	-3.62	2.39
72602	s	—	10:52	1.43	-2.31	0.62
80402	s	—	11:18	1.73	-5.64	-0.51
72502	s	—	10:58	0.77	-4.35	0.38
80302	s	—	11:14	2.49	-5.02	0.85
80502	s	—	10:52	1.92	-3.92	2.06
72709	s	—	—	—	—	—
72506	s	—	—	—	—	—
72710	f	—	0:28	0.84	-0.67	6.25
72910	f	—	0:14	0.12	-2.08	6.22
80804	f	—	0:12	-0.84	-1.25	9.32
80505	f	—	0:08	1.44	-3.78	17.01
80507	f	—	0:10	1.26	-2.20	13.66
80508	f	—	0:06	0.57	-3.60	21.89
80906	f	—	0:10	0.54	-5.89	29.62
80306	f	—	0:08	-0.62	-2.67	17.06
72501	f	0:16	0:08	-0.08	-3.43	23.67
72601	f	0:14	0:08	0.12	-0.69	33.13
72607	f	1:30	0:18	1.96	-4.74	13.14
72701	f	0:16	0:08	-1.25	-5.24	15.98
72704	f	0:58	0:24	0.22	-1.18	8.07
72705	f	0:34	0:20	1.50	-4.63	7.27
72711	f	0:58	0:12	0.21	-0.04	5.98
72901	f	0:22	0:08	-0.02	-3.53	34.18
72905	f	0:40	0:08	-1.14	0.46	9.57
72907	f	1:38	0:10	0.02	1.28	11.62
^a s: smoldering, n: nuisance, f: flaming, —: no detection						

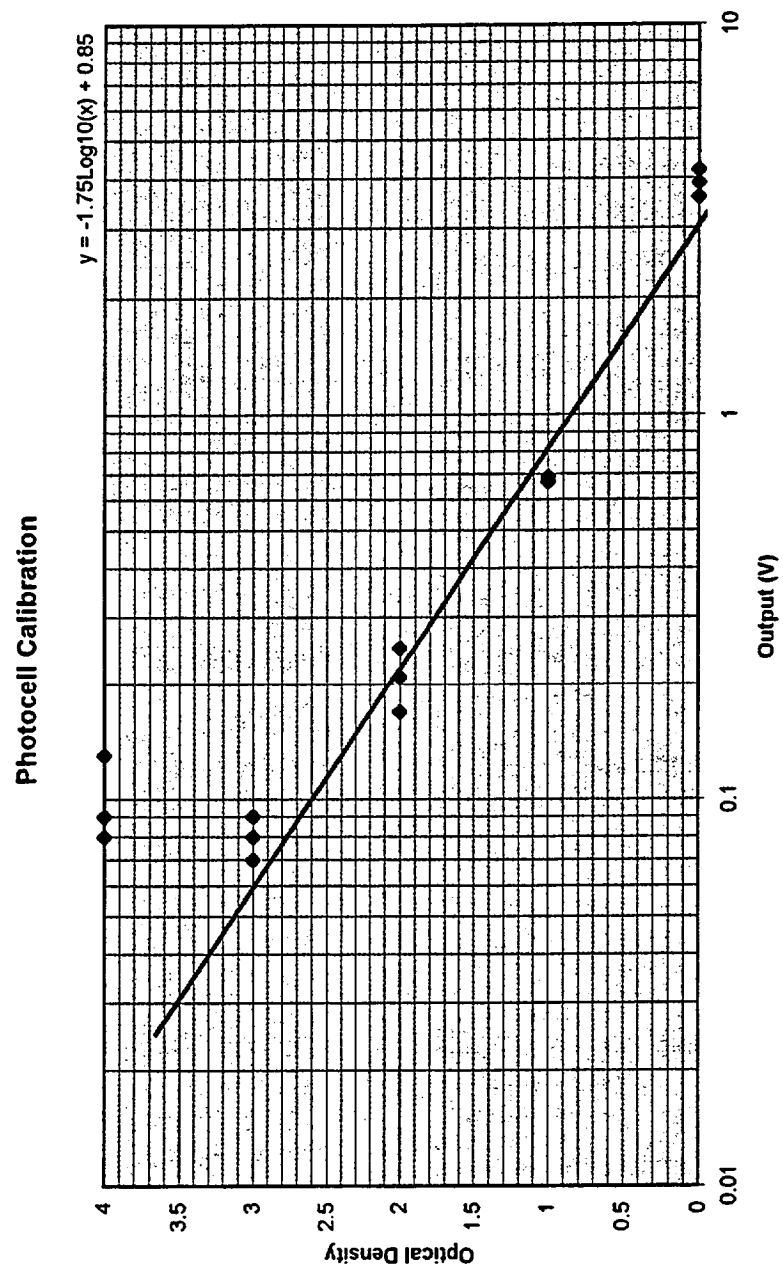
		Detection Time (min)		Scores		
File	Type ^a	Detector	PCA Model	t ₁	t ₂	t ₃
80101	f	0:22	0:08	0.27	-4.26	6.06
80104	f	0:24	0:10	1.19	-2.34	8.47
80105	f	1:50	0:10	-1.31	-2.54	11.80
80108	f	0:20	0:08	0.84	-3.85	16.00
80301	f	0:20	0:08	0.78	-3.66	24.90
80304	f	0:20	0:10	-1.08	-4.63	13.98
80401	f	0:14	0:08	-2.33	-5.45	31.65
80501	f	0:20	0:08	-2.13	-3.48	23.13
80801	f	0:22	0:08	0.71	-0.05	32.18
80802	f	3:40	0:38	-0.15	-0.49	6.51
80803	f	0:32	0:12	-0.54	-3.32	26.71
80805	f	1:20	0:08	-0.65	-3.06	21.44
80808	f	0:40	1:10	-1.38	-4.35	26.26
80809	f	4:20	0:16	-0.27	-2.85	8.23
80810	f	2:08	0:12	-1.42	-2.26	10.47
80901	f	0:22	0:08	0.08	-4.54	25.83
72911	n	0:10	1:04	2.46	-1.61	1.05
72608	n	0:10	0:10	35.27	-79.21	-9.41
80410	n	0:16	0:10	33.41	-81.11	-7.74
80407	n	16:38	9:24	0.55	-5.09	1.61
72708	n	21:02	20:20	1.30	-3.07	-0.39
72503	n	—	0:08	28.54	-56.82	-0.98
72603	n	—	0:08	27.66	-55.60	-0.64
72604	n	—	0:10	34.41	-80.81	-6.58
72605	n	—	0:48	3.14	-6.44	2.47
72609	n	—	1:48	3.24	0.04	1.04
72703	n	—	0:30	23.94	-32.14	2.92
72706	n	—	5:46	2.12	-3.05	0.80
72903	n	—	0:08	29.10	-52.29	-1.26
80303	n	—	0:08	29.46	-57.56	-1.82
80305	n	—	8:30	6.76	-9.24	1.52
80307	n	—	8:30	2.04	-10.74	-1.36
80403	n	—	0:10	29.37	-61.04	-1.64
80404	n	—	3:40	1.65	-2.92	1.11

^a s: smoldering, n: nuisance, f: flaming, —: no detection

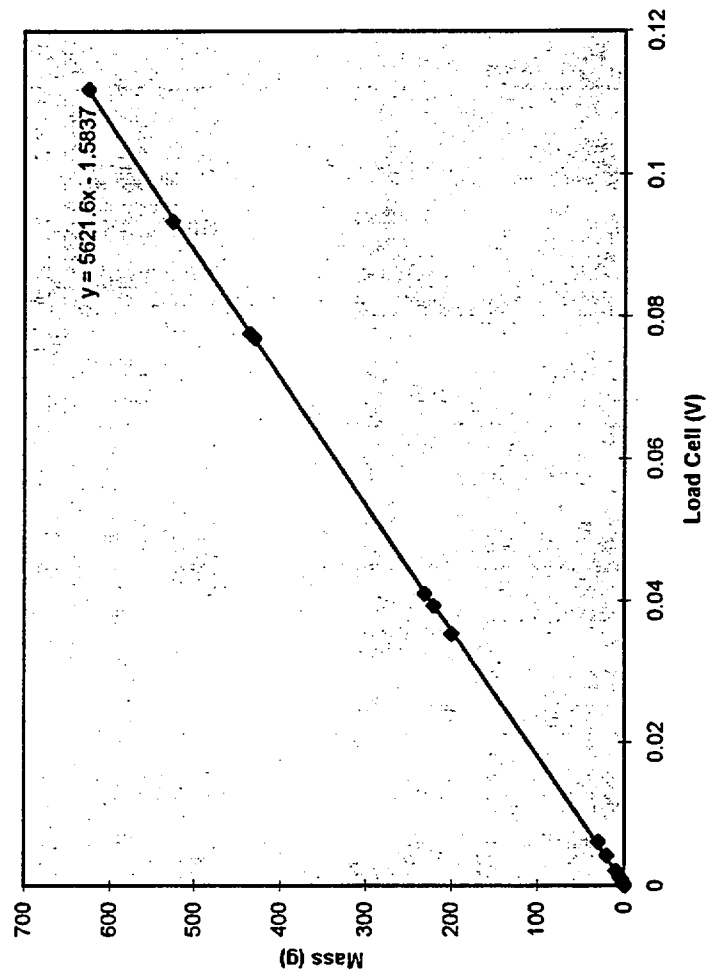
		Detection Time (min)		Scores		
File	Type ^a	Detector	PCA Model	t ₁	t ₂	t ₃
80405	n	—	1:08	0.93	-5.24	1.72
80406	n	—	1:18	3.04	-6.13	0.92
80408	n	—	7:56	1.51	-5.82	0.80
80506	n	—	7:24	7.86	-10.07	1.75
80807	n	—	4:34	2.72	-4.81	0.13
80103	n	—	0:08	28.88	-54.67	-0.39
80106	n	—	0:08	27.38	-55.37	-1.21
80409	n	—	0:10	24.56	-55.39	-2.53
80503	n	—	0:10	31.03	-60.35	-1.85
72909	n	—	—	—	—	—
80107	n	—	—	—	—	—
80504	n	—	—	—	—	—
80902	n	—	—	—	—	—
80903	n	—	—	—	—	—
80904	n	—	—	—	—	—
72504	n	—	—	—	—	—
72706	n	—	—	—	—	—
72707	n	—	—	—	—	—
72908	n	—	—	—	—	—

^a s: smoldering, n: nuisance, f: flaming, —: no detection

Appendix B: Calibration Curves



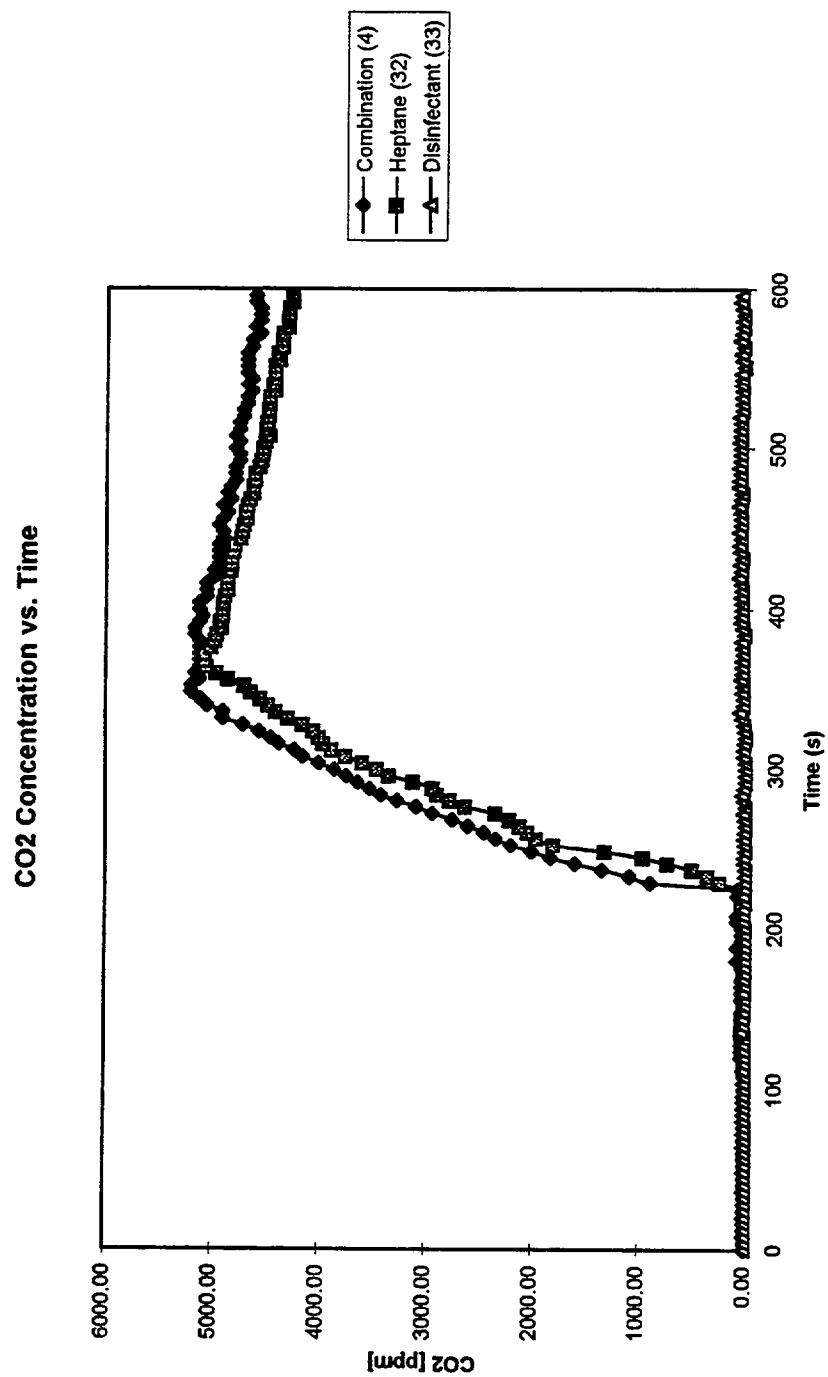
Load Cell Calibration



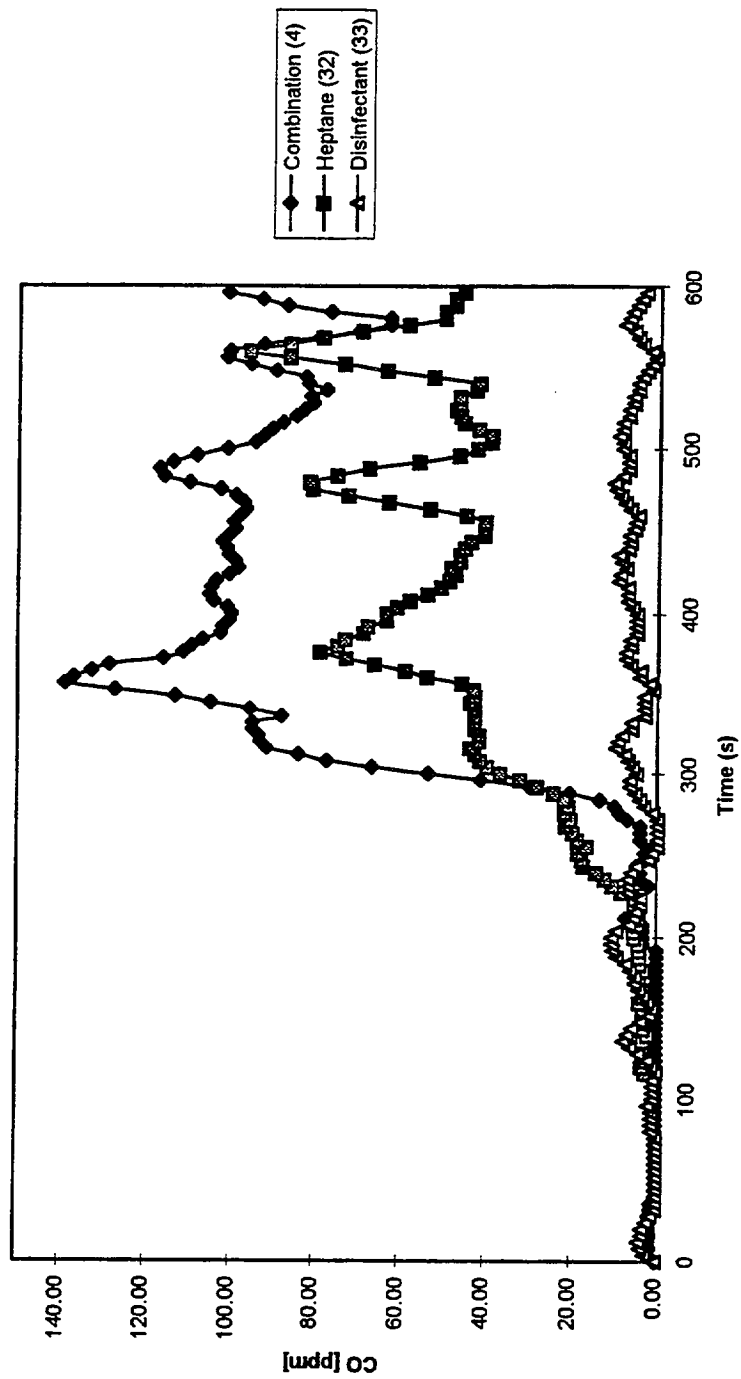
Appendix C: Data Summaries

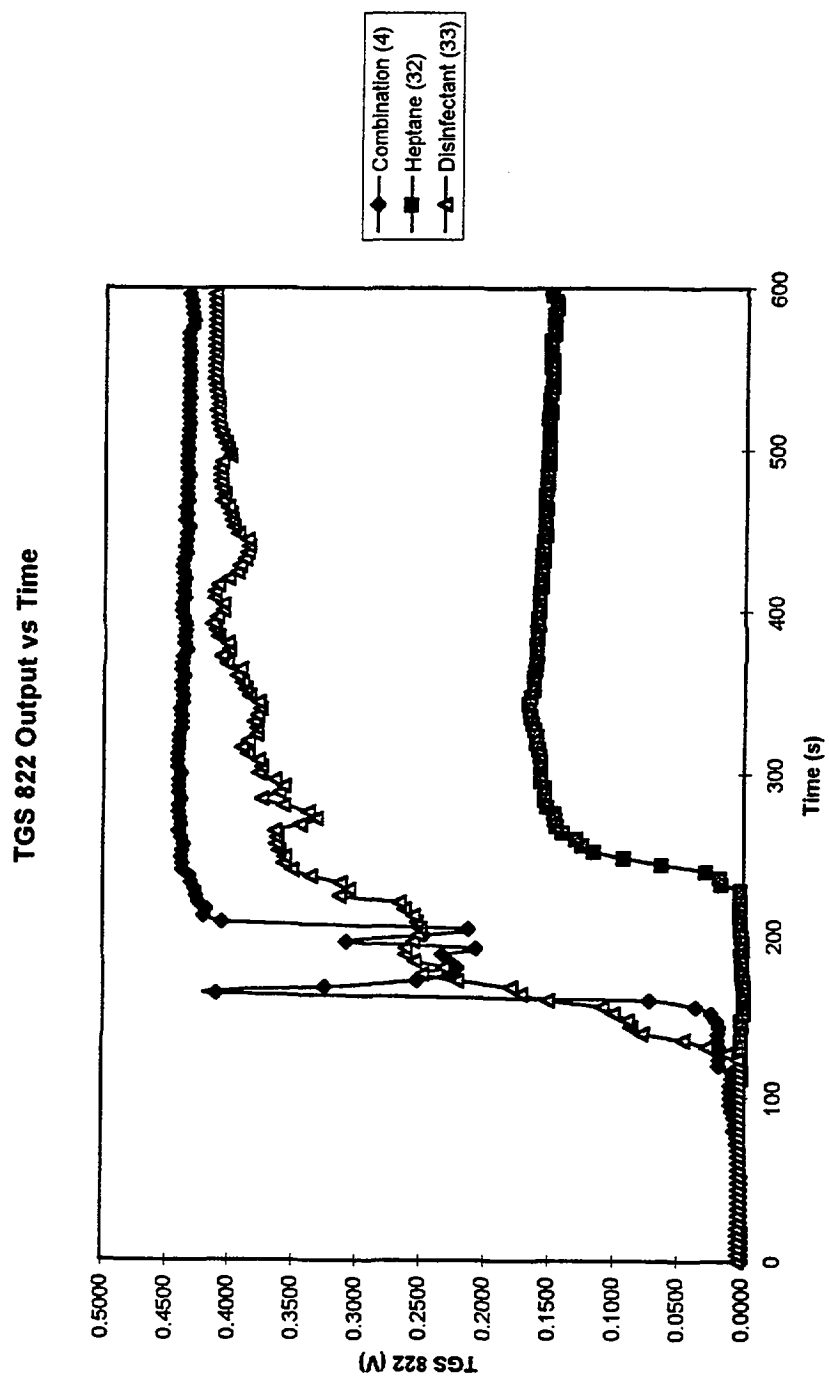
Test	Test Scenario Information				Initiation Time 1 (s)	Initiation Time 2 (s)	Photo cell-#1		Photo cell-#3		Residential-#5	
	Fuel	Mode	Nuisance	Det Time (s)			Det Time (s)	Det Time (s)	Det Time (s)	Det Time (s)	Det Time (s)	
4	heptane-50ml	flaming	disinfectant	120	208	259	232	259	238	223	4	
5	heptane-50ml	flaming	window cleaner	120	204	230	224	234	224	219	5	
6	heptane-50ml	flaming	hair spray	120	205	190	226	226	226	217	6	
7	heptane-50ml	flaming	boiling water	110	201	253	237	238	238	239	7	
9	paper-10 sheets	flaming	none	na	120	365	305	350	350	295	9	
10	paper-10 sheets	flaming	disinfectant	120	211	405	266	399	270	257	10	
11	paper-10 sheets	flaming	window cleaner	116	206	217	235	215	239	235	11	
12	paper-10 sheets	flaming	hair spray	115	207	382	262	377	374	362	12	
13	paper-10 sheets	flaming	boiling water	110	203	302	263	302	277	255	13	
32	heptane-50ml	flaming	none	na	120	159	140	157	150	131	32	
33	none	na	disinfectant	121	na	na	na	na	na	na	33	
34	none	na	boiling water	122	na	na	na	na	na	na	34	
35	none	na	window cleaner	120	na	na	na	na	na	na	35	
36	none	na	hair spray	127	na	na	na	na	na	na	36	
37	cloth-50%polyester/50%cotton	smoldering	none	na	123	395	na	493	na	na	37	
38	cloth-50%polyester/50%cotton	smoldering	disinfectant	120	227	400	na	496	na	na	38	
39	cloth-50%polyester/50%cotton	smoldering	window cleaner	122	202	243	na	286	na	na	39	
40	cloth-50%polyester/50%cotton	smoldering	hair spray	109	200	461	na	1406	na	na	40	
41	cloth-50%polyester/50%cotton	smoldering	boiling water	123	219	460	na	808	na	na	41	
42	hamburger - 75.1 grams	smoldering	none	na	130	400	703	508	na	924	42	
43	hamburger - 72.6 grams	smoldering	disinfectant	115	205	486	863	524	na	1237	43	
44	hamburger - 70.4 grams	smoldering	window cleaner	115	200	638	1379	741	na	1380	44	
45	hamburger - 72.1 grams	smoldering	hair spray	115	205	265	816	267	na	775	45	
46	hamburger - 68.2 grams	smoldering	boiling water	111	202	407	703	480	na	551	46	

Appendix D: Representative Sensor Data

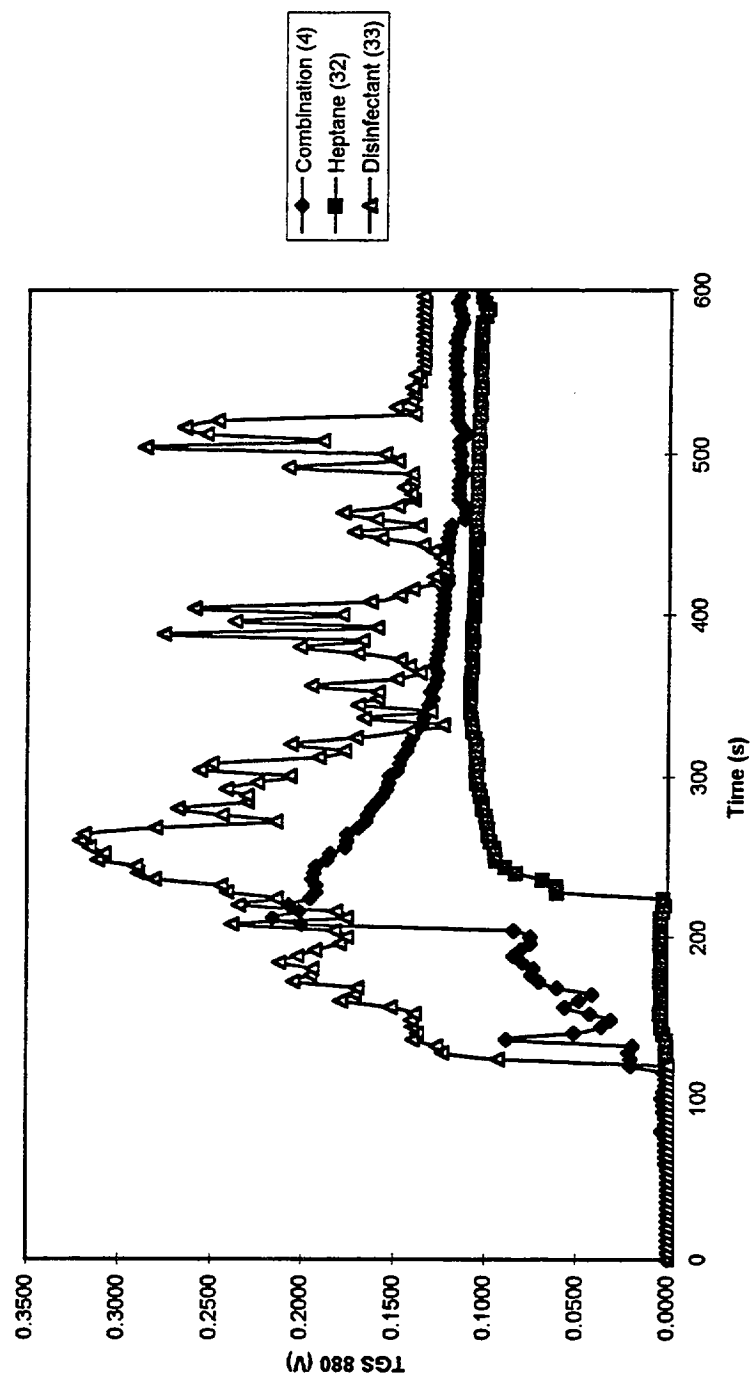


CO Concentration vs. Time

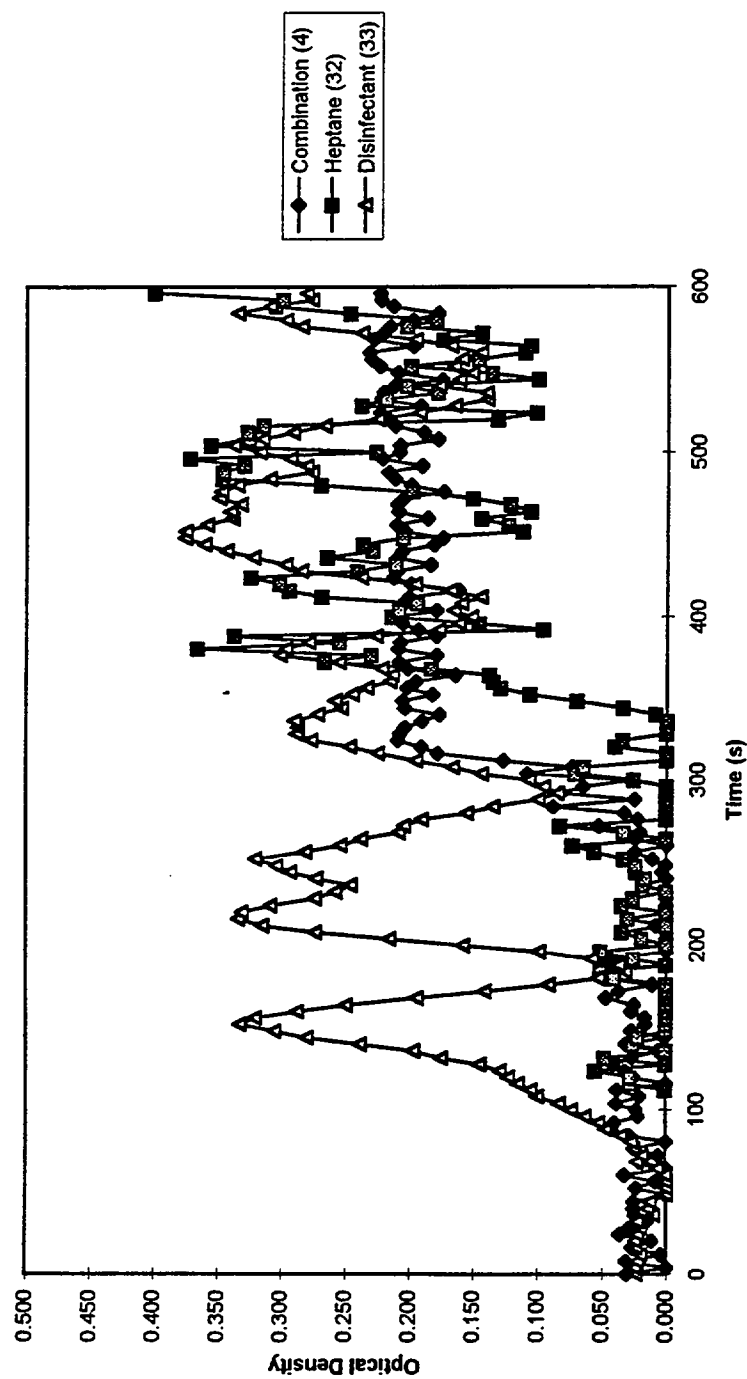




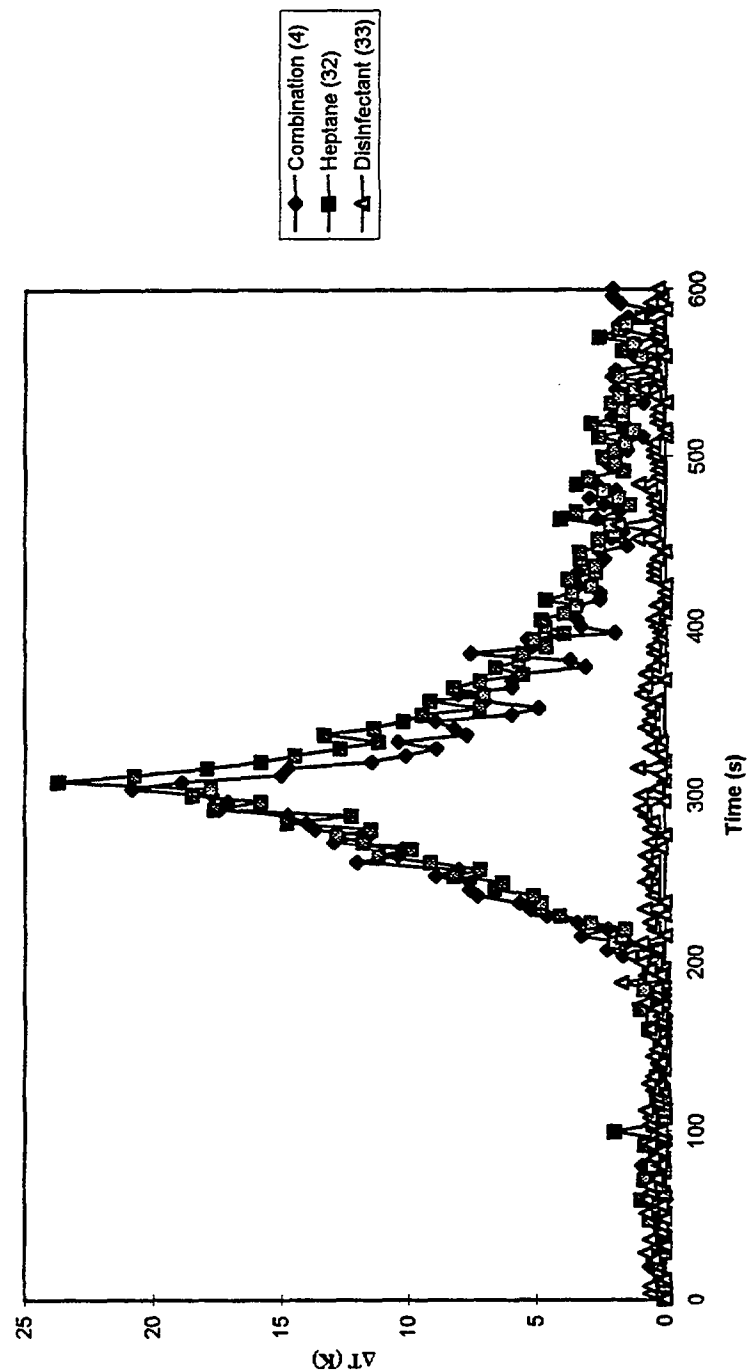
TGS 880 Output vs. Time



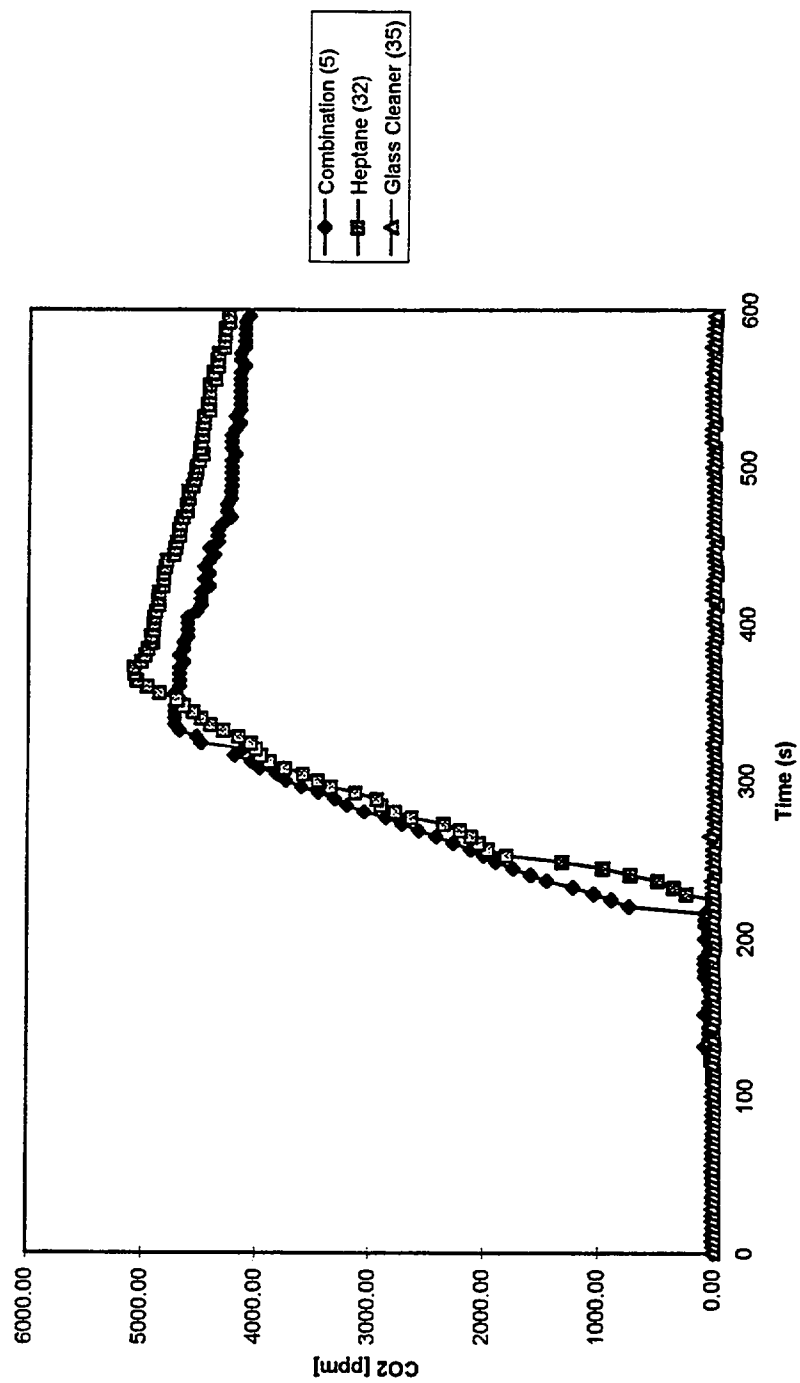
Optical Density vs. Time



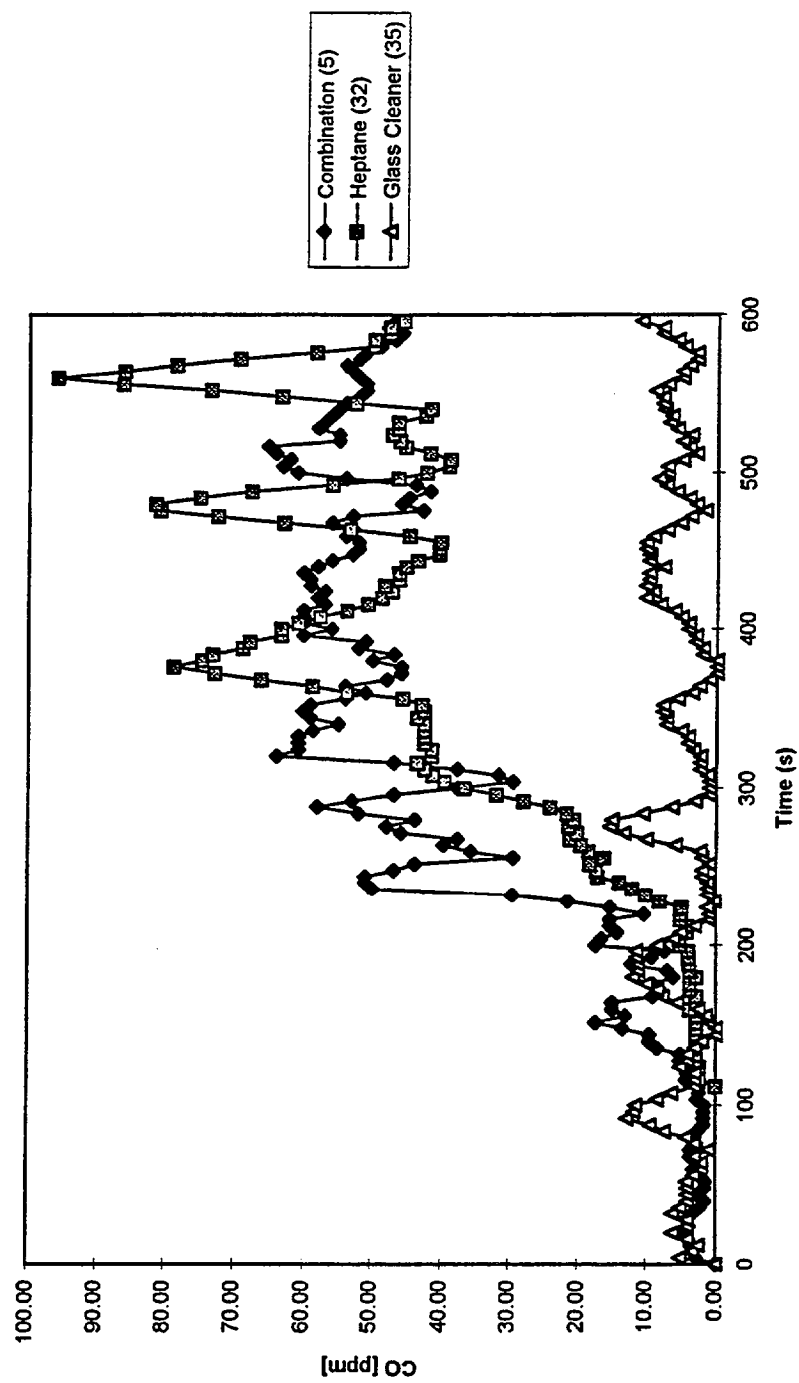
Temperature Rise at TC 13 vs. Time



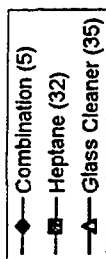
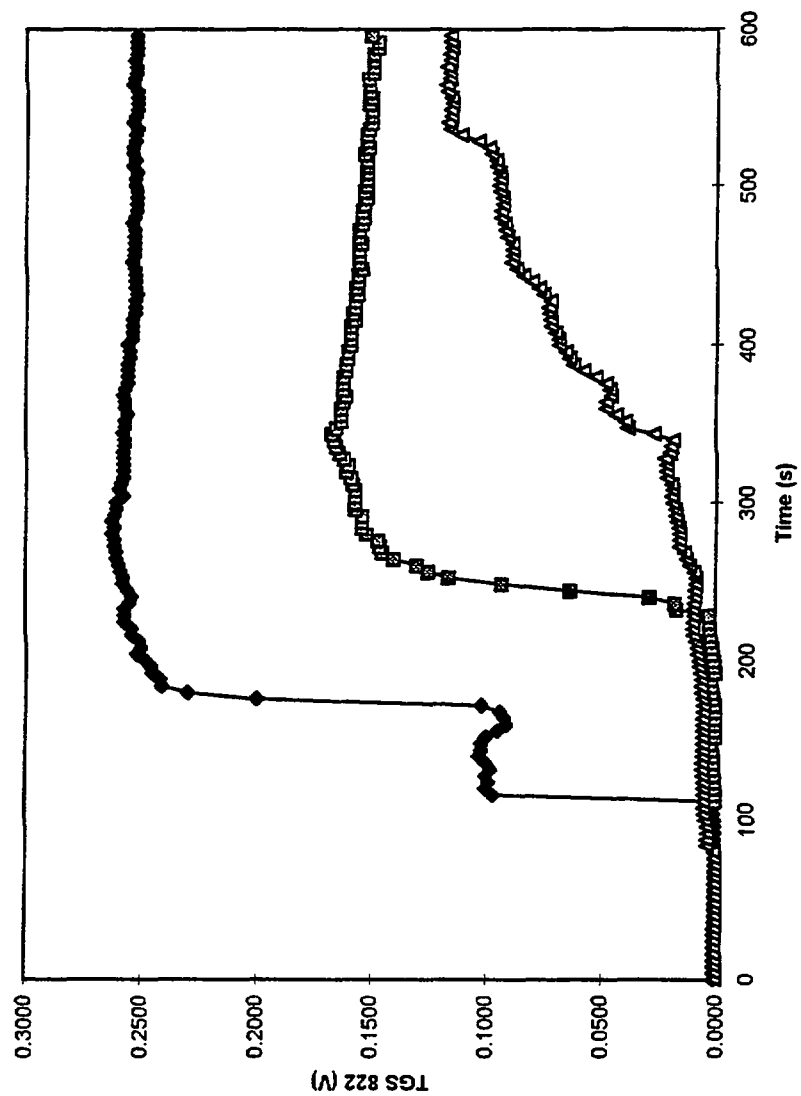
CO2 Concentration vs. Time



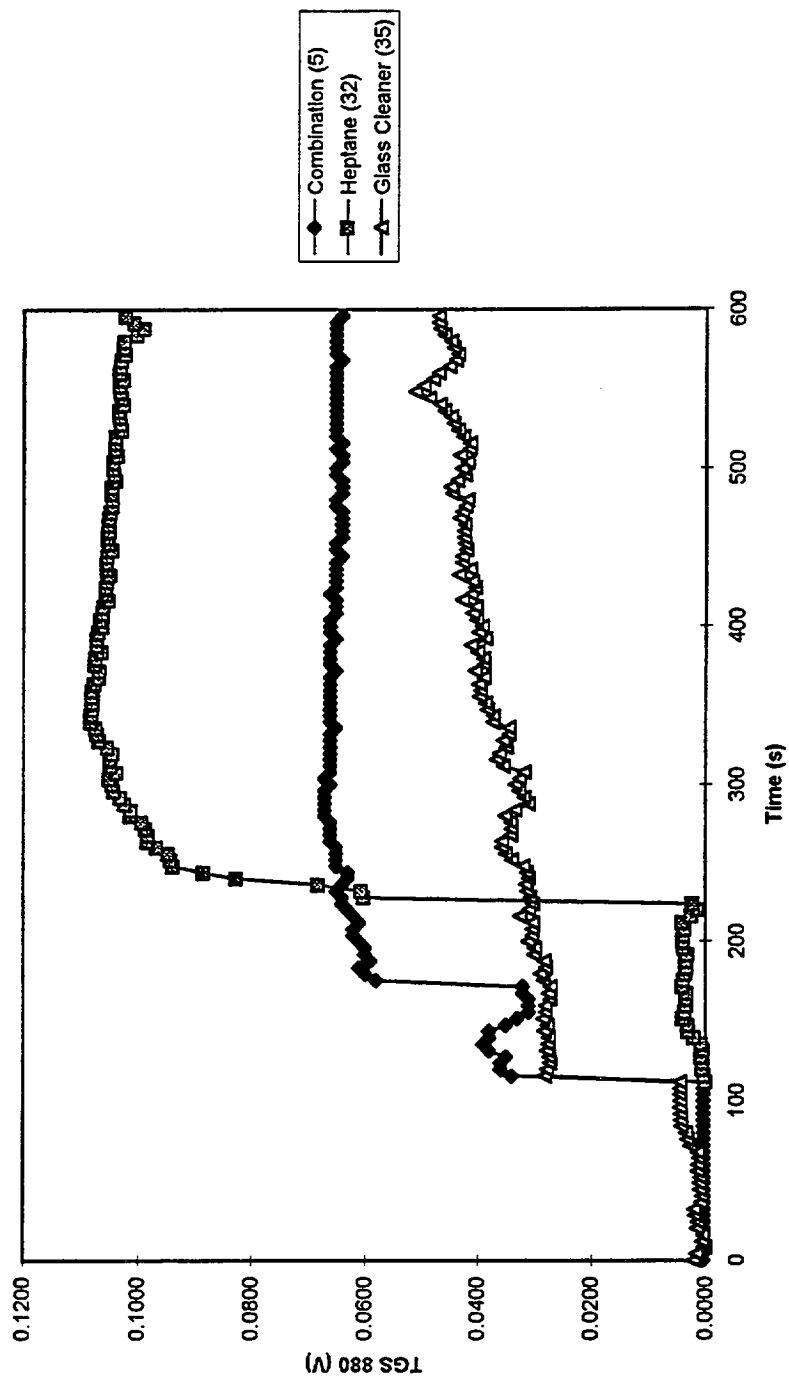
CO Concentration vs. Time



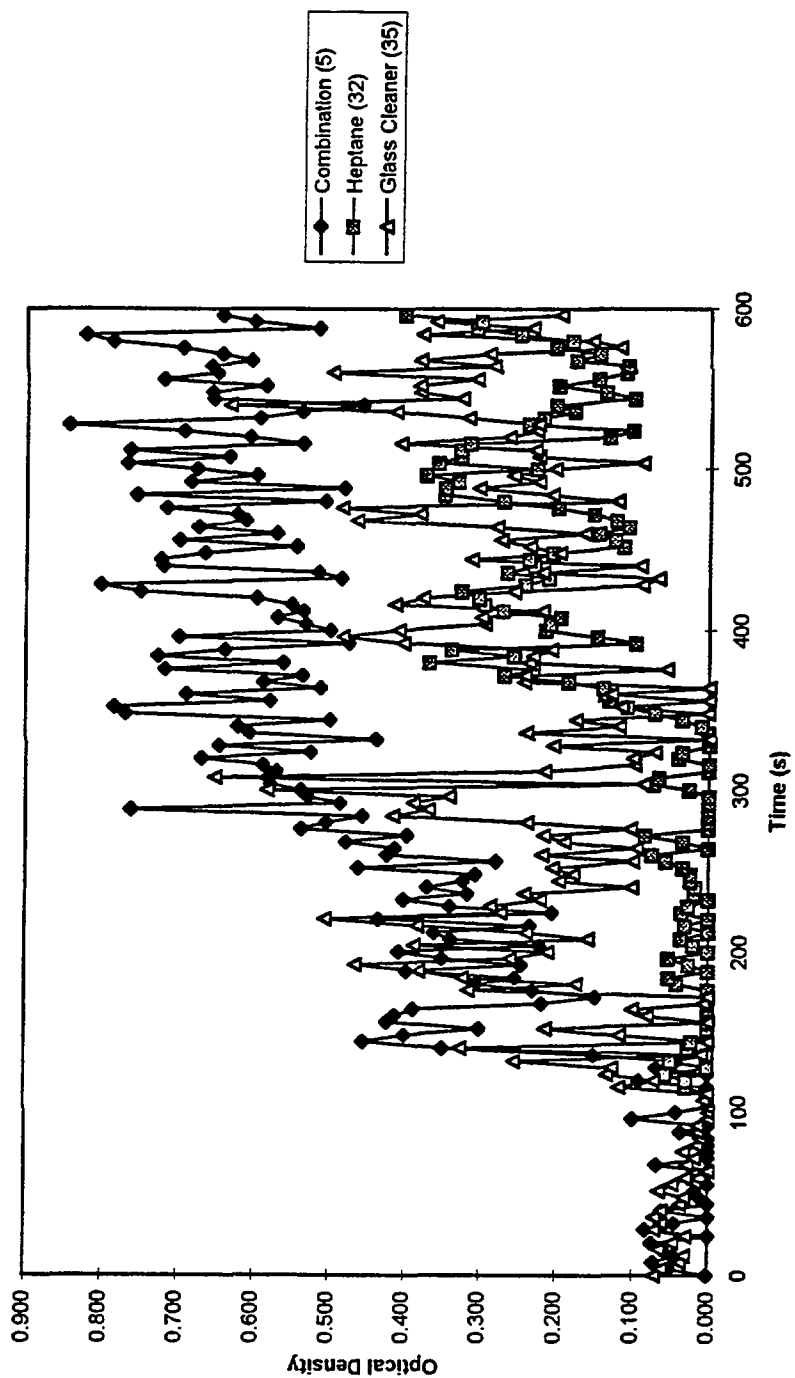
TGS 822 Output vs. Time



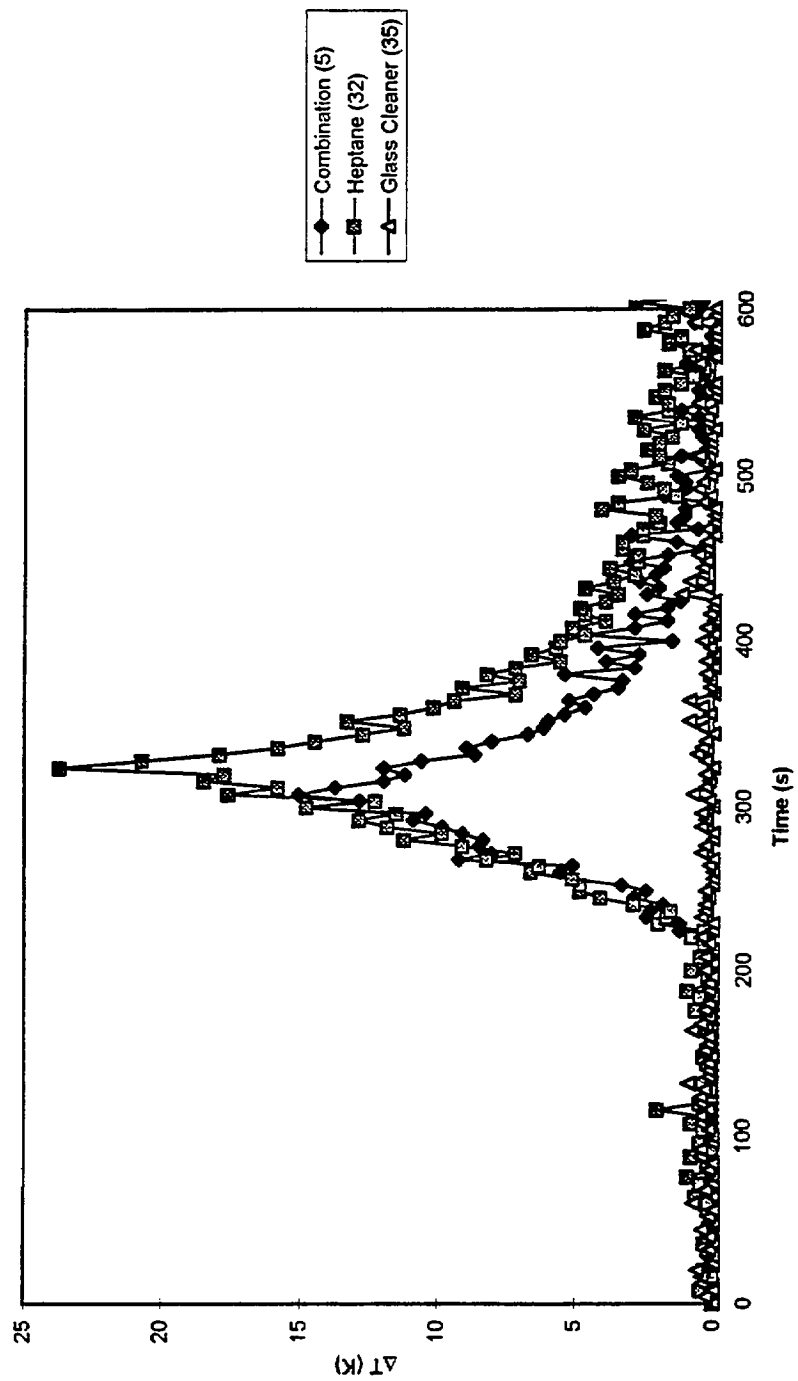
TGS 880 Output vs. Time



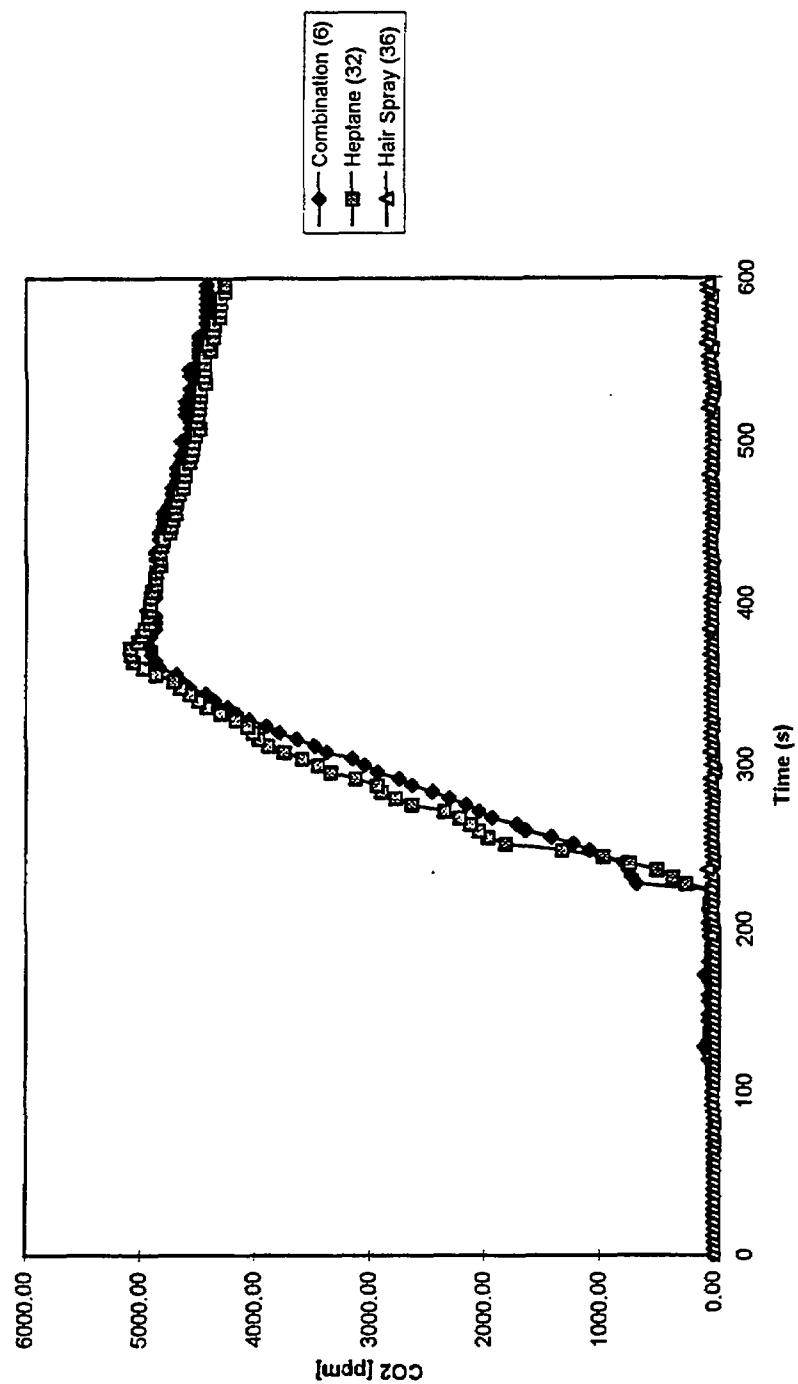
Optical Density vs. Time



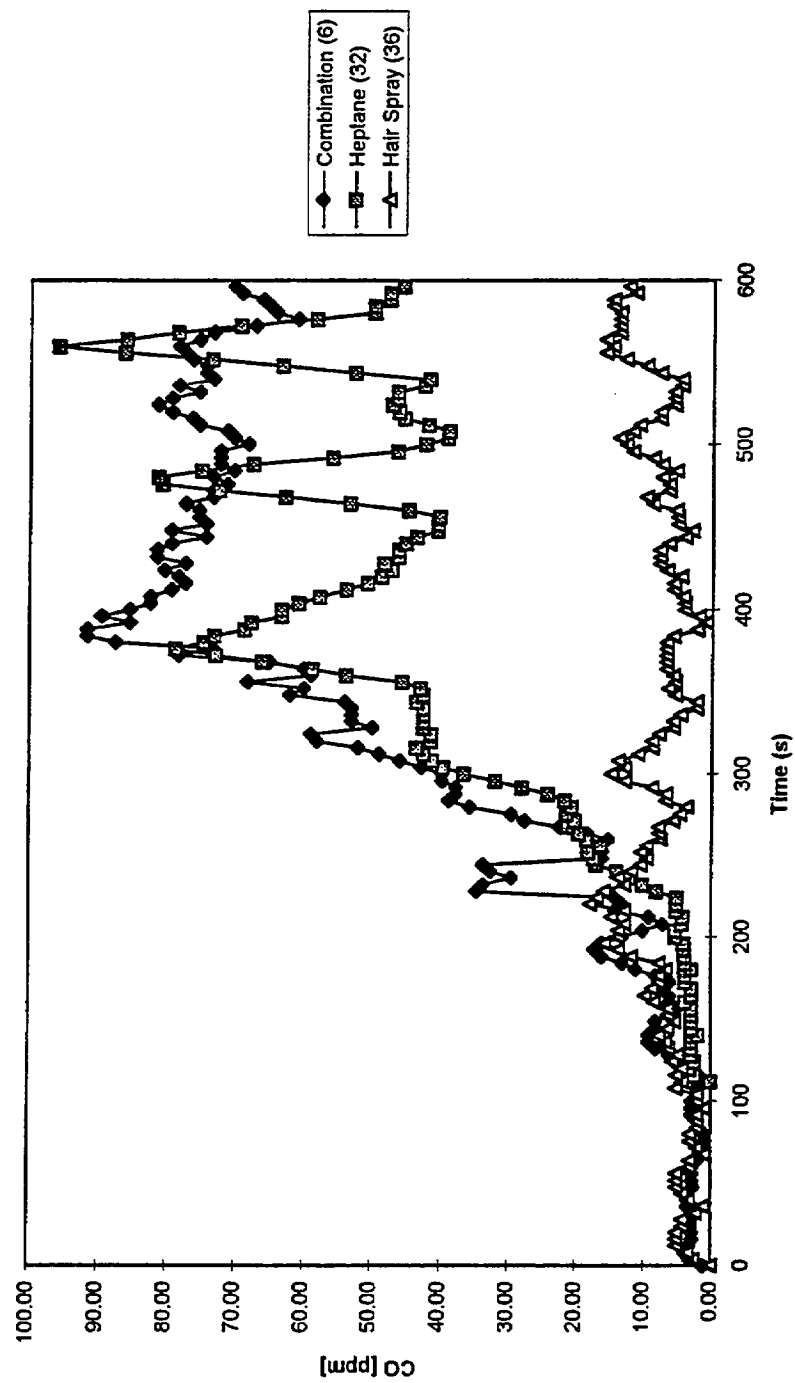
Temperature Rise at TC 13 vs. Time



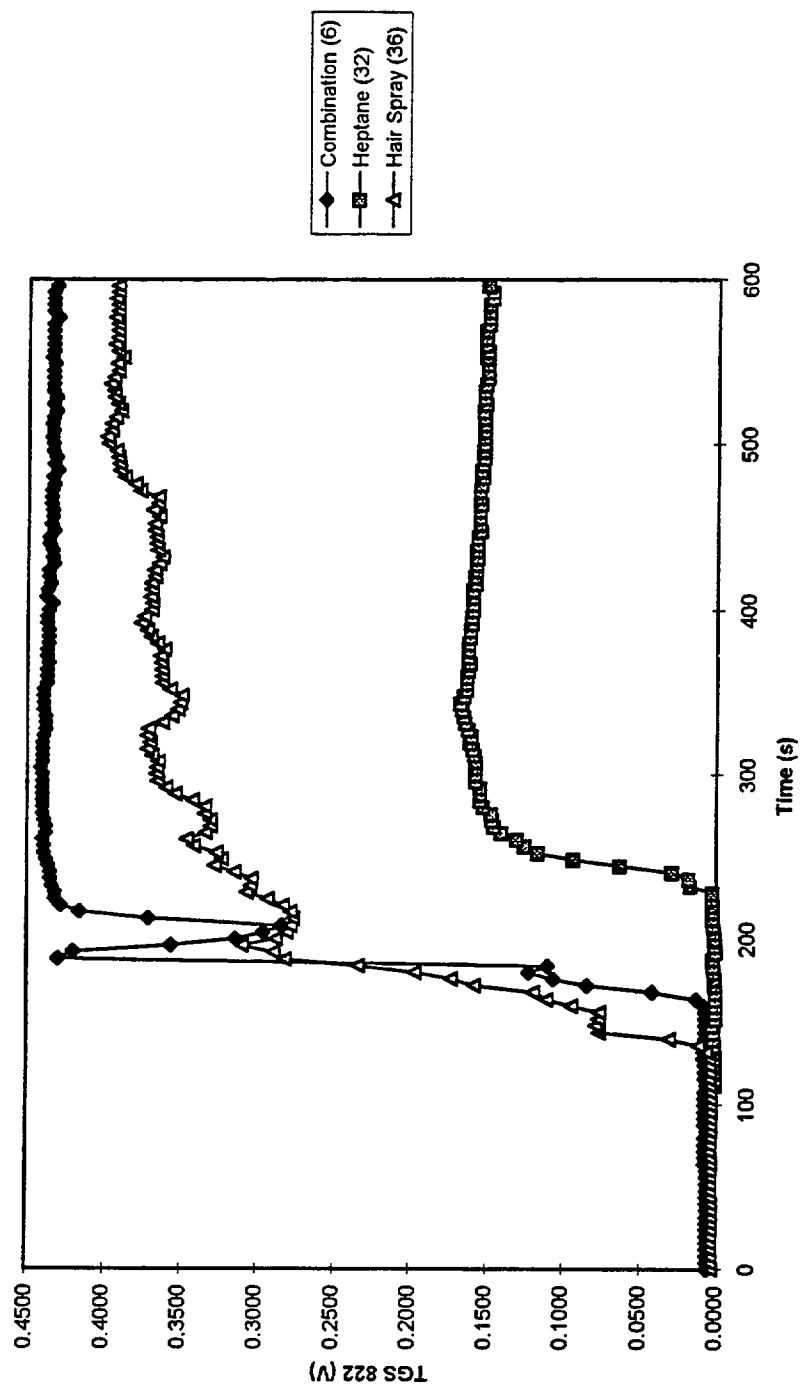
CO2 Concentration vs. Time



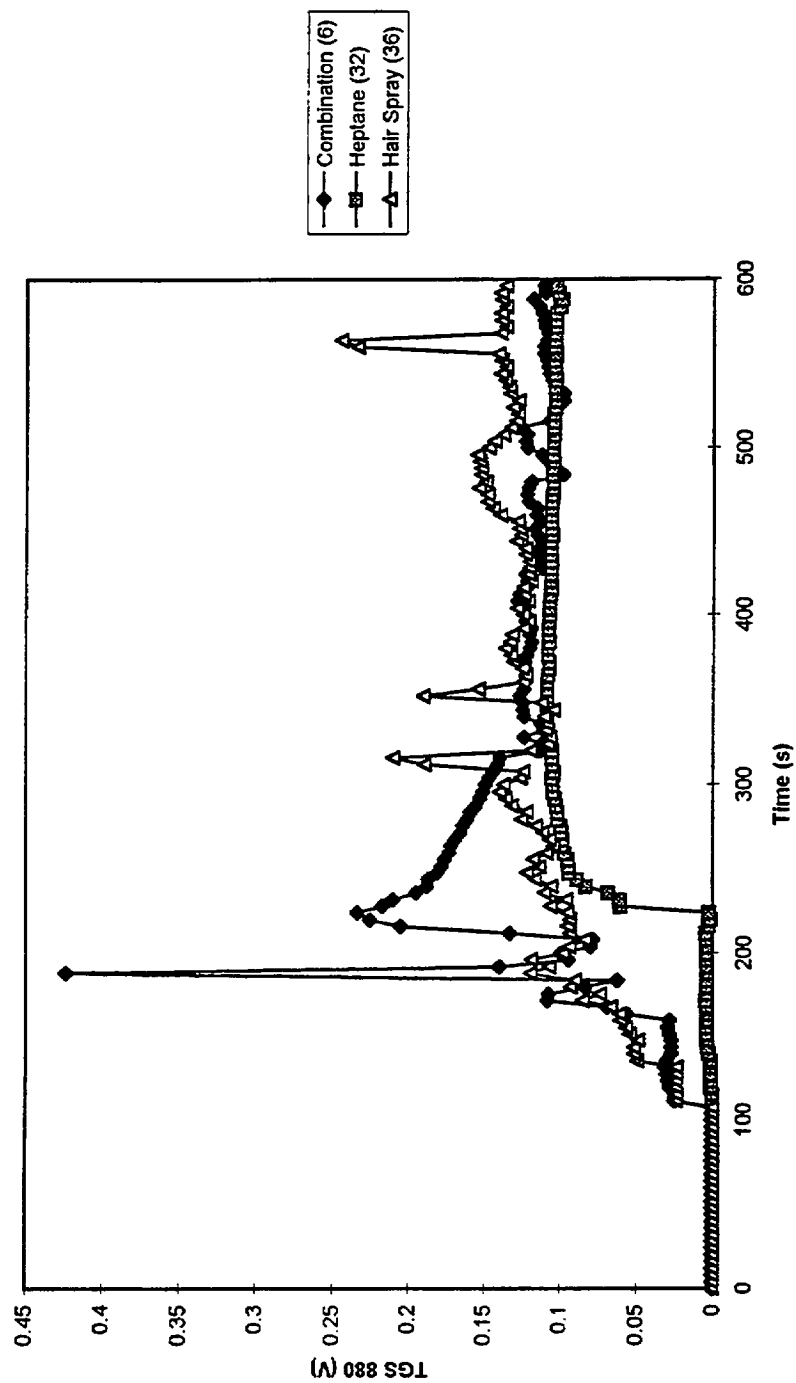
CO Concentration vs. Time



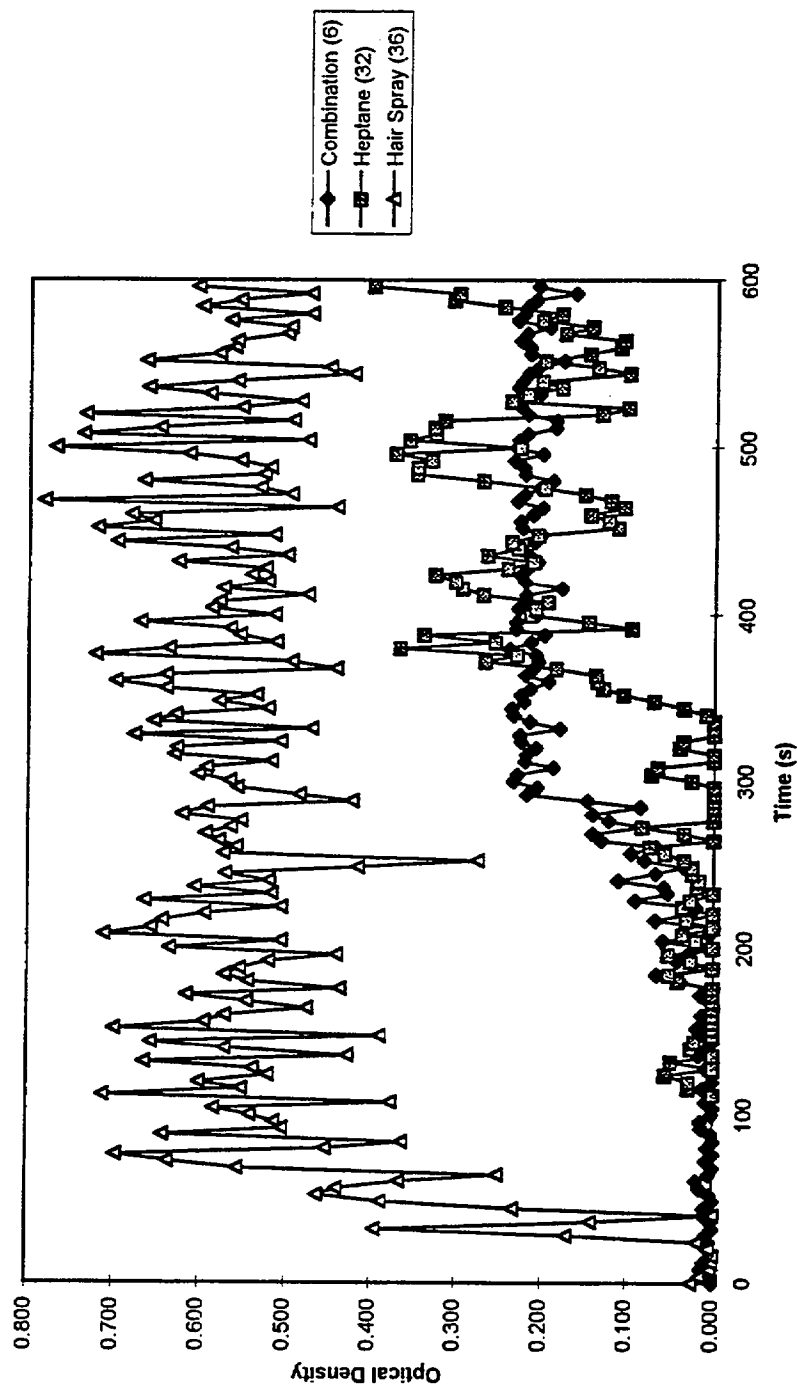
TGS 822 Output vs. Time



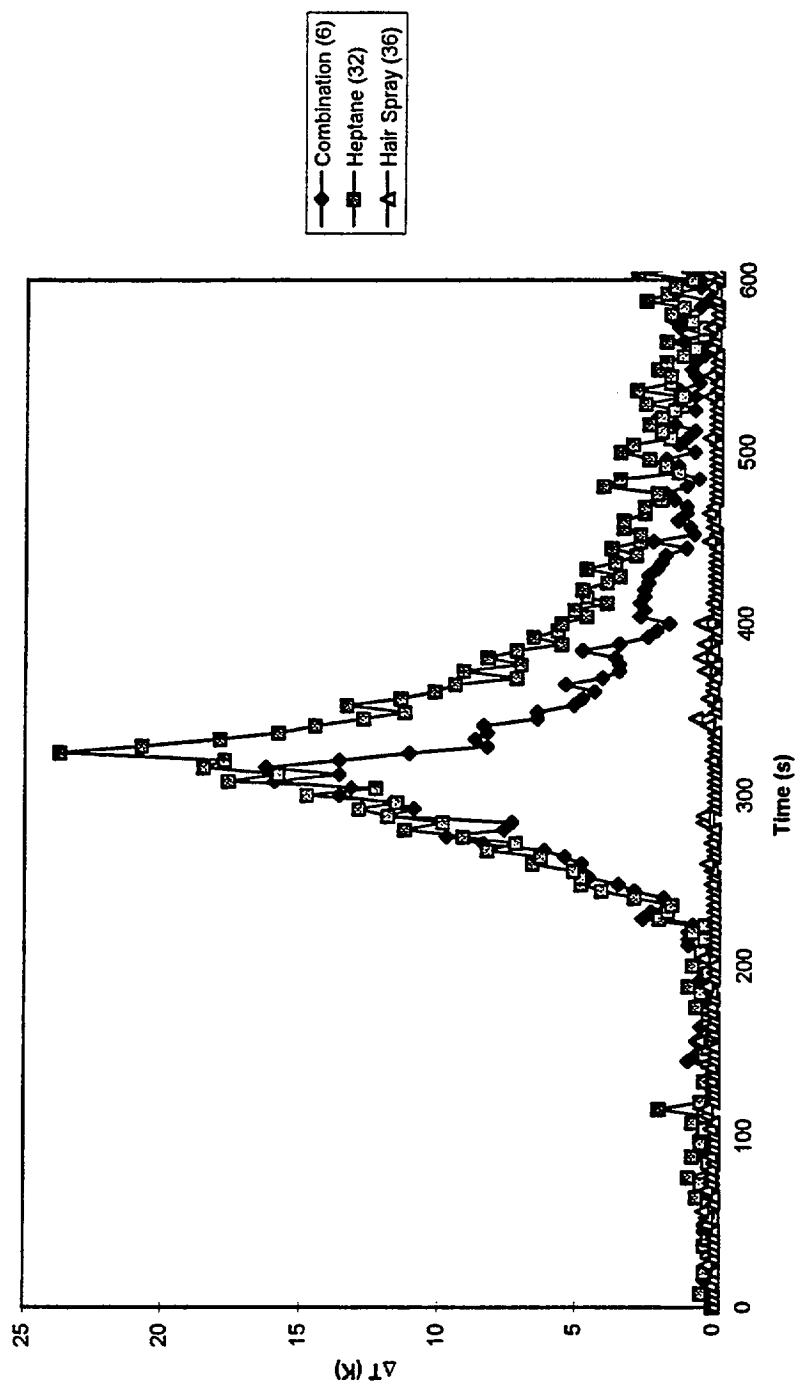
TGS 880 Output vs. Time

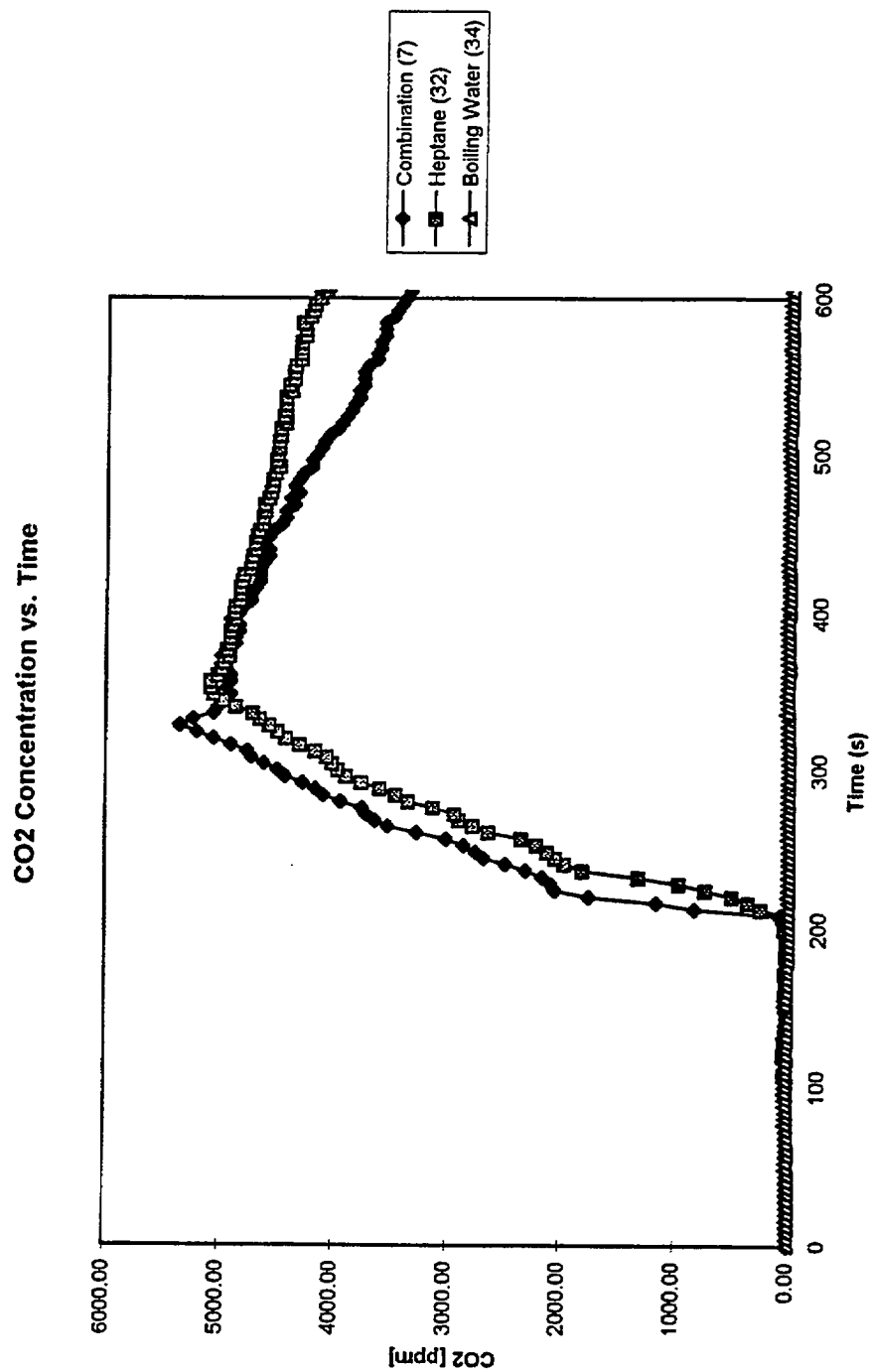


Optical Density vs. Time

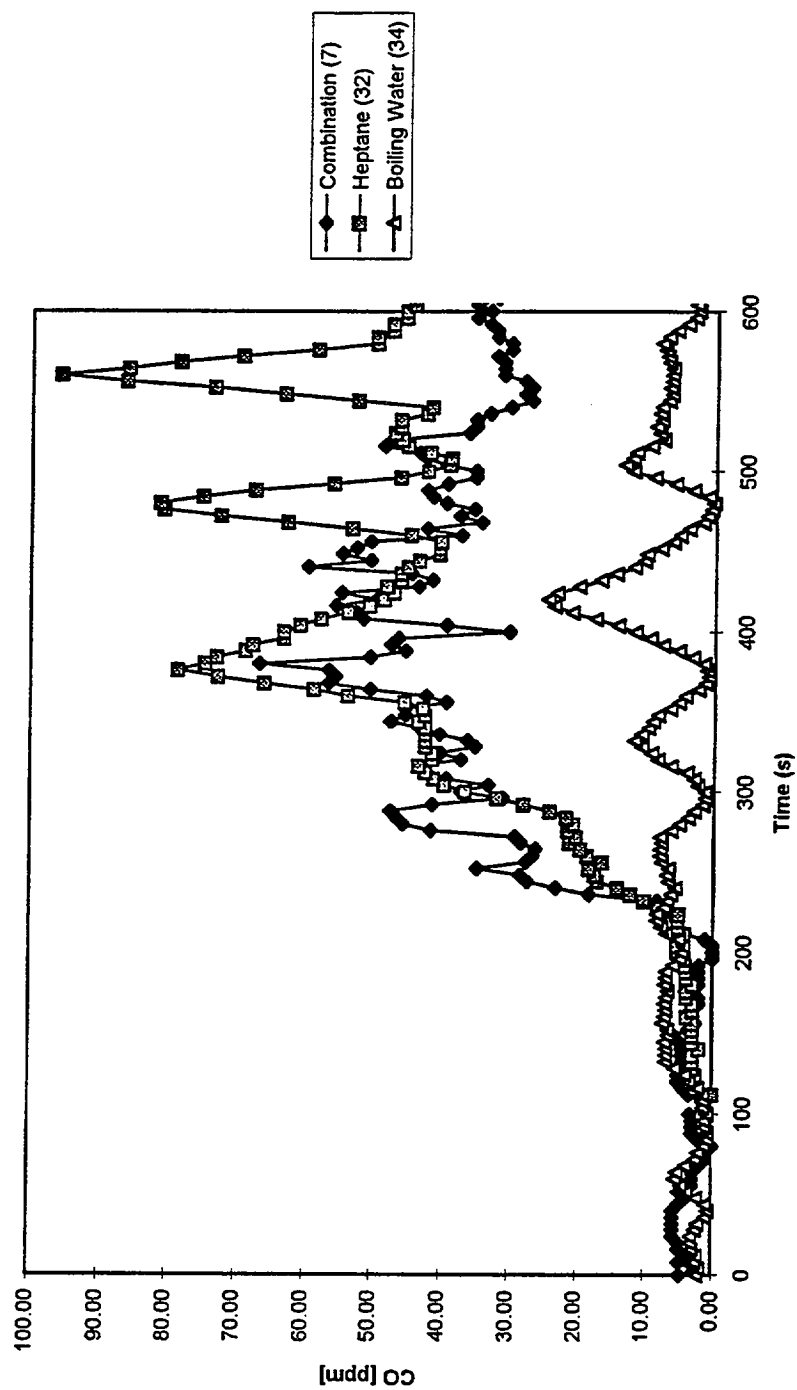


Temperature Rise at TC 13 vs. Time

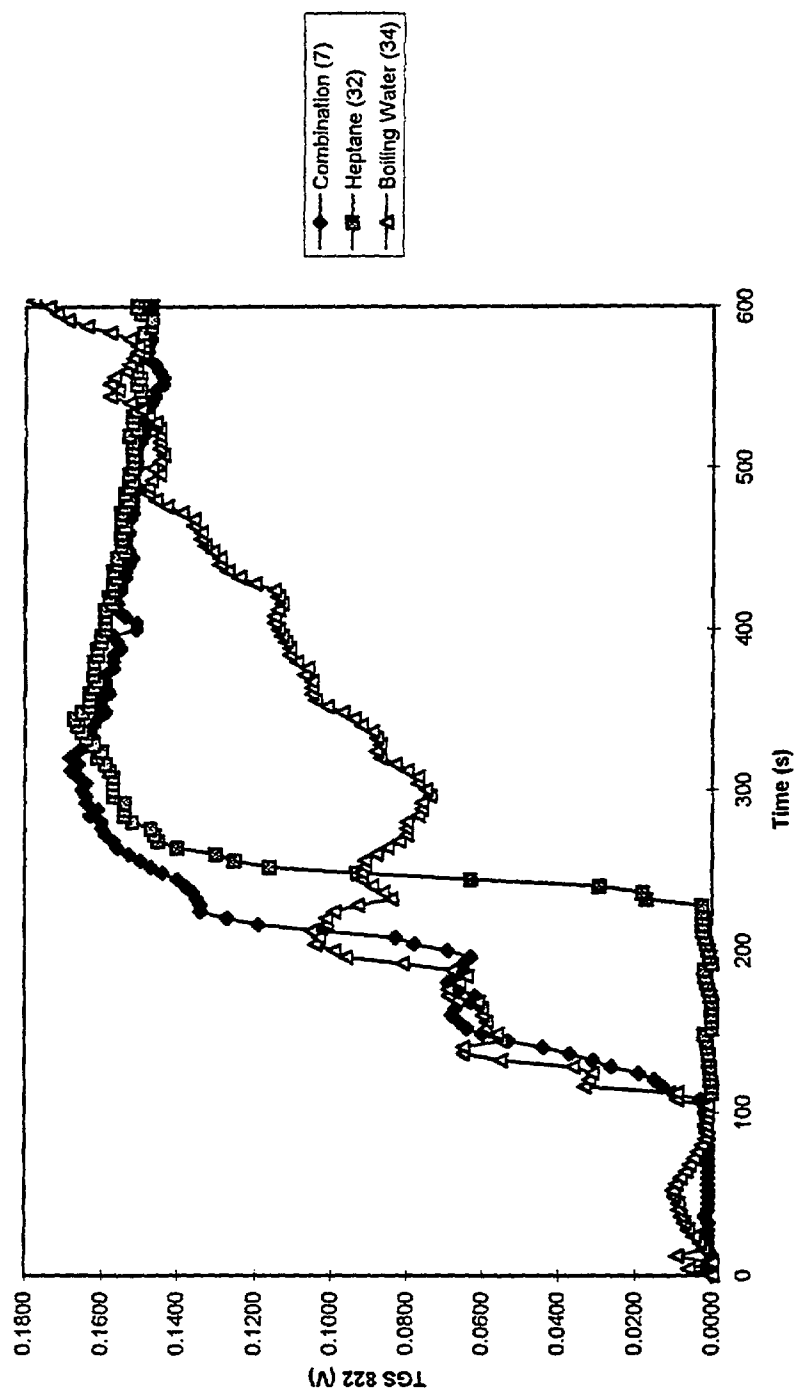




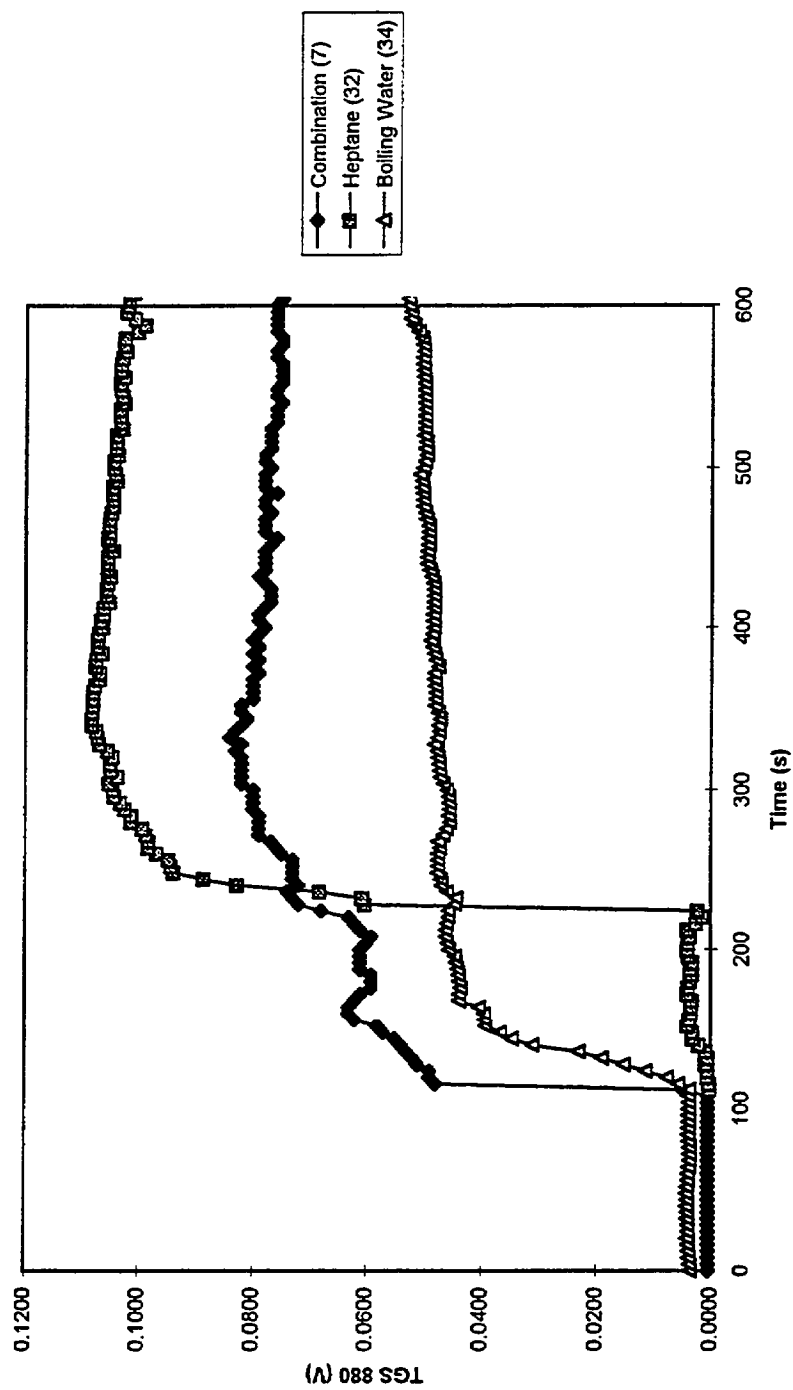
CO Concentration vs. Time



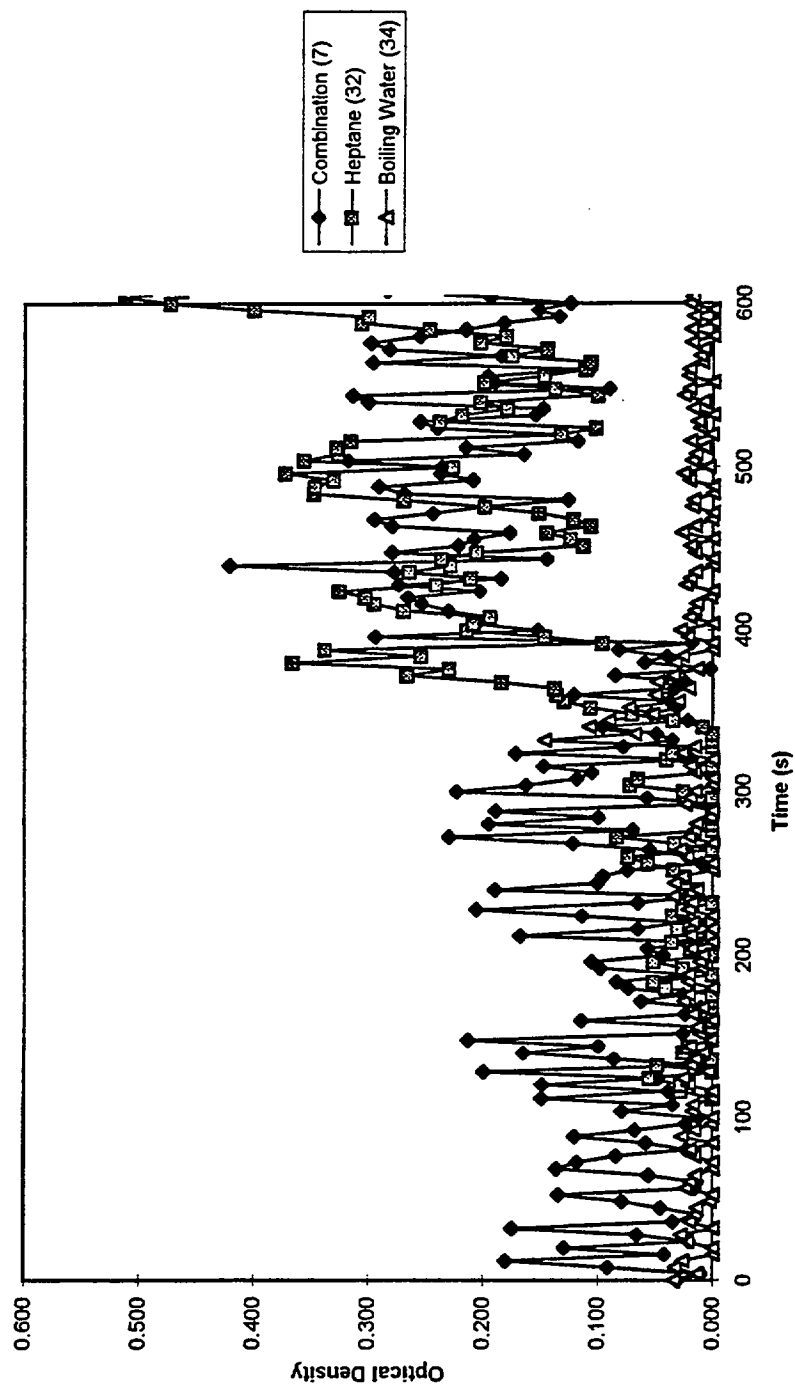
TGS 822 Output vs. Time



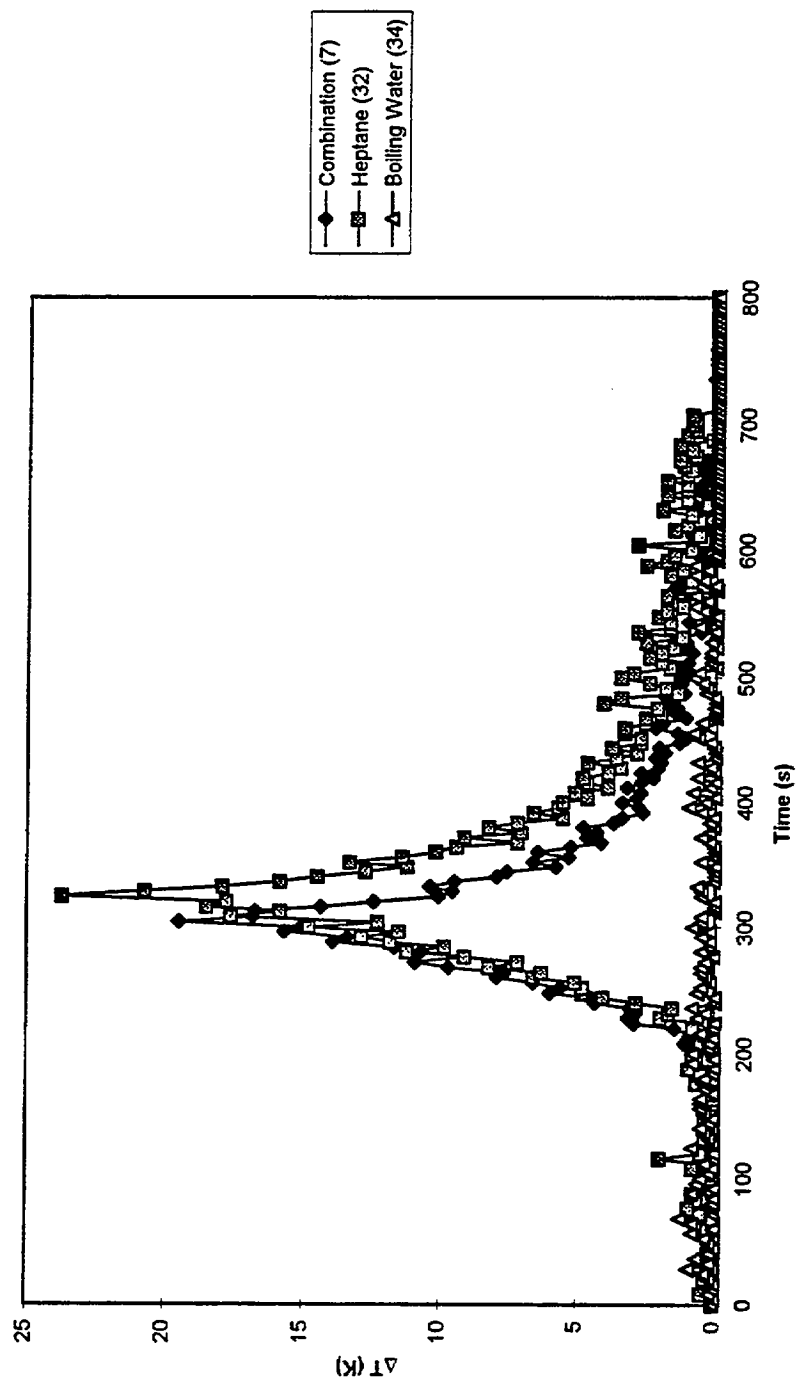
TGS 880 Output vs. Time



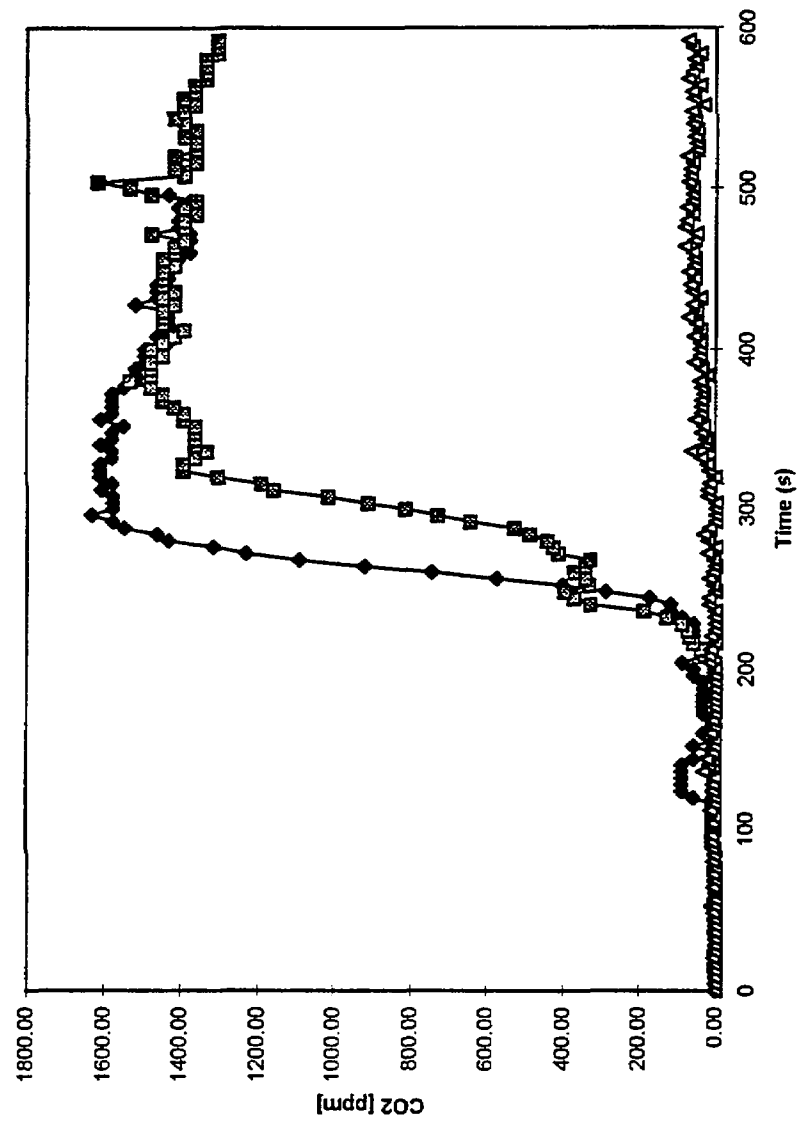
Optical Density vs. Time



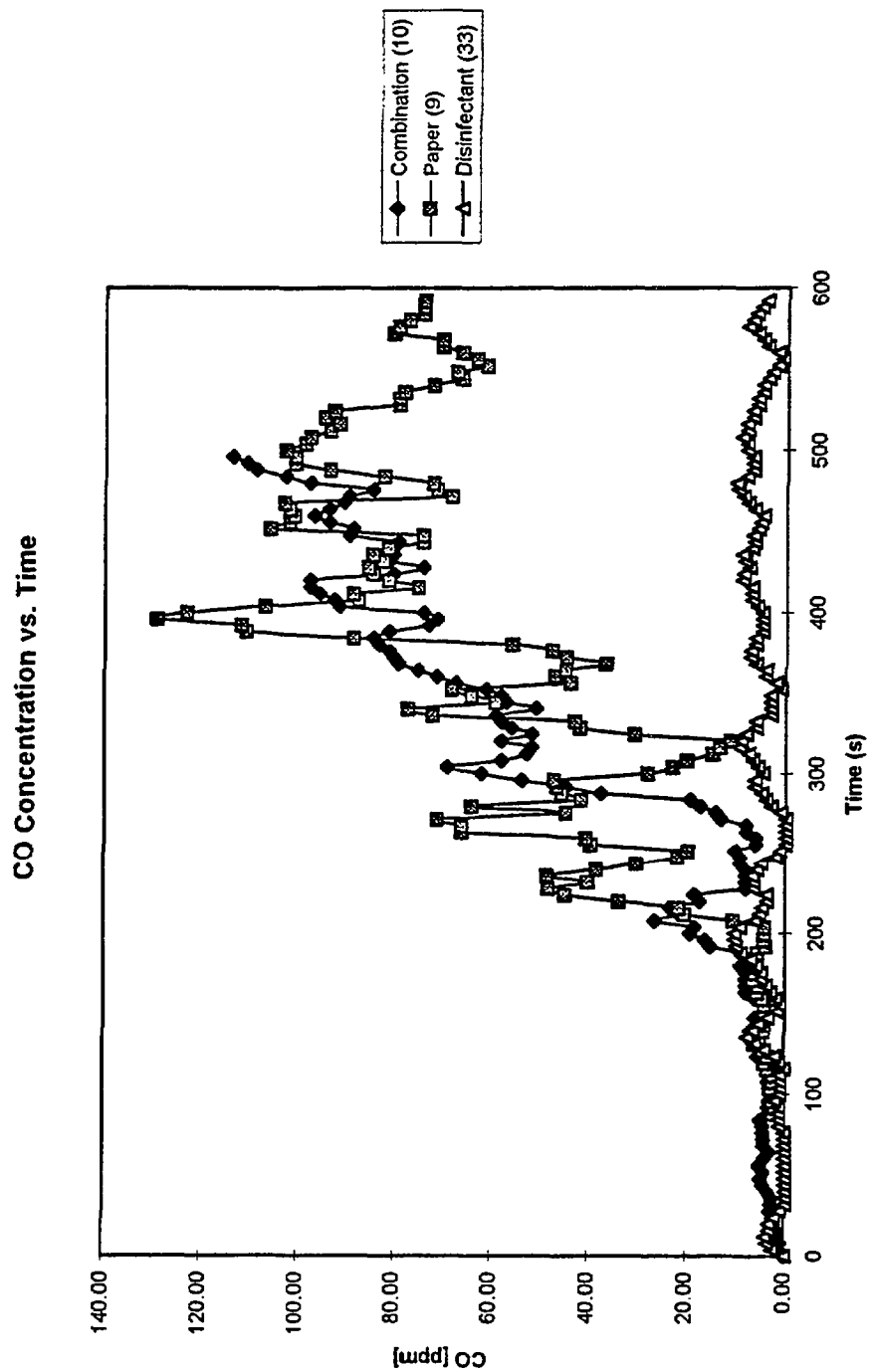
Temperature Rise at TC 13 vs Time



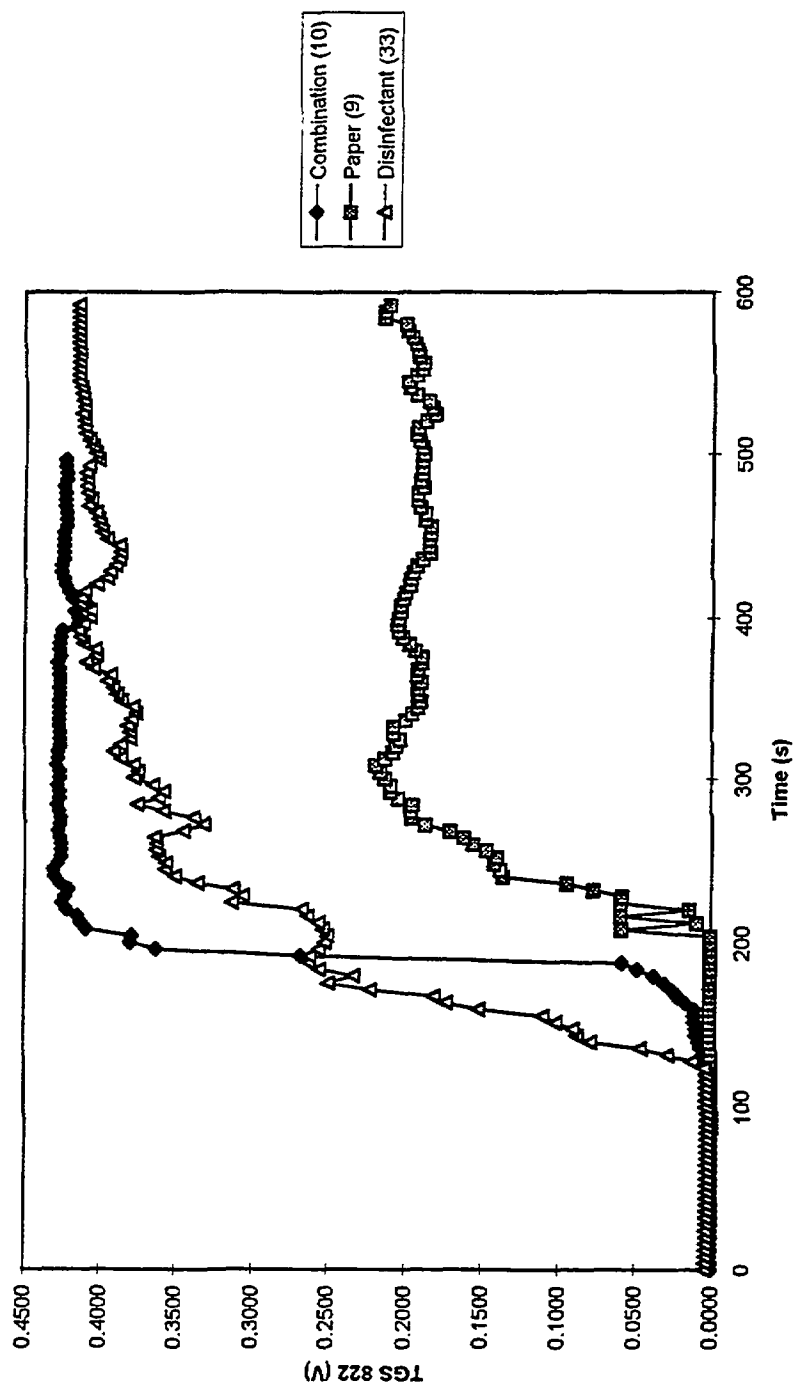
CO2 Concentration vs. Time



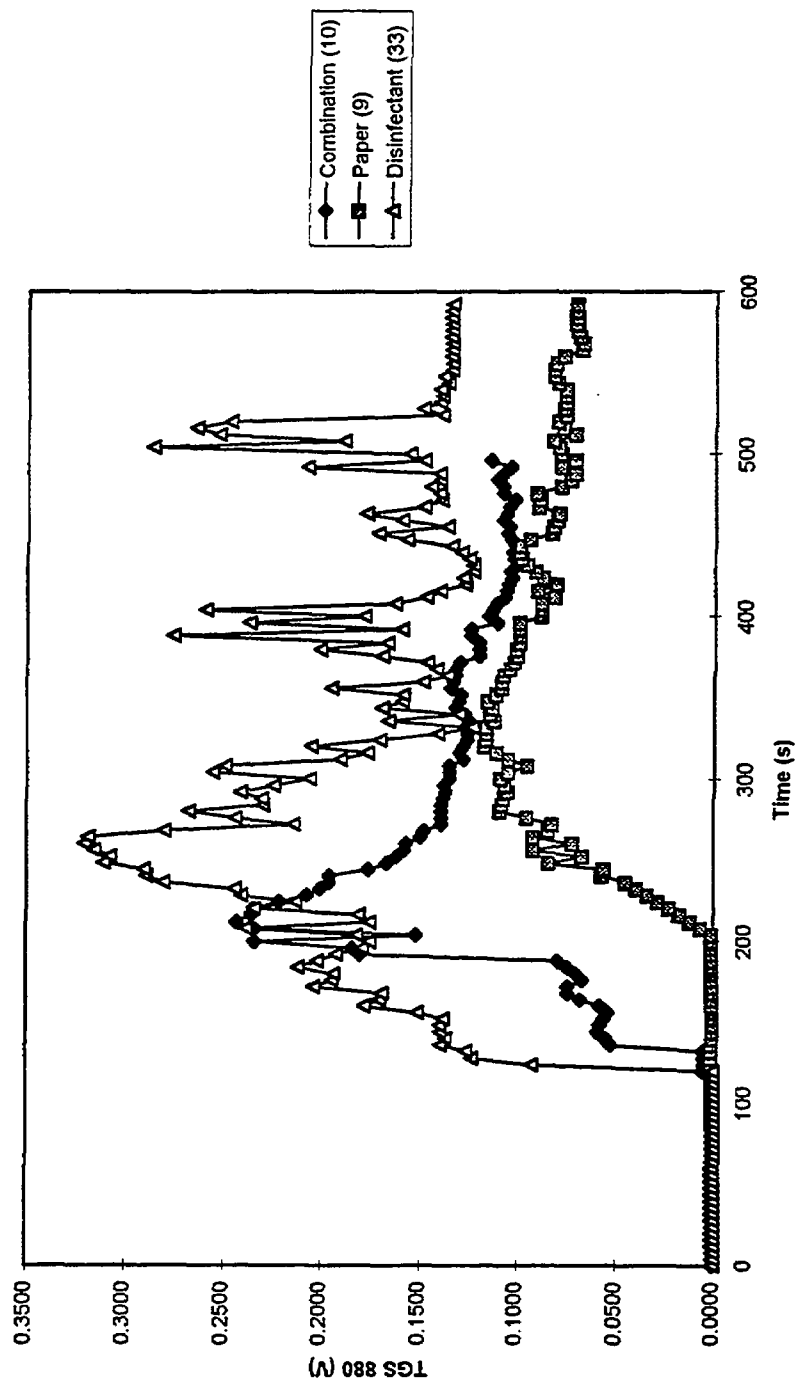
Combination (10)
Paper (9)
Disinfectant (33)

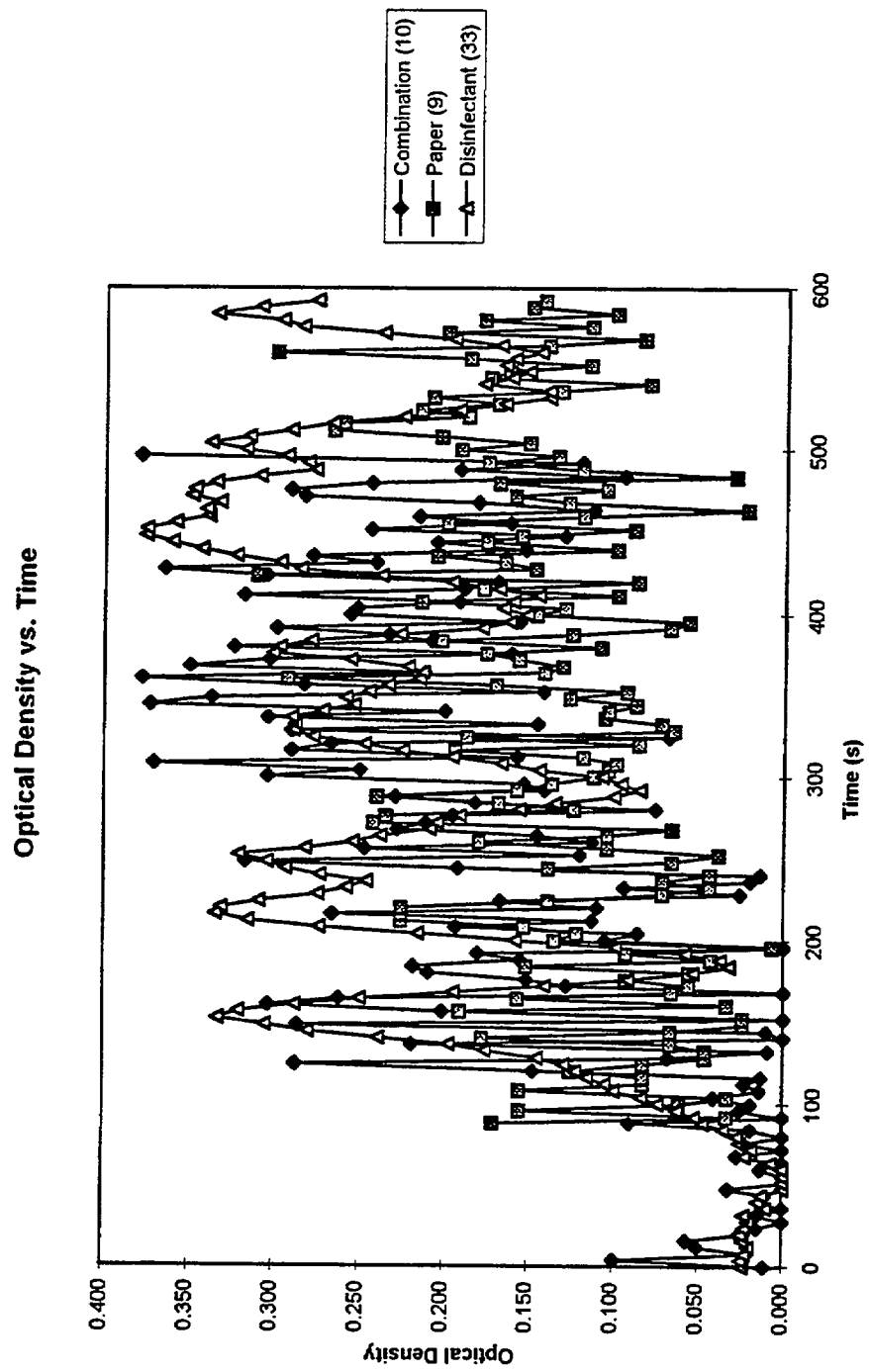


TGS 822 Output vs. Time

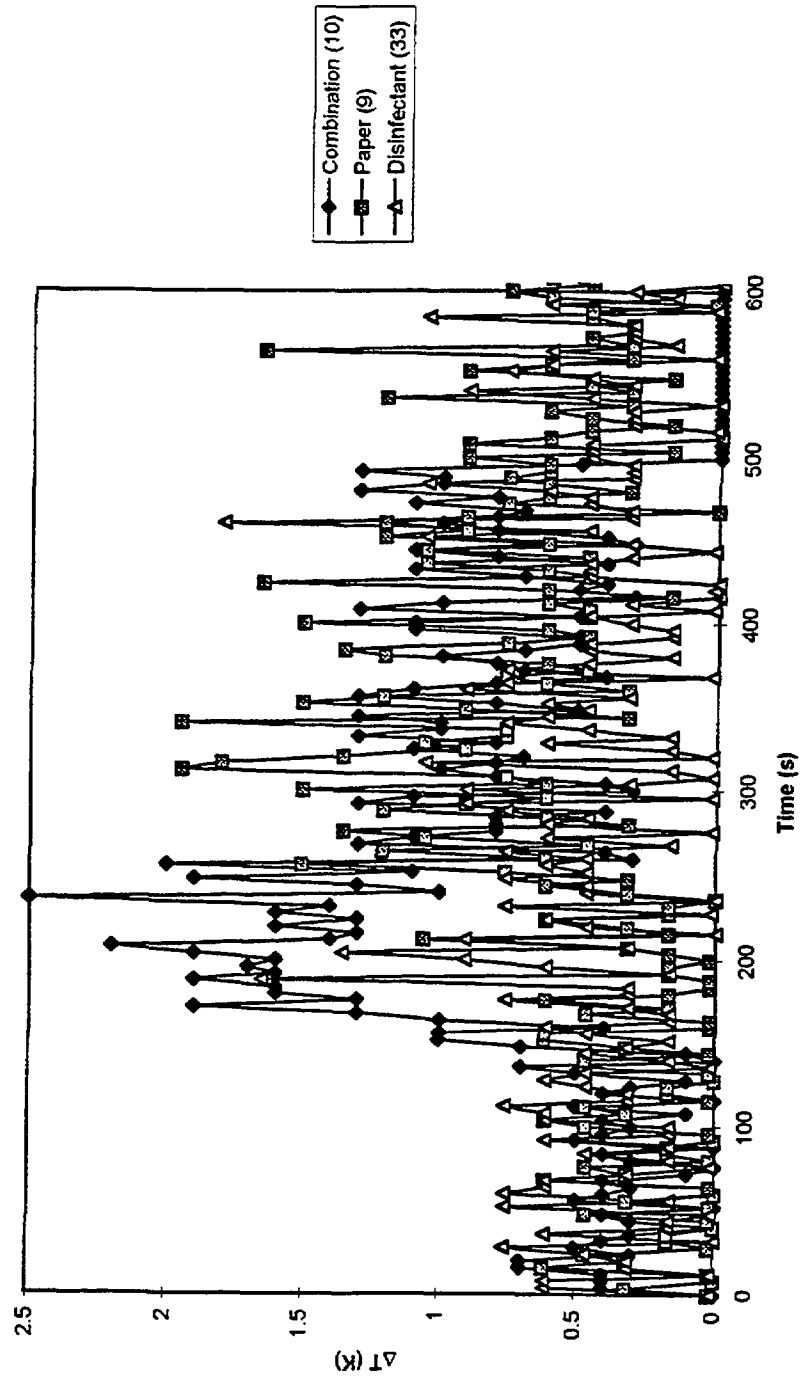


TGS 880 Output vs. Time

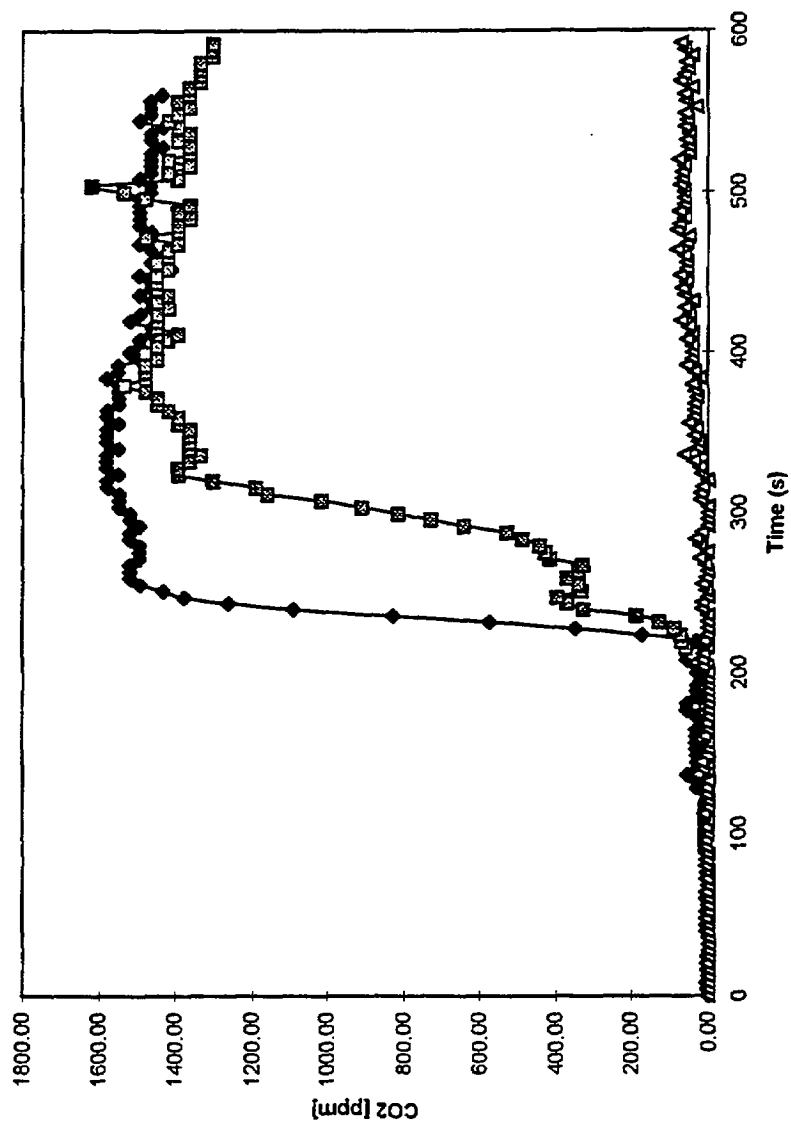


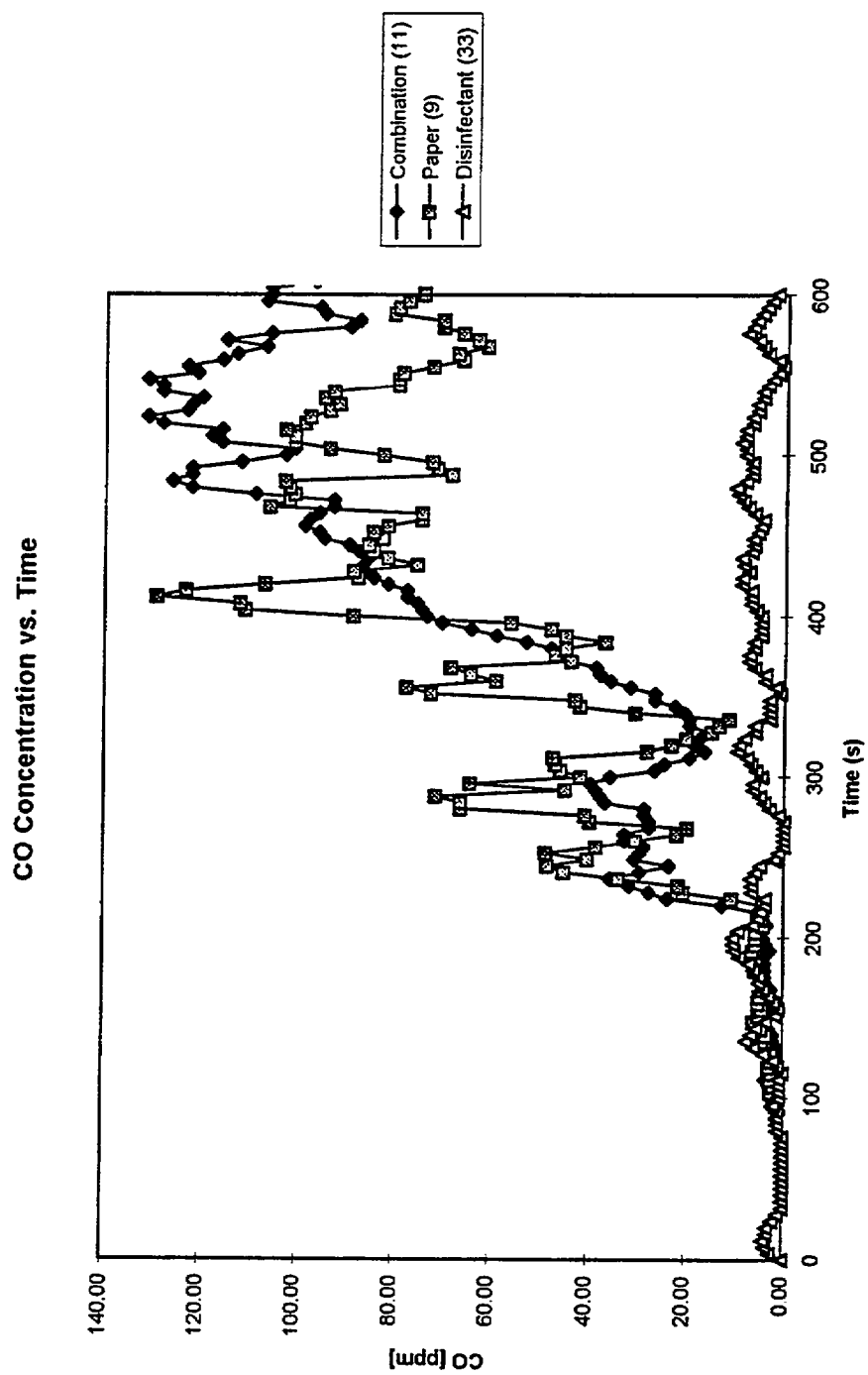


Temperature Rise at TC 13 vs. Time

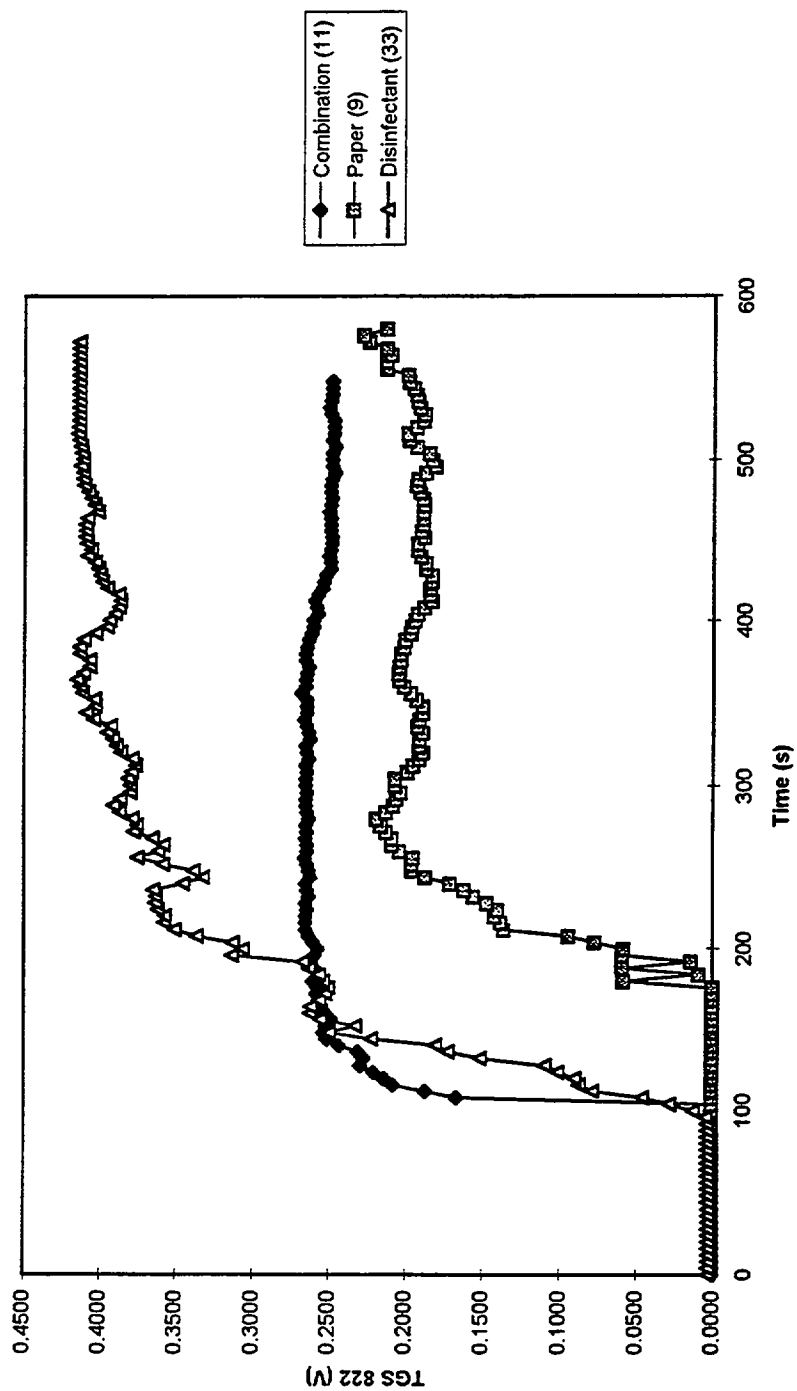


CO2 Concentration vs. Time

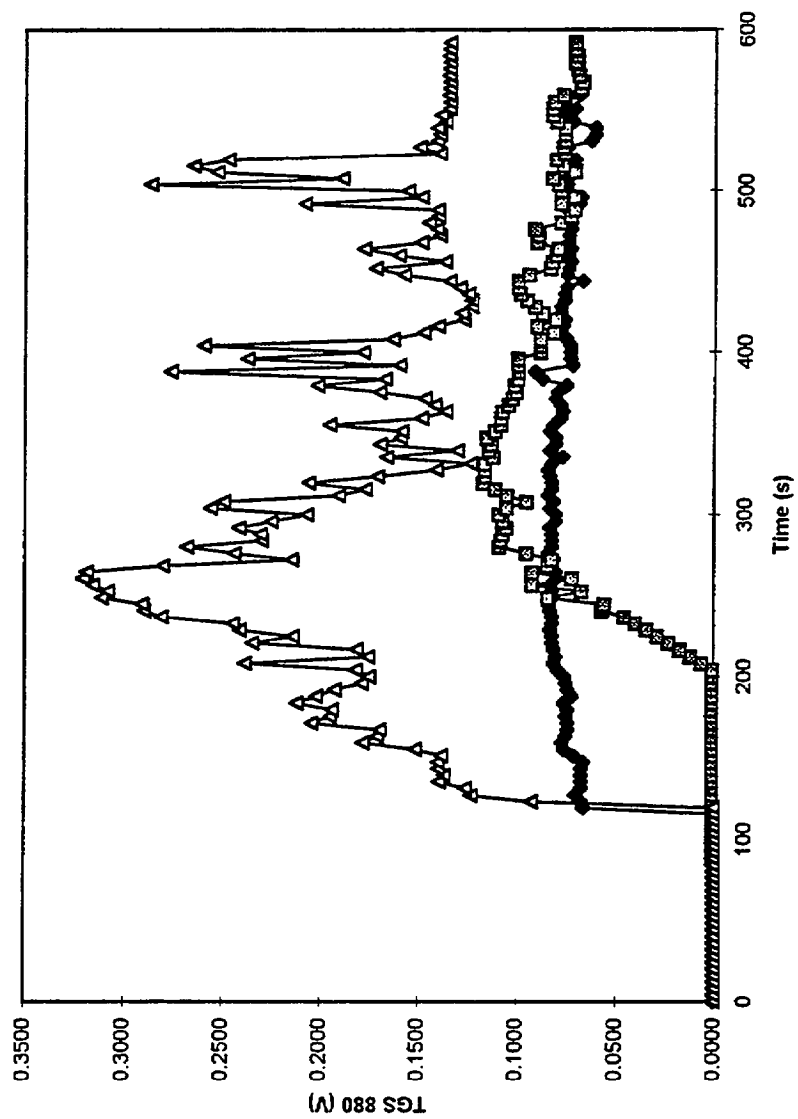


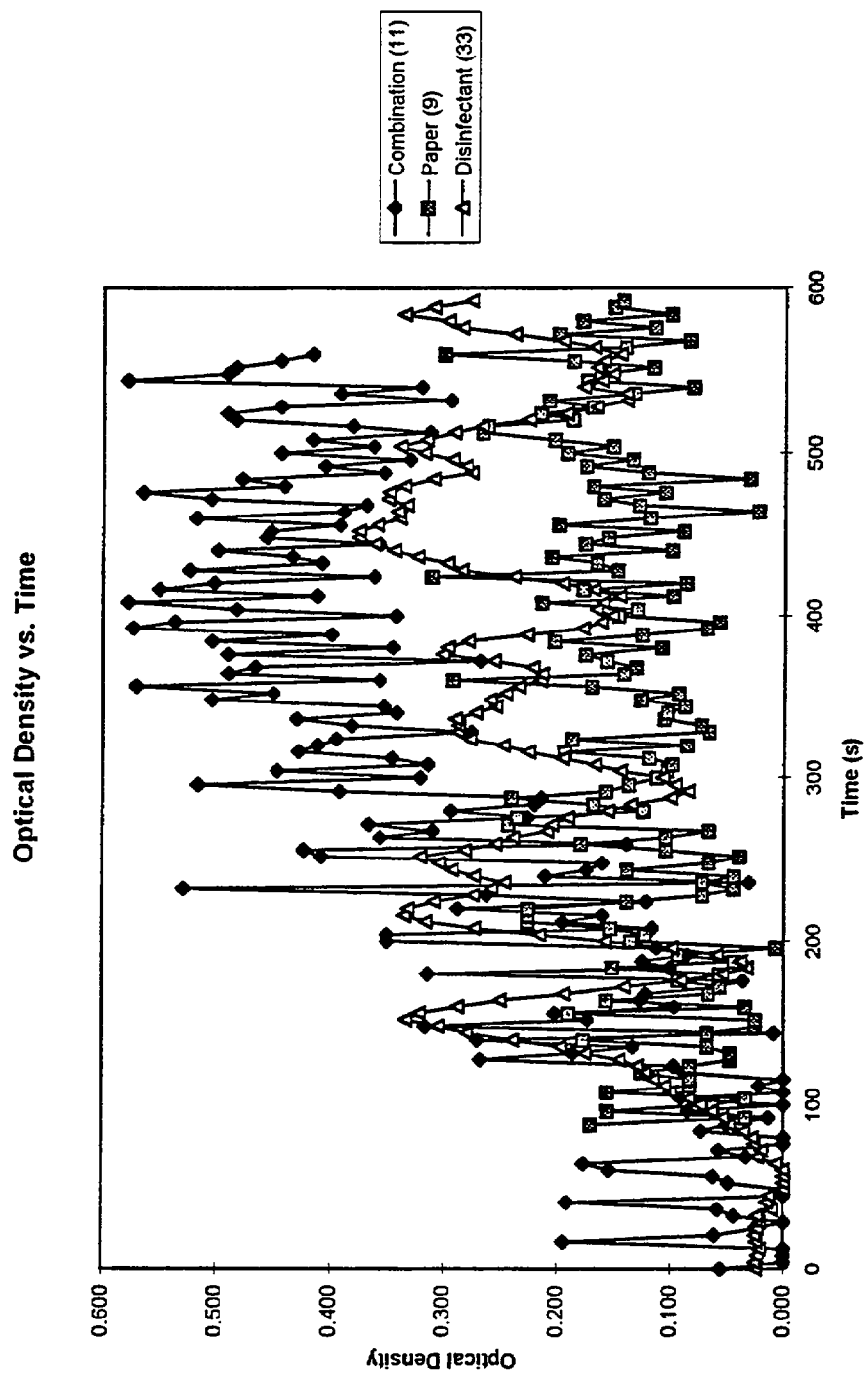


TGS 822 Output vs. Time

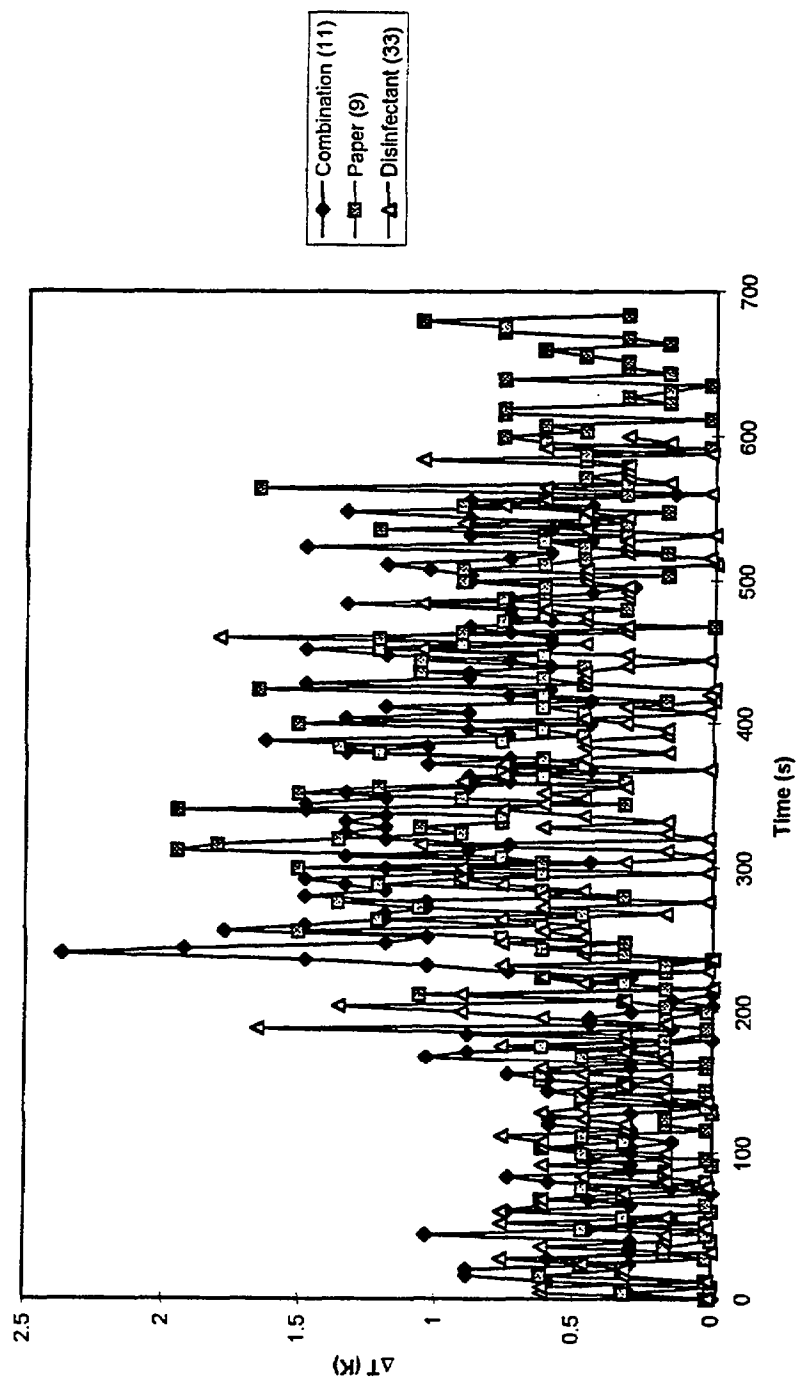


TGS 880 Output vs. Time

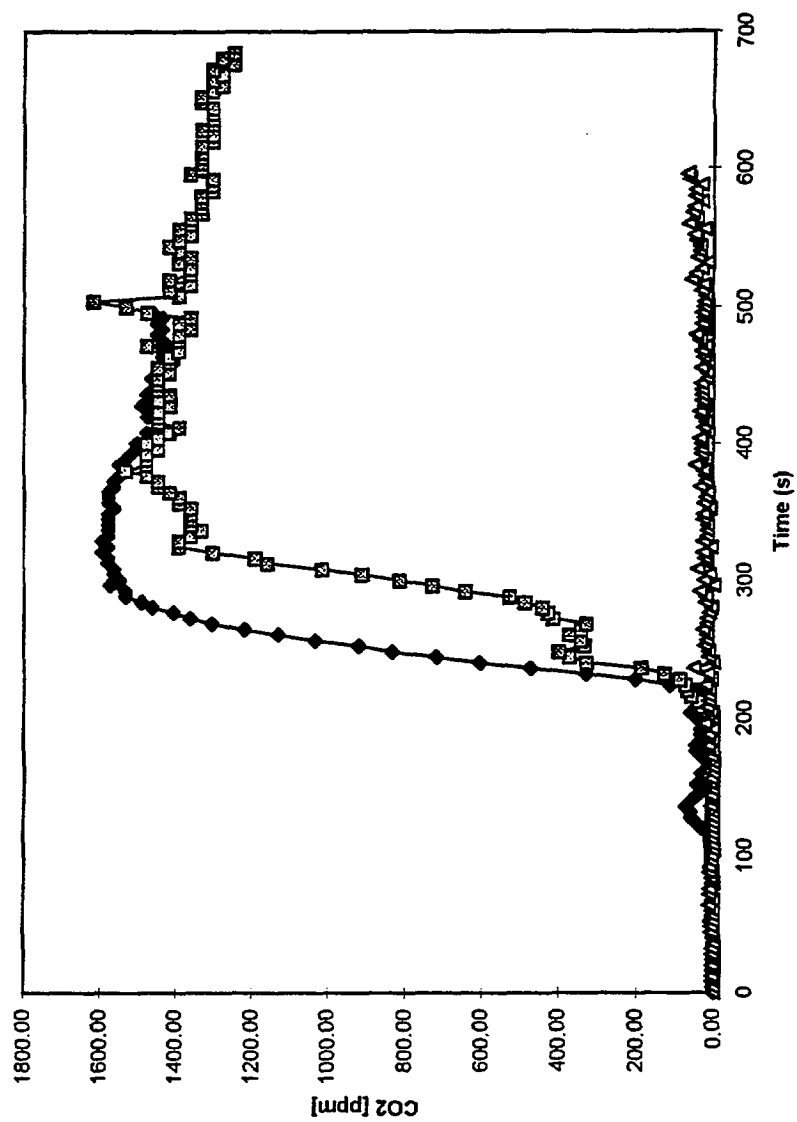


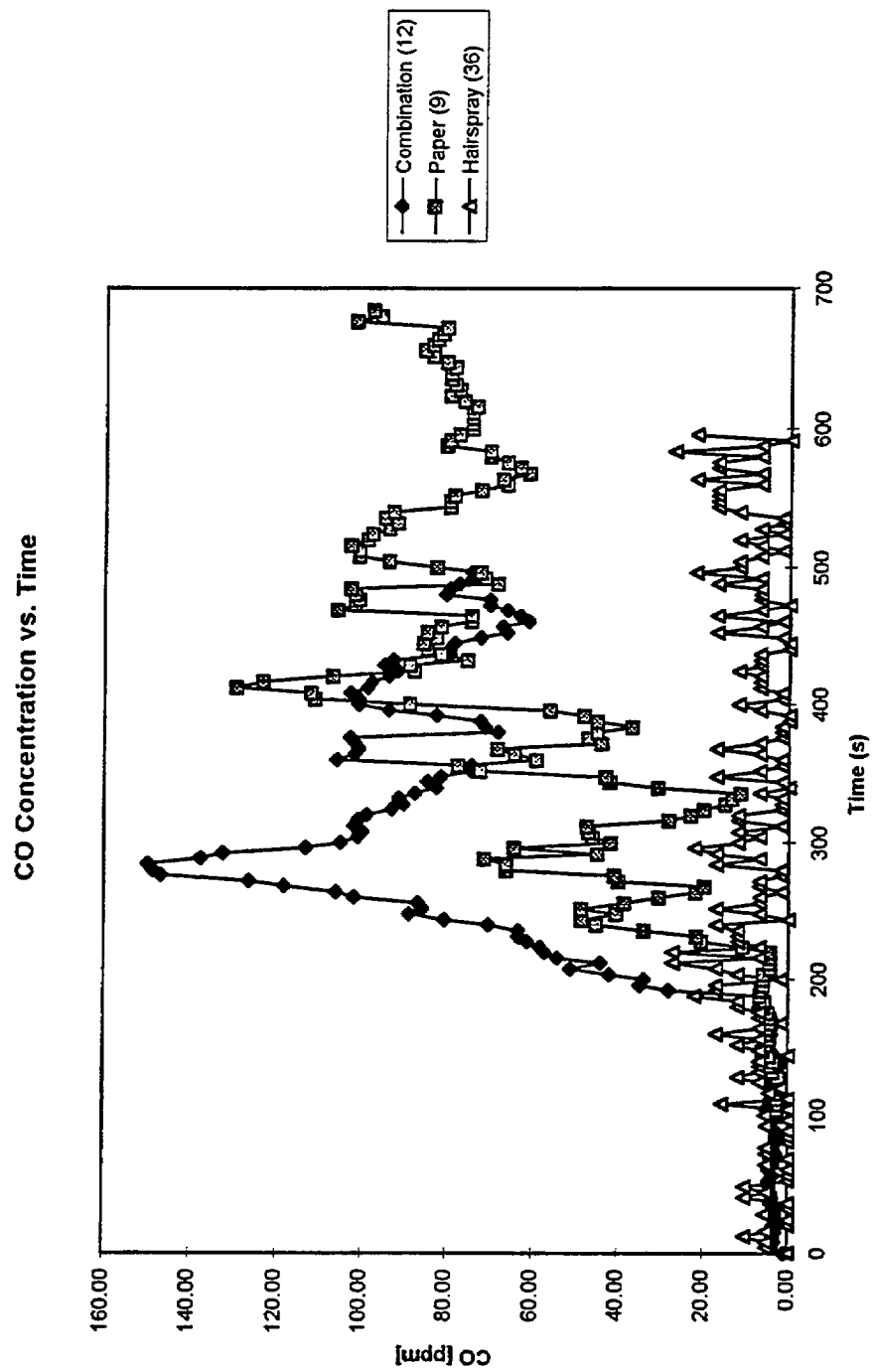


Temperature Rise at TC 13 vs. Time

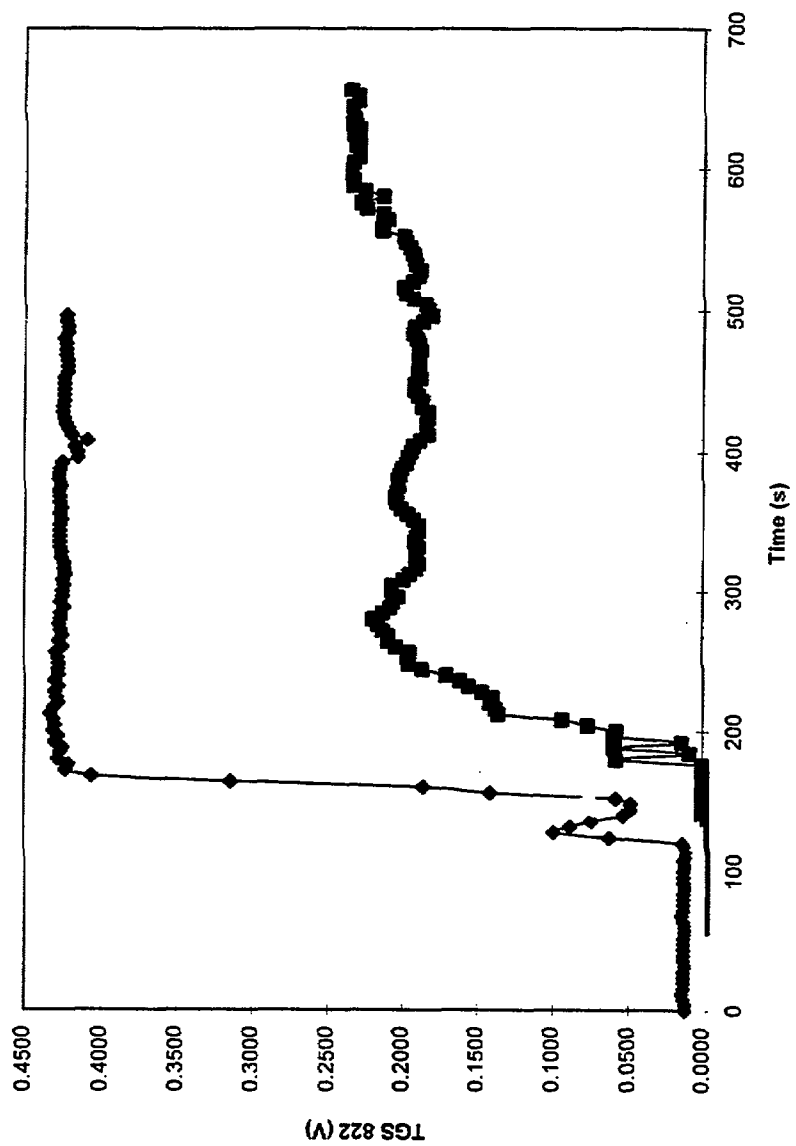


CO2 Concentration vs. Time

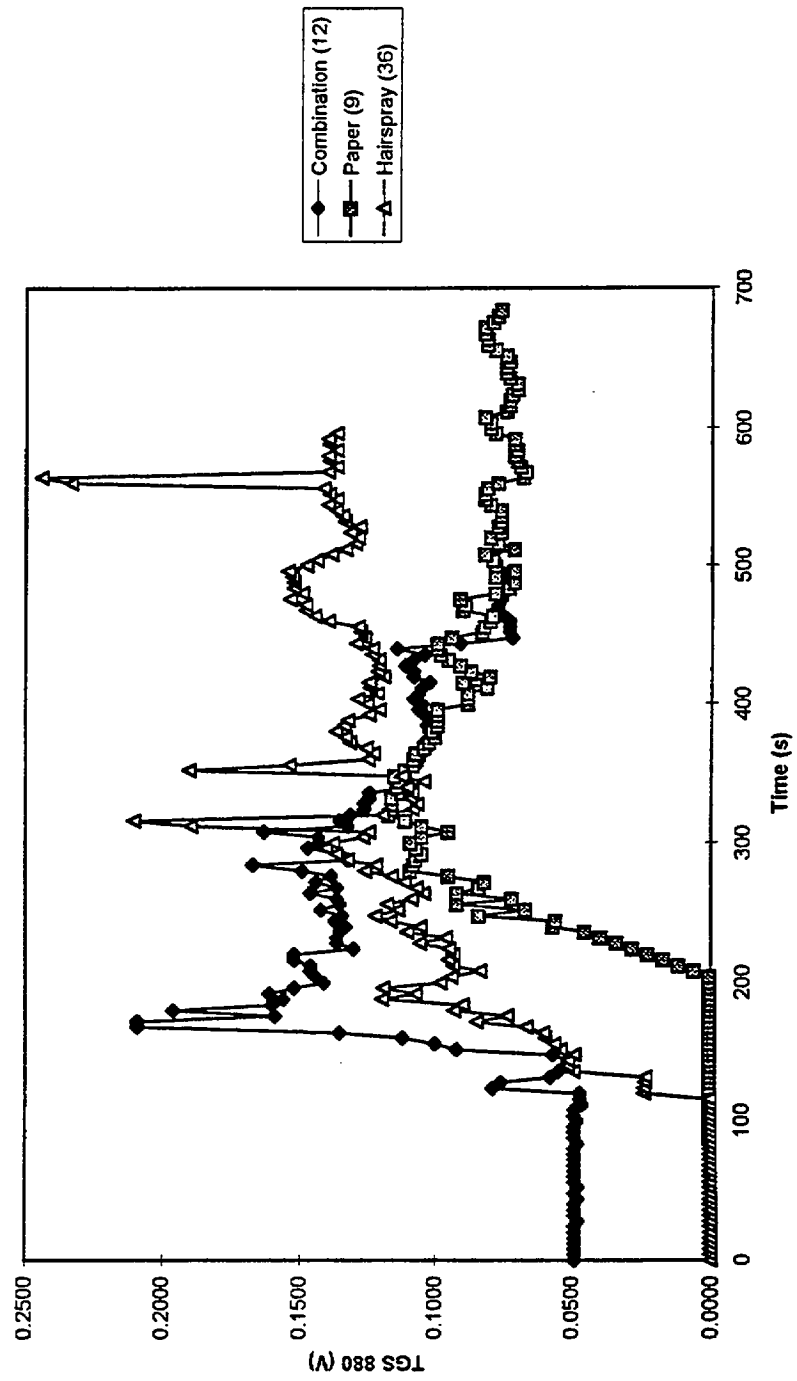




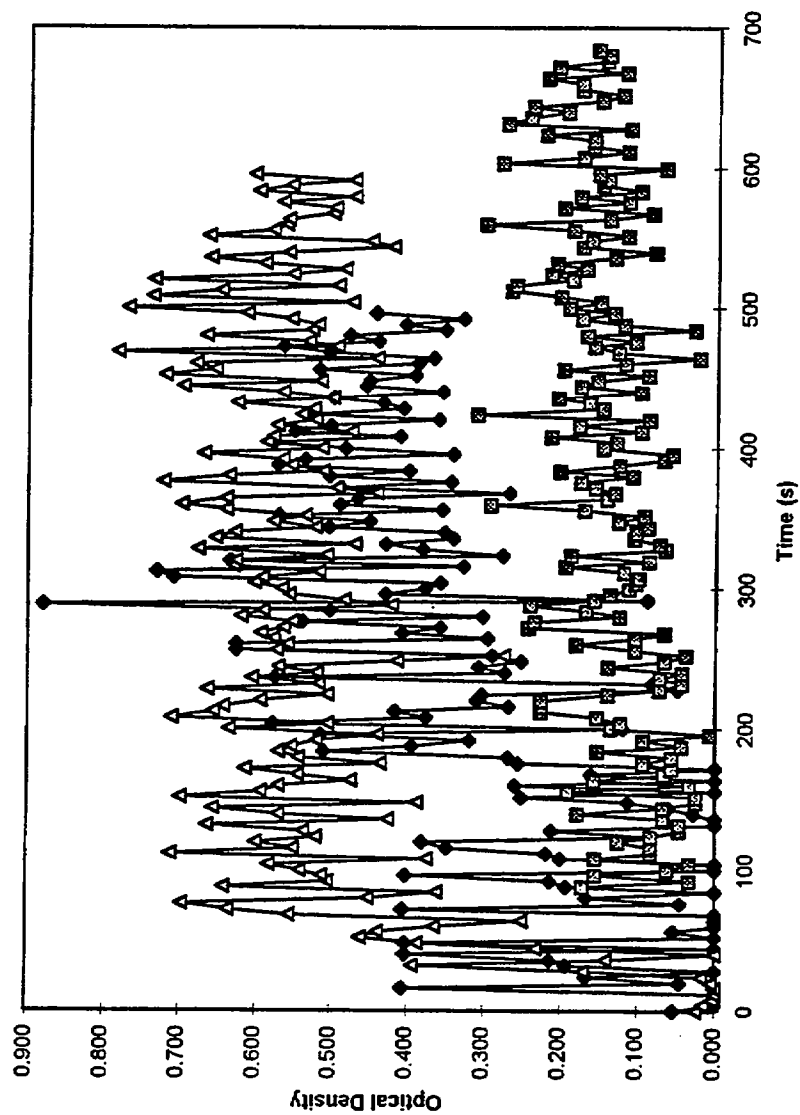
TGS 822 Output vs. Time



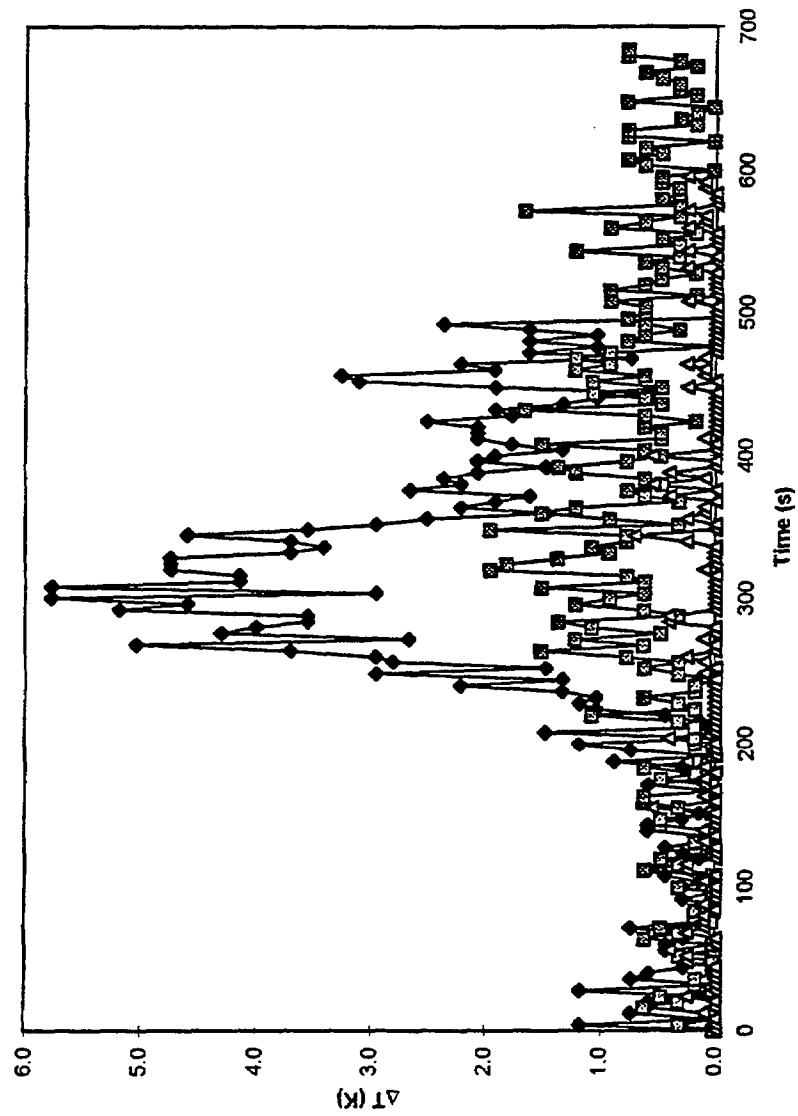
TGS 880 Output vs. Time



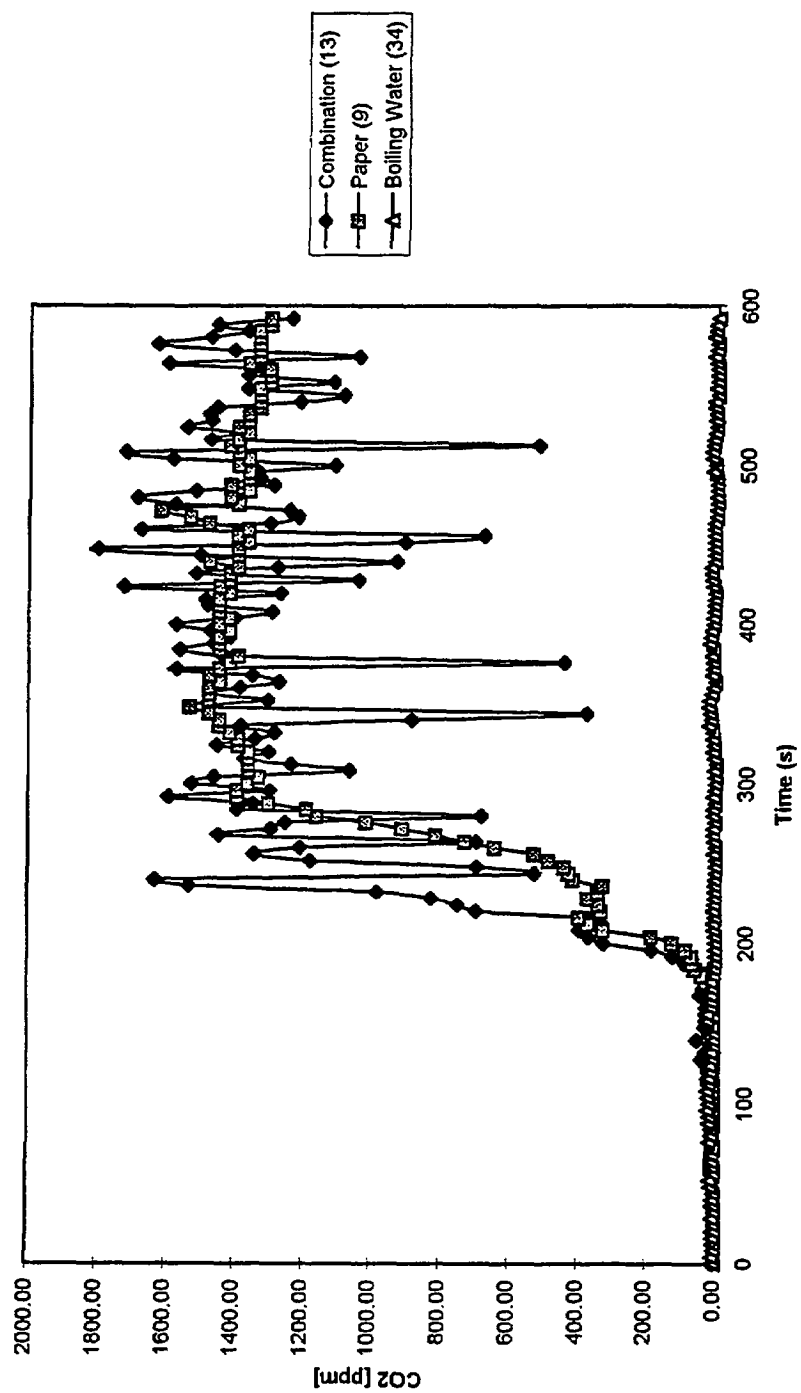
Optical Density vs. Time



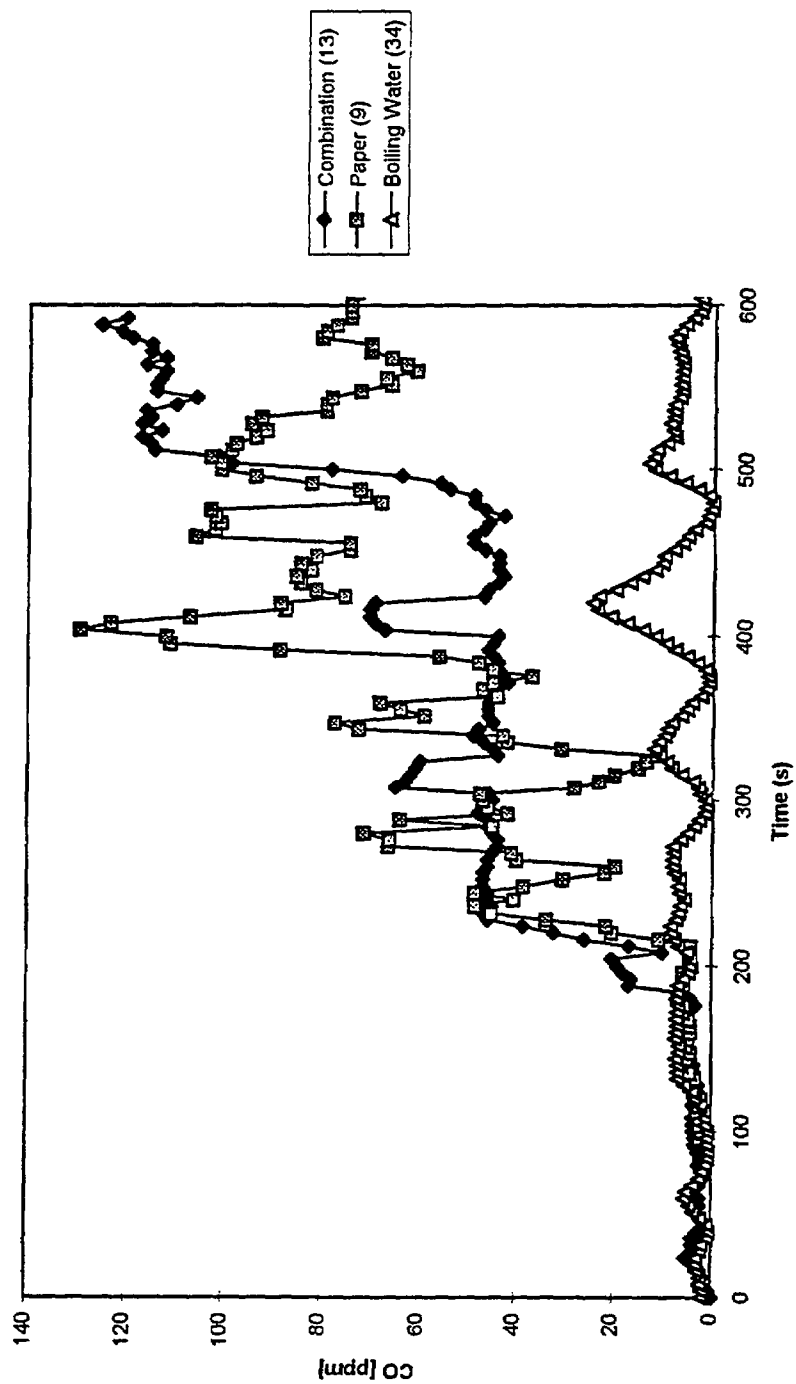
Temperature Rise at TC 13 vs. Time



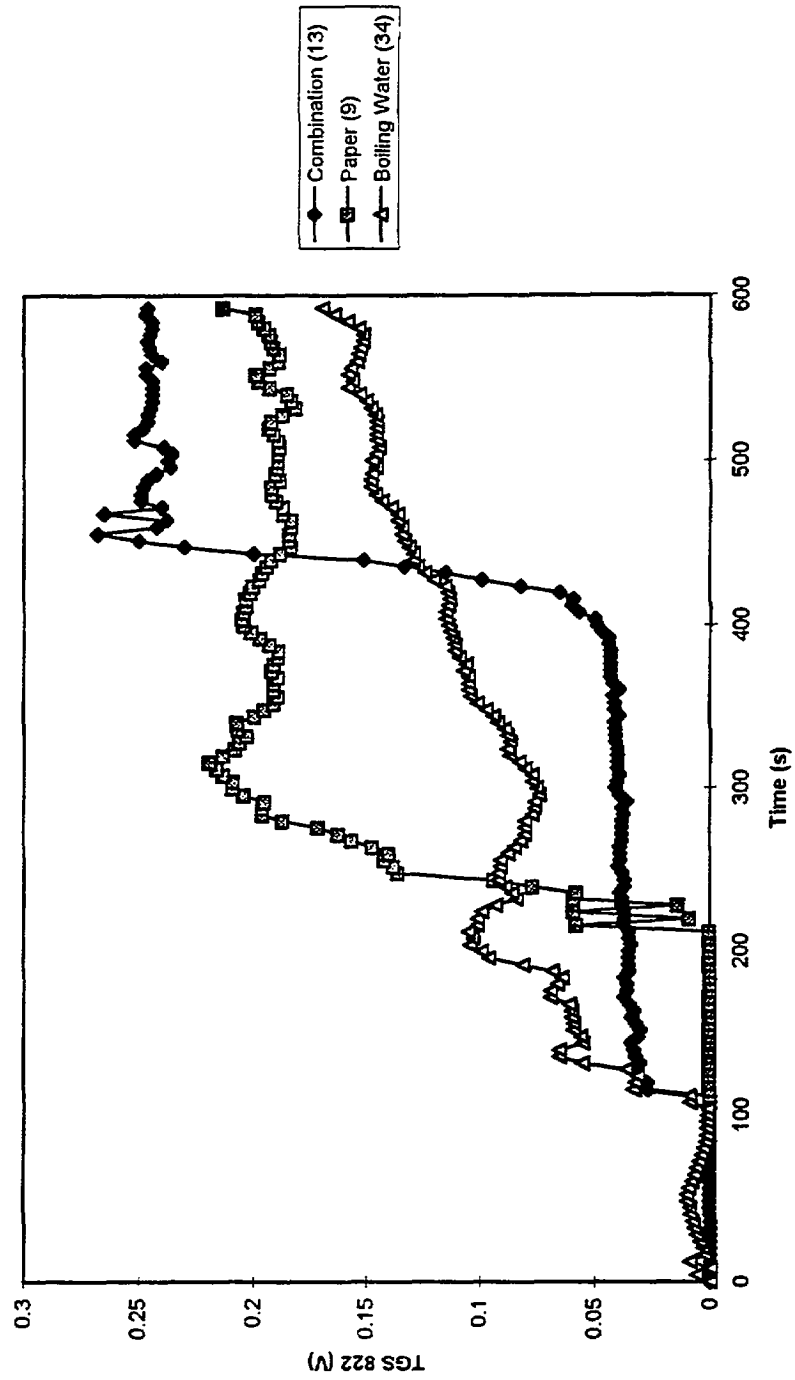
CO2 Concentration vs. Time



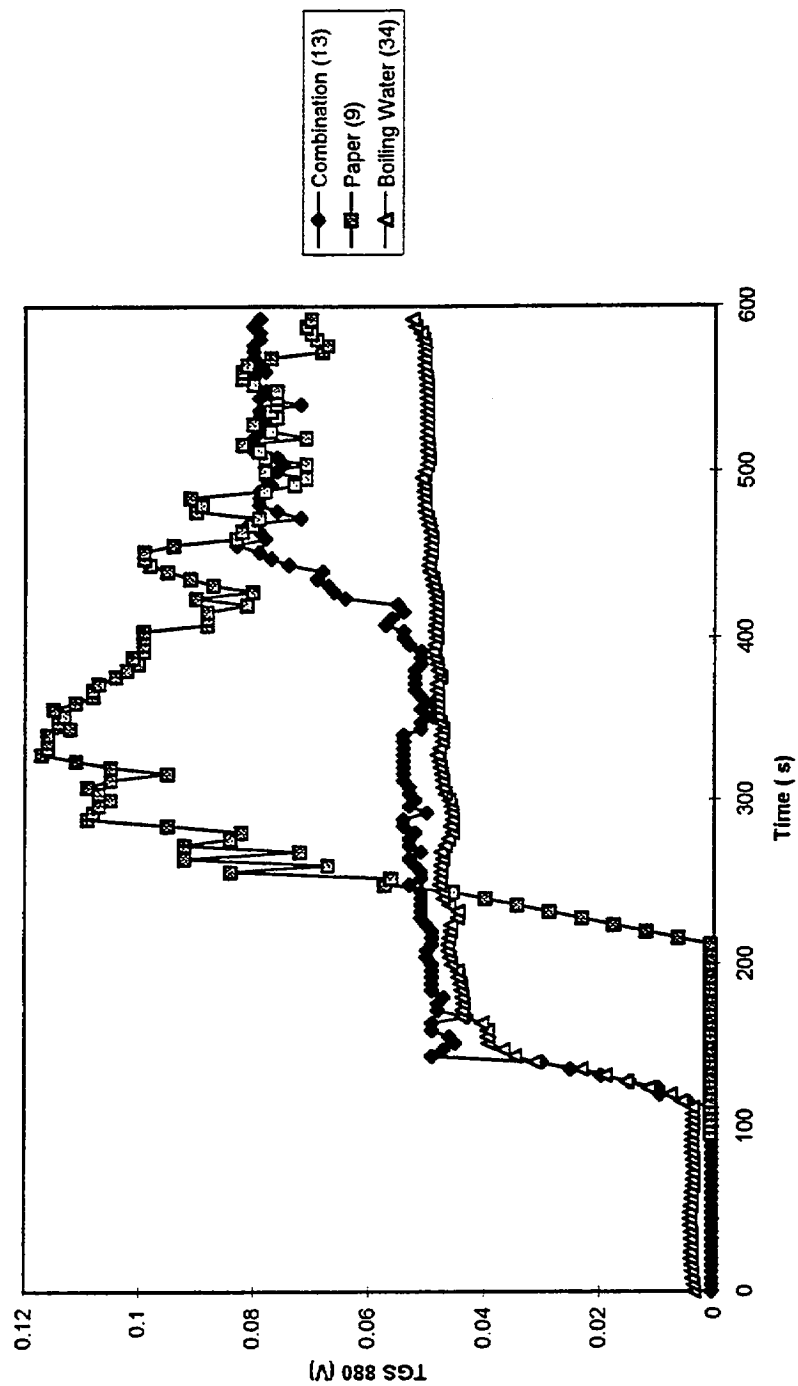
CO Concentration vs. Time



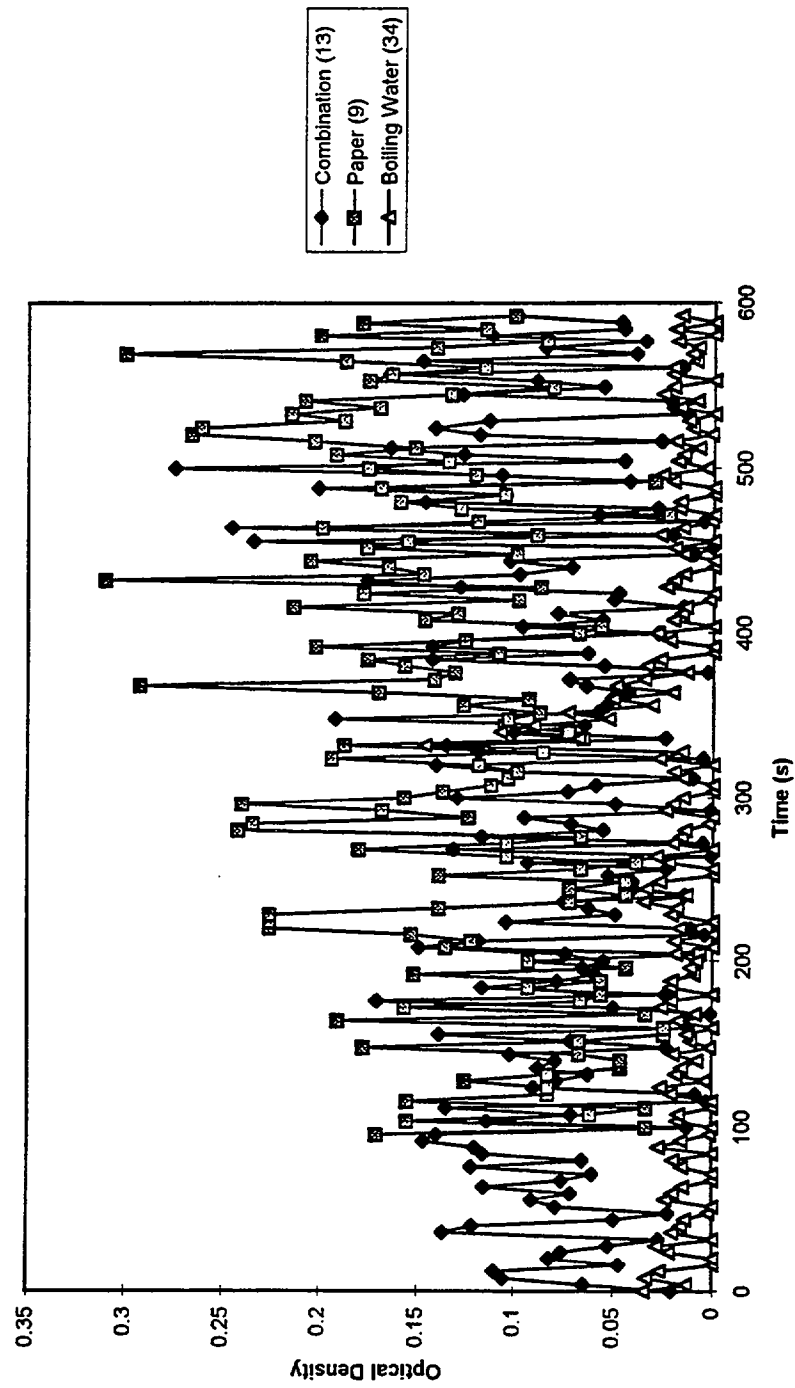
TGS 822 Output vs. Time



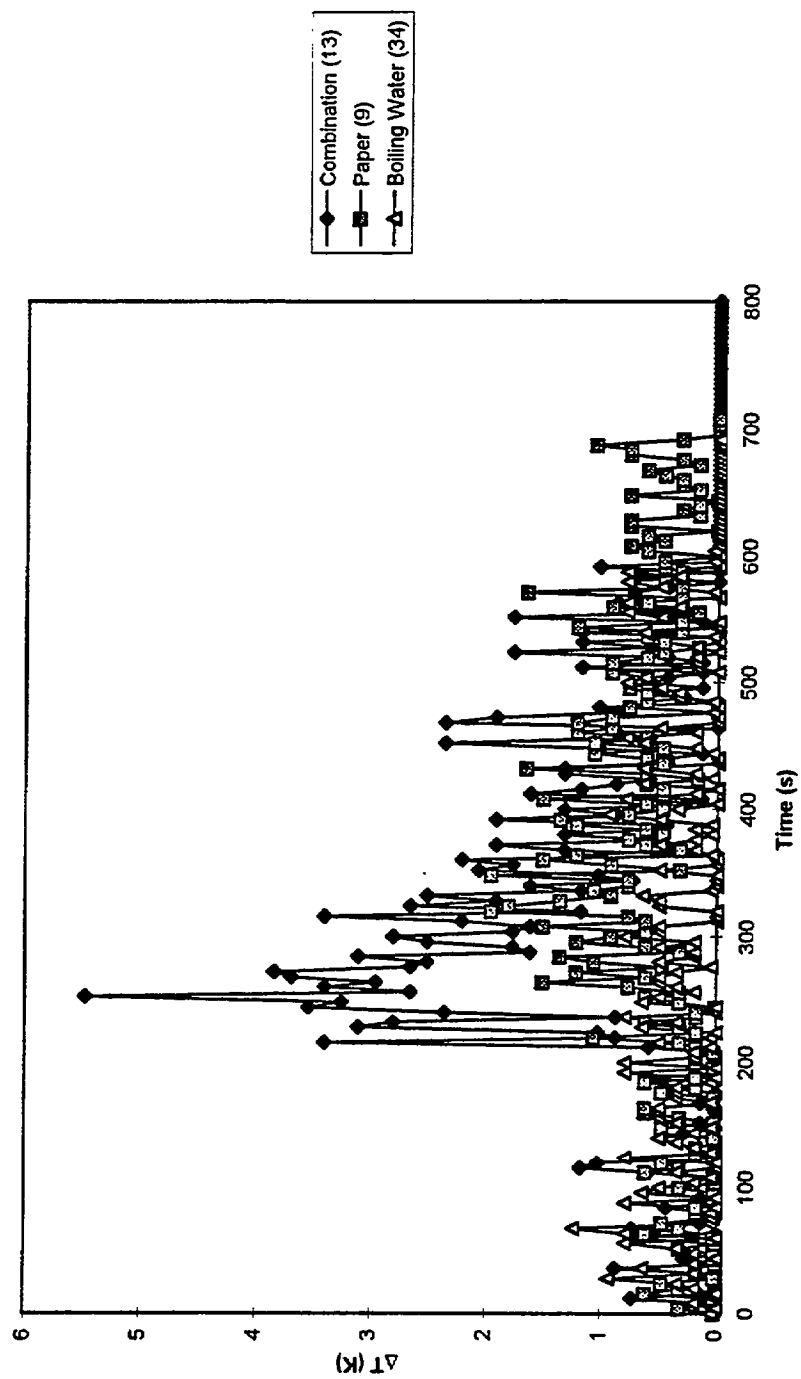
TGS 880 Output vs. Time



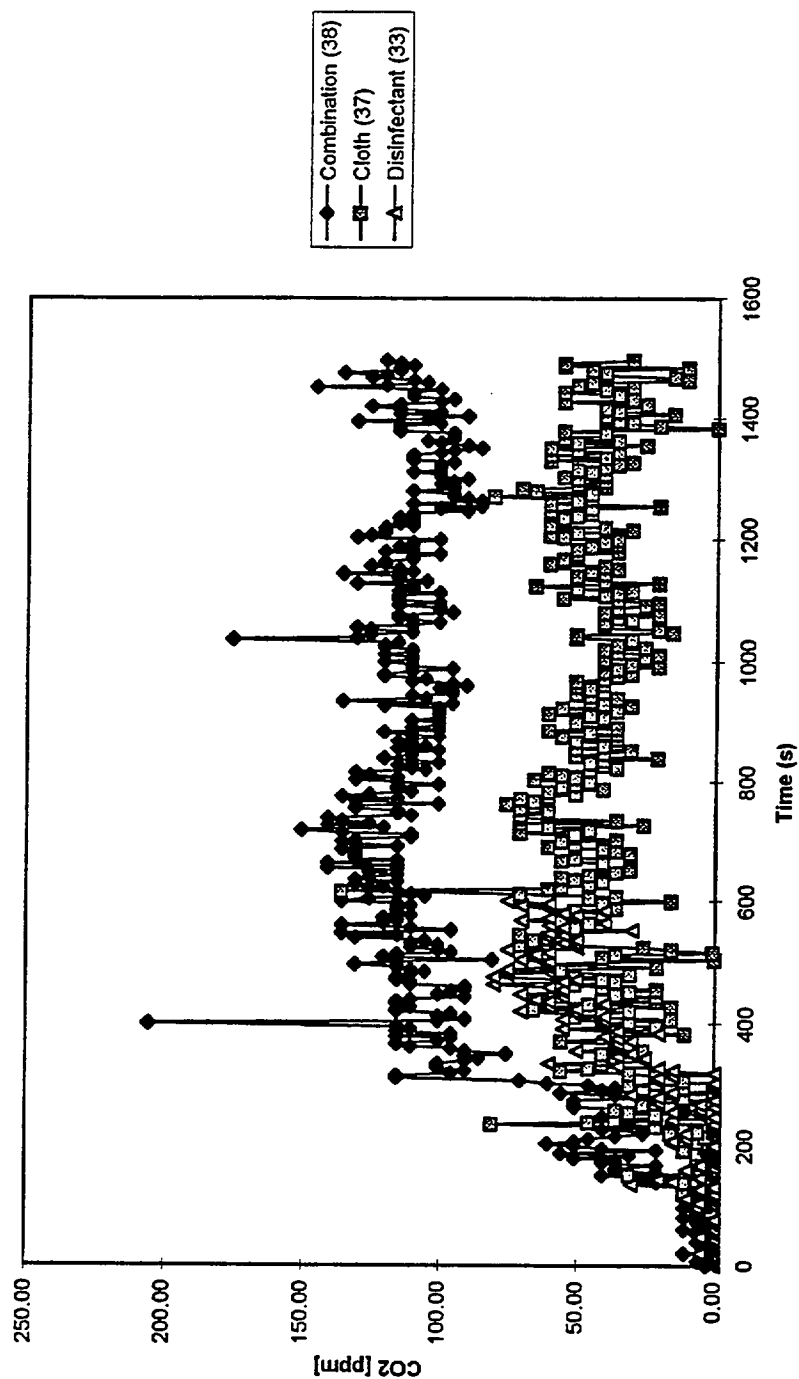
Optical Density vs. Time



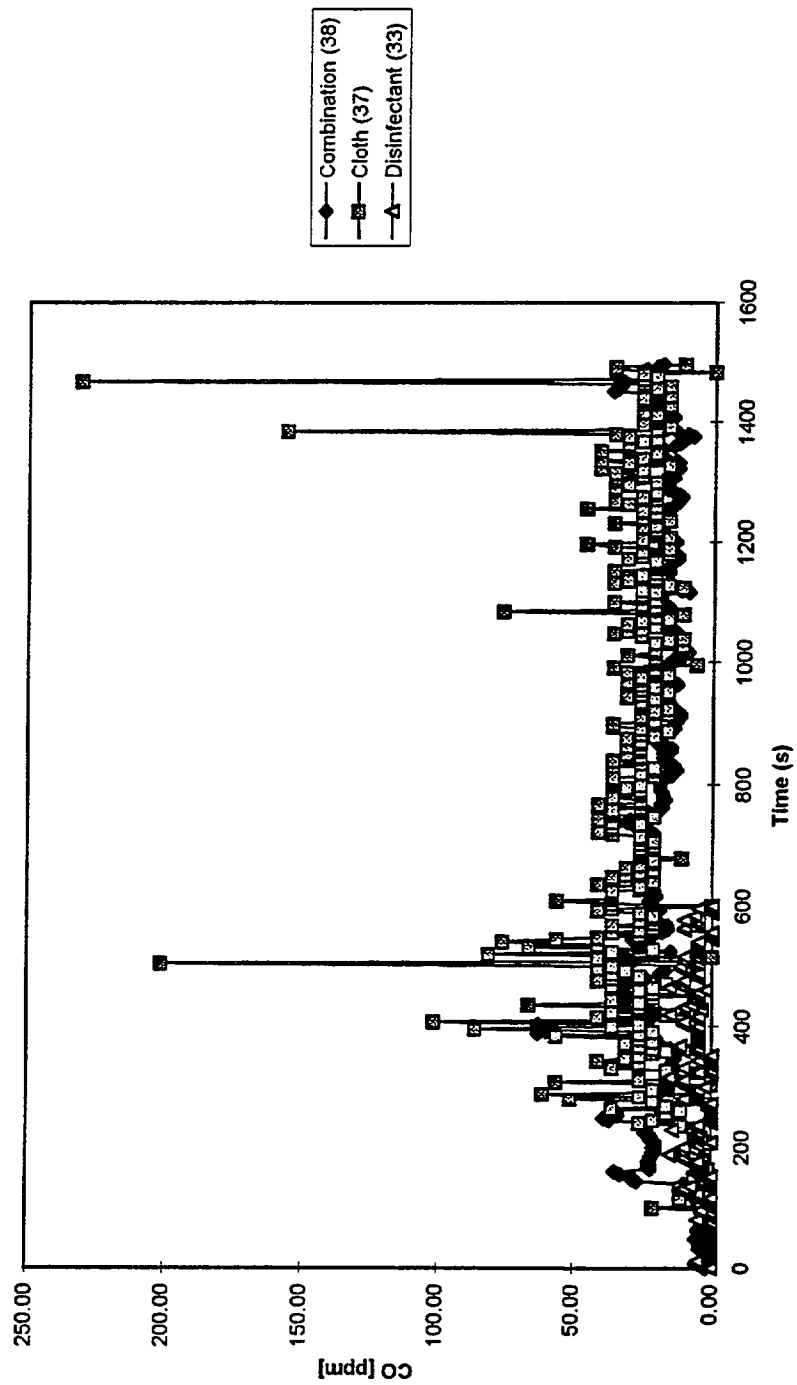
Temperature Rise at TC 13 vs. Time



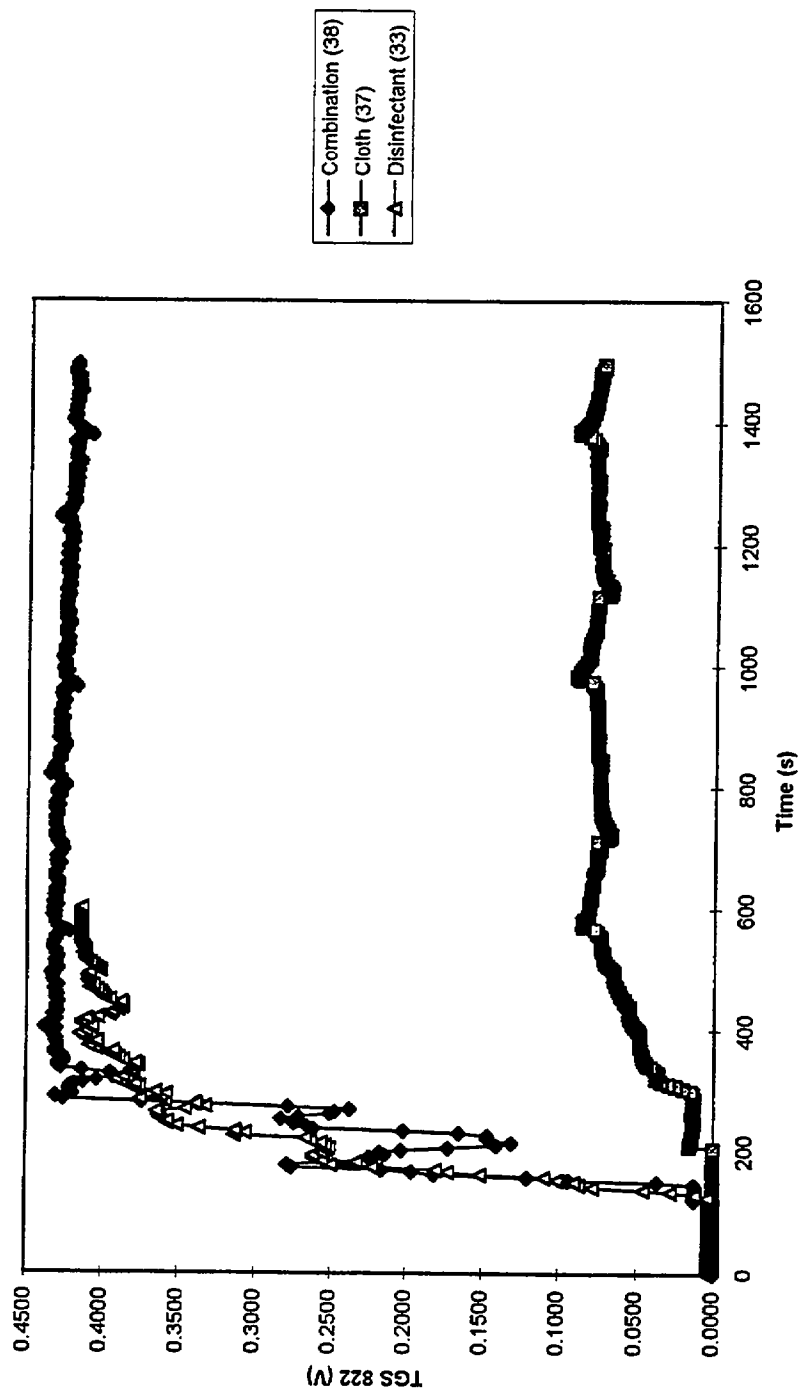
CO2 Concentration vs. Time



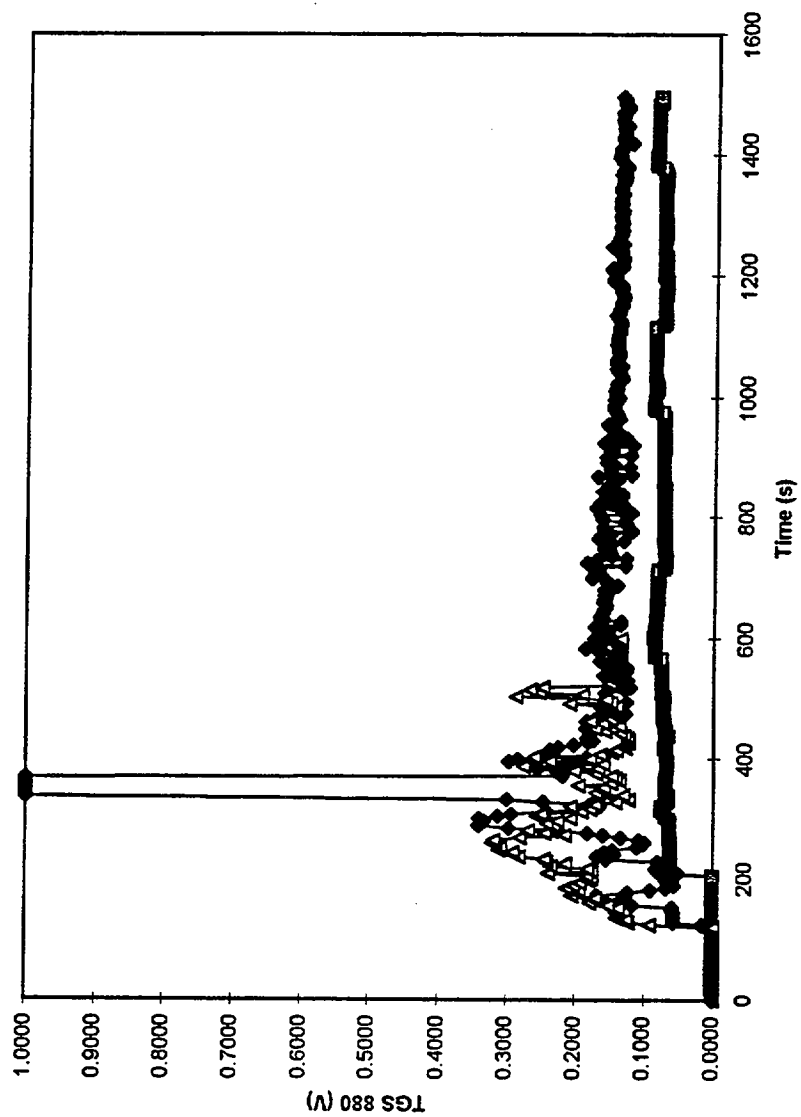
CO Concentration vs. Time



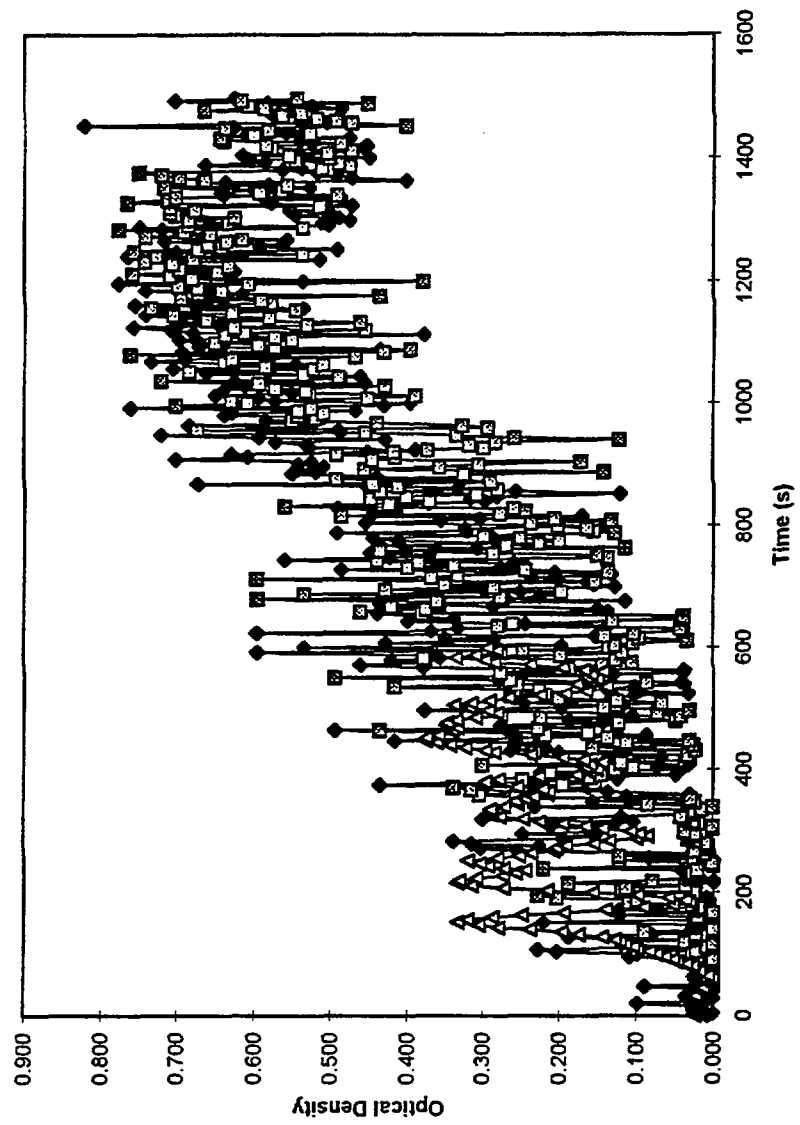
TGS 822 Output vs. Time



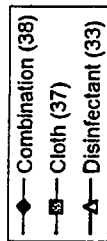
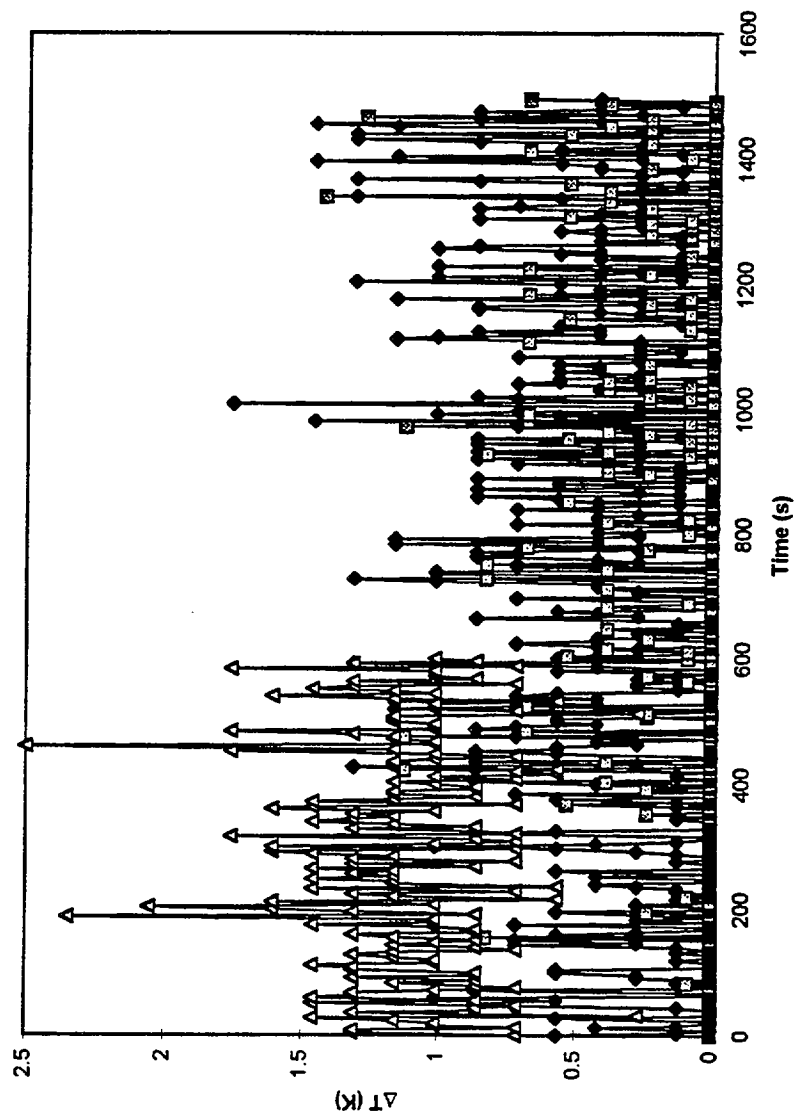
TGS 880 Output vs. Time



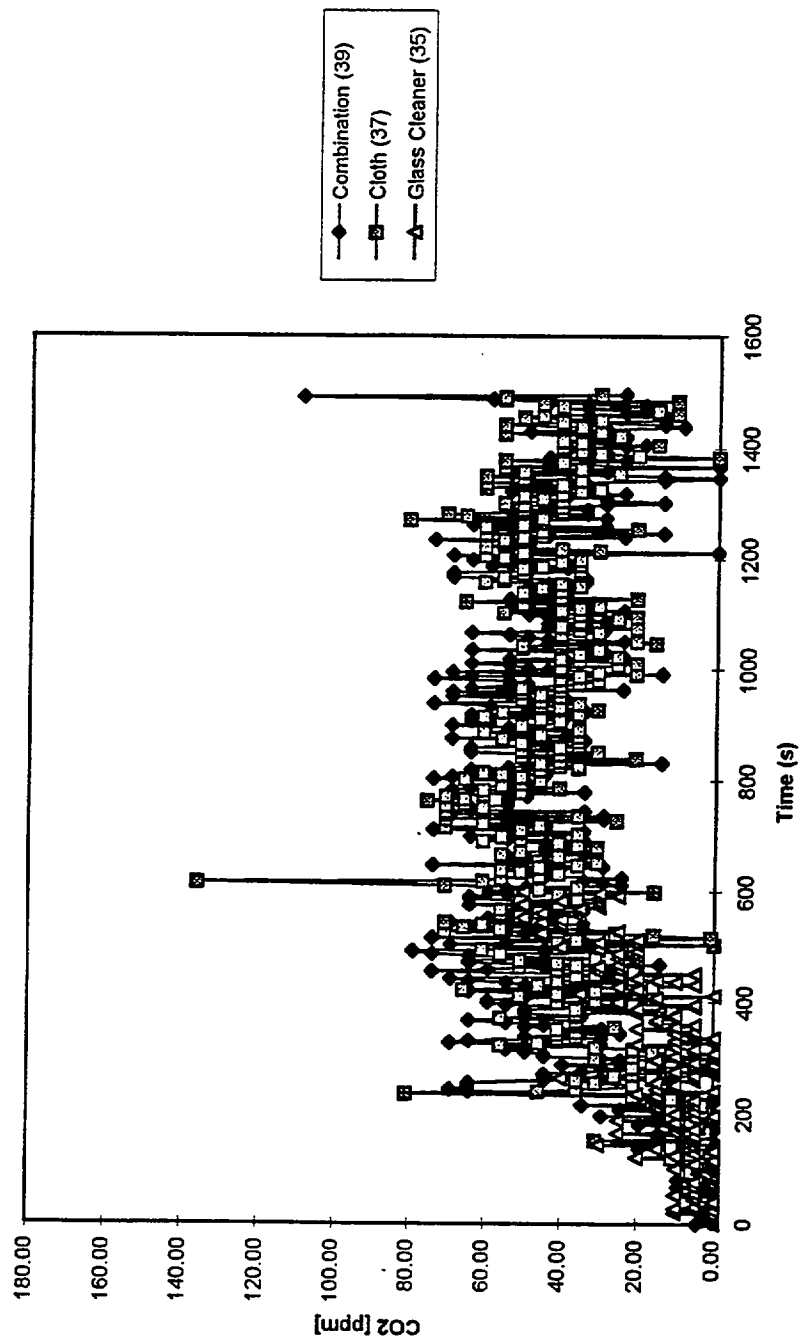
Optical Density vs. Time



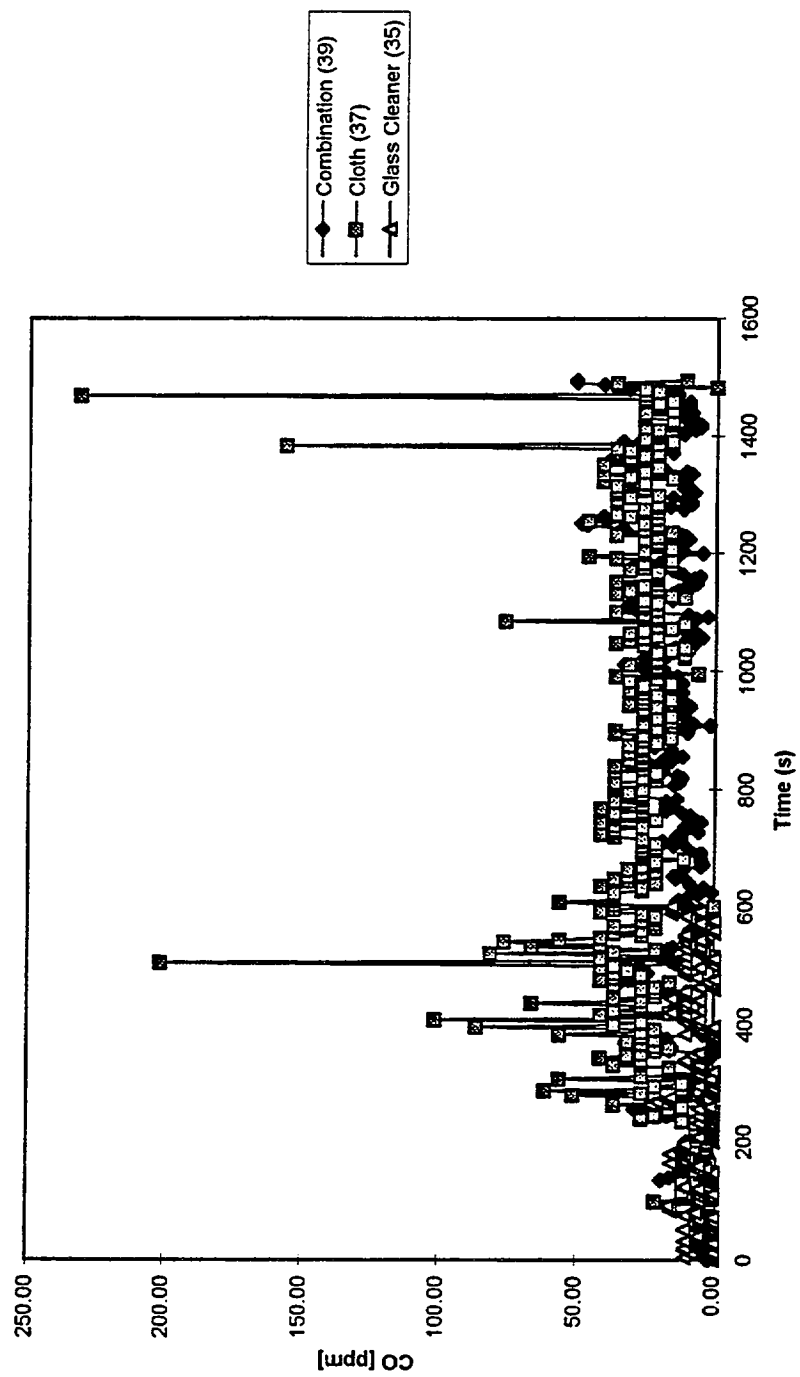
Temperature Rise at TC 13 vs. Time



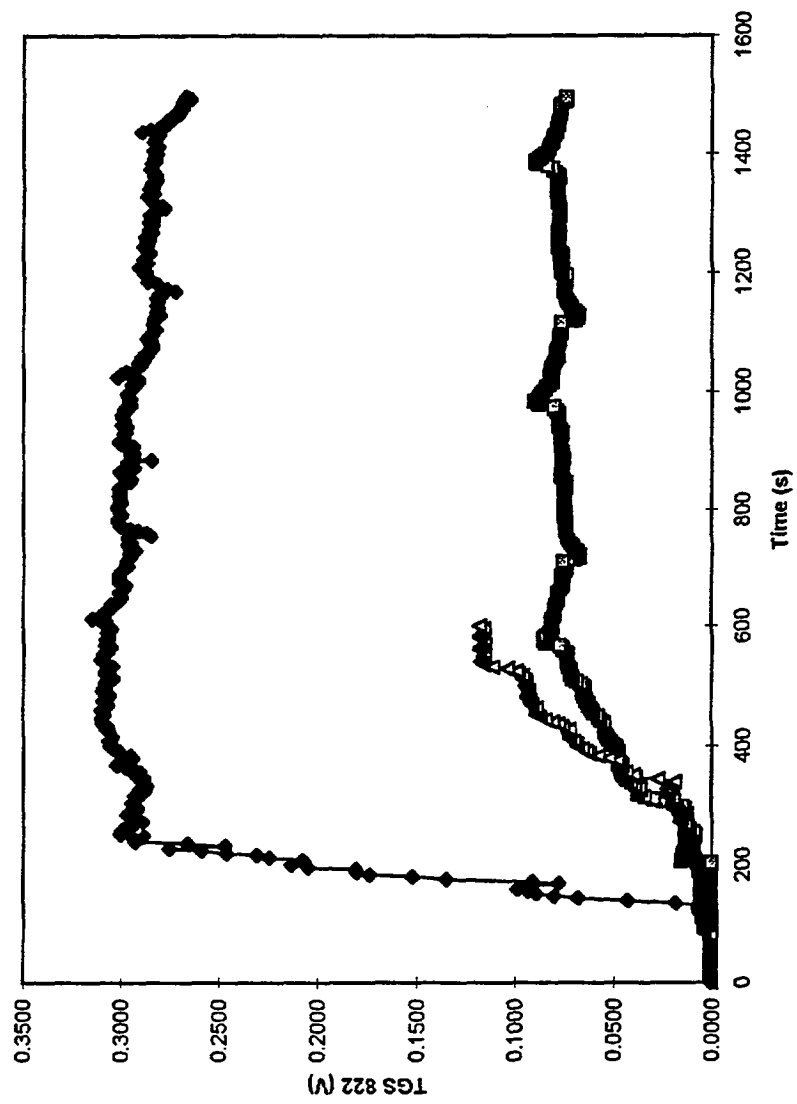
CO2 Concentration vs. Time



CO Concentration vs. Time

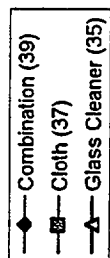
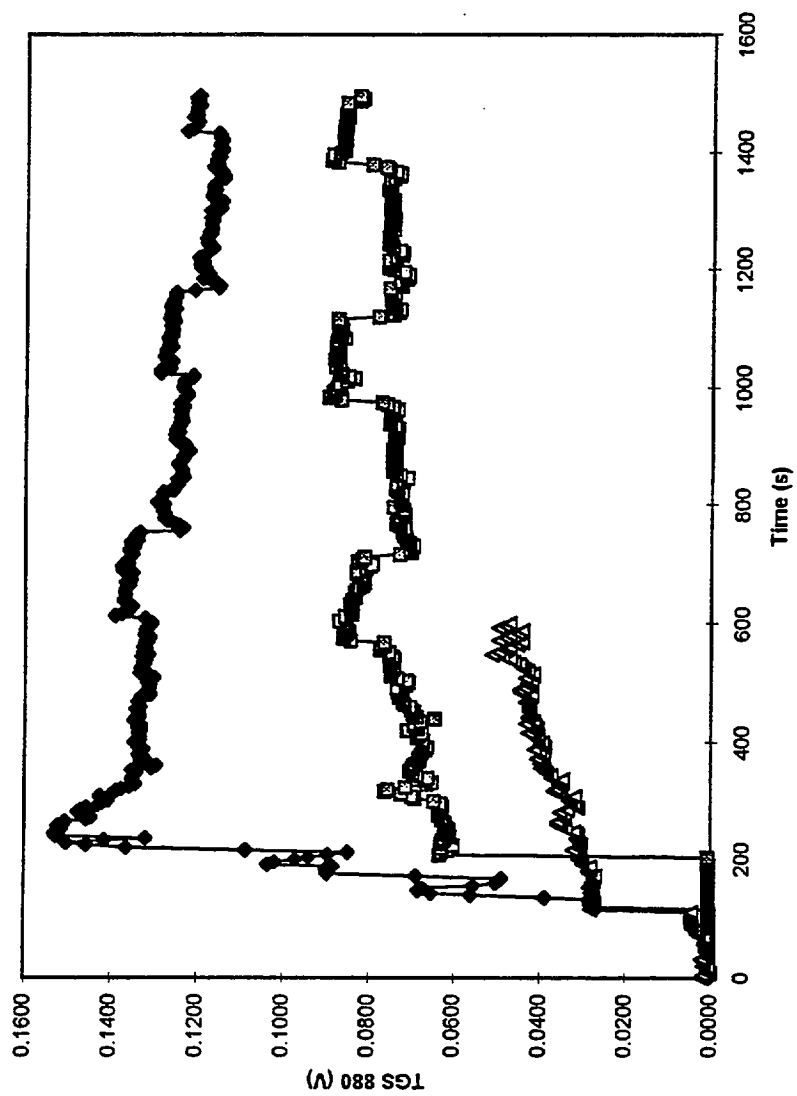


TGS 822 Output vs. Time

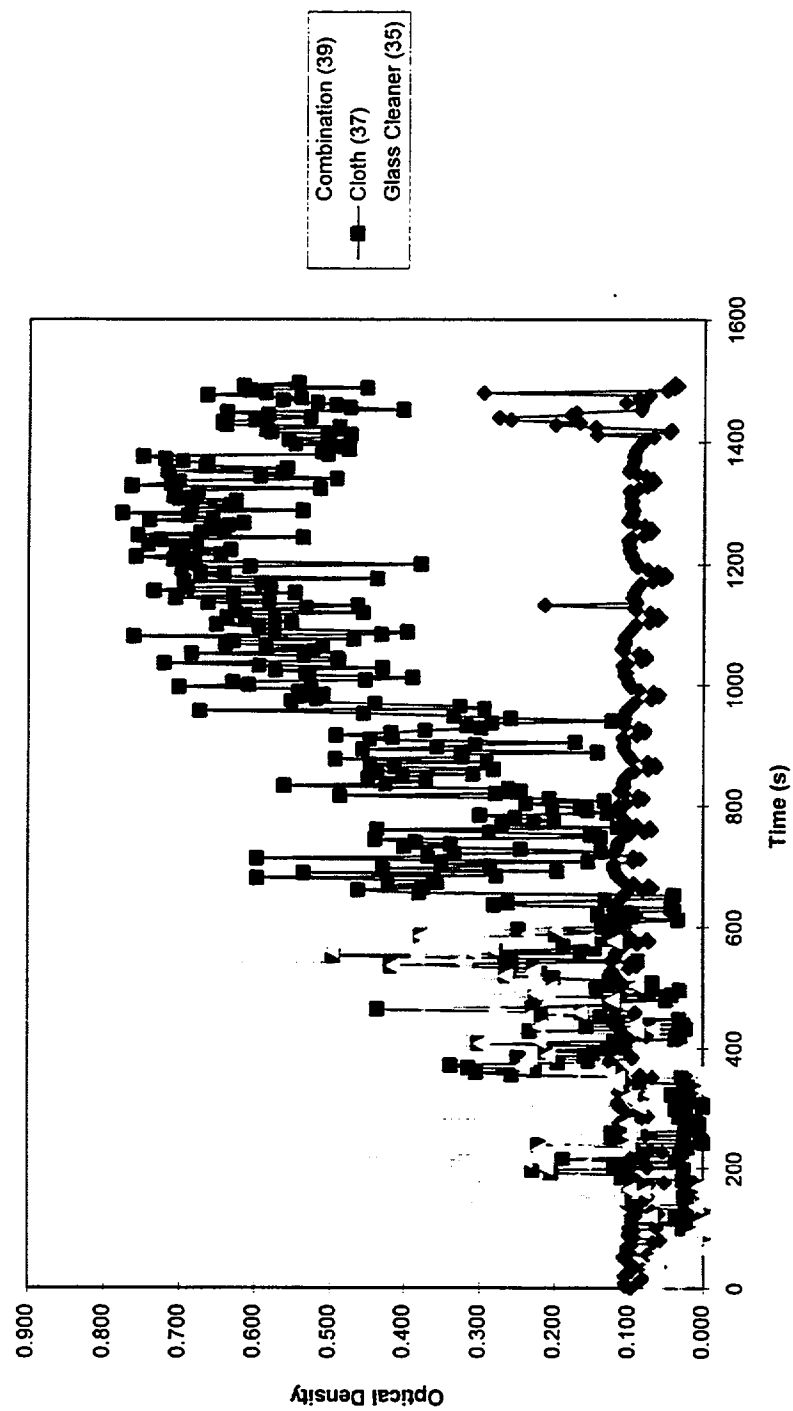


Combination (39)
Cloth (37)
Glass Cleaner (35)

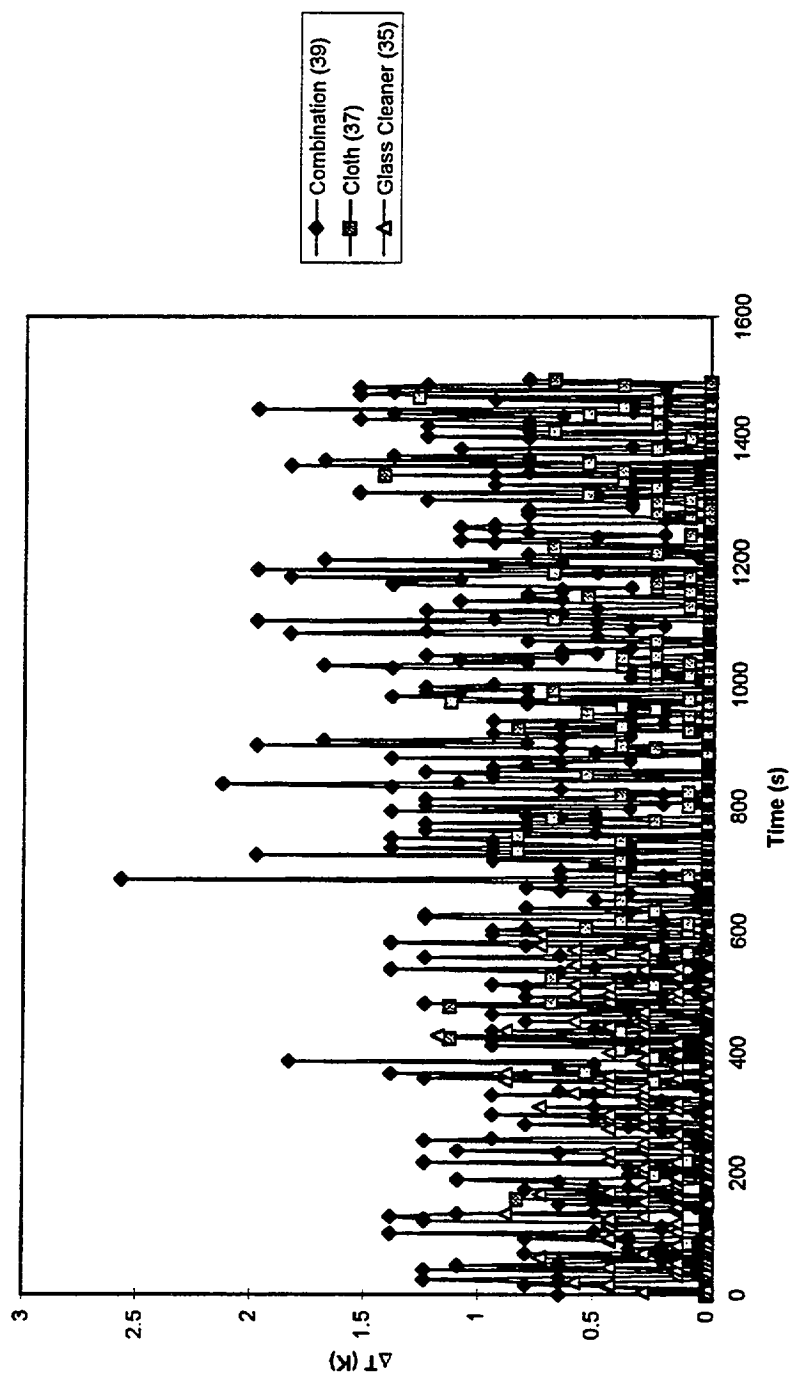
TGS 880 Output vs. Time



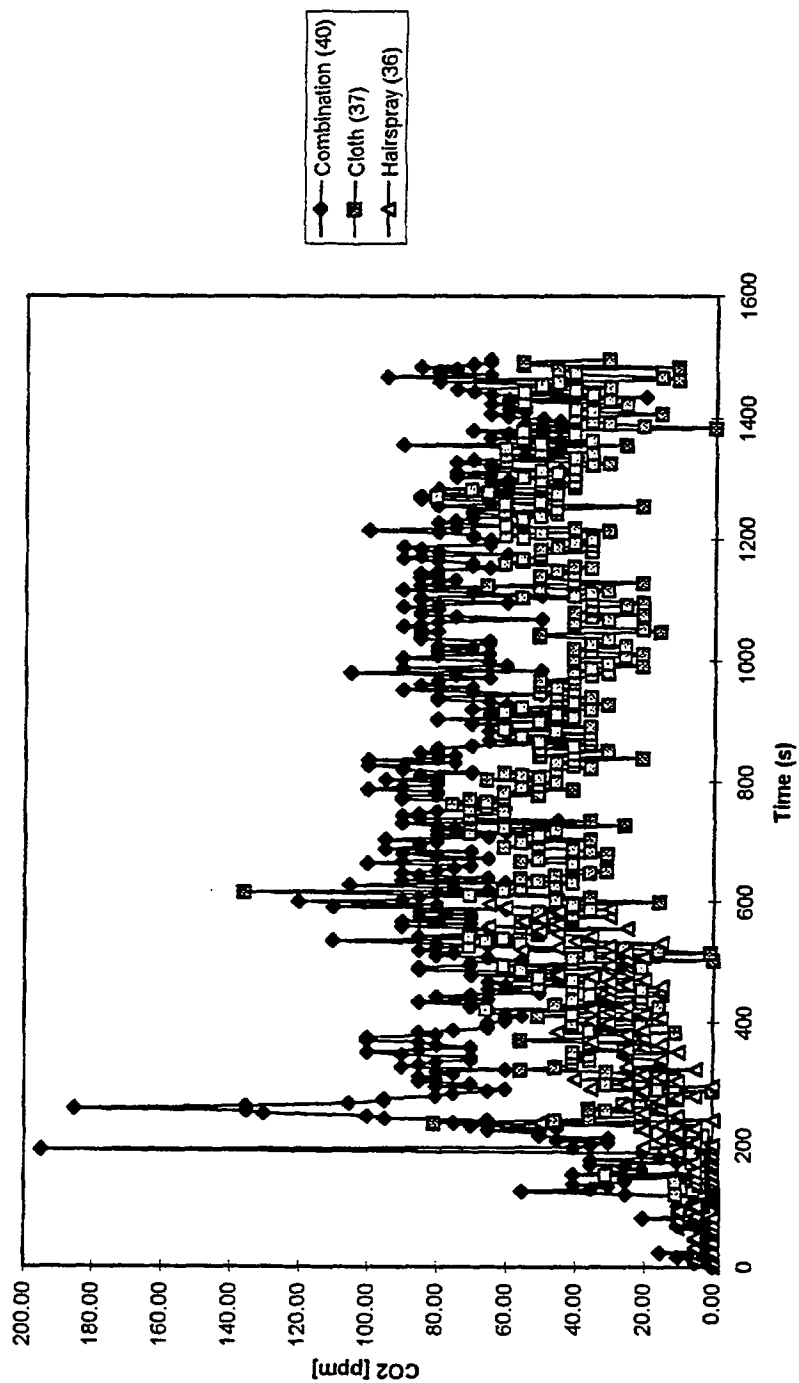
Optical Density vs. Time



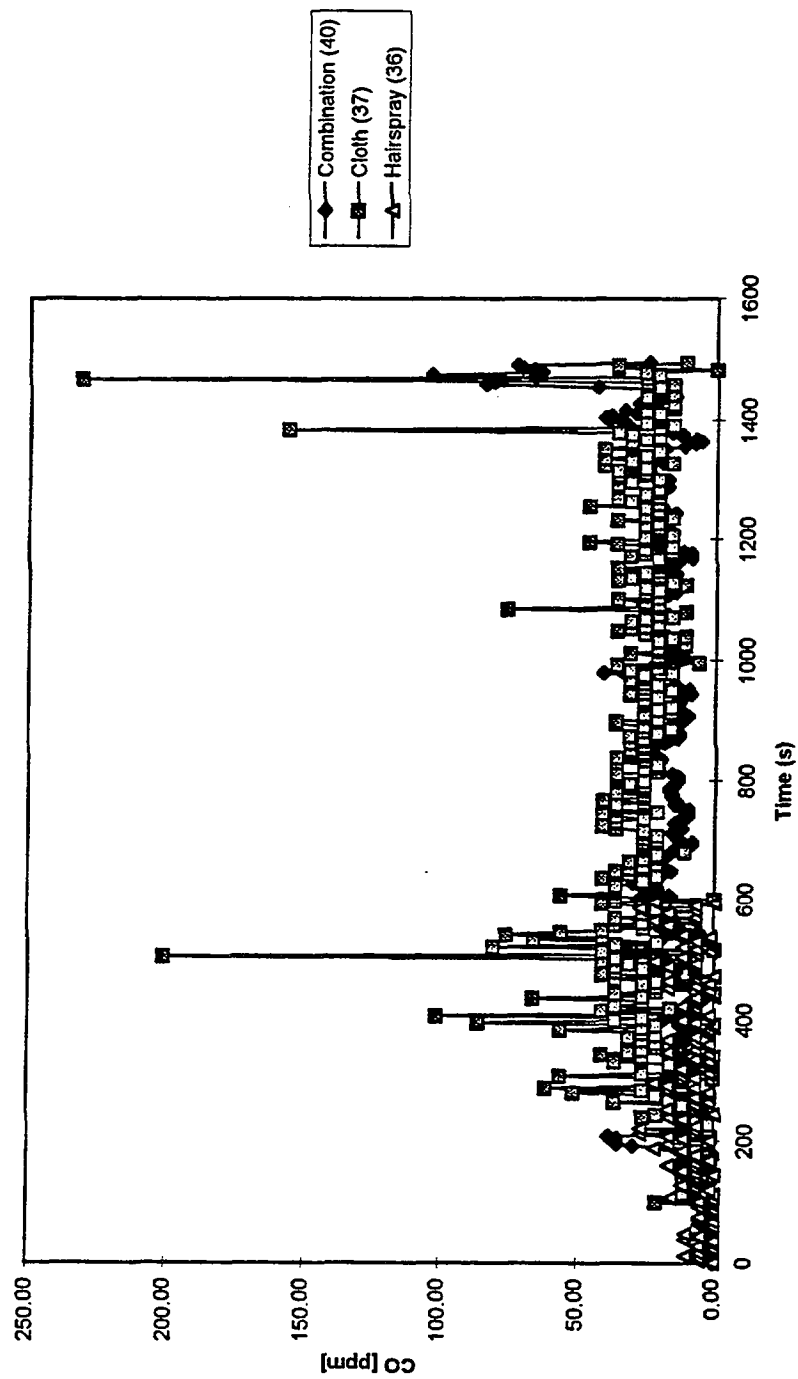
Temperature Rise at TC 13 vs. Time



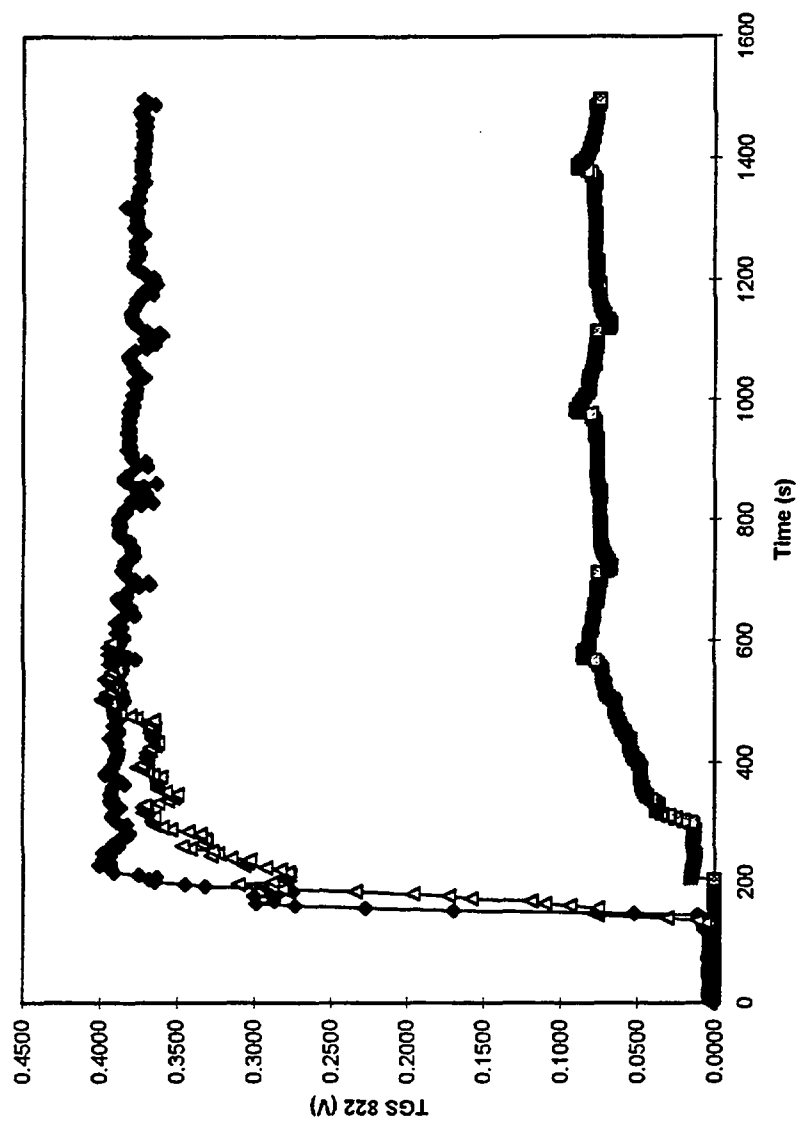
CO2 Concentration vs. Time



CO Concentration vs. Time

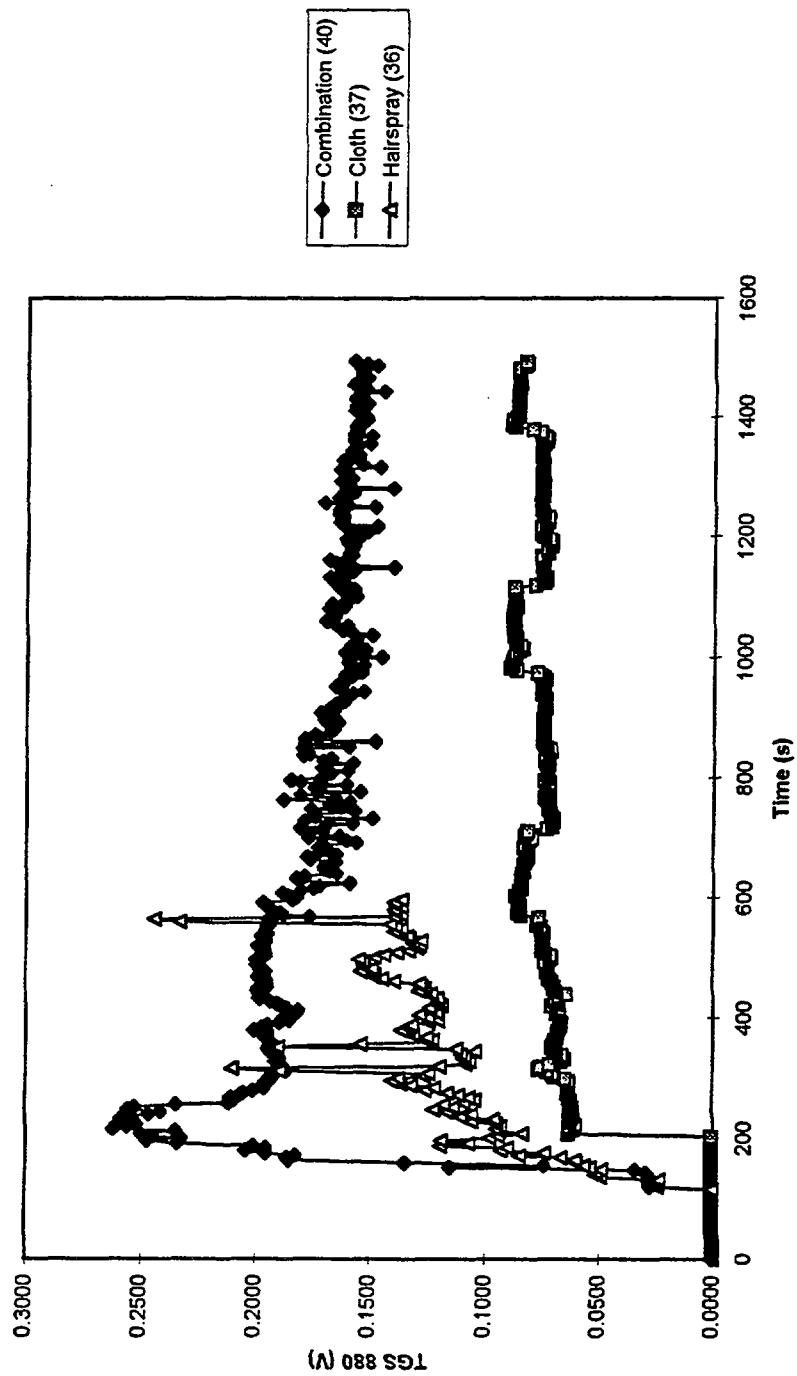


TGS 822 Output vs. Time

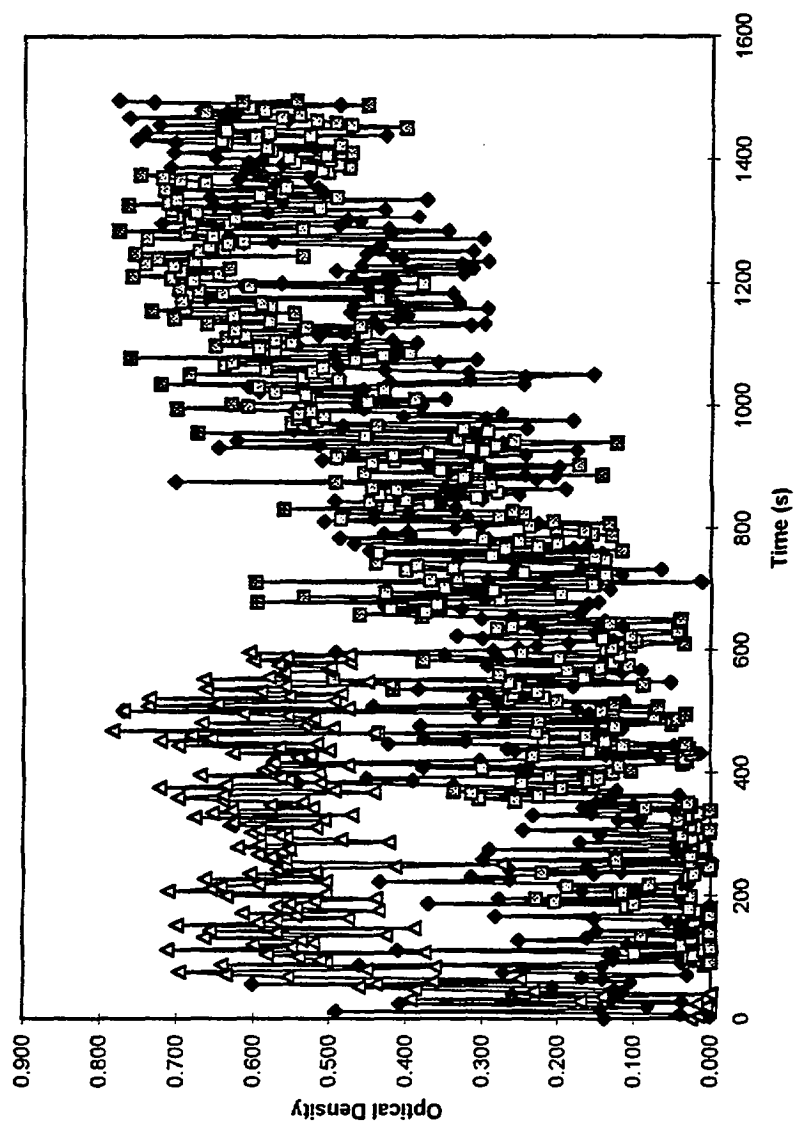


◆ Combination (40)
 ■ Cloth (37)
 ▲ Hairspray (36)

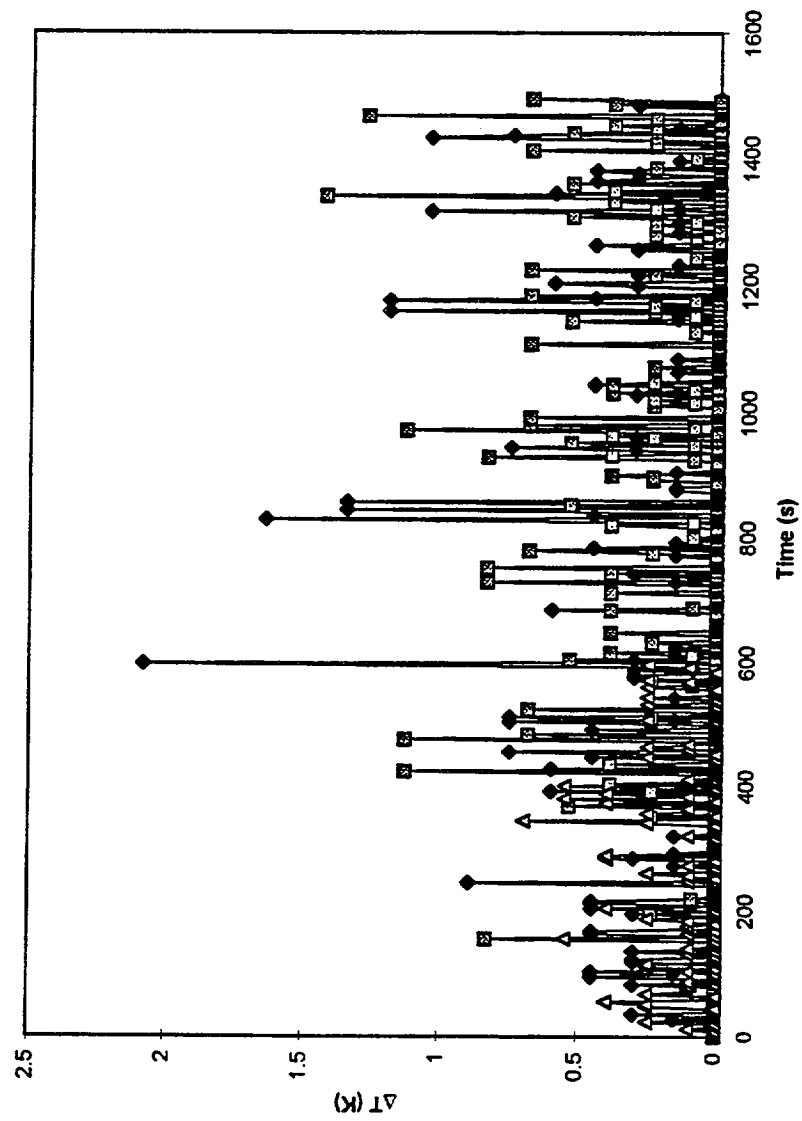
TGS 880 Output vs. Time



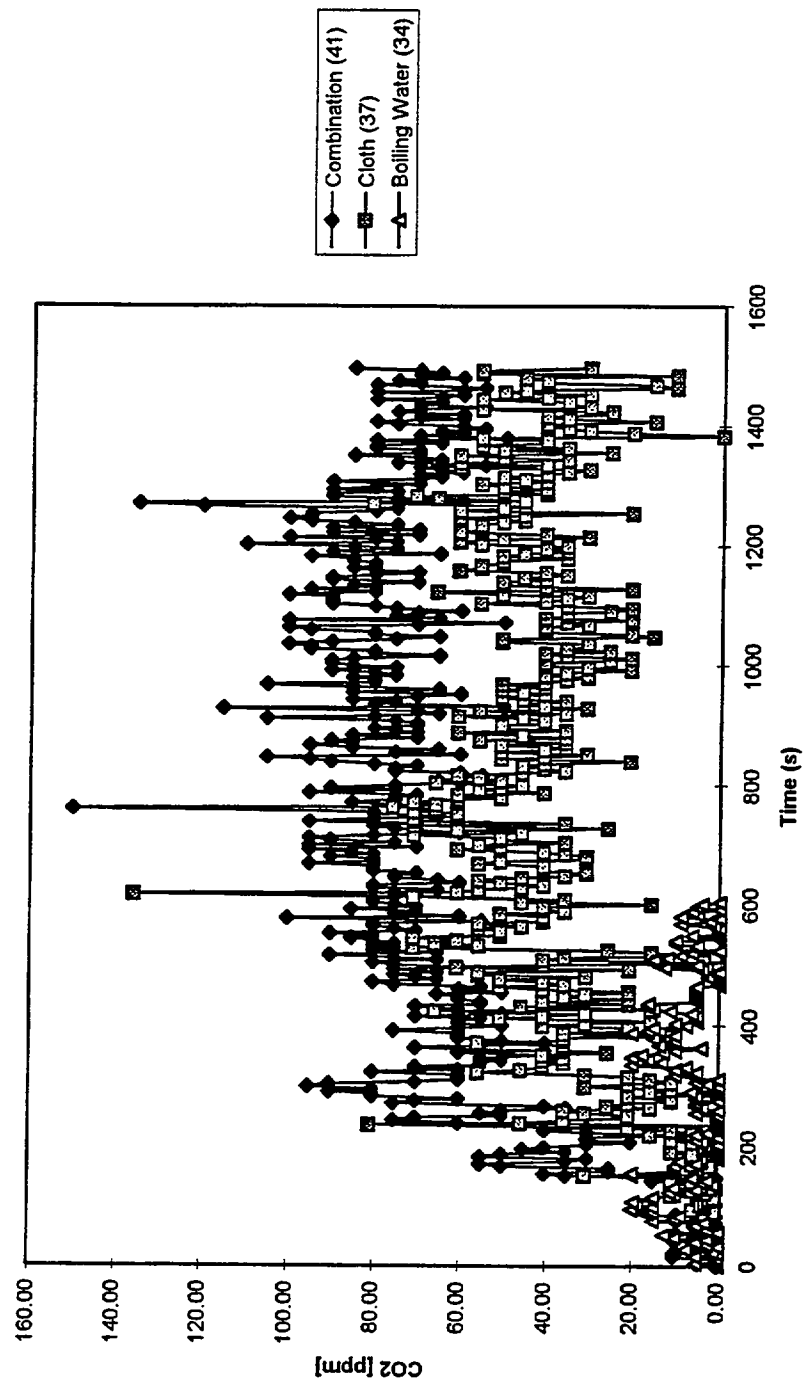
Optical Density vs. Time



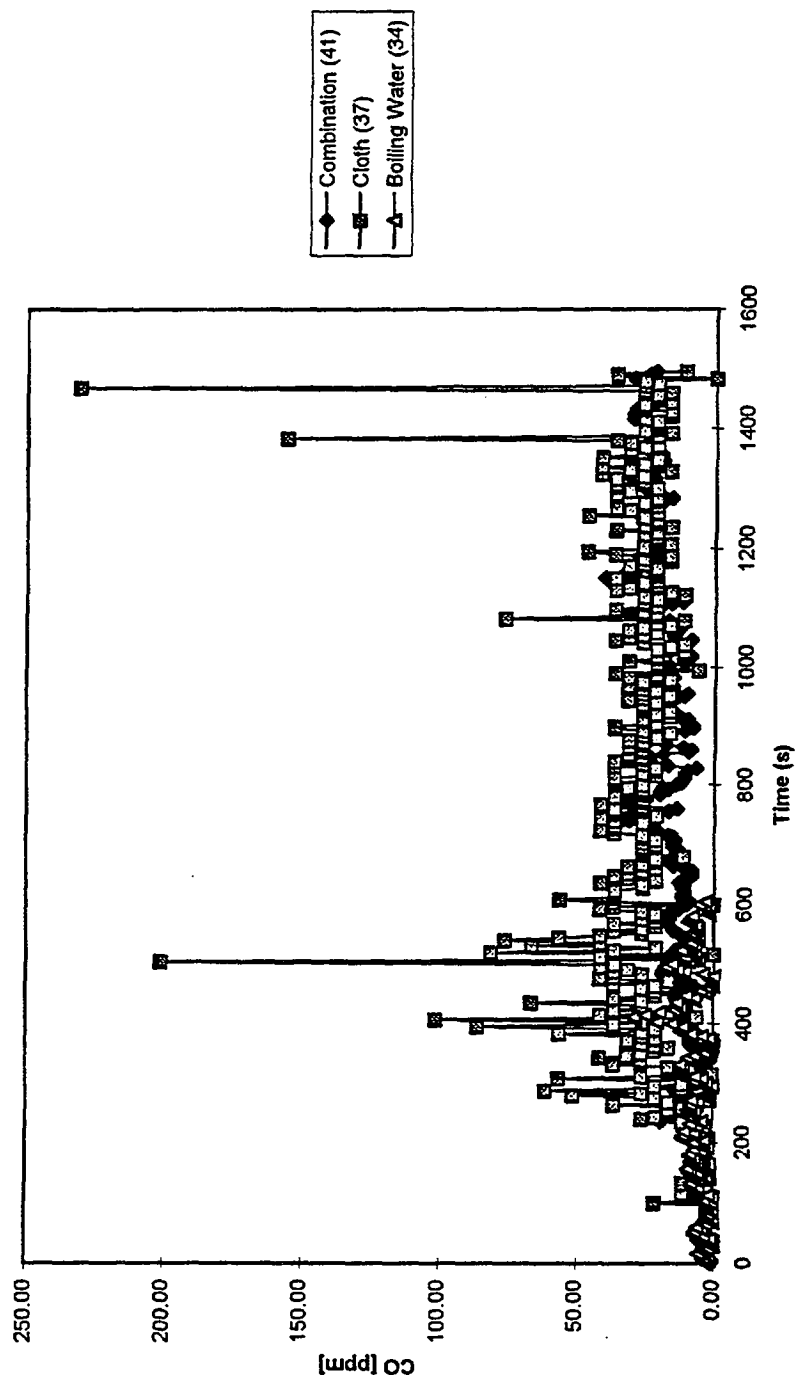
Temperature Rise at TC 13 vs. Time



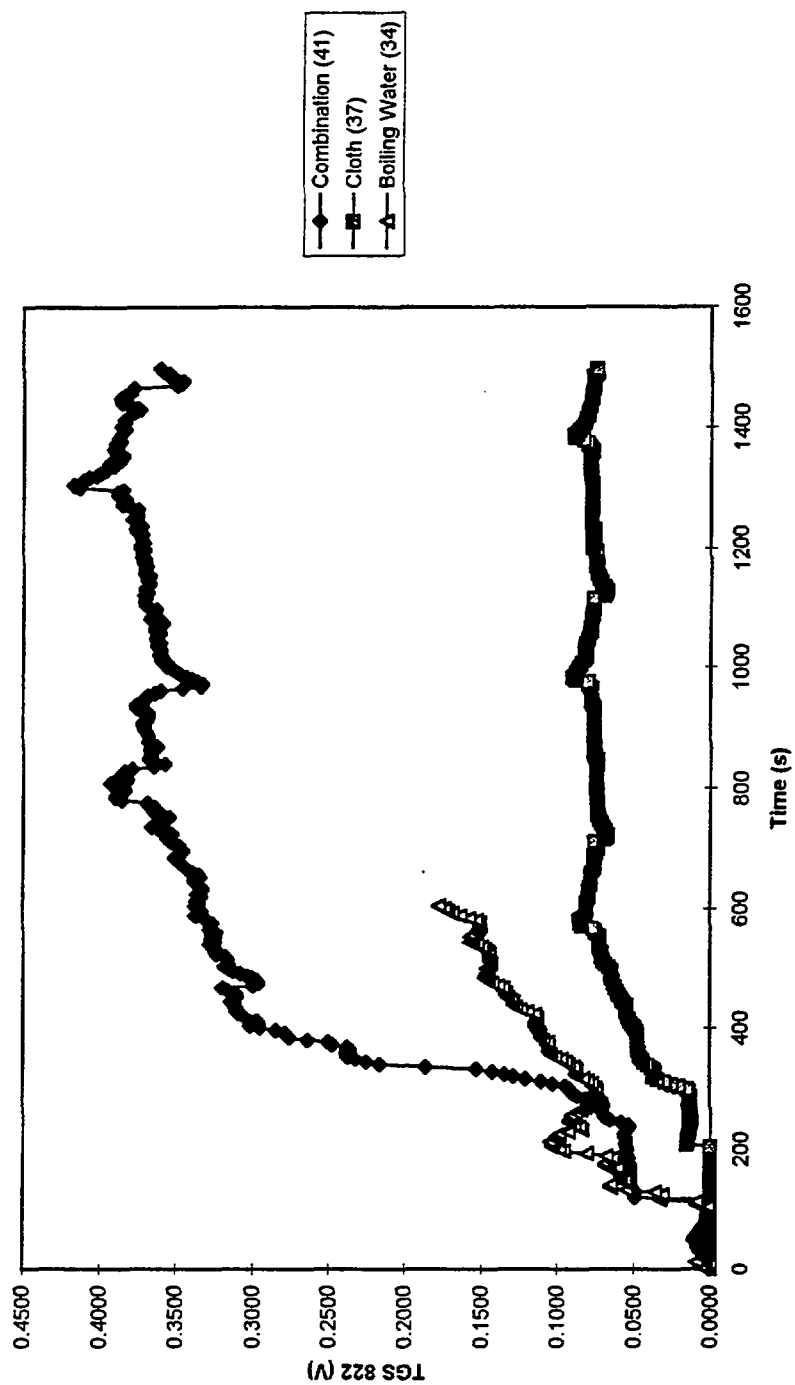
CO2 Concentration vs. Time



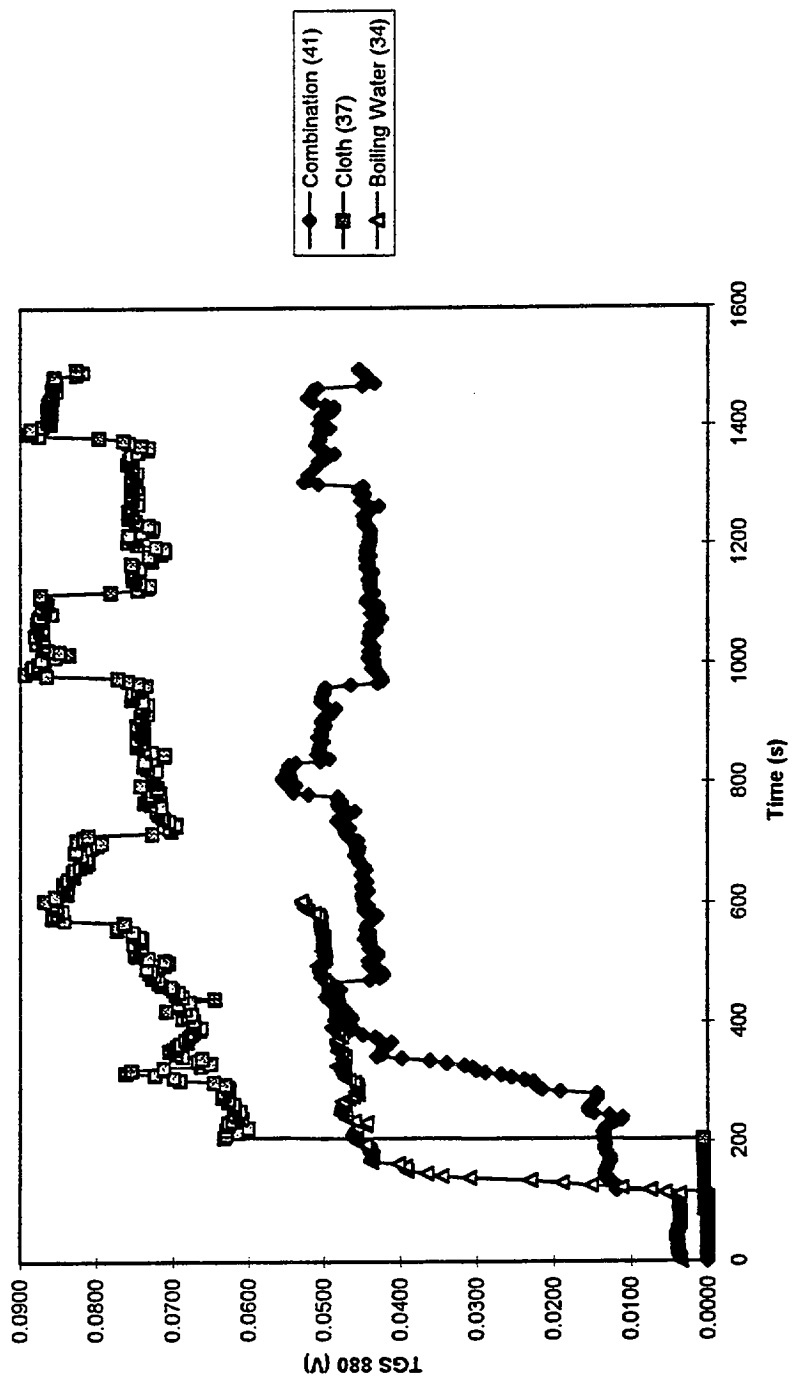
CO Concentration vs. Time



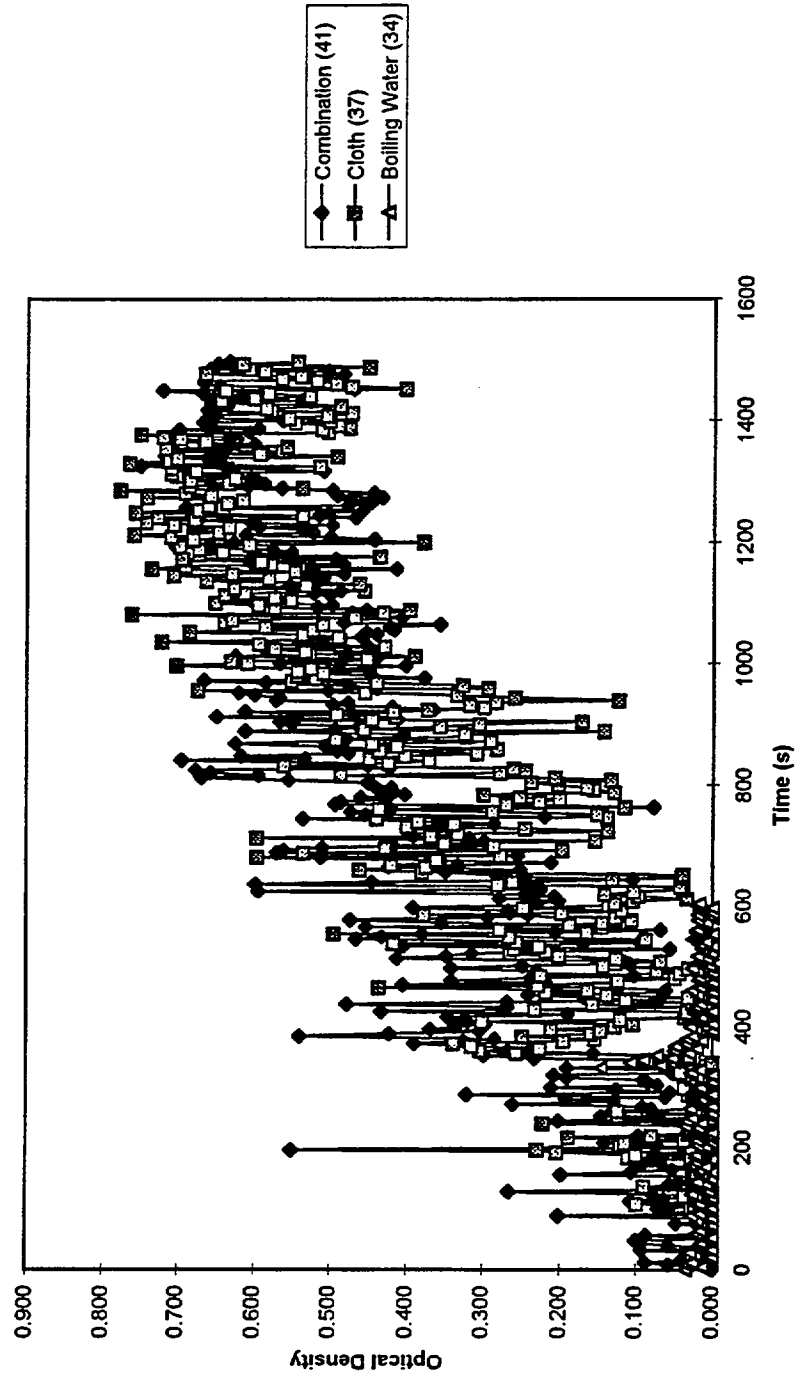
TGS 822 Output vs. Time



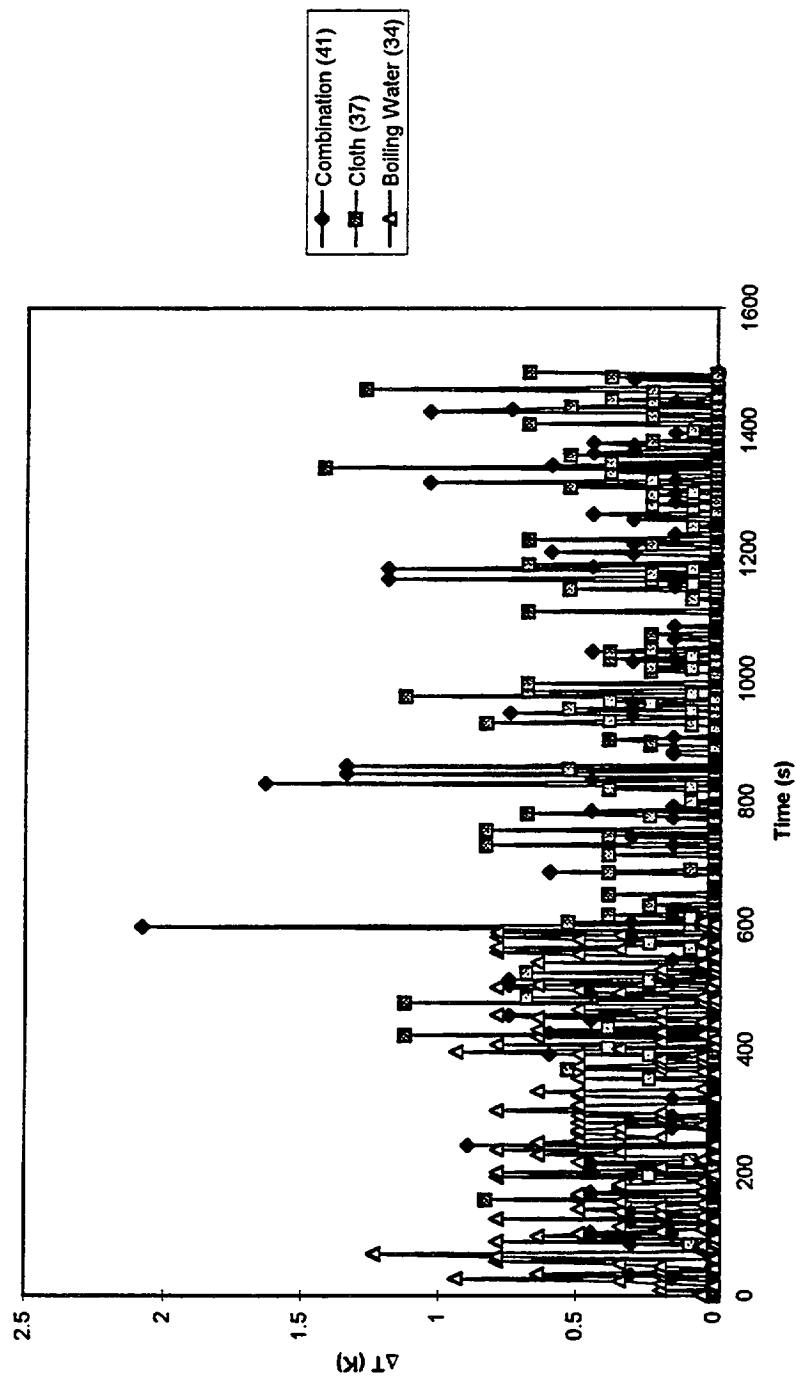
TGS 880 Output vs. Time

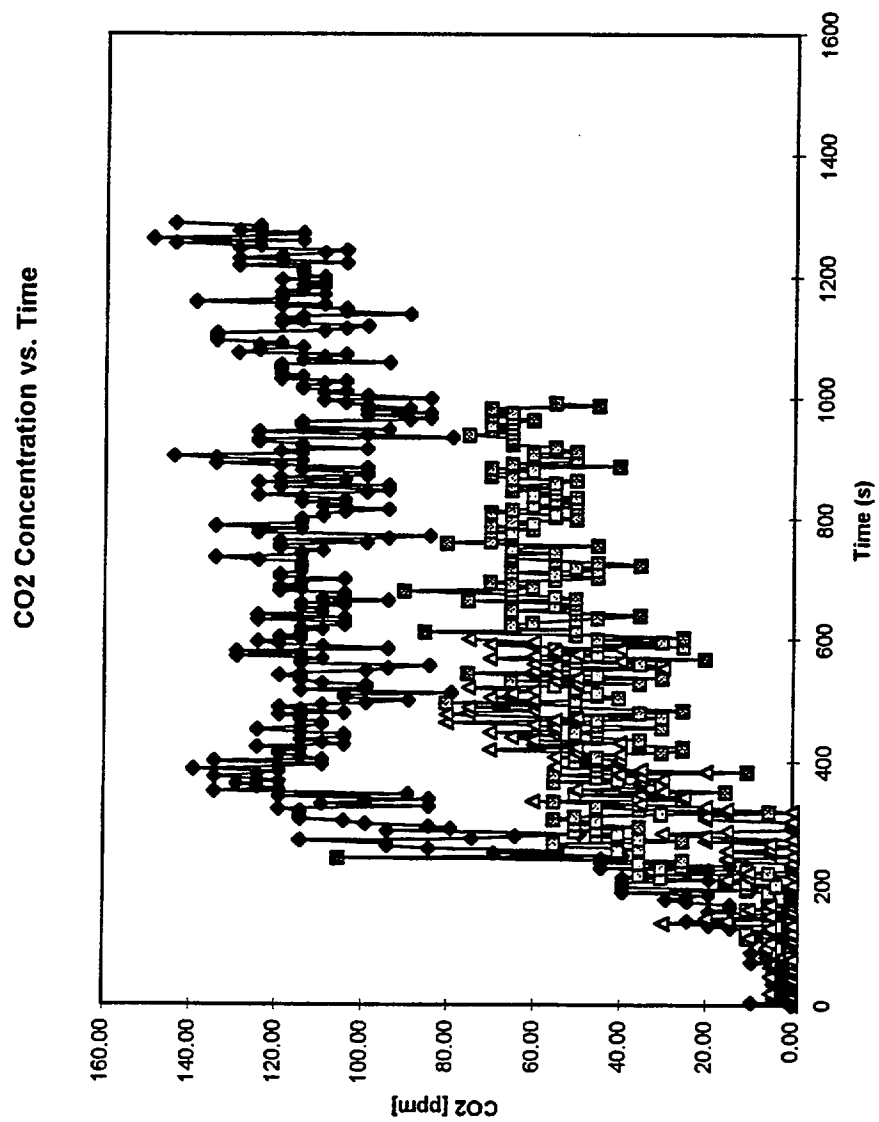


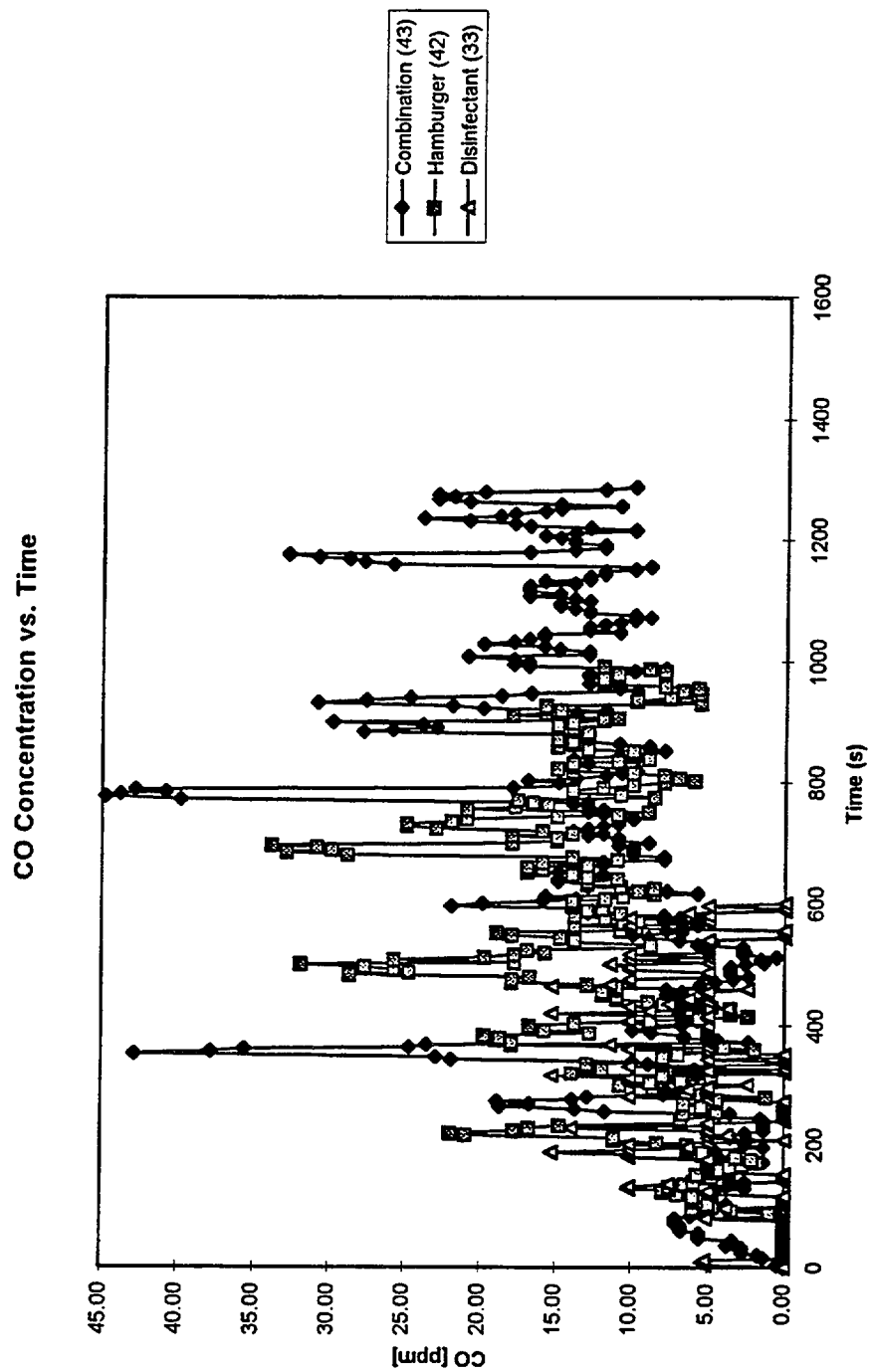
Optical Density vs. Time



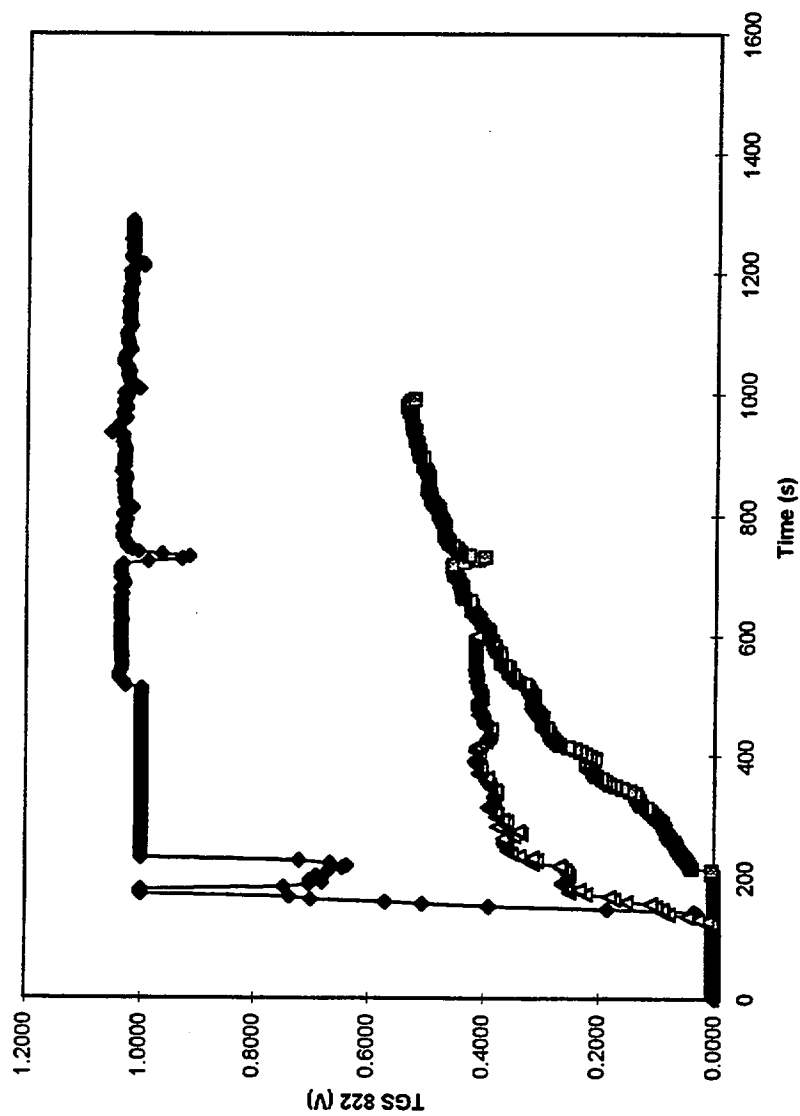
Temperature Rise at TC 13 vs. Time



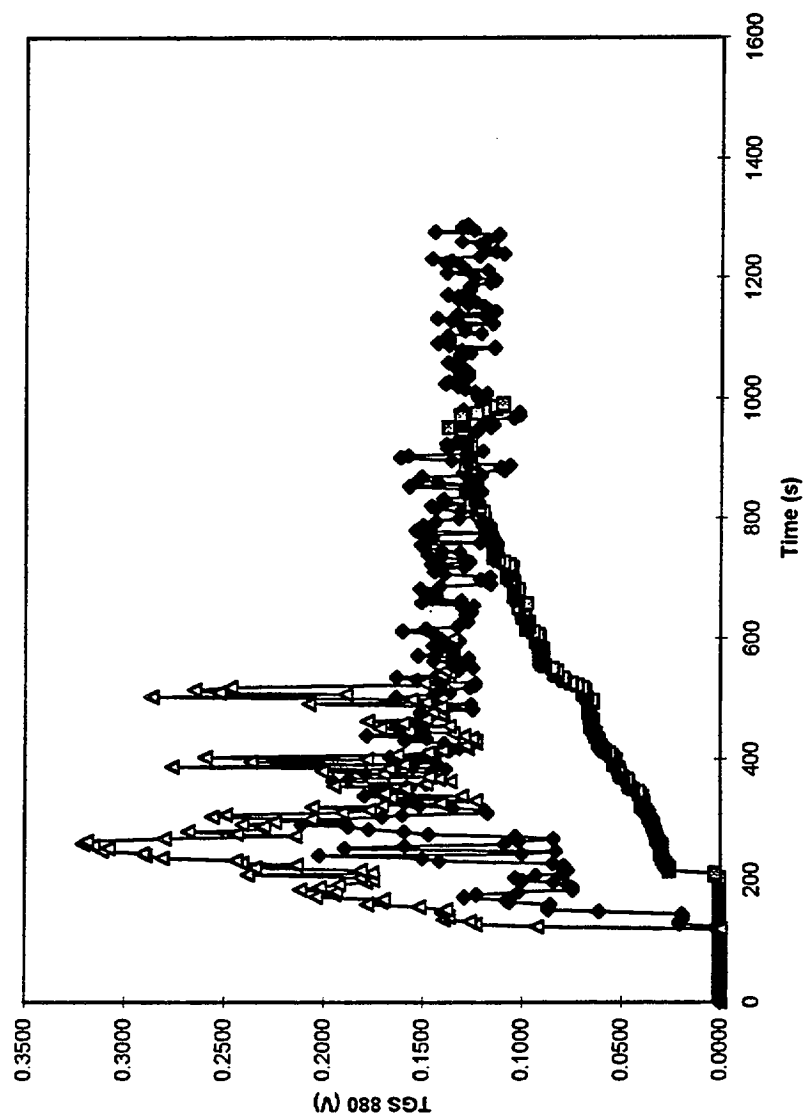




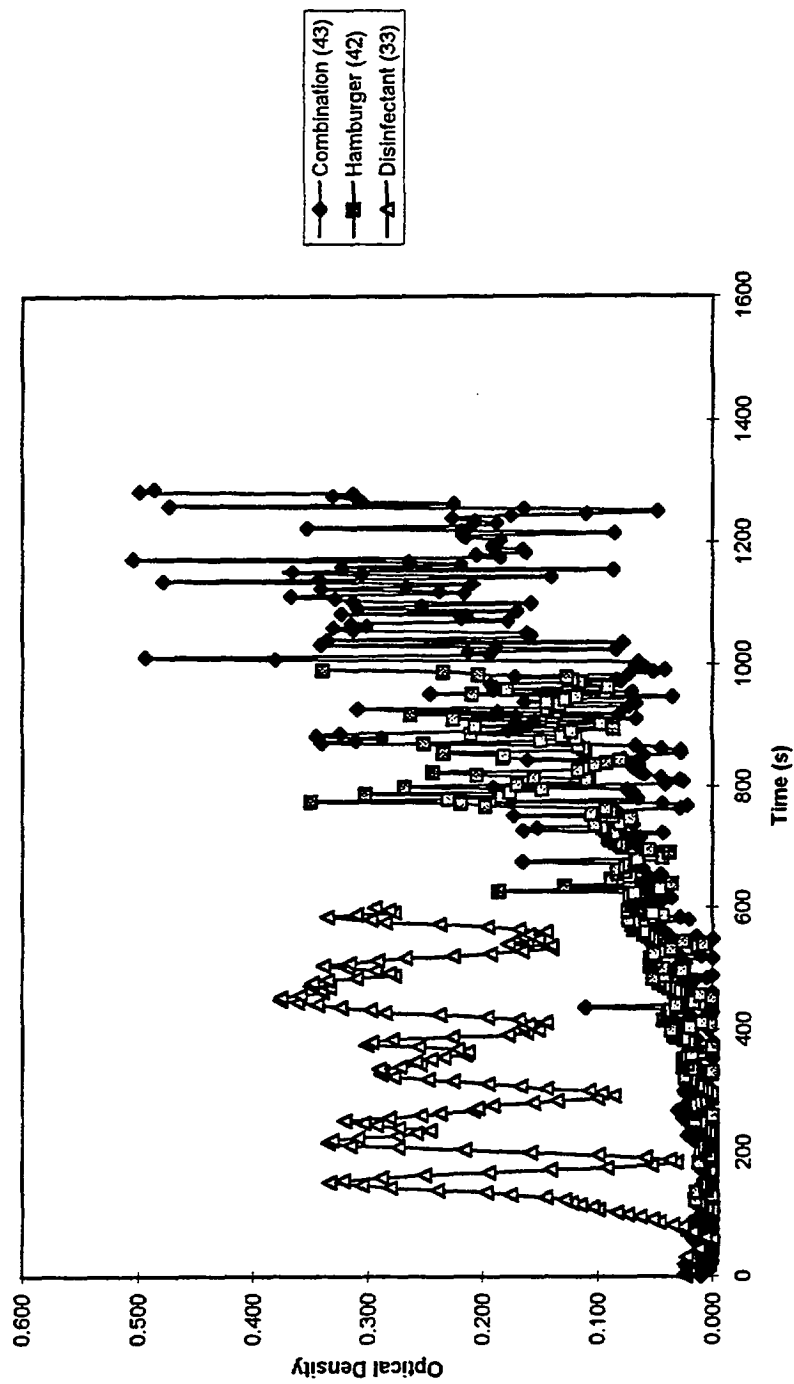
TGS 822 Output vs. Time



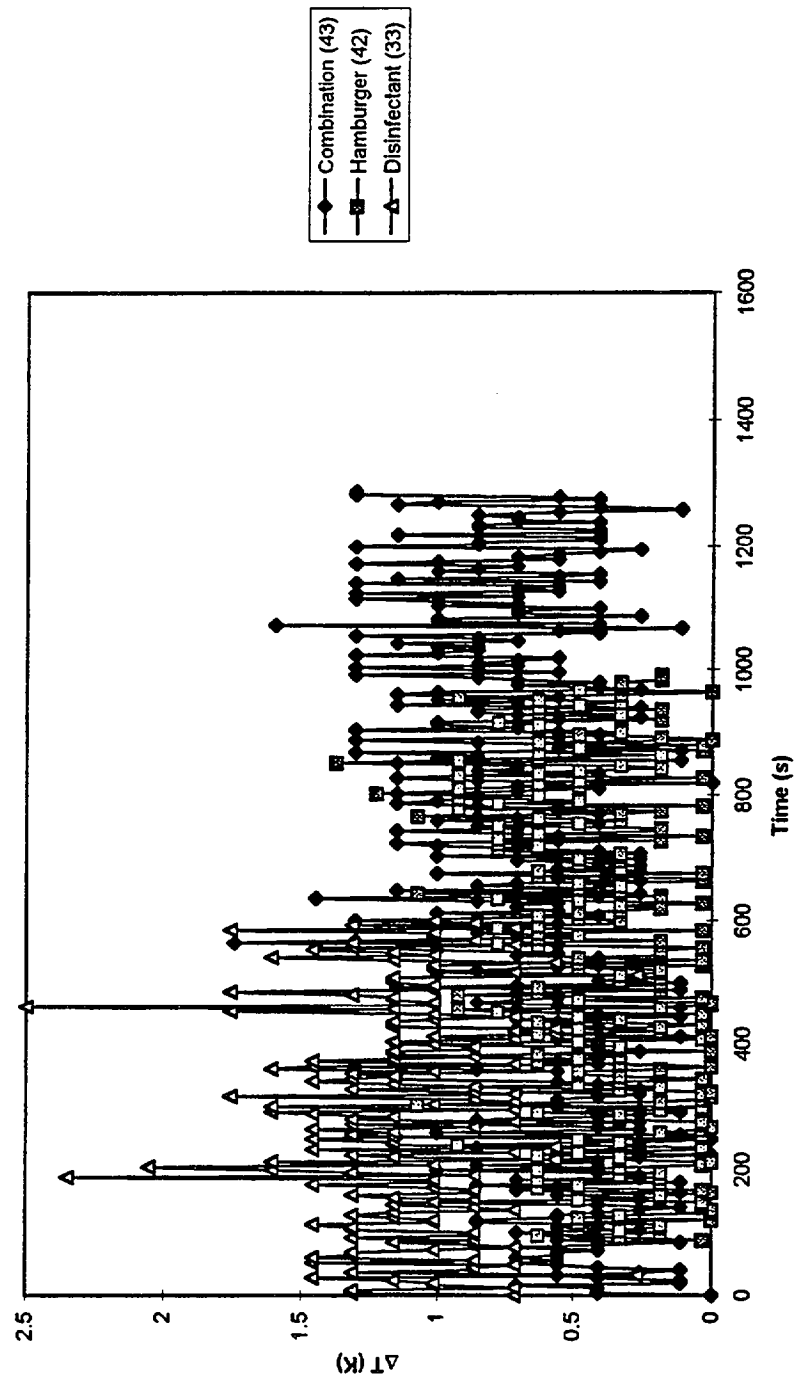
TGS 880 vs. Time



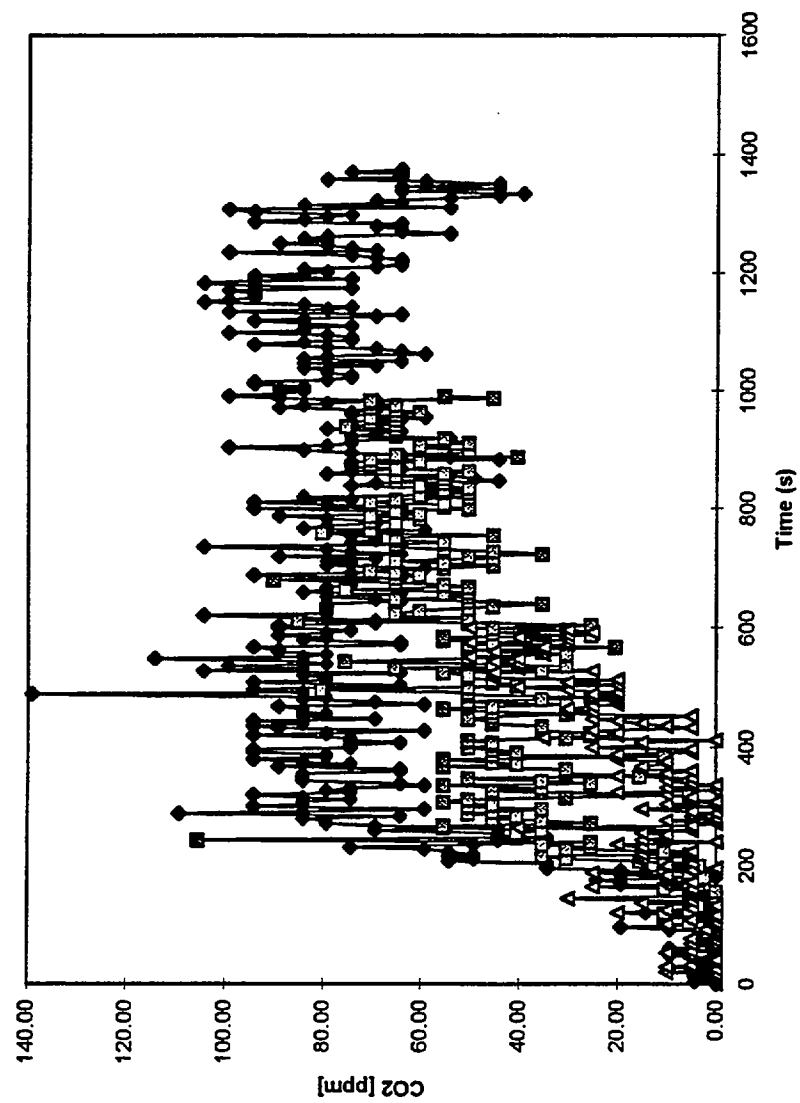
Optical Density vs. Time



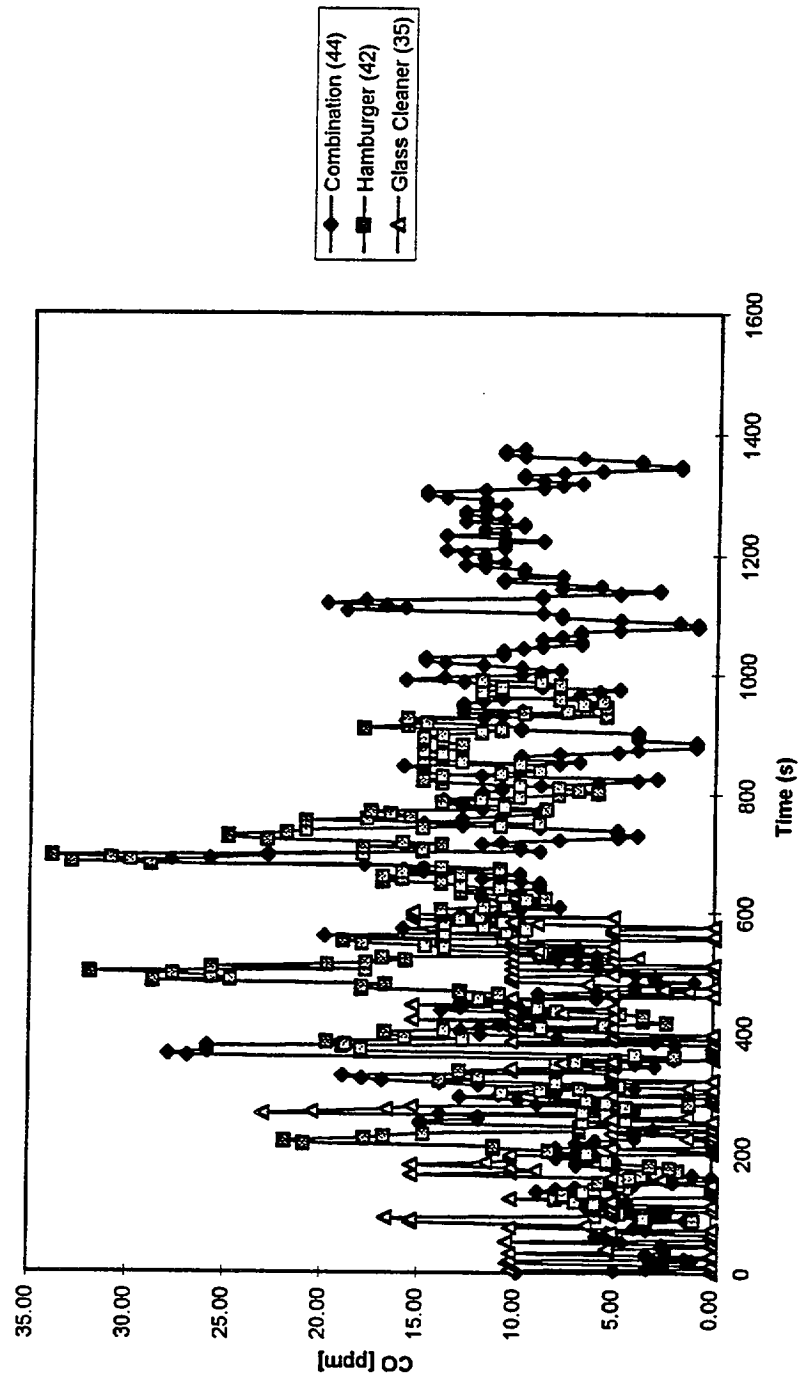
Temperature Rise at TC 13 vs. Time



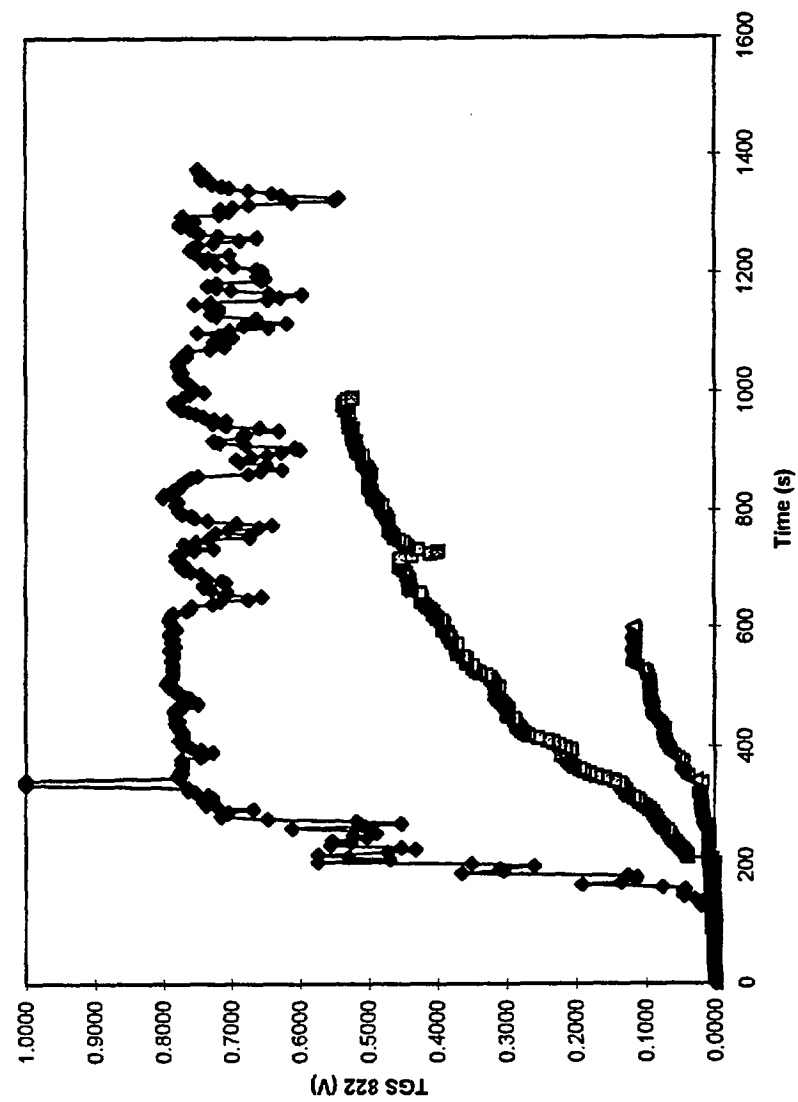
CO2 Concentration vs. Time



CO Concentration vs. Time

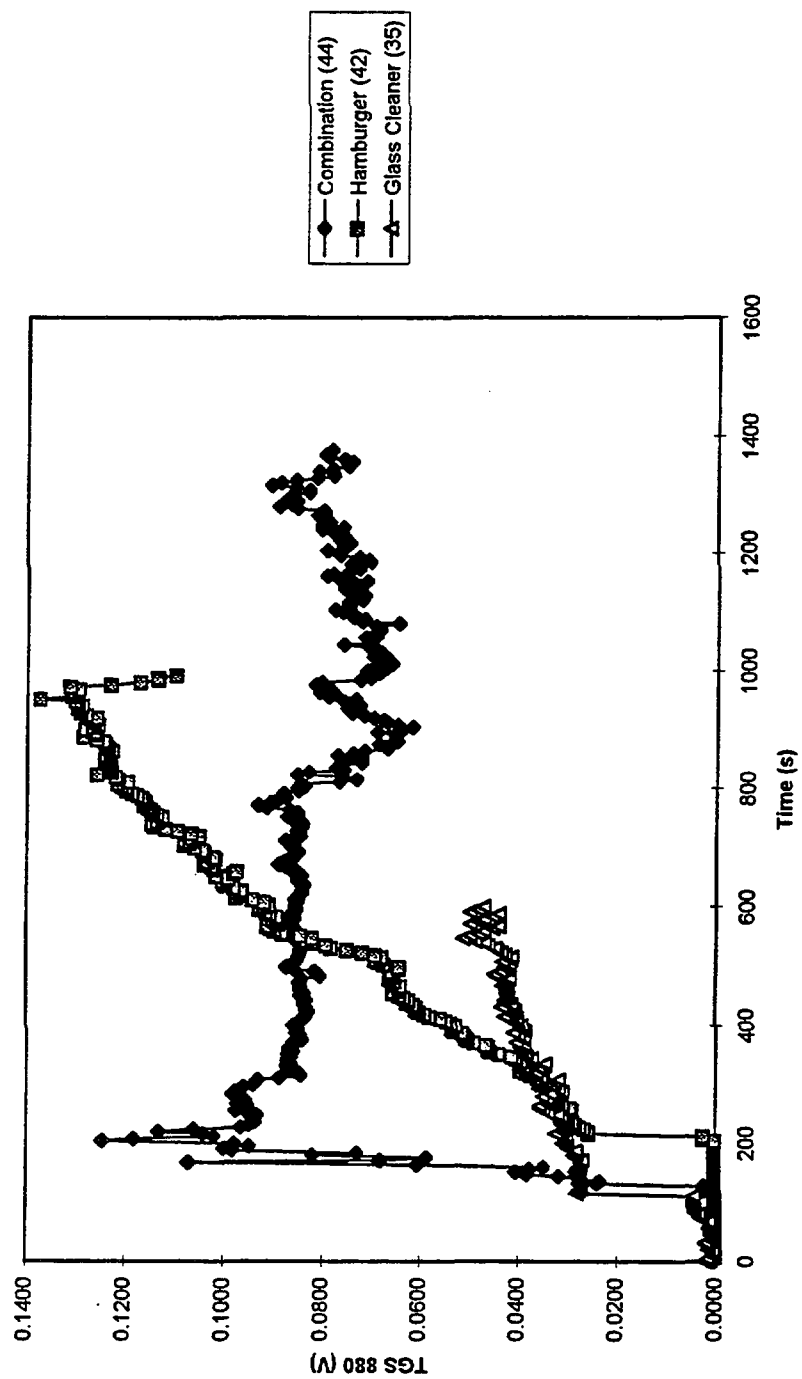


TGS 822 Output vs. Time

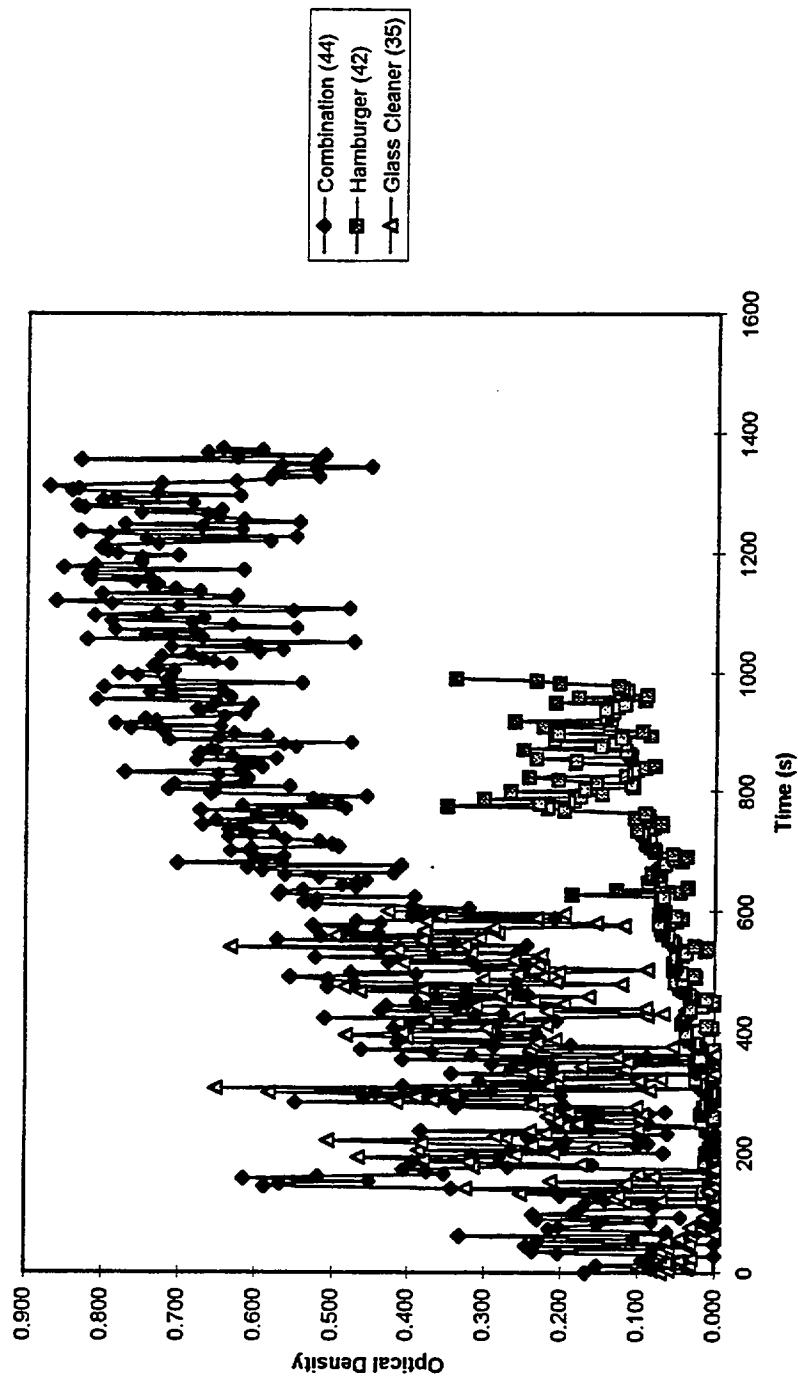


Combination (44)
Hamburger (42)
Glass Cleaner (35)

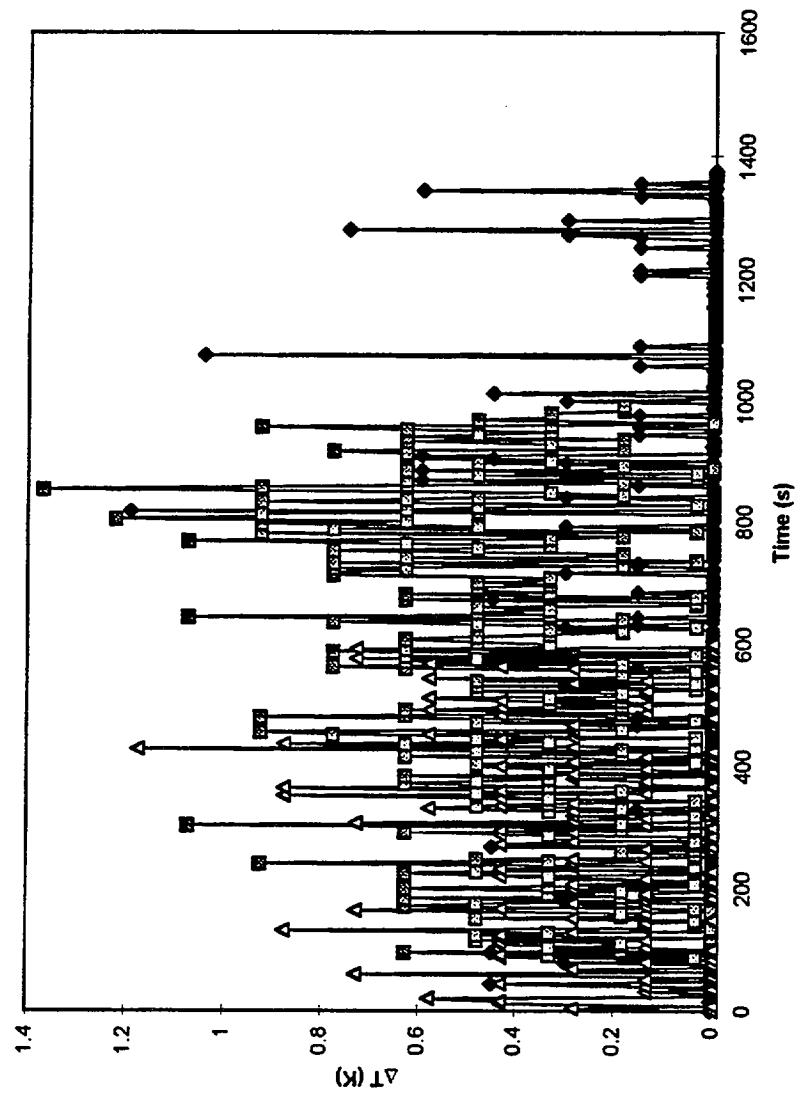
TGS 880 Output vs. Time



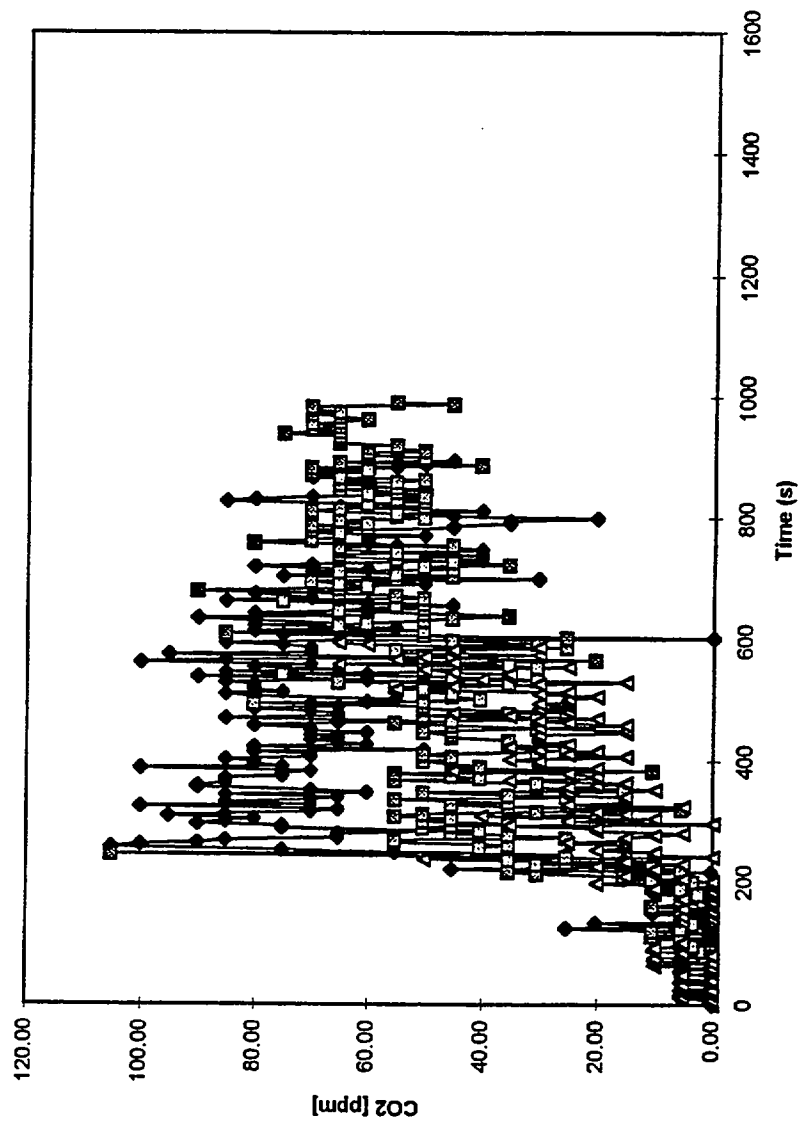
Optical Density vs. Time



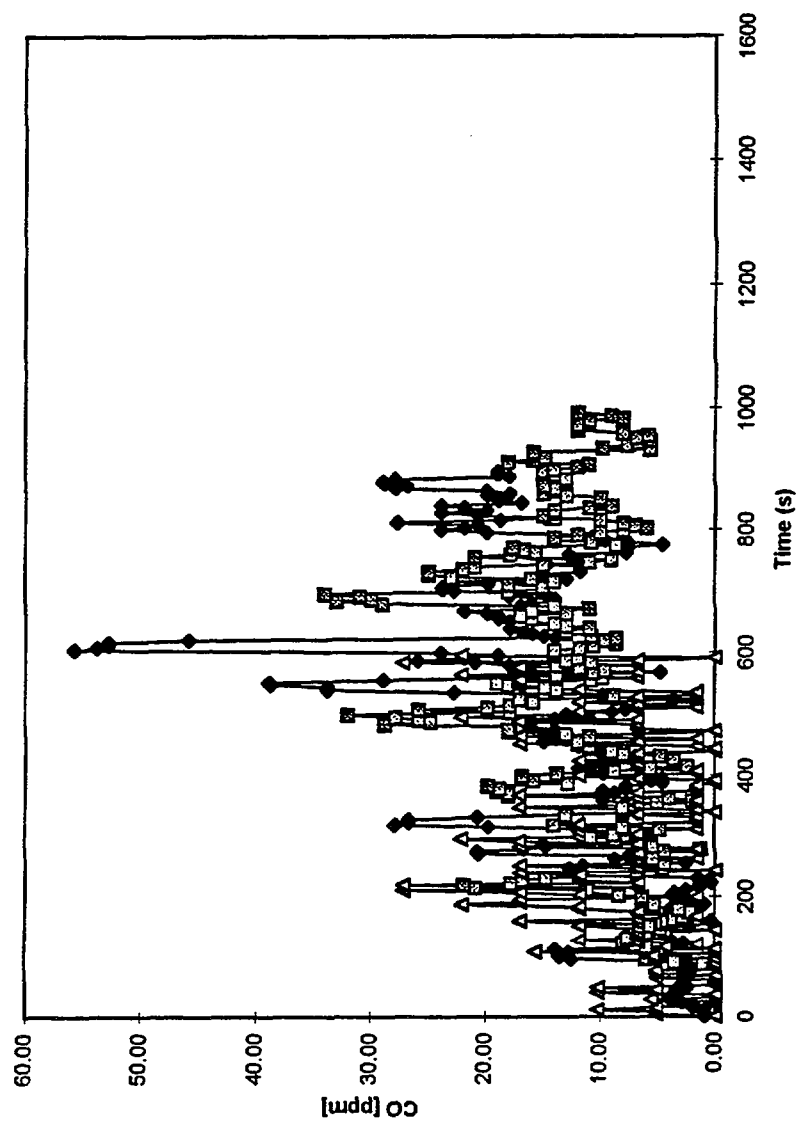
Temperature Rise at TC 13 vs. Time



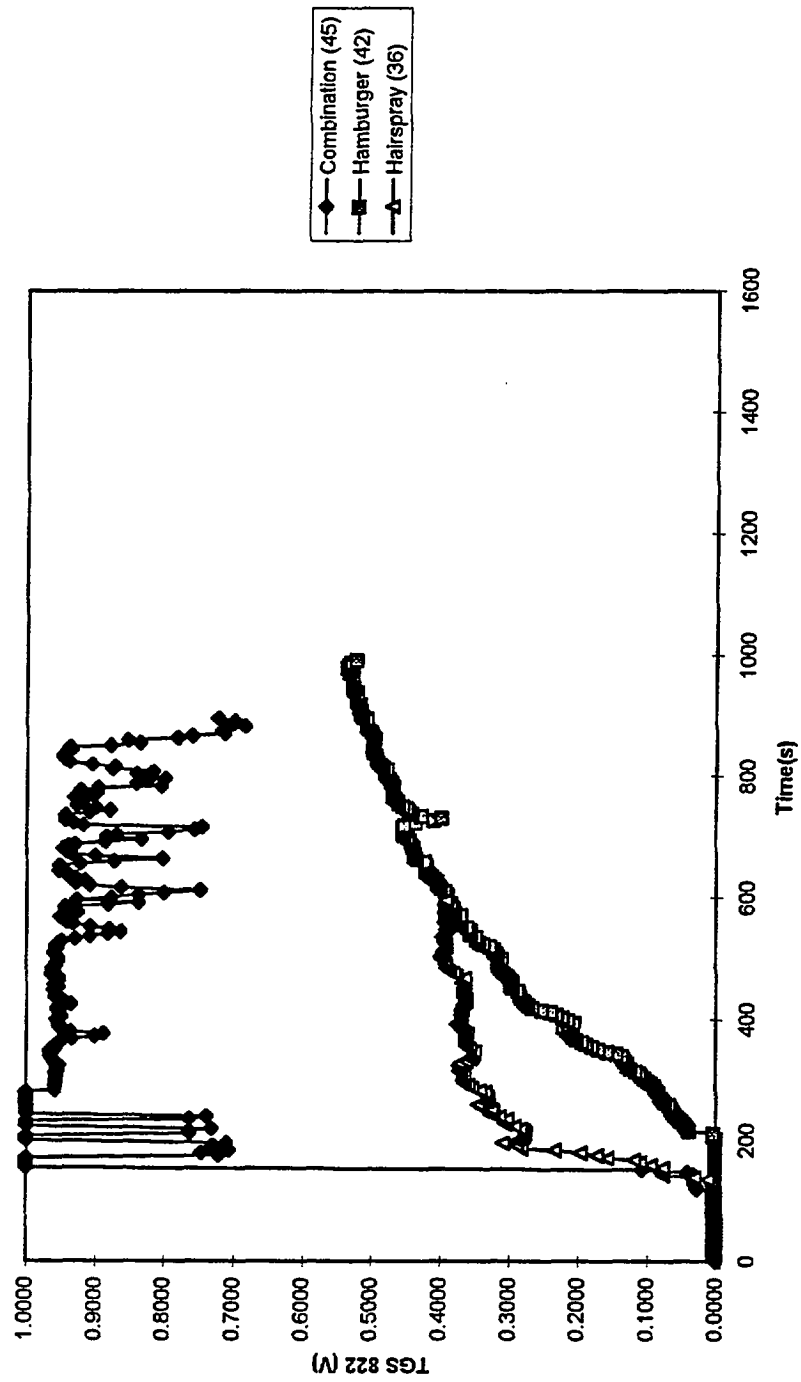
CO2 Concentration vs. Time



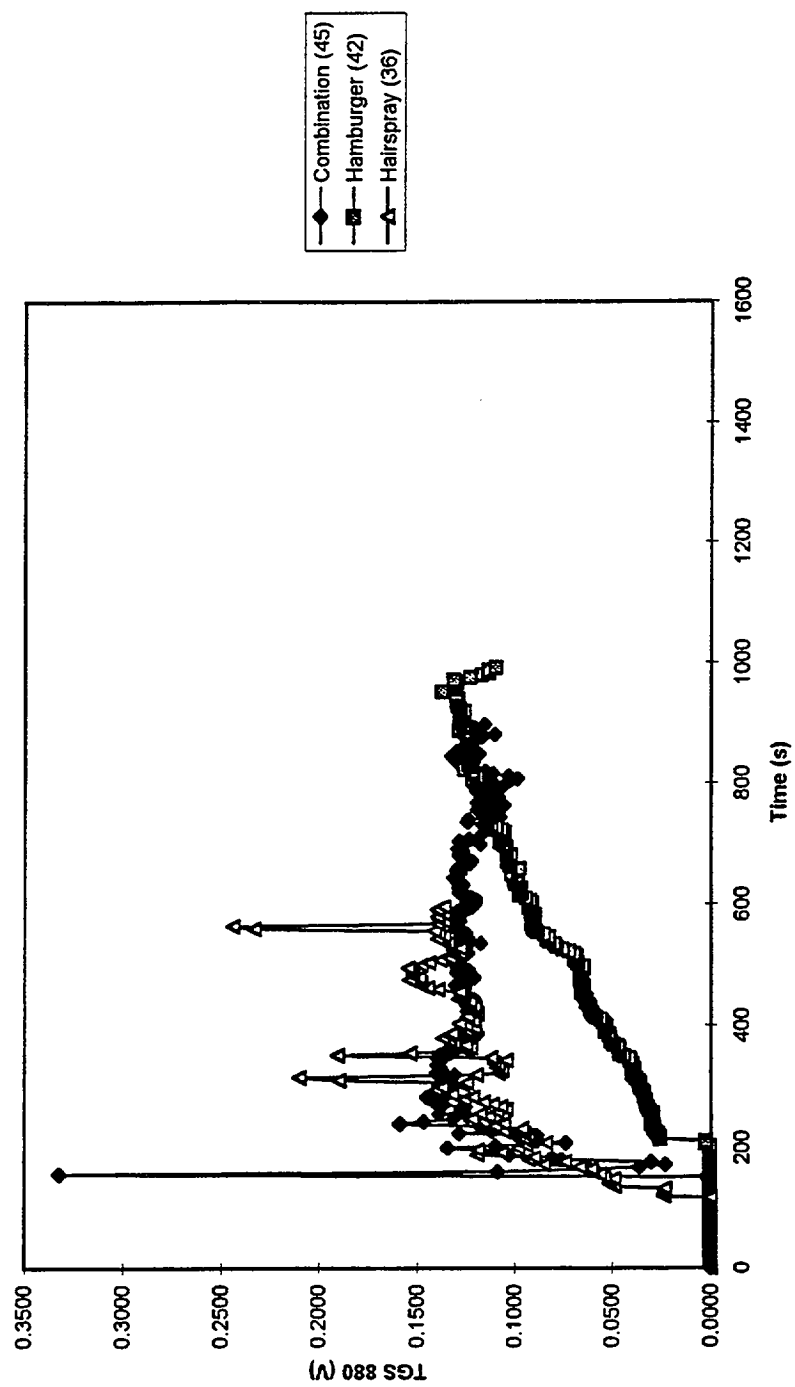
CO Concentration vs. Time



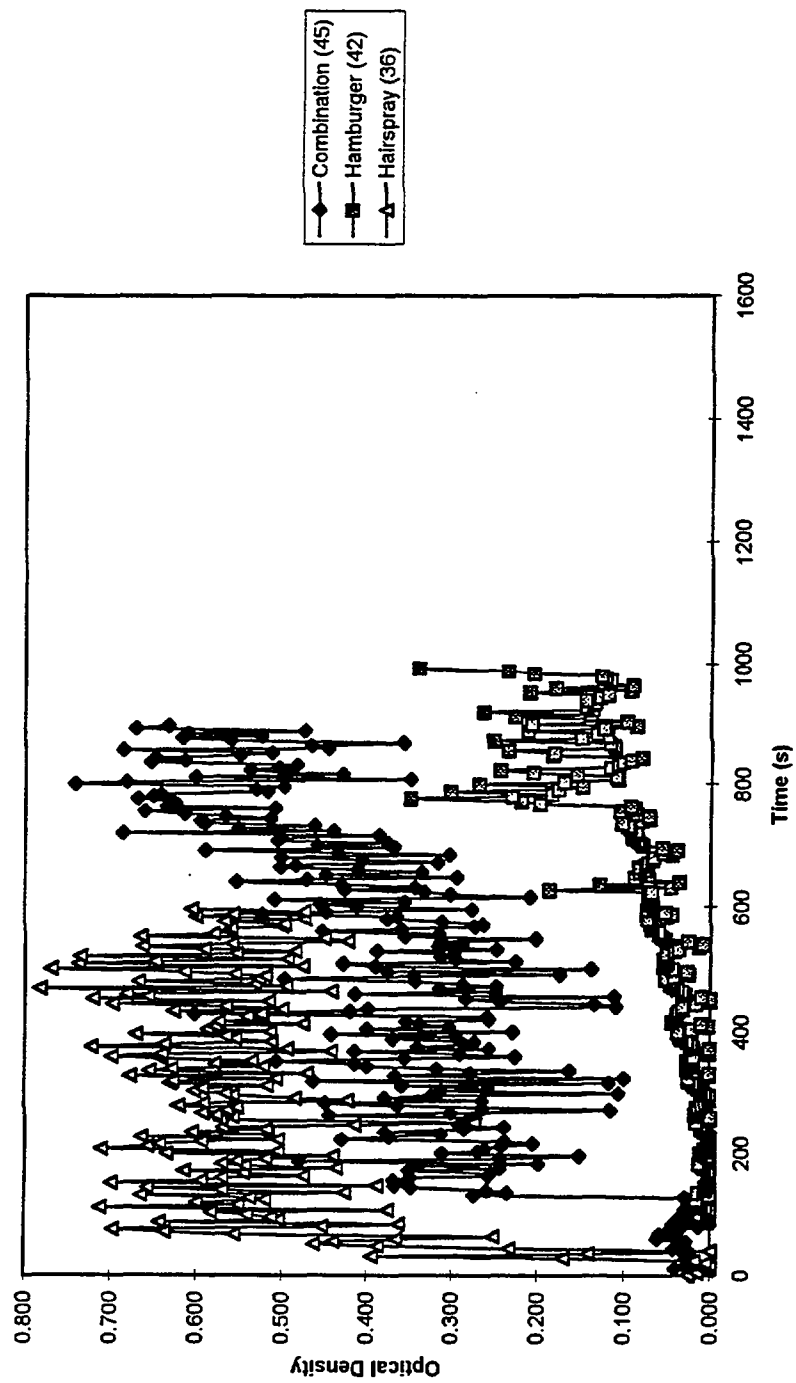
TGS 822 Output vs. Time



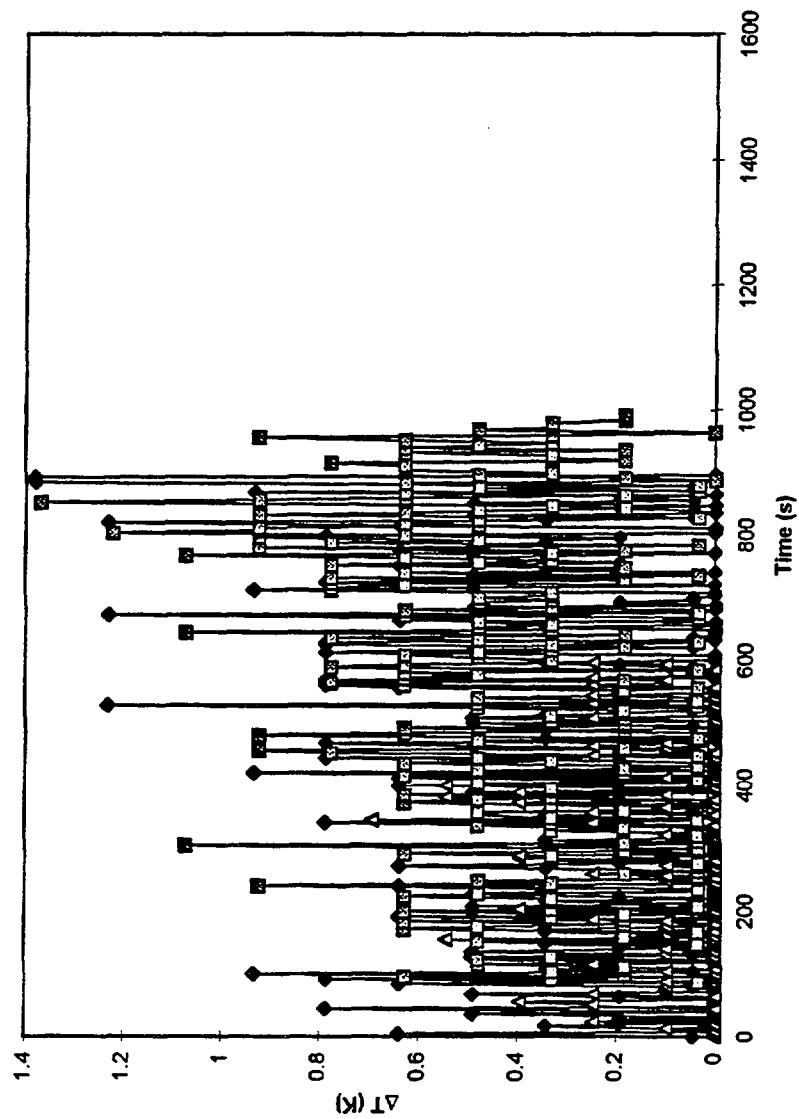
TGS 880 Output vs. Time



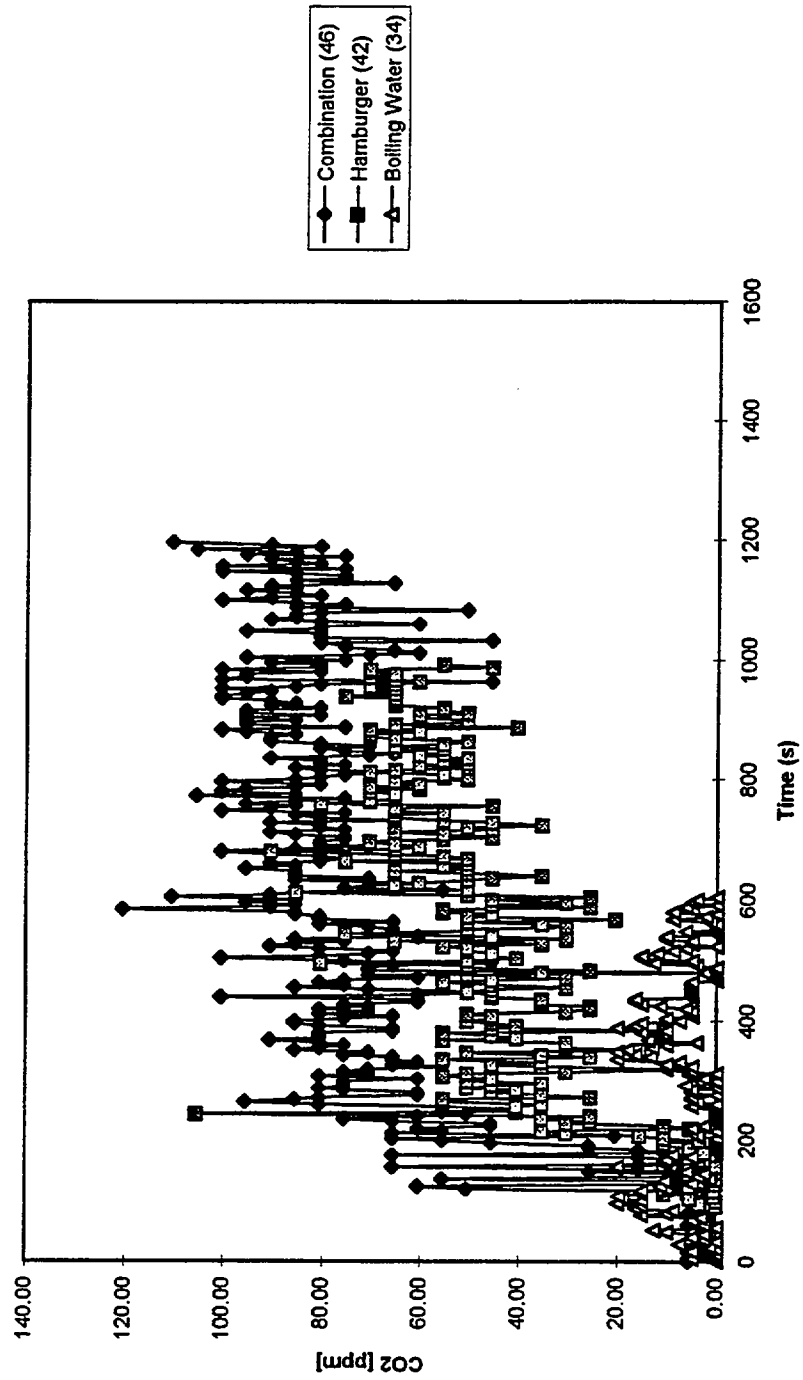
Optical Density vs. Time



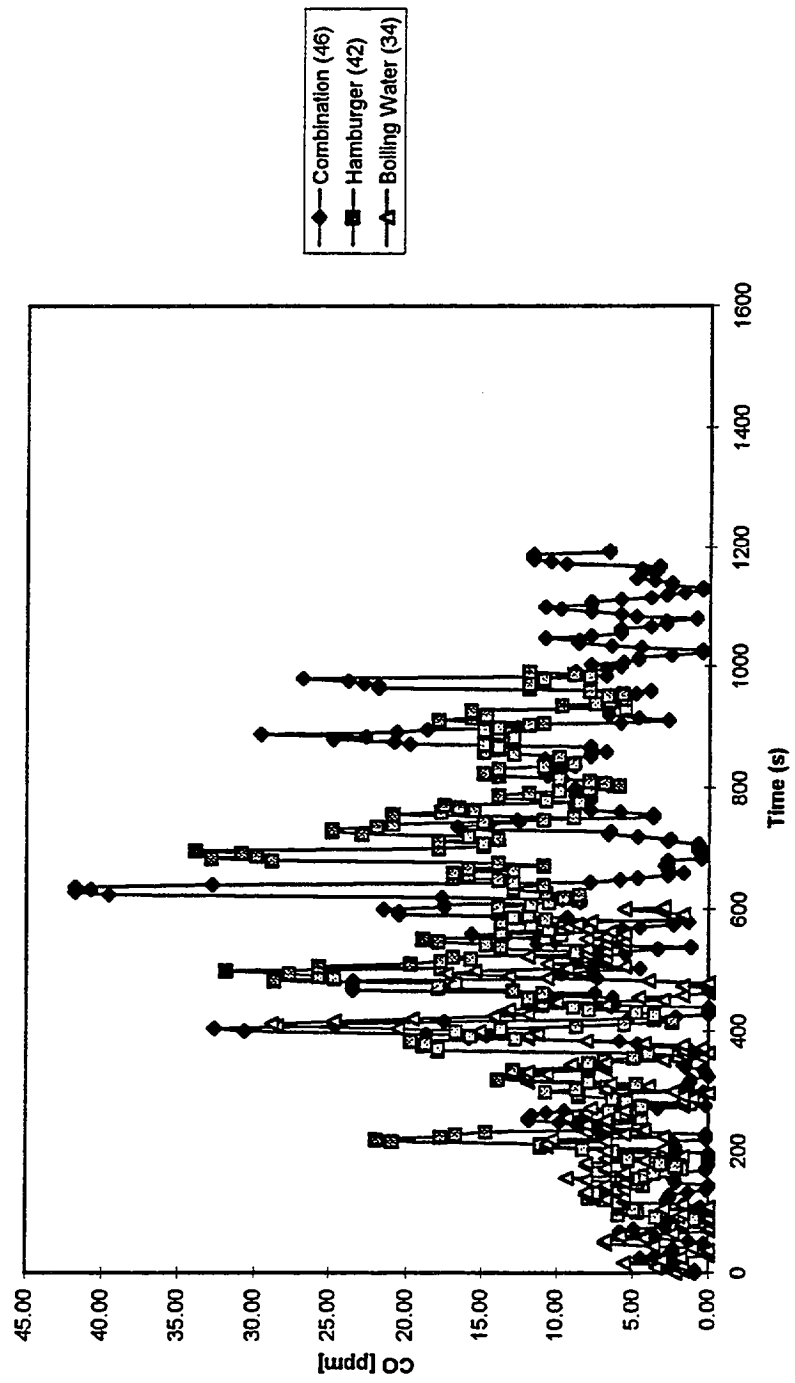
Temperature Rise at TC 13 vs. Time



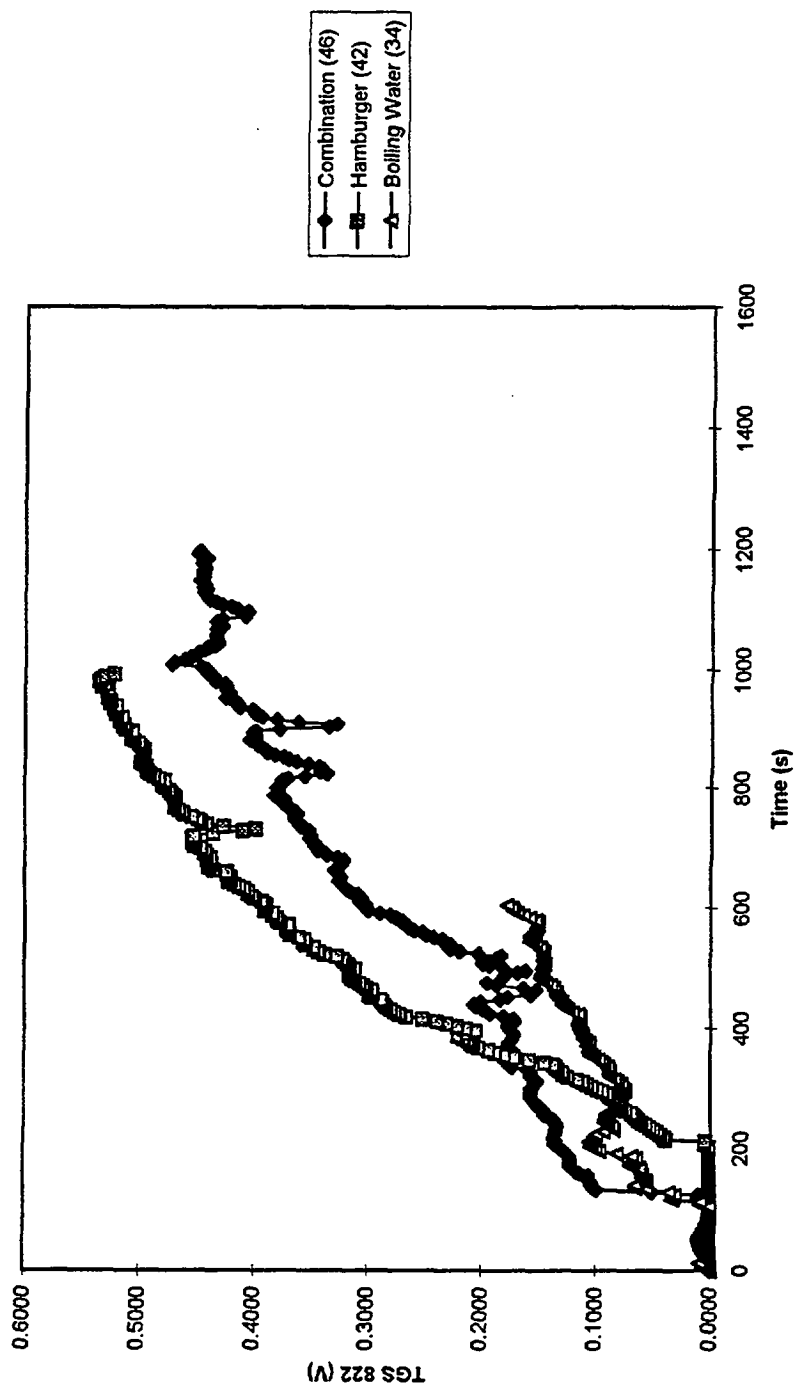
CO2 Concentration vs. Time



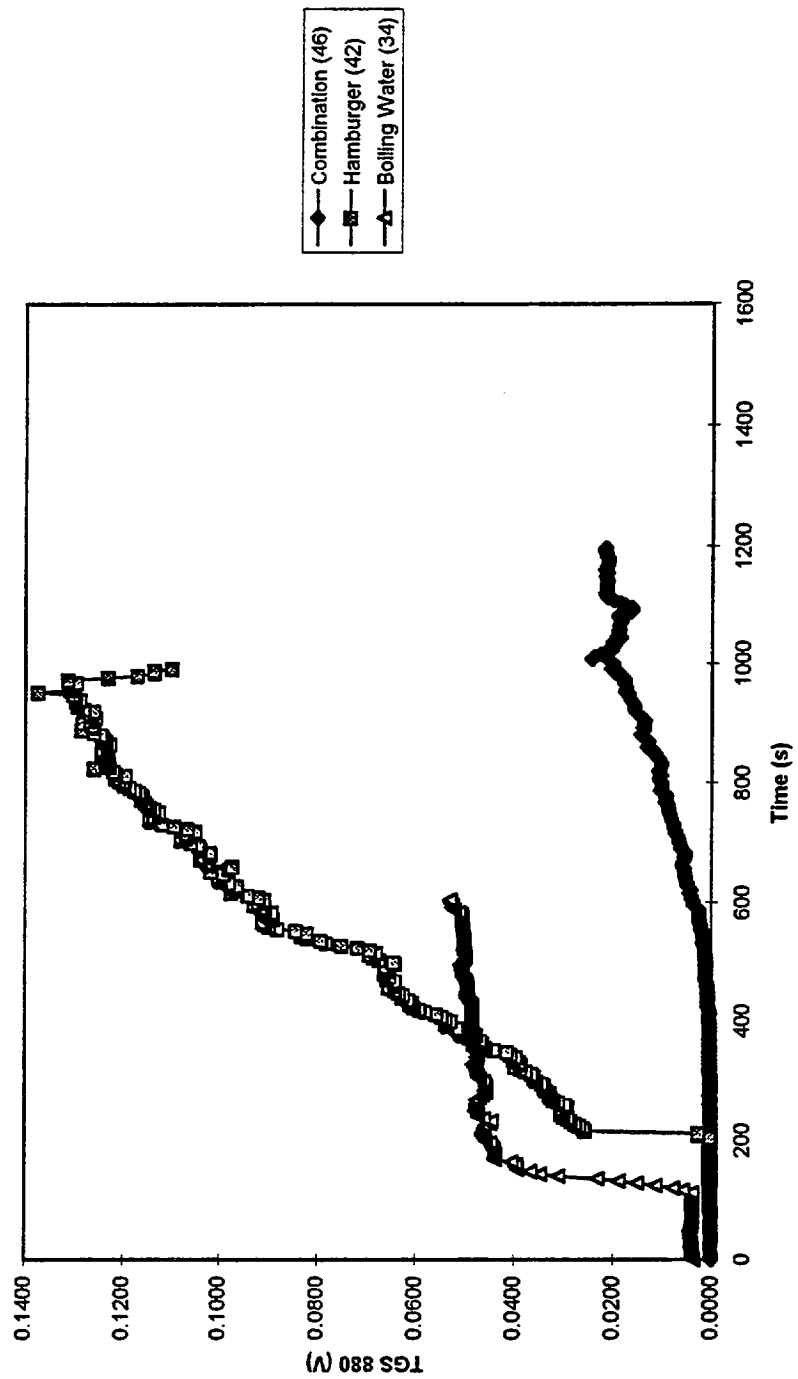
CO Concentration vs. Time



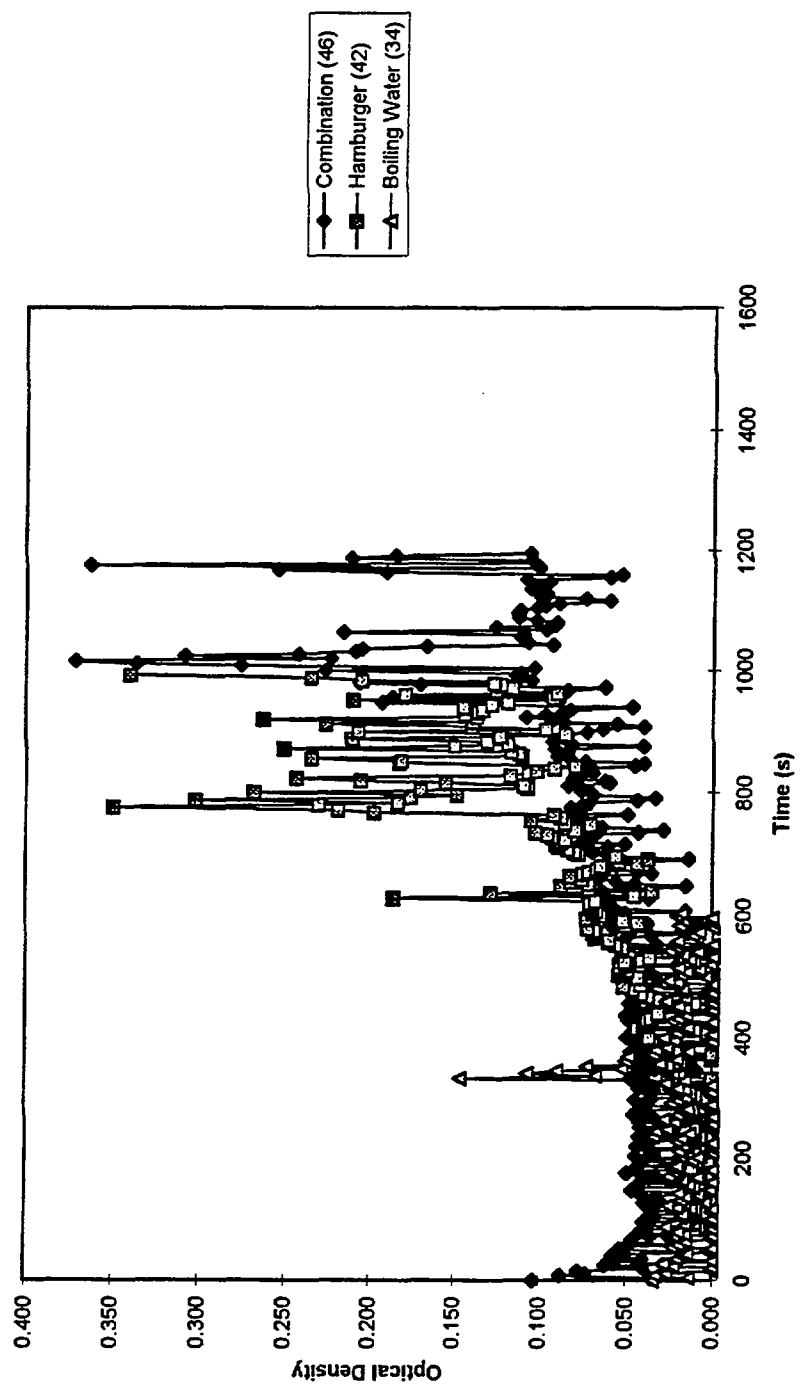
TGS 822 Output vs. Time



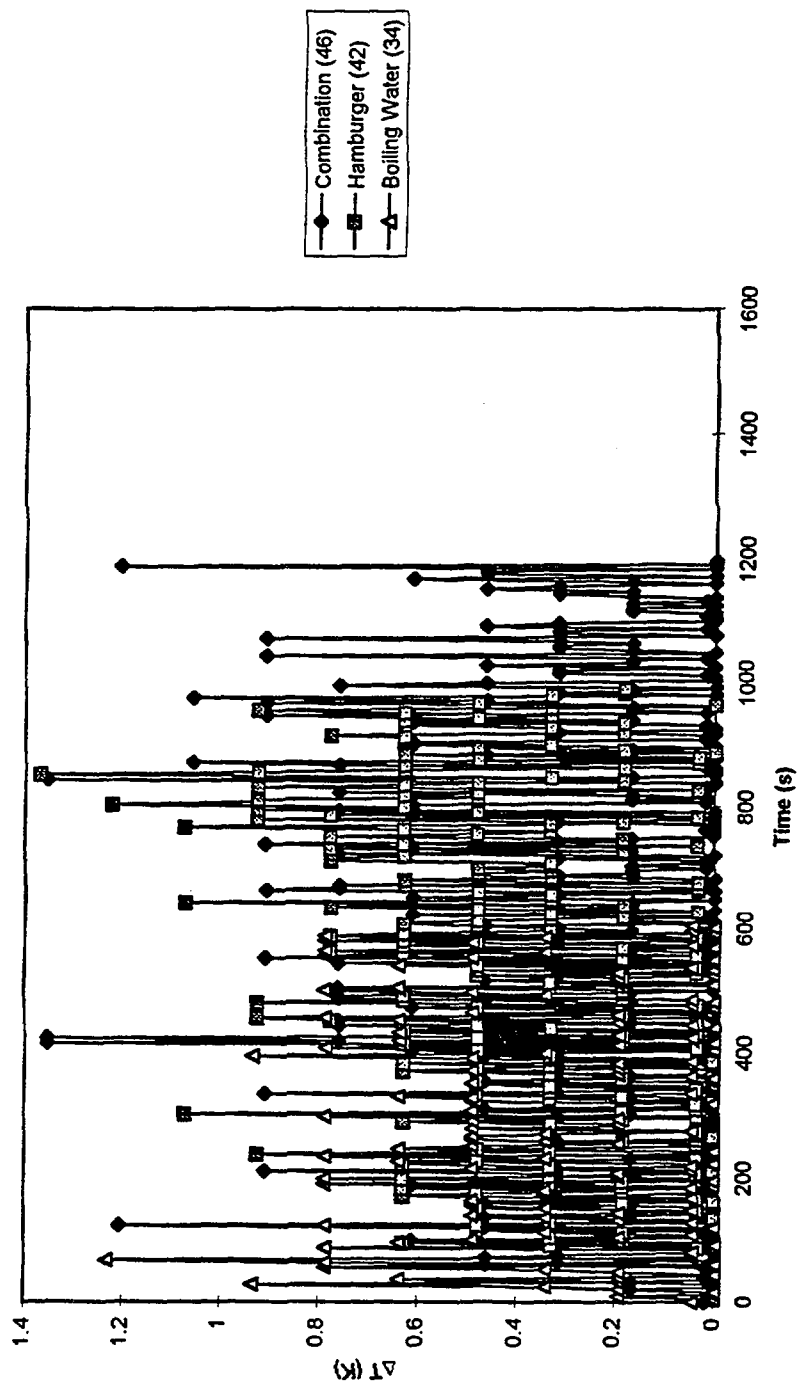
TGS 880 Output vs. Time



Optical Density vs. Time



Temperature Rise at TC 13 vs. Time



Appendix E: Example Calculations Used in Analysis

The carbon monoxide and carbon dioxide yields were estimated by the following method.

1. The total lag time was calculated for the ceiling jet to reach the farthest ceiling-wall interface. The time lag for the plume region, 0.57 seconds, was calculated in section 5.3. Using equation (5.18) with a maximum radius of 3.97 m, a time lag of approximately 8 seconds was calculated for the ceiling jet region, resulting in a total lag time of 8.5 seconds.
2. The volume and cross-sectional area of test room are known. The volume of air entrained into the plume was calculated using equations (5.13) and (5.14) for the Cetegen/Zukoski and Heskestad methods, respectively. The total volume of air entrained using equations (5.13) and (5.14) were 6.6 m³ and 5.3 m³, respectively.
3. The gas concentration was known, therefore, the volume of space occupied by each species and the number of moles, n, could be calculated.

The calculated values are as follows:

	Volume of CO	n _{CO}	Volume of CO ₂	n _{CO2}
Cetegen/Zukoski	0.00035 m ³	0.013 mol	0.034 m ³	1.8 mol
Heskestad	0.00028 m ³	0.010 mol	0.027 m ³	1.5 mol

4. The mass of fuel and the molecular weight of each species is known, therefore, the mass yields can be calculated. The calculated values are as follows:

	Y_{CO}	Y_{CO_2}
Cetegen/Zukoski	0.02	2.1
Heskestad	0.01	1.7

The calculations using the spreadsheet model are as follows.

Calculations of air entrainment in fire plume
using Zukoski/Cetegen and Heskestad methods

test32		Zukoski/Cetegen			Heskestad		
		vroom	vtot		vtot		
		23.61	6.60		5.32		
Time	cet V_{ent}	V_{tot}	z	V_{ent}	V_{tot}	z	
0	0.00	0.00	1.76	0.00	0.00	1.76	
5	0.00	0.00	1.76	0.00	0.00	1.76	
10	0.40	0.40	1.76	0.31	0.31	1.76	
15	0.40	0.80	1.73	0.31	0.62	1.74	
20	0.39	1.18	1.70	0.30	0.92	1.72	
25	0.38	1.56	1.67	0.29	1.21	1.69	
30	0.36	1.92	1.65	0.29	1.50	1.67	
35	0.35	2.28	1.62	0.28	1.78	1.65	
40	0.34	2.62	1.59	0.27	2.05	1.63	
45	0.34	2.96	1.57	0.27	2.32	1.61	
50	0.33	3.28	1.54	0.26	2.58	1.59	
55	0.32	3.60	1.52	0.26	2.83	1.57	
60	0.31	3.91	1.49	0.25	3.08	1.55	
65	0.30	4.21	1.47	0.25	3.33	1.53	
70	0.29	4.50	1.45	0.24	3.57	1.51	
75	0.29	4.79	1.43	0.24	3.81	1.50	
80	0.28	5.06	1.40	0.23	4.04	1.48	
85	0.27	5.34	1.38	0.23	4.26	1.46	
90	0.26	5.60	1.36	0.22	4.48	1.44	
95	0.26	5.86	1.34	0.22	4.70	1.43	
100	0.25	6.11	1.32	0.21	4.91	1.41	
105	0.25	6.36	1.31	0.21	5.12	1.40	
110	0.24	6.60	1.29	0.20	5.32	1.38	

Calculation of CO and CO₂ Yields for Test 32

mass (g)	temp	ΔH_c (kJ/g)	
38	329	44.6	
CO ₂ [ppm]	MW (CO ₂)		
5082	44		
CO [ppm]	MW (CO)		
53	28		
Zukoski/Cetegen		Heskestad	
Vco ₂	Vco	Vco ₂	Vco
0.034	0.00035	0.027	0.00028
mol co ₂	mol co	mol co ₂	mol co
1.805	0.013	1.457	0.010
yield co ₂	yield co	yield co ₂	yield co
2.1	0.02	1.7	0.01

REFERENCES

- Aggarwal, S. and Motevalli, V., 1995, "Study of Smoke Generated by non-Flaming Sources for Fuel Identification", AUBE '95 - Proceedings of the 10th International Conference on "Automatic Fire Detection, pp. 180-192.
- Alpert, R.L., 1971, "Fire Induced Turbulent Ceiling-Jet", FMRC 19722-2, Factory Mutual Research Corporation, Norwood, Massachusetts.
- Alpert, R.L., 1972, "Calculation of Response Time of Ceiling-Mounted Fire Detectors", *Fire Technology*, Vol. 8, pp. 181-195.
- Alpert, R.L. and de Ris, J., 1994, "Prediction of Fire Dynamics", NIST-GCR-94-642, National Institute of Standards and Technology, Gaithersburg, Maryland.
- Bryan, J.L., 1993, Fire Suppression and Detection Systems, Macmillan Publishing Co., New York, New York.
- Bukowski, R.W. and Bright, R.G., 1975, "Taguchi Semiconductor Gas Sensors As Residential Fire/Smoke Detectors", *Fire Journal*, Vol. 69, No. 3, pp. 30-33, 102.
- Bukowski, R.W. and O'Laughlin, R.J., 1994, Fire Alarm Signaling Systems, NFPA, Quincy, Massachusetts.
- Cavicchi, R., Suehle, J., Chaparala, P., Poirier, G., Kreider, K., Gaitan, M., and Semancik, S., 1994, "Micro-hotplate Temperature Control for Sensor Fabrication, Study, and Operation," Proceedings of the Fifth International Meeting on Chemical Sensors, Rome, Italy.
- Cetegen, B.M., Zukoski, E.E. and Kubota, T., 1984, "Entrainment in the Near and Far Field of Fire Plumes", *Combustion Science and Technology*, Vol. 39, pp. 305-331.
- Cooper, L.Y., 1995, "Compartment Fire-Generated Environment and Smoke Filling", SFPE Handbook of Fire Protection Engineering, SFPE, Batterymarch Park, Massachusetts.

Denny, S., 1993, "Development of a Discriminating Fire Detector For Use in Residential Occupancies", Report FP 93-07, Master of Science Thesis, The University of Maryland, College Park, Maryland.

Drysdale, D., 1985, An Introduction to Fire Dynamics, John Wiley and Sons, New York, New York.

Evans, D.D., 1995, "Ceiling Jet Flows", SFPE Handbook of Fire Protection Engineering, SFPE, Batterymarch Park, Massachusetts.

Figaro Products Catalog, 1990, Figaro Engineering Corp., Osaka, Japan.

Fischer, A. and Muller, C., 1995, "A Simulation Technique for the Design of Multi Sensor Based Fire Detection Algorithms", AUBE '95 - Proceedings of the 10th International Conference on "Automatic Fire Detection, pp. 439-451.

Fischer, A. and Luck, H., 1994, "Vector Autoregressive Modelling of Fire Signals", Fire Safety Science - Proceedings of the Fourth International Symposium, pp. 727-738.

Gottuk, D.T., Roby, R.J., Peatross, M. and Beyler, C.L., 1992, "Carbon Monoxide Production in Compartment Fires", Journal of Fire Protection Engineering, Vol. 6, No. 3, pp. 133-150.

Grosshandler, W.L., 1995, "A Review of Measurements and Candidate Signatures for Early Fire Detection", NISTIR 5555, National Institute of Standards and Technology, Gaithersburg, Maryland.

Grosshandler, W.L., 1995, "Proceedings of the 1995 Workshop on Fire Detector Research", NISTIR 5700, National Institute of Standards and Technology, Gaithersburg, Maryland.

Grosshandler, W.L., 1995, "Towards the Development of a Universal Fire Emulator/Detector Evaluator", AUBE '95 - Proceedings of the 10th International Conference on "Automatic Fire Detection, pp. 368-380.

Hagen, B.C., 1994, "Evaluation of Gaseous Signatures in Large-Scale Test", Report FP 94-05, Master of Science Thesis, The University of Maryland, College Park, Maryland.

Hall, J.R. and Cote, A.E., 1991, "America's Fire Problem and Fire Protection", Fire Protection Handbook, ed. 17, NFPA, Quincy, Massachusetts.

Hall, J.R., 1994, "The U.S. Experience with Smoke Detectors: Who Has Them? How Well Do They Work? When Don't They Work?", NFPA Journal, Vol. 88, No.5, pp 36-46.

Heskestad, G., 1995, "Fire Plumes", SFPE Handbook of Fire Protection Engineering, SFPE, Batterymarch Park, Massachusetts.

Heskestad, G. and Newman, J.S., 1992, "Fire Detection Using Cross-Correlations of Sensor Signals", Fire Safety Journal, Vol. 18, No. 4, pp. 355-374.

Heskestad, G., 1984, "Engineering Relations for Fire Plumes", Fire Safety Journal, Vol. 7, pp. 25-32.

Horiba Manual No. 09652, Horiba Instruction Manual for Horiba Model PIR-2000 General Purpose Infrared Gas Analyzer, Irvine, California.

Ihokura, K. and Watson, J., 1994, The Stannic Oxide Gas Sensor, CRC Press, Boca Raton, Florida.

Ishii, H., Ono, T., Yamauchi, Y. and Ohtani, S., 1994, "Fire Detection System by Multi-Layered Neural Network with Delay Circuit", Fire Safety Science - Proceedings of the Third International Symposium, pp. 761-772.

Jackson, M.A. and Robins, I., 1994, "Gas Sensing for Fire Detection: Measurements of CO, CO₂, H₂, O₂, and Smoke Density in European Standard Fire Tests", Fire Safety Journal, Vol. 22, PP. 181-205.

Kohl, D., Kelleter, J. and Petig, H., 1995, "Detection of Smouldering Fires by Gas Emission", AUBE '95 - Proceedings of the 10th International Conference on "Automatic Fire Detection, pp. 223-239.

Lee, G.K. and Mulholland, G., 1977, "Physical Properties of Smokes Pertinent to Smoke Detector Technology", NBSIR 77-1312, National Bureau of Standards, Gaithersburg, Maryland.

Mandelis, A. and Christofides, C., 1993, Physics, Chemistry and Technology of Solid State Gas Sensor Devices, John Wiley and Sons, Inc., New York, New York.

McAvoy, T.J., Milke, J.A. and Kunt, T.A., 1996, "Using Multivariate Statistical Methods to Detect Fires", *Fire Technology*, Vol. 32, No. 1, pp. 6-23.

Meacham, B.J., 1994, "The Use of Artificial Intelligence Techniques For Signal Discrimination in Fire Detection Systems", *Journal of Fire Protection Engineering*, Vol. 6, No. 3, pp. 125-136.

Milke, J.A. and Mowrer, F.W., 1993, "A Design Algorithm for Smoke Management Systems in Atria and Covered Malls", Report FP 93-04, The University of Maryland, College Park, Maryland.

Milke, J.A., 1995, "Applications of Neural Networks for Discriminating Fire Detectors", AUBE '95 - Proceedings of the 10th International Conference on "Automatic Fire Detection", pp. 213-222.

Morton, B.R., Taylor, G.I. and Turner, J.S., 1956, "Turbulent Gravitational Convection from Maintained Instantaneous Sources", *Proc. Royal Society A*, 234, 1956, pp. 1-23.

Mowrer, F.W., 1990, "Lag Times Associated with Fire Detection and Suppression", *Fire Technology*, Vol. 26, No. 3, pp. 244-265.

Nakanishi, S., Nomura, J., Kurio, T., Satoh, K., Kouzeki, D., Tamura, H. and Hosokawa, M., 1995, "Intelligent Fire Warning System using Fuzzy Technology", AUBE '95 - Proceedings of the 10th International Conference on "Automatic Fire Detection", pp. 203-212.

Newman, J.S., 1988, "Principles of Fire Detection", *Fire Technology*, Vol. 24, No. 2, pp. 116-127.

Okayama, Y., 1991, "A Primitive Study of a Fire Detection Method Controlled by Artificial Neural Net", *Fire Safety Journal*, Vol. 17, pp. 409-432.

Okayama, Y., 1991, "Approach to Detection of Fires in Their Very Early Stage by Odor Sensors and Neural Net", *Fire Safety Science - Proceedings of the Third International Symposium*, pp. 955-964.

Okayama, Y., Ito, T. and Sasaki, T., 1994, "Design of Neural Net to Detect Early Stage of Fire and Evaluation by Using Real Sensors' Data", *Fire Safety Science - Proceedings of the Fourth International Symposium*, pp. 751-759.

Roby, R.J. and Beyler, C.L., 1991, "Compartment Fire Combustion Dynamics", NIST-GCR-91-588, National Institute of Standards and Technology, Gaithersburg, Maryland.

Servomex Manual 00540/001A/0, *Servomex 540A Oxygen Analyser Instruction Manual*, Norwood, Massachusetts.

Tewarson, A., 1995, "Generation of Heat and Chemical Compounds in Fires", *SFPE Handbook of Fire Protection Engineering*, SFPE, Batterymarch Park, Massachusetts.

Thuillard, M., 1994, "New Methods for Reducing the Number of False Alarms in Fire Detection Systems", *Fire Technology*, Vol. 30, No. 2, pp. 250-268.

Thuillard, M., 1995, "Development of Fuzzy Inference Rules in a Linear Smoke Detector with a New NeuroFuzzy Method", *AUBE '95 - Proceedings of the 10th International Conference on "Automatic Fire Detection"*, pp. 329-325.

Tsuchiya, Y., 1994, "CO/CO₂ Ratios in Fire", *Fire Safety Science - Proceedings of the Fourth International Symposium*, pp. 515-526.

U.L. 217, 1985, "Standard for Single and Multiple Station Smoke Detectors", Underwriters Laboratories, Northbrook, Illinois.

Zukoski, E.E., T. Kubota, and Cetegen B., 1981, "Entrainment in Fire Plumes", *Fire Safety Journal*, Vol. 3, pp. 107-121.

Section II

Methods to Process Sensor Data for Smart Fire Detection

1. Background

This section of the report summarizes the research results that have been achieved on methods to process sensor data for smart fire detection. The interim progress reports that have been submitted give details of the results that are summarized here. In addition, a reprint giving additional details is included in the Appendix of this section. Finally, the future direction of the research, including collaboration with NIST, is discussed.

The initial research involved a study of an olfactory neural network model that was published by Freeman and co-workers [1-3]. This model was aimed at developing an understanding of how the nose processes information to detect odors. Freeman's work started from animal experiments and progressed over approximately the last 25 years to a systems level model. Simulations of his most detailed model, the KIII model, show that the olfactory network acts as a chaotic oscillatory system. Yao, *et al.*, published an interesting application of Freeman's models to an industrial fault detection problem involving detection of faulty screws from good screws[3]. Yao, *et al.* achieved 100% perfect detection of faulty parts with an olfactory models [3]. Because this fault detection problem is very similar to the problem of detecting fires, the olfactory approach appeared very promising for detecting fires. However, after examining the same data and model, the published results could not be duplicated, leading to a suspicion that the published results were incorrect. Consequently, the olfactory model, while having a number of interesting features, was dismissed for the fire detection application.

Next, the use of expert systems and standard neural networks was investigated. The data used was from the large-scale fire experiments, reported previously in Section I.

Results of applying an expert system by Hagen was summarized in Figure 2.7 and Table 2.9. As indicated in Table 2.9, only 76% of the flaming fires, 50% of the smoldering fires and 89% of the nuisance sources were correctly classified. Improvement of these percentages was pursued through the application of a multivariate statistical technique, principal component analysis (PCA).

2. Principal Component Analysis

The type of statistical analysis, a principal component analysis (PCA), makes use of the maximum values measured by each sensor for each test. The data are arranged in a data matrix, X [8,10-12]. The number of rows in X , n , equals the number of experimental measurements made. methods are available to handle the case where some of the x_i Is are missing for particular rows [4]. PCA determines the linear combinations of the maxima that are capable of explaining most of the variations in the measurements. In most applications, PCA achieves a very large reduction in the number of dimensions, without a significant loss of accuracy. For example, for a set of 41 measurements from a chemical plant, four PCA components were able to account for 80% of the variation in the data [5].

Specifically, the PCA approach seeks to maximize:

$$p_1^T X^T X p_1 \quad (1)$$

with the constraint of $p_1^T p_1 = 1$.

p_1 is a matrix of coefficients, referred to as the principal components. As expressed, the solution of equation (1) yields the most important direction, p_1 , of the maximum variation

of the data. Equation (1) is then re-expressed to determine the second most important direction, p_2 , etc. The number of coefficients selected for the PCA approach is based upon using the least number of principal components which provide sufficiently accurate predictions. For this application, an accuracy of 75-80 percent was judged acceptable.

The predictions of the data are provide by a product of the principal components matrix, P , with a score matrix, T , as presented in equation (2).

$$X = TP^T \quad (2)$$

The column vectors in the P and T matrices are required to be orthogonal, *i.e.*:

$$t_i t_j = \begin{cases} 1, i = j \\ 0, i \neq j \end{cases}$$

$$p_i p_j = \begin{cases} 1, i = j \\ 0, i \neq j \end{cases}$$

The score matrix, T , is determined by:

$$T = XP \quad (3)$$

Consequently, a linear combination of scores, t_i , and coefficients, p_i , are used to reconstruct the raw sensor measurements, as expressed in equation (4) for three principal components.

$$X = t_1 p_1 + t_2 p_2 + t_3 p_3 \quad (4)$$

Measurements from the following six sensors used in the tests are applied to develop the PCA model: CO, CO₂, two Taguchi sensors (T880 and T822), temperature and light obscuration. The data for each sensor is scaled to zero mean and unit variance. The data collected from each sensor prior to the introduction of the source is used to establish normal, background conditions for that test. Characterizing ambient conditions was especially

important given the unconditioned nature of the test room. Three PCA components explain approximately 76% of the variability in the ambient data (collected two minutes prior to the introduction of any source). Consequently, three components are used to classify the sources.

The squared difference between the raw sensor values and the reconstructed values is called the squared prediction error (SPE). The expression for the SPE with three principal components is:

$$\text{SPE} = (x_i \pm t_1 p_1 \pm t_2 p_2 \pm t_3 p_3)^2 \quad (5)$$

Both the scores, t_i , and the SPE reflect all of the sensor measurements because both the scores and the SPE involve data compression as well as synthesis. The SPE is used to identify the existence of an abnormal situation, with its confidence limit set at 99.5%. Where a set of measurements exceed the SPE outside of the established limit in three successive scans (with a scan rate of 2 sec. for all measurements), the identified conditions are considered to be “abnormal”. The SPE successfully identifies conditions generated in all 87 tests as differing from normal conditions.

Following identification of abnormal conditions, the PCA is applied to classify the nature of the source. The scores (t_i) are used to distinguish the type of source, using the following rules:

- if $t_3 > 5$, then the source is a flaming fire
- if $-8 < t_2 < 0$, then the source is a smoldering fire
- otherwise the source is a nuisance source.

The results of applying the above rules are summarized in Table 2.11 of Section I for the test data. All of the flaming sources are properly classified, with smoldering sources

classified properly in 88% of the tests. Nuisance and ambient sources are classified properly in 73% of the tests by the PCA evaluation of the sensor data. 27% of the nuisance source cases are incorrectly identified as smoldering sources and hence represent false alarms. In contrast, at least one of the commercial detectors respond to 97% of the flaming fires (one is missed) and 25% of the non-flaming fires. At least one of the commercial detectors also respond to 11% of the nuisance sources as false alarms.

In addition to the improved classification rate, the time for detection of the signatures from fire sources is significantly less with the measurements included and the PCA-based intelligence than that for either of the commercial detectors. The time required for detection of flaming fires is reduced by an average of 45 s (representing a decrease of 57%), with the detection time for the PCA-based evaluation of the data being 6 to 244 s less than that for the first responding commercial detector. The decrease in detection time was greater for the non-flaming fires, having an average reduction of 245 s and a range of 182 to 332 s.

Two errors and ten false alarms out of 87 cases still has room for improvement. In order to improve this ratio, additional sensors are required. These additional sensors need to be chosen so that a greater difference between the scores for the nuisance and smoldering cases are determined to permit an accurate distinction between each case.

3. Sensors

Sensor research has progressed to the point where it is possible to place a hundred different gas sensors on a chip. While determining which sensors to use remains an open question, such a chip coupled with multivariate statistical approaches holds great promise

as a means of achieving further improvement in discriminating fire detection. The research on gas sensor arrays is continuing in cooperation with Dr. Semancik's group at NIST. The research involves dynamic modeling and optimization of the temperature inputs to a thin film, tin oxide microsensors; and, signal processing to extract information from the raw sensor data. Recently, wavelets have been successfully applied to develop dynamic models of the sensors. These models can then be used to predict how a sensor responds to its temperature input, and then to optimize the temperature input. The optimization approach involves using signal processing to measure the distance between signals produced by different gas species making it easy to recognize the presence of a chemical specie.

Three standard signal processing approaches have been investigated: Gram-Schmidt orthogonalization, Fast Fourier Transforms, and the Haar wavelet. Two other models based on olfaction have been reviewed. A paper describing the initial results of the reviews has been submitted for publication (a copy is included in the Appendix).

4. Summary

As a result of the experimental effort, an early fire detector consisting of an array of gas sensors appears feasible, with discrimination provided by a principal component analysis (PCA). It has been shown that discrimination among a flaming fire, smoldering fire, and a nuisance source can be accomplished using the PCA factors. However, many questions still remain prior to the application of this technology as a means of early fire detection. Due to the small number of sensors used, numerous false alarms occurred for

nuisance sources, which were classified as smoldering fires. Adding more sensors should help to alleviate this problem. Additional research is required to optimize the number and types of sensors to be included in the array, while still providing the desired level of sensitivity and discrimination ability. In addition, most of the data acquired has been from experiments conducted with one type of source, *e.g.*, a flaming source without a nuisance source being present. Additional components are needed to assess the potential for a nuisance source to mask a flaming or smoldering source.

5. References

1. Freeman, W., (Feb. 1991), Scientific American, pp. 78-85.
2. Yao, Y., and Freeman, W., (1990) Neural Networks, 3, pp. 153-170.
3. Yao, Y., Freeman, W., Burke, B., and Qing, Y. (1991), Neural Networks, 4, pp. 103-121.
4. Kresta, J., MacGregor, J., and Marlin, T., "Multi-variate Statistical Monitoring Of Process Operating Performance," Canadian J. Chemical Engineering, 69, 35-47, 1991.
5. Dong, D., and McAvoy, T., "Nonlinear Principal Component Analysis - Based on Principal Curves and Neural Networks", Computers and Chemical Engineering, 20: 1996, 65-78.

APPENDIX

A Comparative Study of Signal Processing Techniques for Clustering Microsensor Data (A First Step Towards an Artificial Nose)

Laurent Ratton¹
Tekin Kunt¹
Thomas McAvoy¹
Thomas Fuja¹
Richard Cavicchi²
Steve Semancik²

Abstract

Microsensor technology has progressed to the point where it is now feasible to place several hundred sensors on a computer chip. Such a sensor array can potentially be used in many applications including detecting hazardous chemical emissions, food processing, and fire detection. This paper addresses an important aspect involved in microsensor applications, namely how the sensor signals are processed. The problem treated involves classifying whether a sensed signal is generated by one of four chemicals. Two broad approaches to processing the sensor signals are discussed, one based on classical signal processing approaches, and one based on a model of how the olfactory system in animals functions. The classical approaches used include: Gram Schmidt orthogonalization, fast Fourier transforms, and Haar wavelets. For the experimental signals treated, the classical approaches give superior results compared to those produced by the olfactory model.

1. Introduction

The olfactory systems of animals and humans are exceptional at detecting and classifying odors even when exposed to only trace amounts of an odorant. Recordings from single olfactory receptors have shown that the receptors are

¹Institute for Systems Research, Department of Chemical Engineering, University of Maryland, College Park, MD 20742

²National Institute of Science and Technology, Chemical Science and Technology Laboratory, Gaithersburg, MD 20899

broadly tuned, and that they respond to a number of different odorants [1]. This finding favors the hypothesis that a pattern of receptor firings is the means of coding odorant presence, rather than the hypothesis that each odorant is associated with one receptor type. The fact that olfactory information is coded as a pattern requiring higher order recognition means that signal processing plays an important role in odor detection. There is a continuous turnover of olfactory receptors, as well as a high degree of redundancy. As many as 1000 receptors can converge to a single processing neuron in the olfactory bulb. It has been estimated that humans have on the order of 1000 olfactory receptor groups (each with numerous individual receptors) and that they are capable of distinguishing approximately 5000 odors. The number of receptor groups in the olfactory system is very much larger than the minimum number needed to distinguish 5000 odors, and a large redundancy exists. Nature seems to use numerous, non-specific sensors and a good signal processing algorithm to achieve excellent odor detection and classification.

In a recently published history of electronic noses [2] it is pointed out that olfactory cells suffer from a number of deficiencies, including low sensitivity ($\cong 1$ ppm), low specificity, and a short lifetime (about 22 days). Yet, subsequent neural processing is able to increase sensitivity by about 3 orders of magnitude, remove drift, and allow humans to discriminate between several thousand odors. Considerable improvements in electronic noses can be achieved both through improved signal processing and improved materials [2]. It is also pointed out that to date no use has been made of the transient information in a sensed signal through appropriate signal processing [2]. In this paper approaches to using transient information from sensors to detect the presence of a pure chemical species are discussed.

One significant target application for an artificial nose is detecting hazardous emissions from chemical plants, particularly at trace levels. Additional important applications involve: detection and control of automobile emissions, odor control in chemical and food processing, fire detection, and possibly improved fault detection. For the target application it is envisioned that the artificial nose would make use of an array of sensors and reside on a computer chip. Such a chip could be placed at all potential sites for a leak in a chemical plant, e.g. valves, flanges, pumps, etc. The chip would be located outside of the process streams. Thus, extensive safety precautions would not be required, as they would be if the chip were placed inside a process stream.

The purpose of the chip would be to raise an alarm that a leak of a particular chemical beyond a threshold is suspected. Such an alarm would be followed by a team taking air samples back to the laboratory for detailed analytical assay. If successful, the use of an artificial nose chip in this manner could be a cost effective approach to the increasingly important problem of hazardous emission detection. One of our research goals is to develop a design methodology for a complete sensor array system. For detecting chemicals, there is a trade-off between having one exceptionally accurate sensor for a particular species, versus achieving the same result by using a number of less accurate sensors, as the olfactory system does. It is this trade-off that we are addressing in our research.

Today, one can duplicate the key parts of the olfactory system in silicon to produce an artificial nose [3-9]. Indeed, commercial artificial noses have appeared on the market [10-12]. From the information available it appears that in some applications these commercial approaches target applications where relatively strong odor concentrations are present, e.g. beer brewing, and coffee roasting. However, some success with detection of trace quantities in the parts per trillion range has been reported [13]. Also, the commercial approaches appear to use a straightforward technique for signal processing and classification, namely a backpropagation neural network, sometimes with some signal conditioning. This paper discusses initial results from an interdisciplinary research program whose objective is the development of an artificial nose for use in the applications discussed above. There are several technical components of an artificial nose that can be identified. These are the sensors, signal processing, classification, and overall system design. Preliminary results on using signal processing methods to help sharpen the interpretation of the signals from a tin oxide micro-sensor are presented in this paper.

2. Modern Si-Based Sensor Arrays

Various forms of silicon-based, chemical sensor arrays are now being developed at research institutions around the world. In a number of cases, and in at least a general sense, these are micromachined structures that serve as analogue bases to the olfactory system for detection and monitoring of gases and vapors. The integrated multiple elements provide for the use of multiple active films of differing chemical functionality, within one device, to achieve analyses of practical mixtures. The combined chemical and electronic characteristics needed for these devices has led some to use custom process-

ing methods for fabrication. However, for low cost production, and efficient transfer of technology to sensor manufacturers, it is advantageous to keep fabrication steps as standard as possible. This not only allows reproducible production of large batches of sensor arrays at relatively low cost, but also opens the door to using existing libraries of proven circuitry or control and signal handling to be included, on chip, when appropriate.

While many different solid state sensing principles can be applied for sensing gases, the responses examined in this study are from conductometric (i.e.—gas-induced changes in conductance provide the response signal) micro-sensors developed at NIST using semiconducting oxide active films such as SnO_2 , ZnO and TiO_2 . The microsensor arrays are constructed by micro-machining a multi-level, Si-based CMOS (complementary metal oxide semiconductor) structure formed at a Si foundry according to our specific set of design parameters. The post-fab micromachining produces an array of suspended pixel elements with 4 exposed contact pads for electrical characterization of the active film on each sensor [14]. A schematic of one such micro-hotplate element is shown in Figure 1. The microsensor used in the analysis here was 1 element of a 2×2 array, like that shown in Figure 1. The suspended structure, which is $100\text{ }\mu\text{m}$ on a side, contains three functional layers: a polysilicon resistor for heating, an aluminum hotplate for distributing heat and measuring the temperature, and four aluminum contact pads for connection to the sensing film. These layers are separated by insulating layers of SnO_2 .

Two inter-related schemes are used to impart selectivity to the sensor elements [15]. The first approach involves using a variety of oxide films deposited on the microhotplates within an array. These oxide films are either used pure, or with surfaces that have been decorated with monolayer regime (catalytic) metals. The compositionally-varied interfaces produce a matrix of conductance changes, due to their differing adsorption/desorption and electronic transport characteristics. For added selectivity, individually-addressable temperature control of each pixel (each with its own built-in heater and leads, for use between 20° C and 550° C) is used as a means to exercise kinetic manipulation of chemisorption processes. Due to the extremely low mass (approximately $0.2\mu\text{g}$) of the micromachined pixels, our microsensor elements can each be thermally pulsed with a 1-5 msec time constant, in addition to being held at (variable) fixed temperatures. Response characteristics for varied array compositions and thermal schedules are collected as the

data to be used in recognition and quantification. Although semiconducting oxides are not highly specific, they do have the advantage of being quite robust, and thereby provide considerable latitude in tuning arrays for a wide range of applications. Additional advantages for these CMOS microsensors relate to their small size, which makes them relatively nonobtrusive even when packaged, and requires only low power consumption for temperature control.

While research studies on our arrays thus far have been concentrated on technological aspects for single microelements, or small (2×2) arrays, many tasks for hardware replication to larger arrays are straight-forward. The signal recognition analysis that follows is based on single microsensor data, and is a stepping stone toward the operation of larger systems under more complex conditions.

3. Signal Processing Issues

3.1 Classical Approaches

Suppose a micro-hotplate sensor is heated according to a temperature profile $u(t)$ during the time interval $[0, T_0]$. Suppose further that this takes place in the presence of one of M different chemicals and that the conductance exhibited by the sensor during the interval $[0, T_0]$ depends on which of the chemicals is present. Specifically: if chemical i is present ($1 \leq i \leq M$), the conductance of the sensor is given by the function $s_i(t)$.

Signal processing provides the tools necessary to make an estimate as to which chemical is present based on an observed conductance. That is, if we observe a conductance “signal” $r(t)$ that is the result of a temperature profile $u(t)$ in the presence of chemical i , then $r(t)$ is a (possibly noisy) version of $s_i(t)$. Signal processing techniques can be used to make this classification decision in an optimal fashion.

This is similar in many ways to the classic M -ary detection problem from digital communication theory. That problem may be described as follows: Every T seconds one of M signals is transmitted; if $M = 2^b$, then each signal can represent b bits of data, and communication at a rate of b/T bits per second is effected. Every T seconds the receiver observes a corrupted version of the corresponding transmitted signal and makes a decision as to which was the most likely transmitted waveform. In this way, the transmitted data can be recovered with a probability of error that depends on the ratio of the power of the transmitted signal and that of the noise. (See [16] for details.) We

intend to use the insight gained from detection and communication theory to attack the classification problem for the artificial nose.

A common approach used in communication systems is the representation of the “signal set” – i.e., $\mathcal{S} = \{s_i(t) : 1 \leq i \leq M\}$ – in terms of an orthonormal basis. We now describe three methods based on this approach.

3.1.1 Gram-Schmidt Approach: Given $\mathcal{S} = \{s_i(t) : i = 1, 2, \dots, M\}$, every signal in \mathcal{S} can be expressed as a linear combination (i.e., a weighted sum) of $N \leq M$ *orthonormal signals*. The set of signals $\{\phi_i(t) : 1 \leq i \leq N\}$ are said to be *ortho-normal* if they satisfy the following:

$$\int_0^{T_0} \phi_i(t) \phi_j(t) dt = \begin{cases} 1, & \text{if } i = j; \\ 0, & \text{otherwise.} \end{cases} \quad (1)$$

Orthonormal signals have a geometric interpretation; they are at “right angles” to one another, in the sense that varying a signal’s $\phi_i(t)$ -component has no effect on its $\phi_j(t)$ -component for $i \neq j$. This will be made more clear shortly.

Given the signals $\{s_i(t) : 1 \leq i \leq M\}$ we must first construct the orthonormal “basis set” $\{\phi_i(t) : 1 \leq i \leq N\}$. This can be accomplished via the “Gram-Schmidt procedure,” [16, pp. 167-173] as follows:

(1.) Let N be the *dimension* of the signal set $\mathcal{S} = \{s_i(t) : 1 \leq i \leq M\}$. This means that \mathcal{S} contains N *linearly independent* signals but does not contain $N + 1$ linearly independent signals. Recall that the signals $\{x_i(t) : 1 \leq i \leq n\}$ are linearly independent if the only constants c_1, c_2, \dots, c_n satisfying $\sum_{i=1}^n c_i x_i(t) = 0$ are $c_1 = c_2 = \dots = 0$. Assume without loss of generality that $\{s_1(t), s_2(t), \dots, s_N(t)\}$ are linearly independent.

(2.) The signal $\phi_1(t)$ is just a scaled version of $s_1(t)$; specifically,

$$\phi_1(t) = \frac{s_1(t)}{\sqrt{E_1}}, \quad (2)$$

where

$$E_1 = \int_0^{T_0} s_1^2(t) dt. \quad (3)$$

(3.) Set $i = 2$.

(4.) If $i = N + 1$ then stop. Otherwise, the signal $\phi_i(t)$ is obtained by subtracting off that part of $s_i(t)$ that can be represented as a linear combination of the signals $\{\phi_1(t), \dots, \phi_{i-1}(t)\}$ and scaling appropriately. Specifically, let

$$f_i(t) = s_i(t) - \sum_{\ell=1}^{i-1} s_{\ell,i} \phi_\ell(t) \quad (4)$$

where

$$s_{\ell,i} = \int_0^{T_0} \phi_\ell(t) s_i(t) dt. \quad (5)$$

Then $\phi_i(t)$ is given by

$$\phi_i(t) = \frac{f_i(t)}{\sqrt{E_i}} \quad (6)$$

where

$$E_i = \int_0^{T_0} f_i^2(t) dt. \quad (7)$$

(5.) Increment i and go to step (4.).

The net result of this procedure is the basis set $\{\phi_i(t) : 1 \leq i \leq N\}$ such that

$$\begin{pmatrix} s_1(t) \\ s_2(t) \\ \vdots \\ s_M(t) \end{pmatrix} = \begin{pmatrix} s_{1,1} & s_{1,2} & \dots & s_{1,N} \\ s_{2,1} & s_{2,2} & \dots & s_{2,N} \\ \vdots & \vdots & \ddots & \vdots \\ s_{M,1} & s_{M,2} & \dots & s_{M,N} \end{pmatrix} \begin{pmatrix} \phi_1(t) \\ \phi_2(t) \\ \vdots \\ \phi_N(t) \end{pmatrix}, \quad (8)$$

where

$$s_{i,j} = \int_0^{T_0} s_i(t) \phi_j(t) dt. \quad (9)$$

We associate the vector $\mathbf{s}_i = [s_{i,1}, s_{i,2}, \dots, s_{i,N}]$ with the signal $s_i(t)$. The important characteristics of the signal $s_i(t)$ are replicated in the vector \mathbf{s}_i . In particular, the “squared distance” between the signals $s_i(t)$ and $s_j(t)$ is

$$d^2(s_i, s_j) = \int_0^{T_0} [s_i(t) - s_j(t)]^2 dt = \sum_{k=1}^N |s_{i,k} - s_{j,k}|^2. \quad (10)$$

Now suppose $r(t) = s_i(t) + n(t)$, where $i \in \{1, 2, \dots, M\}$ and $n(t)$ is noise. Our goal is to estimate i from our observation of $r(t)$. If $n(t)$ is additive white Gaussian noise (AWGN), then the optimal detection algorithm is to compute the vector $\mathbf{r} = [r_1, r_2, \dots, r_{r_N}]$ defined by

$$r_i = \int_0^{T_0} r(t) \phi_i(t) dt \quad (11)$$

and to then make our decision \hat{i} according to the rule

$$\hat{i} = \arg \min \left\{ \sum_{k=1}^N |r_k - s_{i,k}|^2 : 1 \leq i \leq M \right\}. \quad (12)$$

The effectiveness of this approach is determined totally by the “distance structure” between the signals – i.e., $d^2(s_i, s_j)$ defined above.

3.1.2 Discrete Fourier Transform Approach: The Gram-Schmidt approach uses an orthonormal signal set $\{\phi_i(t) : 1 \leq i \leq N\}$ constructed from the signals one expects to observe – $\mathcal{S} = \{s_i(t) : 1 \leq i \leq M\}$. An alternative approach is to use complex sinusoids as the basis.

Suppose we sample a signal $x(t)$ on the interval $[0, T_0]$. The result is a sequence of n samples $\{x[k] : 0 \leq k \leq n-1\}$, where $x[k] = x(kT_s)$ and T_s is the sampling period. Associated with this sequence of n samples is a sequence of n complex-valued numbers – the *discrete Fourier transform* (DFT) of the sequence, denoted $\{X[m] : 0 \leq m \leq n-1\}$ and defined by

$$X[m] = \sum_{k=0}^{n-1} x[k] e^{-j(2\pi/n)km}. \quad (13)$$

The samples $\{x[k] : 0 \leq k \leq n-1\}$ can be recovered from the transform components under the inverse-transformation, as follows:

$$x[k] = \frac{1}{n} \sum_{m=0}^{n-1} X[m] e^{j(2\pi/n)km}. \quad (14)$$

(A detailed explanation of DFT’s and their efficient implementation is given in [17].)

We use the DFT of the sampled conductance profiles much as we used the vectors obtained through the Gram-Schmidt procedure. Given the conductance “signature” $s_i(t)$, we sample $s_i(t)$ and compute the associated DFT

of length n – i.e., let $\sigma_i = [\sigma_{i,0}, \sigma_{i,1}, \dots, \sigma_{i,n-1}]$ denote the DFT associated with $s_i(t)$:

$$\sigma_{i,m} = \sum_{k=0}^{n-1} s_i[k] e^{-j(2\pi/n)km}. \quad (15)$$

Here, $s_i[k]$ is the k^{th} sample of the signature $s_i(t)$.

The M different DFT's – one for each signal $s_i(t)$ – are computed in advance and stored. When the conductance signal $r(t)$ is observed, the DFT of $r(t)$ is computed and is compared with each of the stored DFT's; let $\rho = [\rho_0, \rho_1, \dots, \rho_{n-1}]$ denote the DFT of the observed signal. Whichever stored DFT is closest (in squared Euclidean distance) to that of $r(t)$ is assumed to be the DFT of the “correct” signature. More simply, we assume that chemical \hat{i} is present, where

$$\hat{i} = \arg \min \left\{ \sum_{k=1}^N |\rho_k - s_{i,k}|^2 : 1 \leq i \leq M \right\}. \quad (16)$$

3.1.3 Haar Wavelet Transform:

Over the past few years, wavelets have been used extensively in many signal processing applications [18]-[20] such as signal and image analysis, filtering, compression, decomposition, and more recently system identification [21]. Indeed, the wavelet transform provides a means of overcoming the limitations of Fourier analysis in defining a representation of one dimensional signals with both time and frequency information. Wavelets are often compared to the observation of a signal through a microscope: by increasing the power of the microscope, one hides the gross changes but zooms in on details. On the other hand, one gets the general shape of a signal without the details by decreasing the power of the microscope. Although wavelet theory is beyond the scope of this paper, a brief discussion of its essential properties and definitions is given below.

Consider the basic function $\psi(t)$, called a “mother wavelet”, and its Fourier transform $\Psi(w)$, that satisfy the “admissibility condition”:

$$\int_{-\infty}^{+\infty} \frac{|\Psi(w)|^2}{w} dw = C_\Psi < +\infty, \quad (17)$$

which implies that

$$\int_{-\infty}^{+\infty} \psi(t) dt = 0. \quad (18)$$

One can perform dilation and translation operations on $\psi(t)$ and create a family of scaled and translated versions of the mother wavelet function:

$$\psi_{a,b}(t) = \frac{1}{\sqrt{|a|}} \psi\left(\frac{t-b}{a}\right) \quad (19)$$

where a and b are the scaling and translation parameters. The continuous wavelet transform (CWT) of a function $f(t)$ is defined from $\mathbb{R}^* \times \mathbb{R}$ to \mathbb{C} by:

$$CWT_f(a, b) = \frac{1}{\sqrt{|a|}} \int_{-\infty}^{+\infty} f(t) \psi^*\left(\frac{t-b}{a}\right) dt \quad (20)$$

where the asterisk stands for the complex conjugate.

In the discrete case, time-scale parameters are discretized such as $a = a_0^{-m/2}$ and $b = n \cdot b_0 \cdot a_0^m$ and the family of wavelets $\{\psi_{m,n}(t)\}$ is given by:

$$\psi_{m,n}(t) = a_0^{-m/2} \psi(a_0^{-m}t - nb_0) \quad n, m \in \mathbb{Z} \quad (21)$$

The discrete version of the wavelet transform (DWT) of function $f(t)$ becomes:

$$DWT_f(m, n) = a_0^{-m/2} \int_{-\infty}^{+\infty} f(t) \psi(a_0^{-m}t - nb_0) dt \quad (22)$$

A standard and simple example of a function that defines an orthonormal family of wavelets in the discrete case is the Haar function:

$$h(t) = \begin{cases} 1 & \text{for } 0 \leq t \leq 1/2 \\ -1 & \text{for } 1/2 < t \leq 1 \\ 0 & \text{otherwise} \end{cases} \quad (23)$$

$$h_{m,n}(t) = 2^{-m/2} \psi(2^{-m}t - n) \quad (24)$$

The Haar transform, which is a linear operation, has been modified for computational efficiency [22] and it can be obtained by the use of the matrix W :

$$W = \begin{pmatrix} h_{0,0}(0) & h_{0,0}(1) & \cdots & h_{0,0}(N-1) \\ h_{0,1}(0) & h_{0,1}(1) & \cdots & h_{0,1}(N-1) \\ h_{1,1}(0) & h_{1,1}(1) & \cdots & h_{1,1}(N-1) \\ h_{1,2}(0) & h_{1,2}(1) & \cdots & h_{1,2}(N-1) \\ h_{2,1}(0) & h_{2,1}(1) & \cdots & h_{2,1}(N-1) \\ \vdots & & & \\ h_{2,2^2}(0) \cdots & h_{2,2^2}(N-1) & & \\ \vdots & & & \\ h_{m,1}(0) \cdots & h_{m,1}(N-1) & & \\ \vdots & & & \\ h_{m,2^m}(0) \cdots & h_{m,2^m}(N-1) & & \end{pmatrix} \quad (25)$$

where $h_{m,n}(k)$ comes from the sampling of $h_{m,n}(t)$, with $k = 0, 1, \dots, N-1$, $0 \leq m \leq \log_2(N) - 1$ being the scale and $1 \leq n \leq 2^m$ the translation parameter. $h_{0,0}(k) = 1$, for $k = 0, 1, \dots, N-1$.

For each scale m one has 2^m rows corresponding to the translated versions of the wavelet at this scale. Thus, the Haar transform of the sampled function f over the interval $[0, N-1]$ is simply:

$$y = W.[f(0)f(1) \dots f(k) \dots f(N-1)]^T \quad (26)$$

In this manner, the initial bidimensional representation of the DWT is reduced to a one dimensional vector by concatenation of the scaled observations.

The Haar basis defined in eqs. (23) and (24) is an orthonormal basis into which a discrete function f can be decomposed. Similar to the approach taken in Sections 3.1.1 and 3.1.2, this provides us with a finite-dimensional representation of the chemical signatures against which we can compare the transform of the observed conductance; once again, by minimizing the Euclidean distance between the observed transform and the signature transforms, we can determine which gas (if any) is present.

3.2 Approaches Based On Models Of The Olfactory System

R. Granger, G. Lynch and J. Ambros-Ingerson [23] have developed a model to explain the interaction between the olfactory bulb and the piriform cortex by observing rats. A team at Oklahoma State University is designing a chip on which a modified version of this model is implemented [24]. A

a chip on which a modified version of this model is implemented [24]. A simulation of this chip has been used to classify data generated from sensor experiments. The simulation is composed of two main parts, shown in Figure 2. These parts are extensively connected by both feedforward and feedback links. The first part is a 16-level thermometer coder which calculates a binary coding of the intensity of the main input components, thereby simulating the olfactory bulb. Then, this binary code is input to the second part which simulates the piriform cortex: this second part is a sparsely connected network described by a sparse weight matrix, which produces a non-binary output. A winner-take-all (WTA) procedure is applied to obtain a final binary output of the model. Finally, the output is sent back to the sparse matrix generating an inhibitory feedback which is combined with the input signal, in order to remove the influence of the components that have already been analyzed. The procedure is repeated as many times as necessary, each time going into more detail in the signal than the previous time. In this way, the model performs a hierarchical analysis of the original input, determining at each level a binary output for the corresponding sub-class.

Initially, the model needs to be trained before it can recognize an odor. Several signals for each class and sub-class are presented, and the training consists of reinforcing the weights of the sparse matrix which have contributed to the selection of the WTA. The underlying weights are increased at each loop, and they are constrained to values between 1.0 and 3.2, which corresponds to saturation. Then, references for each level are defined. These references are used to compare coded outputs, so that a choice can be made at all nodes of this tree-structured hierarchical classifier. This choice is determined by calculating the Hamming distance (number of different bits) between the code and the reference. After training, the performance of the classifier can be evaluated.

In addition to thermometer coding, an investigation of Gray coding [25] which is more widely utilized in communication applications, was studied. Gray coding uses n bits to code 2^n different levels with a constraint of “continuity” in the code, i.e. 2 successive levels are coded by changing only one bit. In the communication field this code prevents small detection errors from making large changes in the associated data. In our application, the goal is to get very different codes for different gases, and at the same time to identify a gas even in presence of disturbances. An advantage of using the Gray code is that the size of our olfactory model can be reduced significantly,

especially the dimensions of the sparse matrix since 4 bits are enough to code 16 different levels. Note that for the 16-bit thermometer coder two successive level codes differ by one bit out of 16. The same levels coded with the 4-bit Gray code will have a larger relative difference in their representation (1 bit out of 4), which might result in a classification that is sensitive to small changes on the inputs.

4. Experimental Results

4.1 Data Collection

The sensing film on this microsensor was Pd-dosed SnO_2 . The fabrication details of this microsensor can be found in [26]. The miniaturized device has a thermal time constant of 1 msec and a thermal efficiency of 7.5°C/mW . The fast thermal response time allows rapid variation of the sensor's temperature pulses. In this case temperatures within a cycle ranged from $20\text{--}550^\circ \text{C}$ in a linearly ramped manner with 5°C increments for successive pulses. The cycle then repeated. In this pulsed mode, conductance is measured at room temperature between each temperature pulse. All temperature pulses have equal duration (100 msec) and are separated by 6 msec of delay to measure the conductance. Four test gases (methanol, ethanol, formaldehyde, and acetone) were examined for investigating different signal processing approaches. Each gas was introduced to the sensor chamber at room temperature, and saturated vapor pressures are assumed throughout the experiments. The input temperature sequence is shown in Figure 3. Conductance is recorded after each temperature pulse, and shown in Figure 4. It should be noted that the duration of each heating pulse as well as the delay between them and the specific pulse sequence will affect the final, cyclic conductance response.

Although the conductance responses, shown in Fig. 4, seem to repeat identically for each cycle, the mean changes slightly from one period to another. In addition, this phenomenon is amplified from week to week with the occurrence of long term drift. Therefore, a statistical analysis, based on mean and variance, would not be effective for signal identification. For the cycles shown in Fig. 4, 107 conductance measurements were made for each cycle. These measurements were resampled, leading to 32 samples per cycle for use in the calculations. In addition to the raw data, the performance of the signal processing methods was evaluated on noisy and drifting data. For the noisy data, uniformly distributed white noise was added, with variances of 10%, 20% and 30%, to test the capability of each scheme to deal with

second test, drift was artificially added to the original signals. The drift was added as a positive linear ramp varying from zero to half the mean of the signal. This magnitude of drift was more drastic than that usually encountered experimentally. It was chosen in order to compare the different signal processing methods. The conductance cycles were normalized for each cycle to zero mean and unit variance before any processing. The normalization prevents the signal processing approaches from being affected by the mean and variance of the data. Note also that the drift effect is not removed by the normalization. Finally, for the classical approaches as well as the olfactory model, references for the classification task have to be defined. The reference for each of the four gases is an average cycle, calculated using the five available experimental cycles for each gas in Figure 4.

4.2 Classical Approaches

We now turn to the techniques described in Sections 3.1.1, 3.1.2, and 3.1.3 for representing the signals of interest in terms of orthonormal bases.

4.2.1 Gram Schmidt Approach. First, the Gram-Schmidt approach was applied to build an orthonormal basis. The basis is obtained by successively using the methanol, ethanol, acetone, and formaldehyde references. The dimension of the signal space is $n = 4$ and the resulting basis is $S = \{\phi_1(t), \phi_2(t), \phi_3(t), \phi_4(t)\}$ as shown in Fig. 6. If all five cycles of methanol, ethanol, acetone and formaldehyde are projected onto this basis, four clear “clusters” of vectors, corresponding to the four gases, are shown, as in Fig. 7. In Figure 7, the components are very well separated, and their projection is characterized by a small variance within each region, compared to the distance between the regions. Note that in Figure 7b formaldehyde is the only species to have four non-zero components. This results from using formaldehyde as the last component in generating the orthonormal basis. Figure 7b also illustrates that one cannot separate methanol from ethanol using only their ϕ_3 and ϕ_4 components, since these components are approximately zero. Figure 7 suggests that the Gram Schmidt approach is able to classify the components based on their raw data without any difficulty.

Next, the robustness of the procedure to the effect of noise is investigated. After normalizing the noisy data (Figure 5), they are projected onto the $\{\phi_1(t), \phi_2(t), \phi_3(t), \phi_4(t)\}$ basis; the results are shown in Fig. 8a and b. No shift occurs between these noisy data and the references, since this decomposition of 32 sampled signals into 4 vectors is a linear operation and we

composition of 32 sampled signals into 4 vectors is a linear operation and we consider a noise with zero mean. Note, however, that the variance of components *within* the regions increases, due to the variance of the noise. This increase in variance does not hinder classifying which gas is flowing past the sensor.

Finally, the Gram-Schmidt orthogonalization is tested on drifting data. As shown in Fig. 9, a drift in the signals leads to a drift in their representation in the Gram-Schmidt basis. This sensitivity to drift in turn leads to a deterioration in the classification performance, and it is an obvious weakness of the Gram-Schmidt orthonormalization technique.

4.2.2. Fast Fourier Transform (FFT). The fast Fourier transform (FFT) is an efficient algorithm to calculate the discrete Fourier transform (DFT) when the number of samples is a power of two. With this approach, the minimum number of FFT coefficients containing most of the information in each signal is determined first. The minimum number is that which allows one component to be separated from another, while allowing a signal from the same class to be classified correctly. Keeping the lowest frequency coefficients in an FFT tends to keep the main shape of the signal and remove noise. It was determined experimentally that eight coefficients are sufficient to classify the four gases correctly. In Figs. 10a, b and 11a, b, the distance between the 32-coefficient DFT of each cycle and the 8-coefficient DFT of the reference signals is plotted. As can be seen, the distance between classes shrinks when the number of coefficients is reduced from 32 to 8. It is clear that a good separation is maintained even with an 8-point DFT. However, below 8 DFT coefficients, one starts removing relevant information which leads to a deterioration in classification capability.

When the same white noise is added (Figure 5), a comparison of the corresponding 8-coefficient DFT with the 8-coefficient DFT of the references can be made to determine the performance of the FFT method with noise. The result, shown in Fig. 12, confirms that noise does not affect the classification ability of this technique very much. When the behavior of the DFT towards the same drifting data as above is analyzed the results in Fig. 13 are observed. Drift causes the data to move away from the references, which deteriorates the classification performance. This observation can be expected, since drift is nothing but a low frequency signal and therefore it is taken into account when the eight lowest frequency coefficients are kept.

4.2.3. Haar Wavelet Transform. The last classical technique used to process the data is based on a wavelet transform. As explained in Section 3.1.3, the Haar Transform is a very efficient way to take advantage of wavelet properties; moreover, this transform has small memory and computational requirements. Once the Haar matrix of size 32×32 is defined, it can be used for all the calculations. The first line of this matrix contains only 1's and the corresponding coefficient gives the mean of the analyzed signal. The next lines correspond to scales 1 through 5 – scale i has 2^{i-1} lines. The projection of the original signal using the Haar matrix gives a 32-coefficient vector, with subsets of coefficients corresponding to respective scales. The higher the scale, the more details are captured.

Figure 14 shows the Haar Transform of each of the four references. Then, using either less or more scales, one can reconstruct the input signals with less or more accuracy (Figs. 15a to Figs. 15b). The transform is applied to the normalized data to determine the “optimal” number of scales that would clearly separate the four gases. Figures 16 to 20 demonstrate that keeping both scales 3 and 4 leads to an efficient discrimination among gases using only 12 coefficients.

Figures 17 and 20 point out an interesting fact: methanol and ethanol are separated by removing scale 2. This result means that this scale is necessary to reconstruct the original input, but its contribution tends to make methanol and ethanol closer to each other. As with the Gram-Schmidt and FFT approaches discussed above, we can easily achieve gas classification using the Haar Transform, with or without noise in the data, provided that the signal to noise ratio is reasonable. However, the interesting property of the present technique is that it can also handle the effect of drift in the data. By keeping only scales 3 and 4, the very lowest frequencies are removed, and these frequencies correspond to the major part of the drift effect. In addition most of the high frequencies are removed, which correspond to most of the noise. Therefore, as observed in Figures 21 and 22 the component regions stay very close to their original positions with noise and drift using 12 coefficients from scales 3 and 4.

4.3 Olfactory Model(s): In this section results for the Granger model are presented. In our calculations the dimensions of the model were 32 bits for the input, 16- bits for the thermometer coding (respectively, 4-bit Gray coding) for the olfactory bulb with a 512×512 (respectively, 128×128) sparse

matrix for the piriform cortex simulation, and 32 non-zero bits in the 512-bit (respectively, 128-bit) model output. The references used so far for each gas represent the second (bottom) level of the hierarchy in this model. However, references are needed for the first (upper, coarser) level that contains two classes: alcohols and non-alcohols. These references are obtained by calculating an average cycle from the sum of methanol and ethanol to get the alcohol class, and an average cycle from the sum of acetone and formaldehyde to get the non-alcohol class. In addition, the matrix in the model is trained by presenting the first 3 original cycles of each gas, after normalization. Then, the test set consists of all 5 cycles for the 4 gases.

Since the sparse matrix in the Granger model is randomly generated, a statistical analysis is carried out by using 10 different realizations of the matrix. The model was tested first on the original data. Table 1 presents statistical results on the Hamming distances between the references for 10 different sparse matrices, and compares performances of 16-bit thermometer coding with 4-bit Gray code. The first row shows the average distance and its standard deviation between alcohol and non-alcohol reference outputs, while the next 2 rows give the results obtained respectively from the methanol/ethanol and the acetone/formaldehyde references outputs. For accurate classification it is desirable to have a large average distance between the classes, as well as a small variance. As can be seen in Table 1 there is a trade off when comparing the thermometer and Gray coding. In some cases there is a large distance between classes, but there is also a large variance. Although the distance depends on the realizations of the sparse matrices, the small values obtained for the methanol/ethanol outputs, are the result of the strong similarity of these two signals. Note that results are totally different between the 16-bit thermometer coding and the 4-bit Gray code. The Gray code uses a minimum number of bits to encode the amplitude of the signal, while thermometer coding is a more robust but less efficient method, from a compression point of view.

Additional statistical results on classifying the original, noisy and drifting data are presented in Tables 2 to 4. The following observations about these results can be made. First, both methods give comparable results on the original data, although the performance of the thermometer coding is better. In the first level classification using both coding approaches, the olfactory model doesn't have any difficulty in making a classification. At the finer level however, there is some confusion, especially between methanol and ethanol.

This result can be expected for the thermometer coding since the reference outputs were very close (Table 1). The sensitivity of the Gray code is also demonstrated in Tables 2 to 4. Second, both approaches are very sensitive to noise and drift. In fact, even the first level of the hierarchical classification gets affected by a small noise (10% of the variance of the original signals) and by drift.

5. Discussion and Conclusions

Both the classical and biologically inspired signal processing approaches evaluated in this paper are very different. The signal processing methods perform a compression of the information contained in the sensor output. Indeed, no matter what classical technique is used (Gram-Schmidt, FFT, Wavelets), the number of coefficients describing the signal can be shrunk enough to help the classification task without deteriorating the relevant information that remains. On the other hand, the Granger approach provides a model based on a mammalian olfactory system that analyzes an odor through a hierarchical process. Knowledge of human (and animal) sensory coding has proven to be very useful, especially in vision and audio processing, and this fact motivated our study of this approach. Both the classical and Granger approaches promise to be easy to implement in silicon. The Granger model mainly deals with binary numbers and it only needs a weight matrix which is trained off-line, and then stored for later real-time classification. Operations are basically inner products and winner-take-all computations. In the Haar Transform, initially a matrix is needed (whose size depends on the length of original cycles) that contains the Haar wavelet basis vectors. Then, inner products are calculated during the processing. The Gram-Schmidt procedure needs a pre-computation of the basis vectors using previous data and then inner products are calculated. The FFT technique requires a real-time Fast Fourier Transform, which is a commonly used circuit.

For the sensor responses studied here the classical methods give the best results, and the wavelet transform (Haar Transform) was the best. The Haar Transform can efficiently compress information while removing the noise and drift effects, at least in the range encountered for the sensor studied.

6. Bibliography

- [1] Klivington, K. A., The Science of Mind, MIT Press, Cambridge, Mass., pp. 125-127, (1989).

- [2] Gardiner, J., and Bartlett, P., "A Brief History of Electronic Noses", *Sensors and Actuators B*, 18-19, 211-220 (1994).
- [3] Gardner, J., Hines, E., and Tang, H., "Detection of Vapours and Odours from a Multisensor Array Using Pattern Recognition, Part 2. Artificial Neural Networks", *Sensors and Actuators B*, 9, pp. 9-15 (1992).
- [4] Hines, E., and Gardner, J., "An Artificial Neural Emulator for an Odour Sensor Array", *Sensors and Actuators B*, 19, pp. 661-664 (1994).
- [5] Persaud, K., and Pelosi, P., "Sensor Arrays Using Conducting Polymers for an Artificial Nose", presented at NATO Workshop on Electronic Noses, Reyjavik, Iceland (Aug., 1991).
- [6] Persaud, K., "Electronic Gas and Odour Detectors That Mimic Chemoreception in Animals", *Trends in Analytical Chemistry*, 11, pp. 61-67 (1992).
- [7] Nakamoto, T., Fukunishi, K., and Moriizumi, T., "Identification Capability of Odor Sensor Using Quartz-Resonator Array and Neural-Network Pattern Recognition", *Sensors and Actuators B*, 1, pp. 473-476 (1990).
- [8] Nakamoto, T., Fukuda, A., Moriizumi, T., and Asakura, Y., "Improvement of Identification Capability in an Odor-Sensing System", *Sensors and Actuators B*, 3, pp. 221-226 (1991).
- [9] Gestri, G., and Starita, A., "A Neural Network for Odour Recognition", *Proc. of Fifth International Meeting on Chemical Sensors*, Rome, Italy, pp. 1089-1092 (1994).
- [10] "The Neural Nose", marketed by Neutronics Technology Plc, Bishops Stortford, Hertfordshire, U.K.
- [11] "Multielement Gas and Odour Detector", marketed by OdourMapper Limited, Manchester, U.K.
- [12] "Rhino", marketed by Mosaic Industries, Inc., Newark, California.
- [13] Abrahms, C., AromaScan Corporation, private communication.

- [14] J. S. Suehle, R. E. Cavicchi, M. Gaitan, and S. Semancik, *IEEE Electron Device Lett.* 14, 118 (1993).
- [15] S. Semancik and R. E. Cavicchi, *Appl. Surf. Sci.* 70/71, 337 (1993).
- [16] John G. Proakis, *Digital Communications* (3rd edition), McGraw-Hill, 1995.
- [17] Alan Oppenheim and Ronald Schafer, *Discrete-Time Signal Processing*, Prentice-Hall, 1989.
- [18] Rioul, O. and Vetterli, M., "Wavelets and signal processing", *IEEE Signal Processing Magazine*, October 1991.
- [19] Meyer, Y., "Wavelets - Algorithms and Applications", translated and revised by R. D. Ryan, SIAM, Philadelphia, 1993.
- [20] Zhang, Z. and Benveniste, A., "Wavelet networks", *IEEE Trans. on Neural Networks*, Vol. 3, nb. 6, 1992.
- [21] Motard R. and Babu, J., *Wavelet Applications in Chemical Engineering*, Kluwer Academic Publishers, Massachusetts, 1994.
- [22] Yang, X., "Detection and classification of neural signals and identification of neural networks", Ph.D. Thesis, University of Maryland, College Park, MD, 1989.
- [23] Ambros-Ingerson J., Granger R., Lynch G., "Simulation of Paleocortex Performs Hierarchical Clustering", *Science*, Vol. 247, March 1990.
- [24] Ramanathan M., "Statistical Model of an Electronic Olfactory", Master's Thesis, Oklahoma State University, May 1995.
- [25] Hamming, R.W., "Coding and Information Theory", Second Edition, Prentice-Hall, 1986.
- [26] Cavicchi, R., Suehle, J., Kreider, K., Gaitan, M., and Chaparala, P., *IEEE Electron Device Letters*, 16, No. 6, 1 (1995).

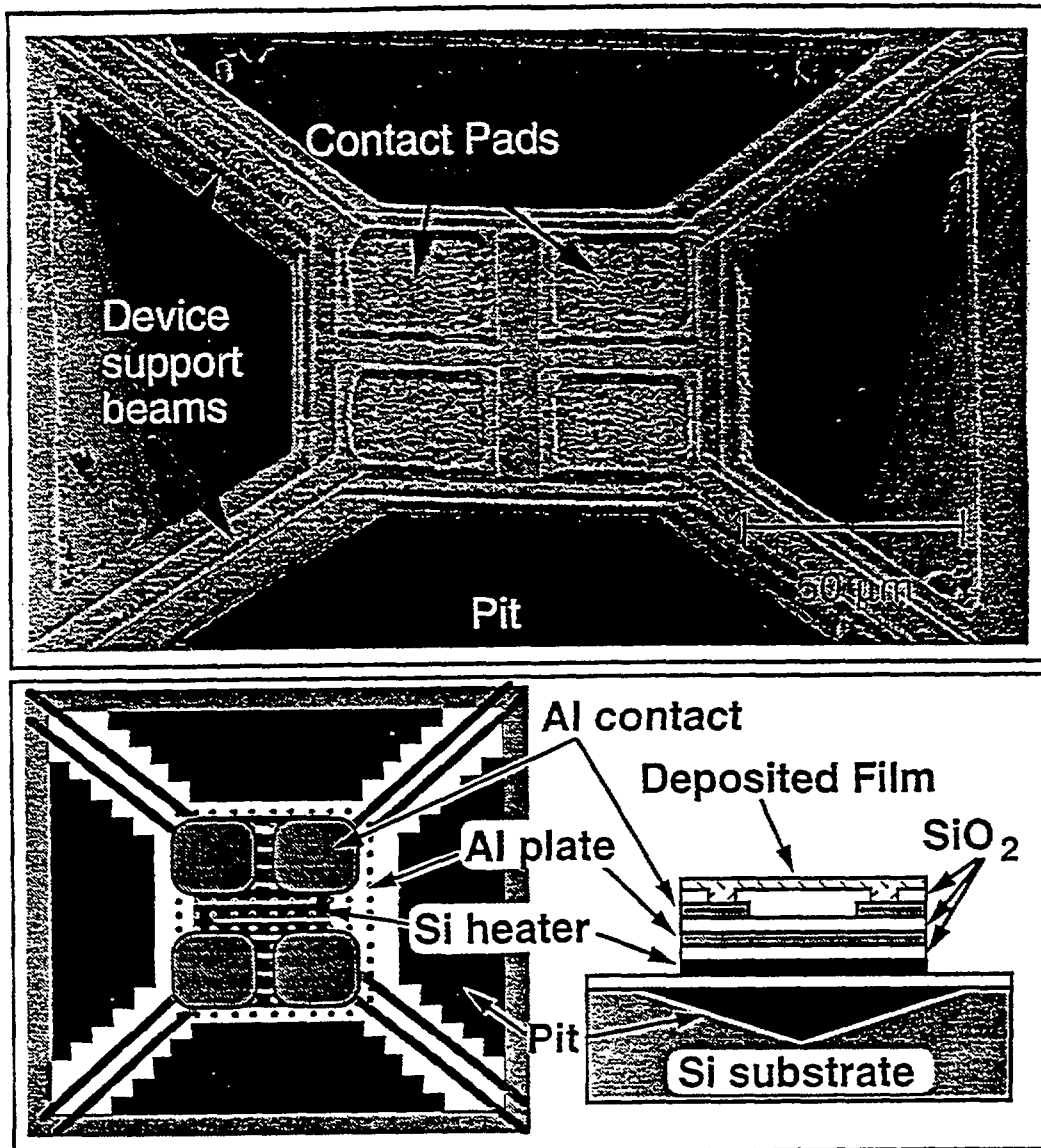


Figure 1. Scanning electron micrograph showing a suspended microhotplate structure with 4 top-surface contact pads for conductance measurements on an active film. Top and cross-sectionnall view schematics (not to scale) are shown in the lower panel.

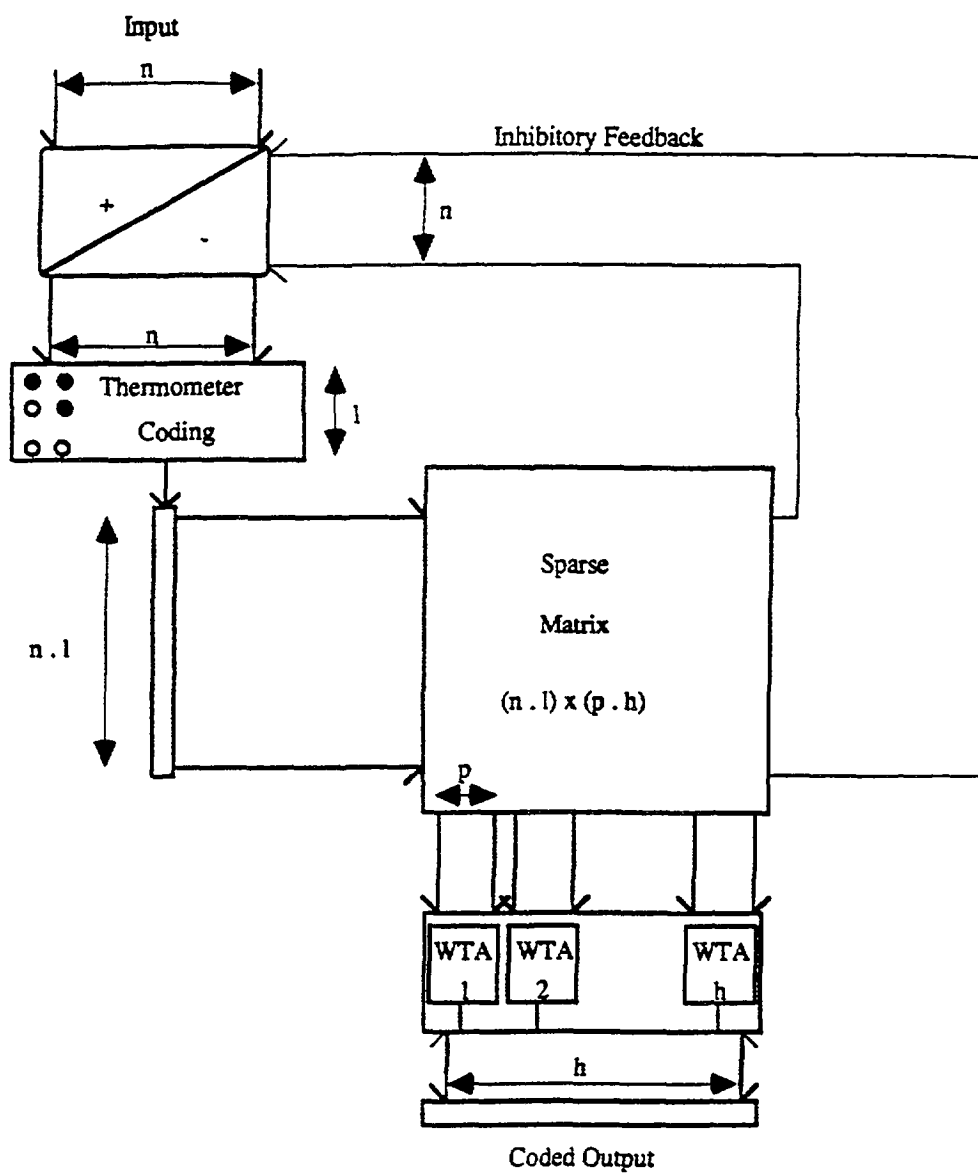


Figure 2. Architecture of the simulation of the Granger olfactory model.

Figure 3 : Temperature Profile

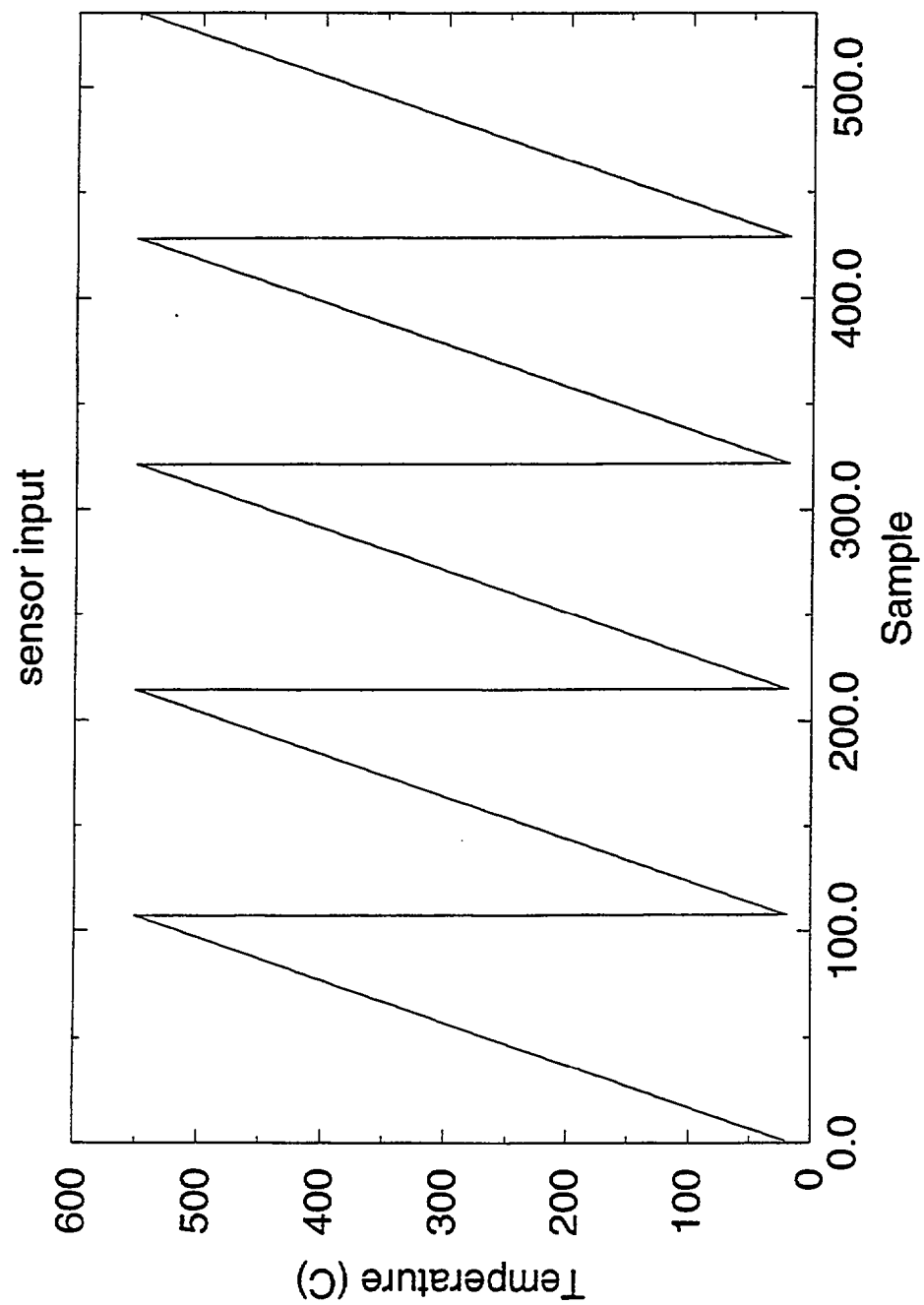


Figure 4 : Actual Conductance Measurement

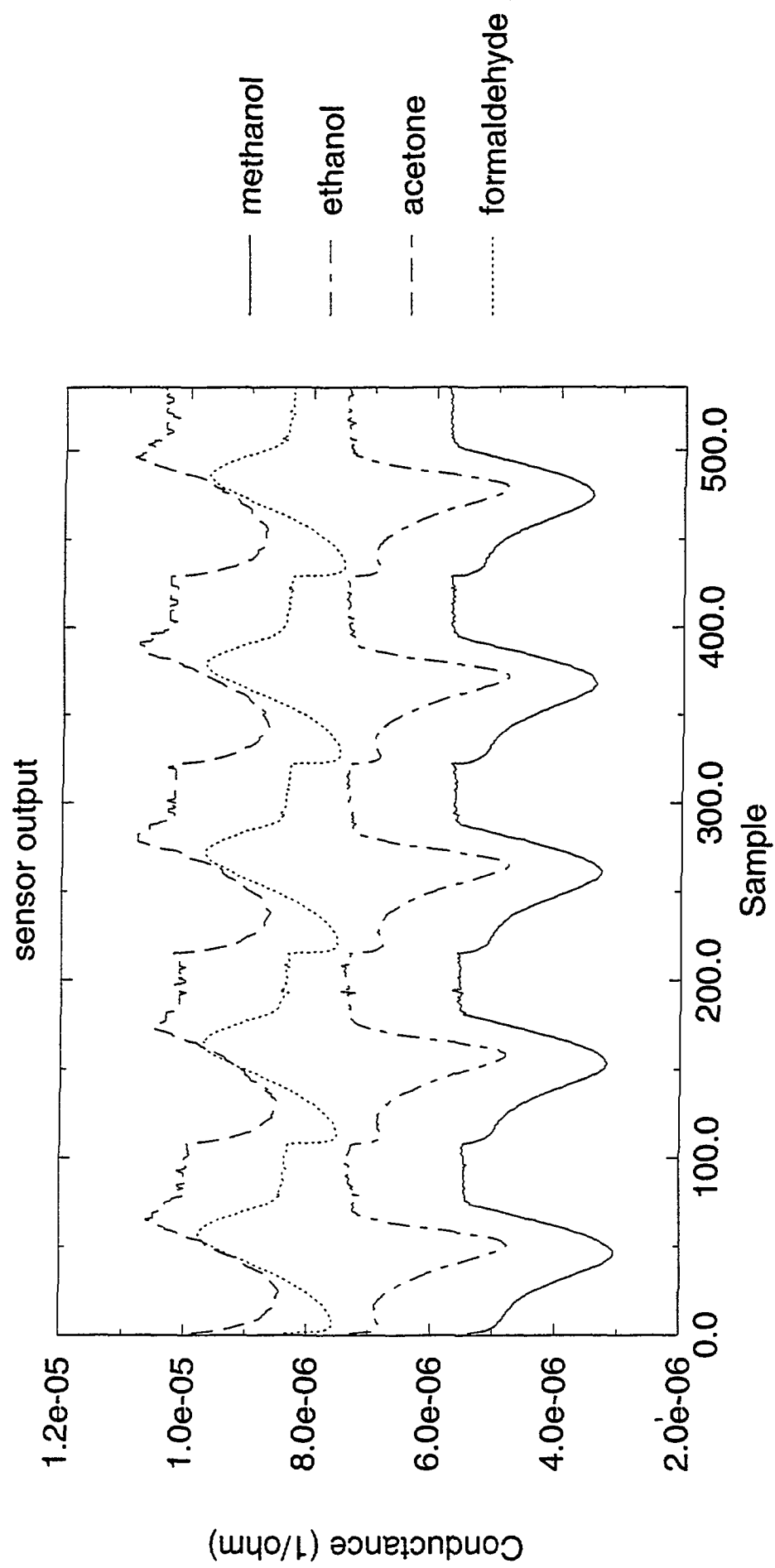


Figure 5 : Conductance with added noise

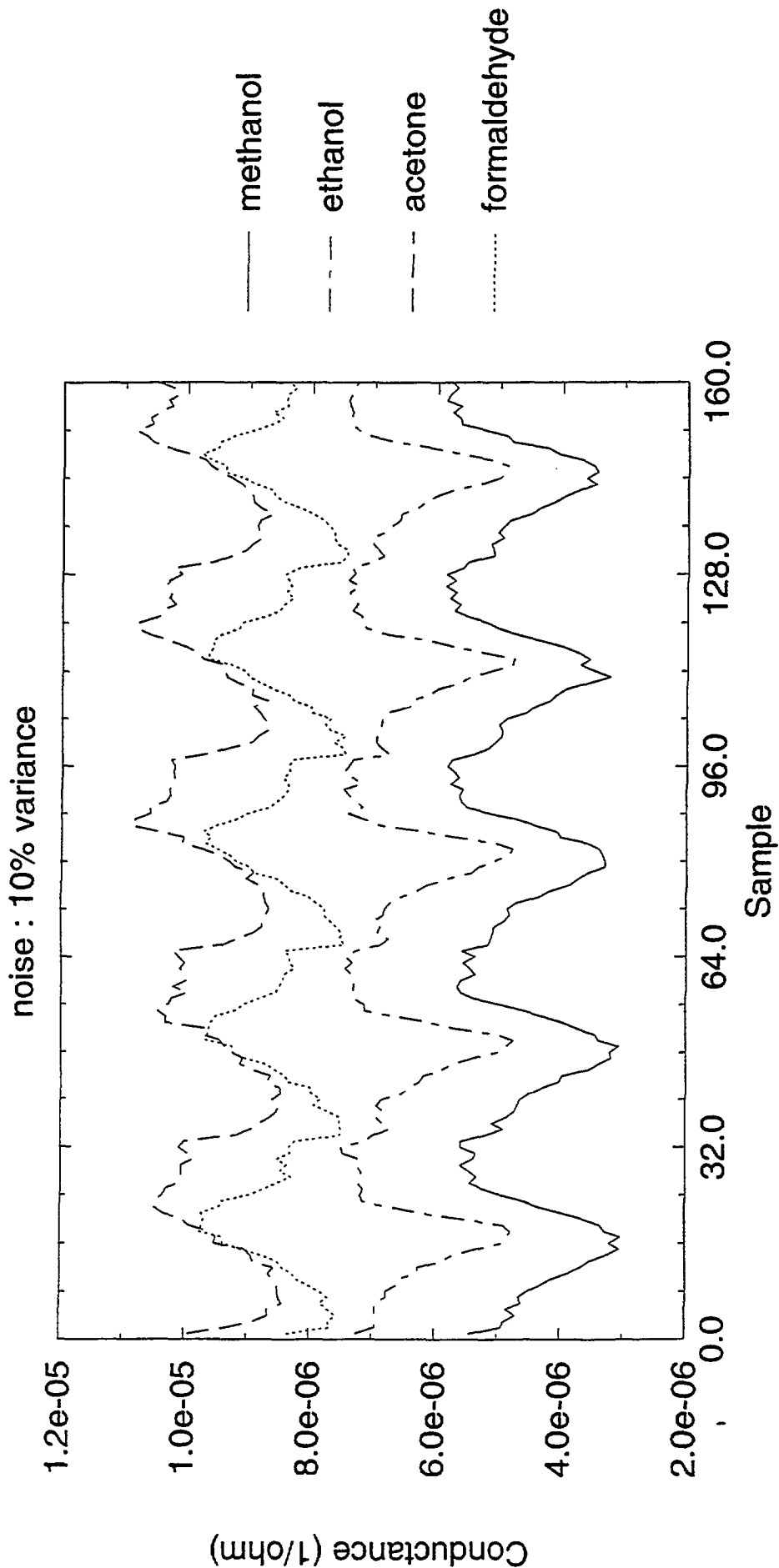


Figure 6 : Vectors of the Gram-Schmidt basis

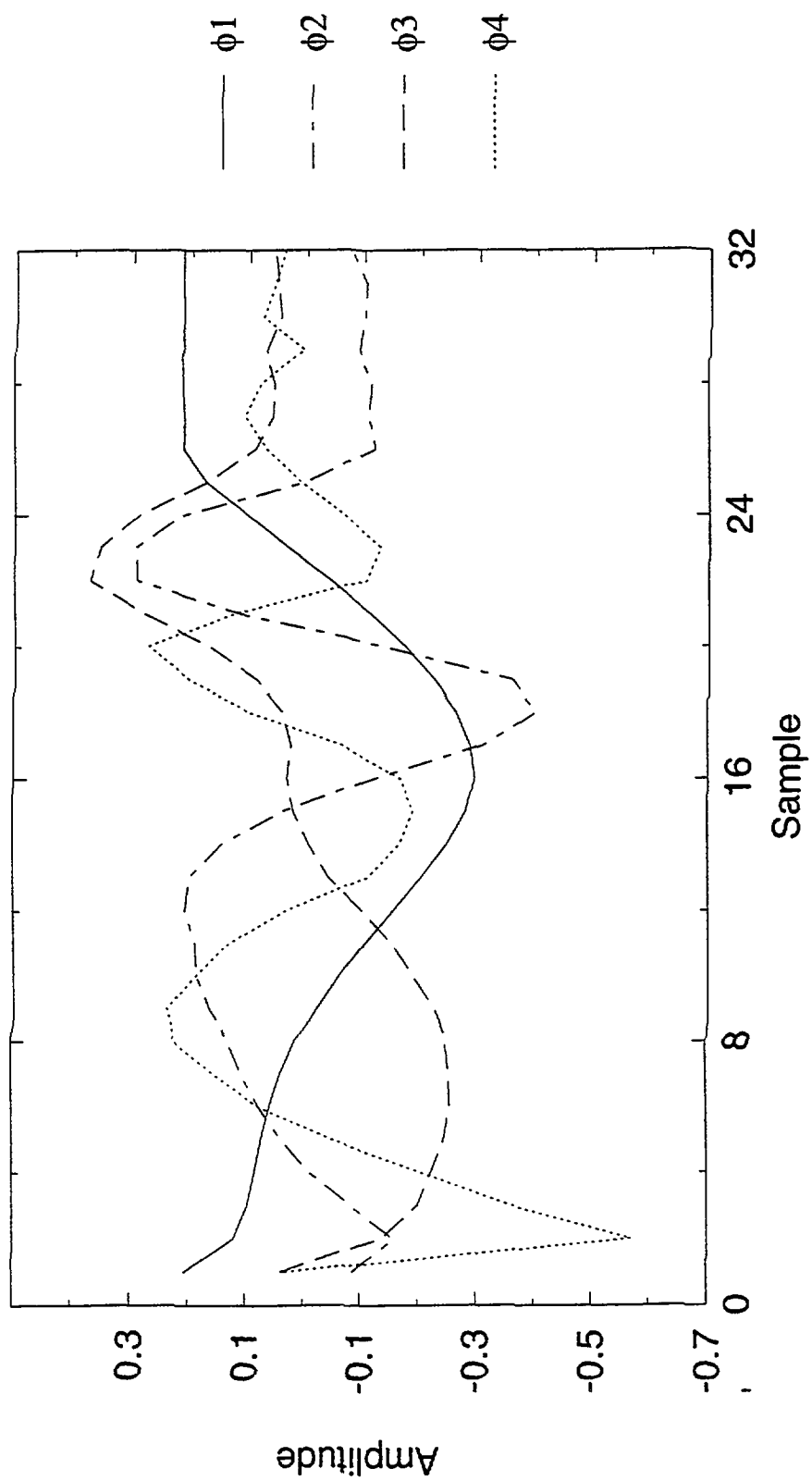


Figure 7a : Gram-Schmidt - 5 cycles and references

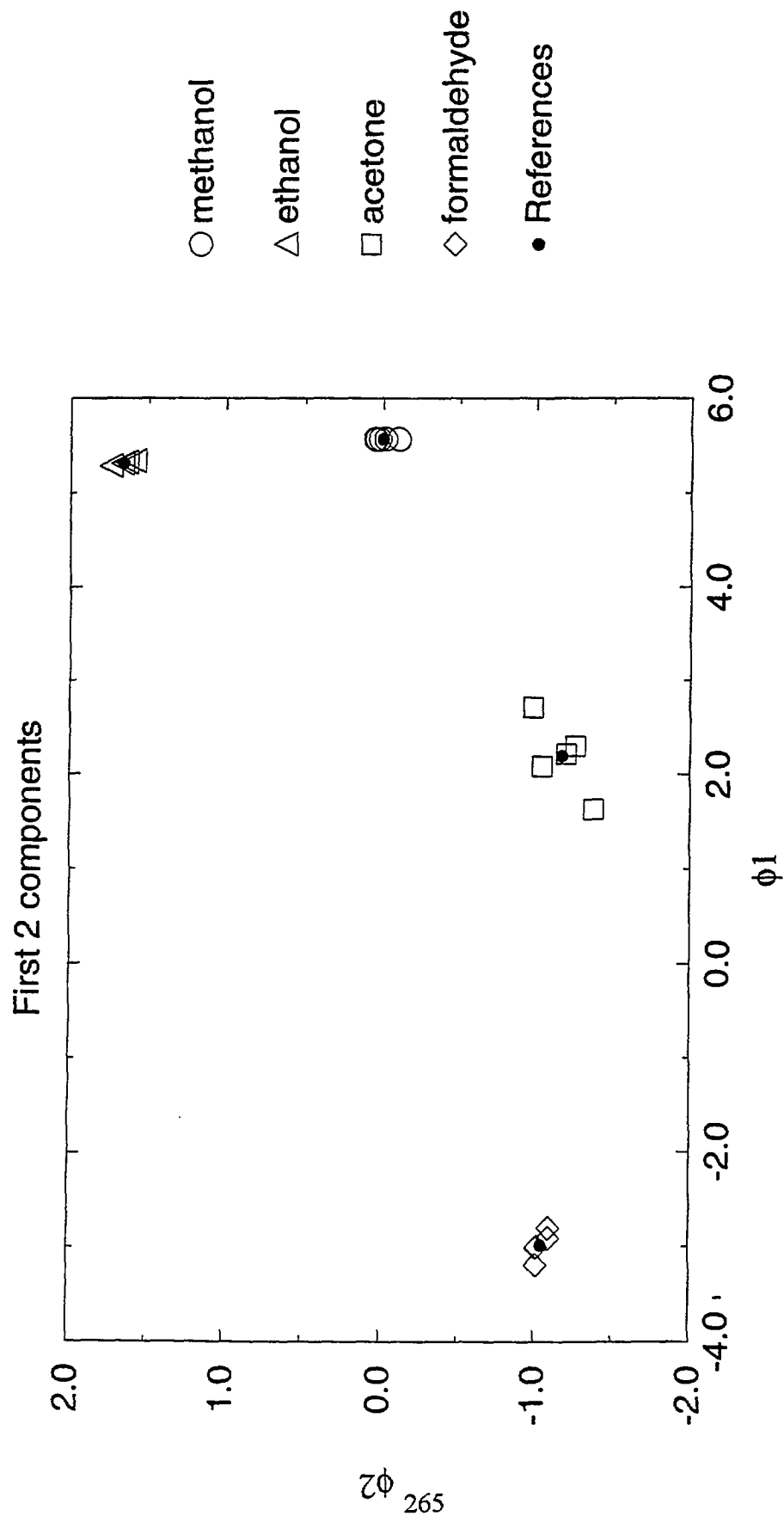


Figure 7b : Gram-Schmidt - 5 cycles and references

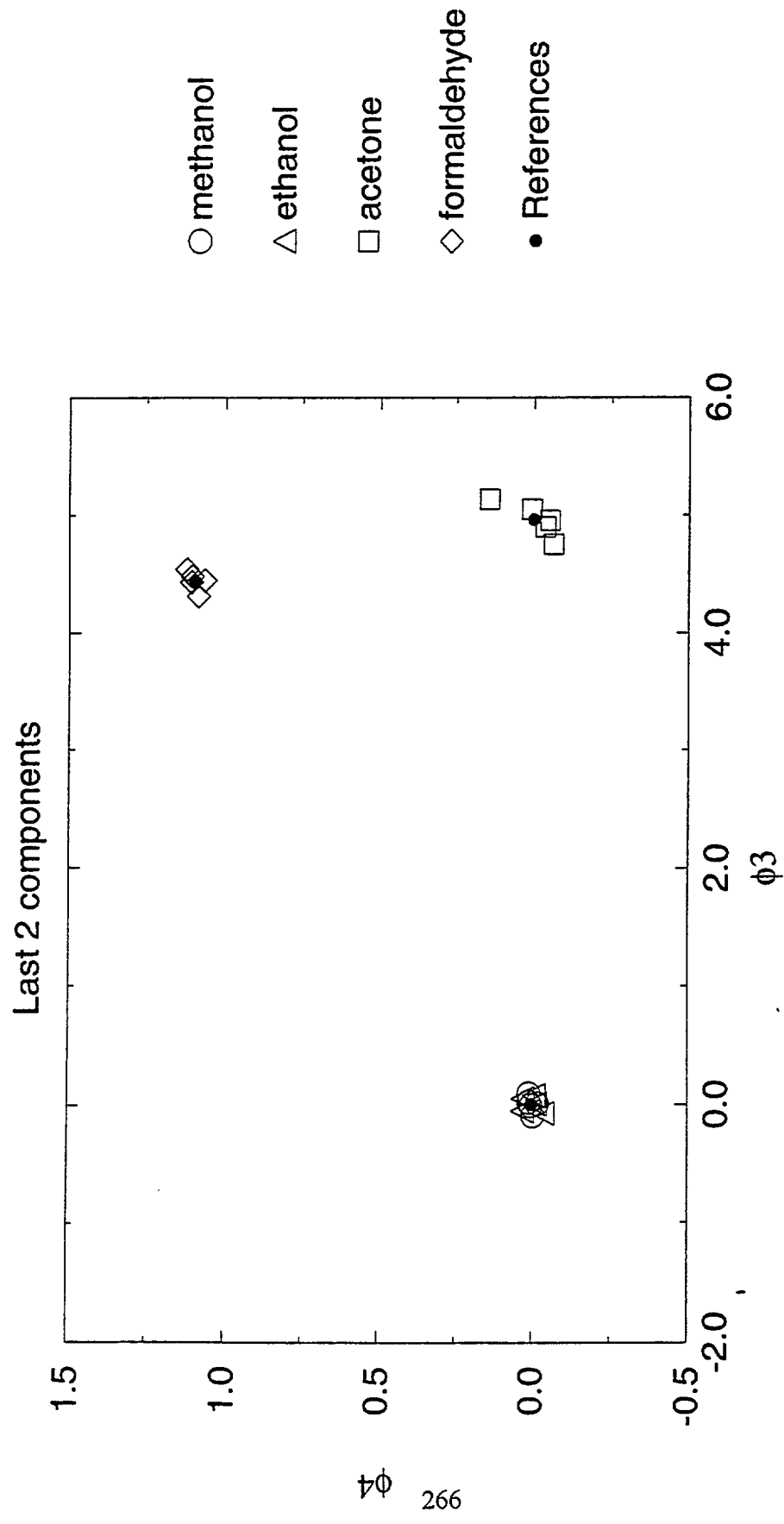


Figure 8a : Gram-Schmidt - 10% noisy data - 5 cycles + ref.

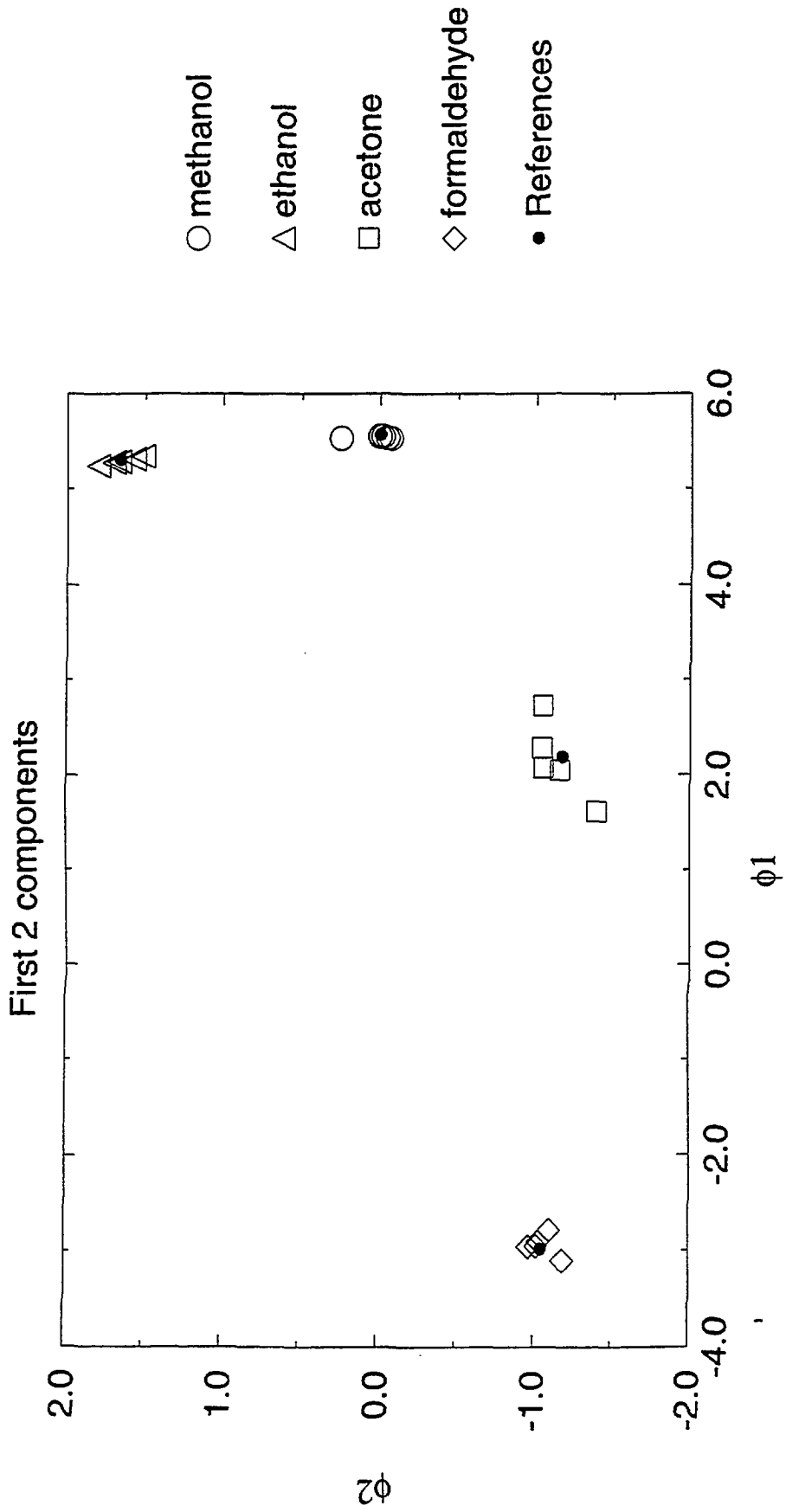


Figure 8b : Gram-Schmidt - 10% noisy data - 5 cycles + ref.

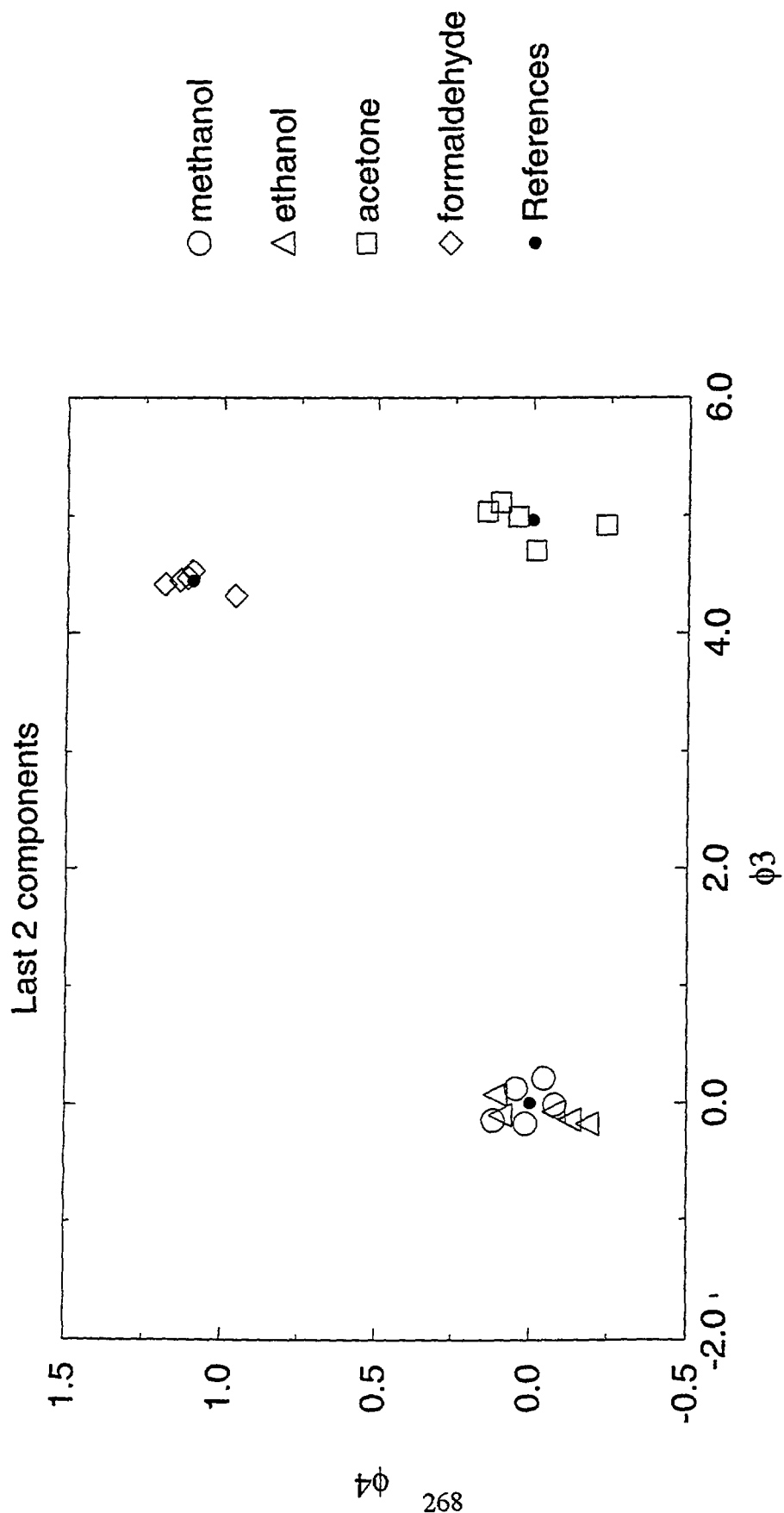


Figure 9a : Gram-Schmidt - drifting data - 5 cycles + ref.

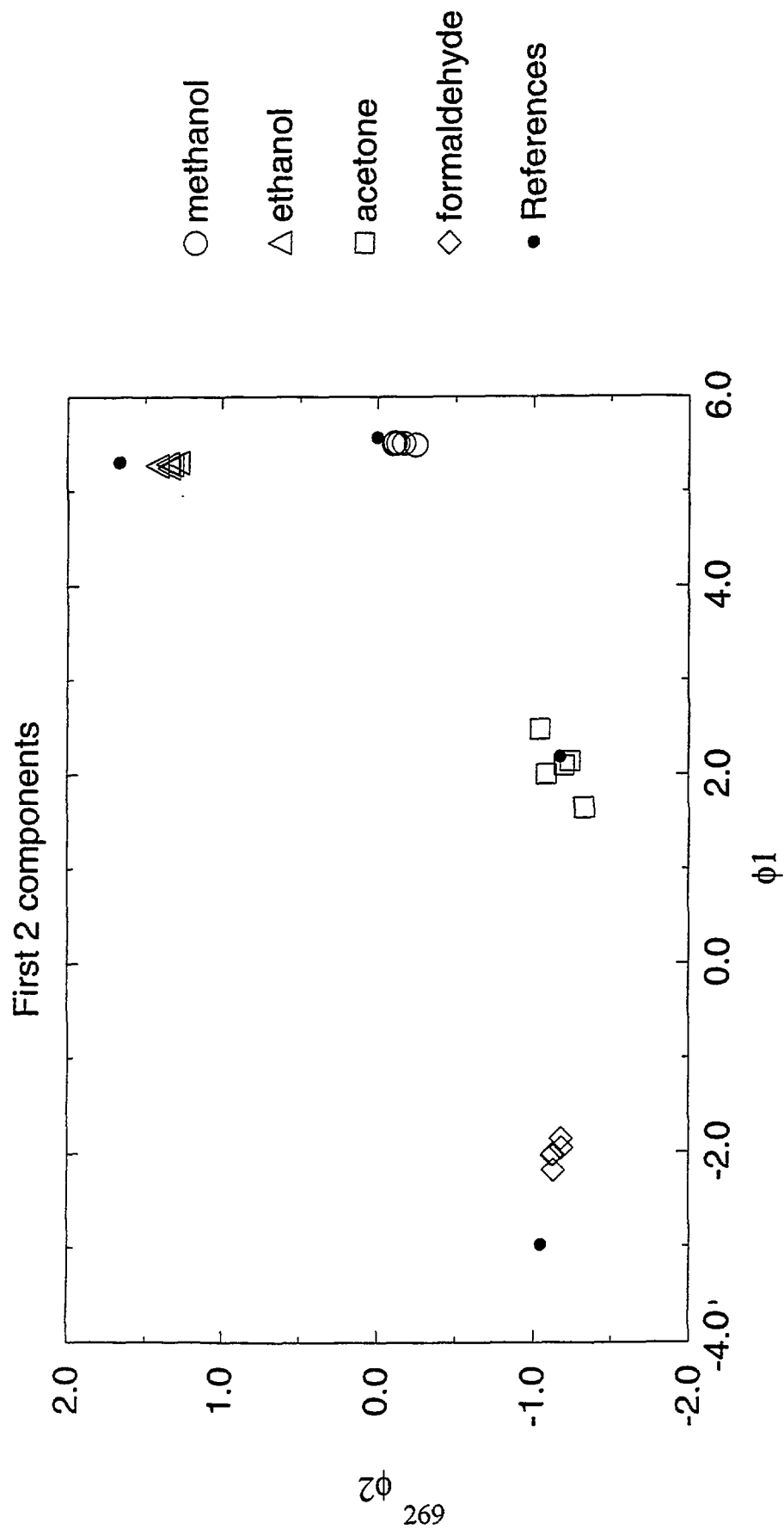


Figure 9b : Gram-Schmidt - drifting data - 5 cycles + ref.

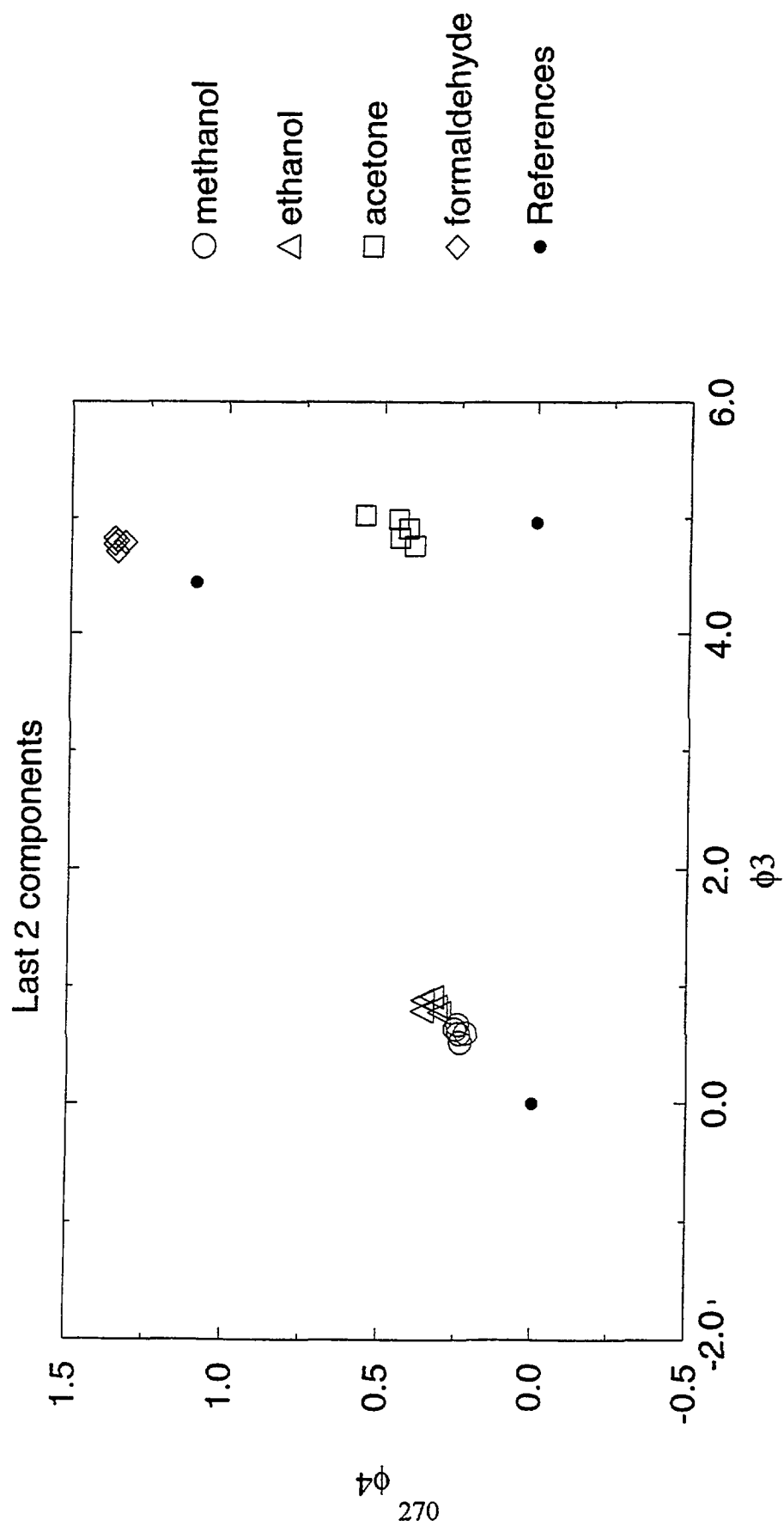


Figure 10a : FFT 32 coef. - original data - 5 cycles + ref.

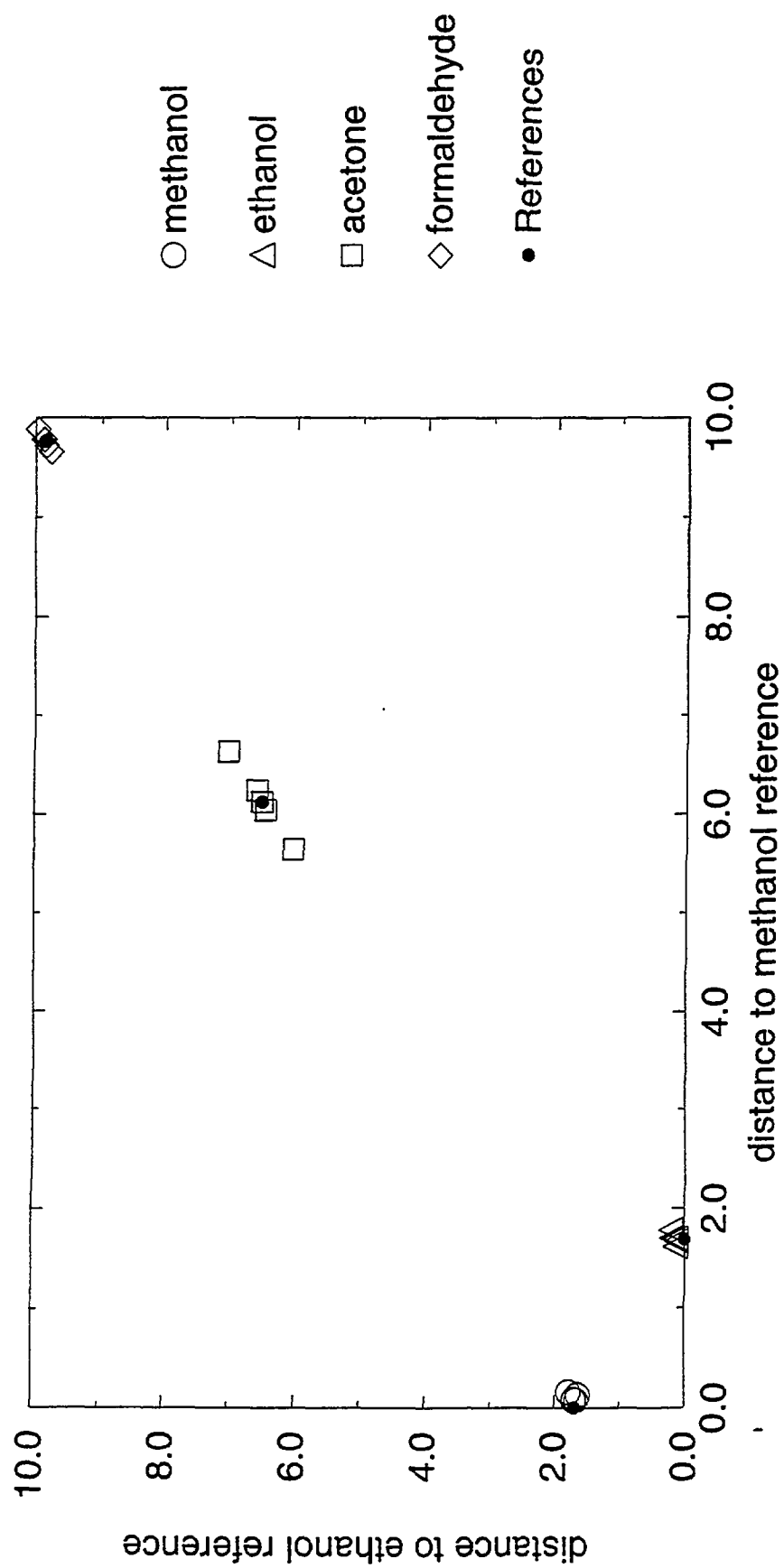


Figure 10b : FFT 32 coef. - original data - 5 cycles + ref.

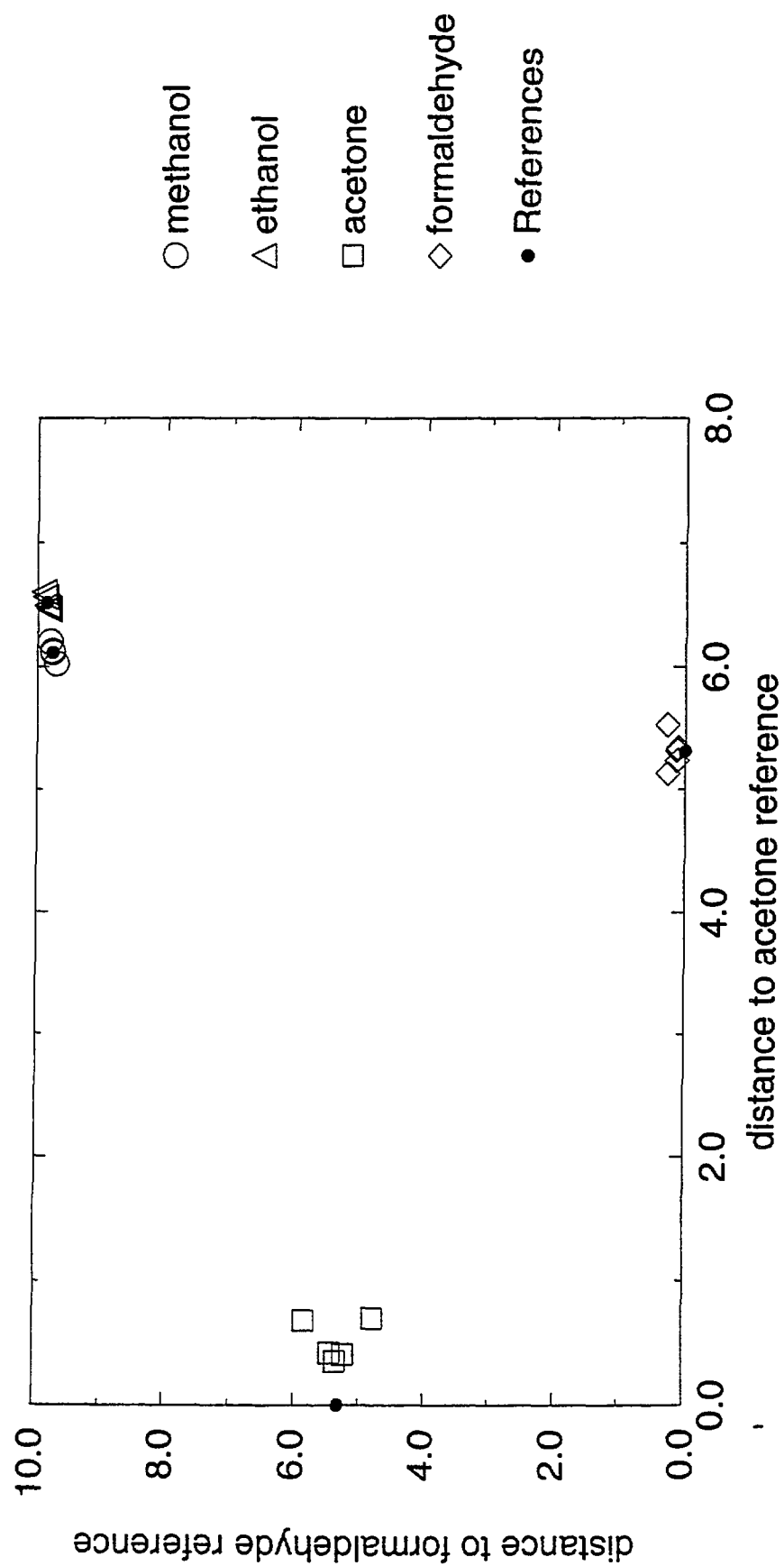


Figure 11a : FFT 8 coef. - original data - 5 cycles + ref.

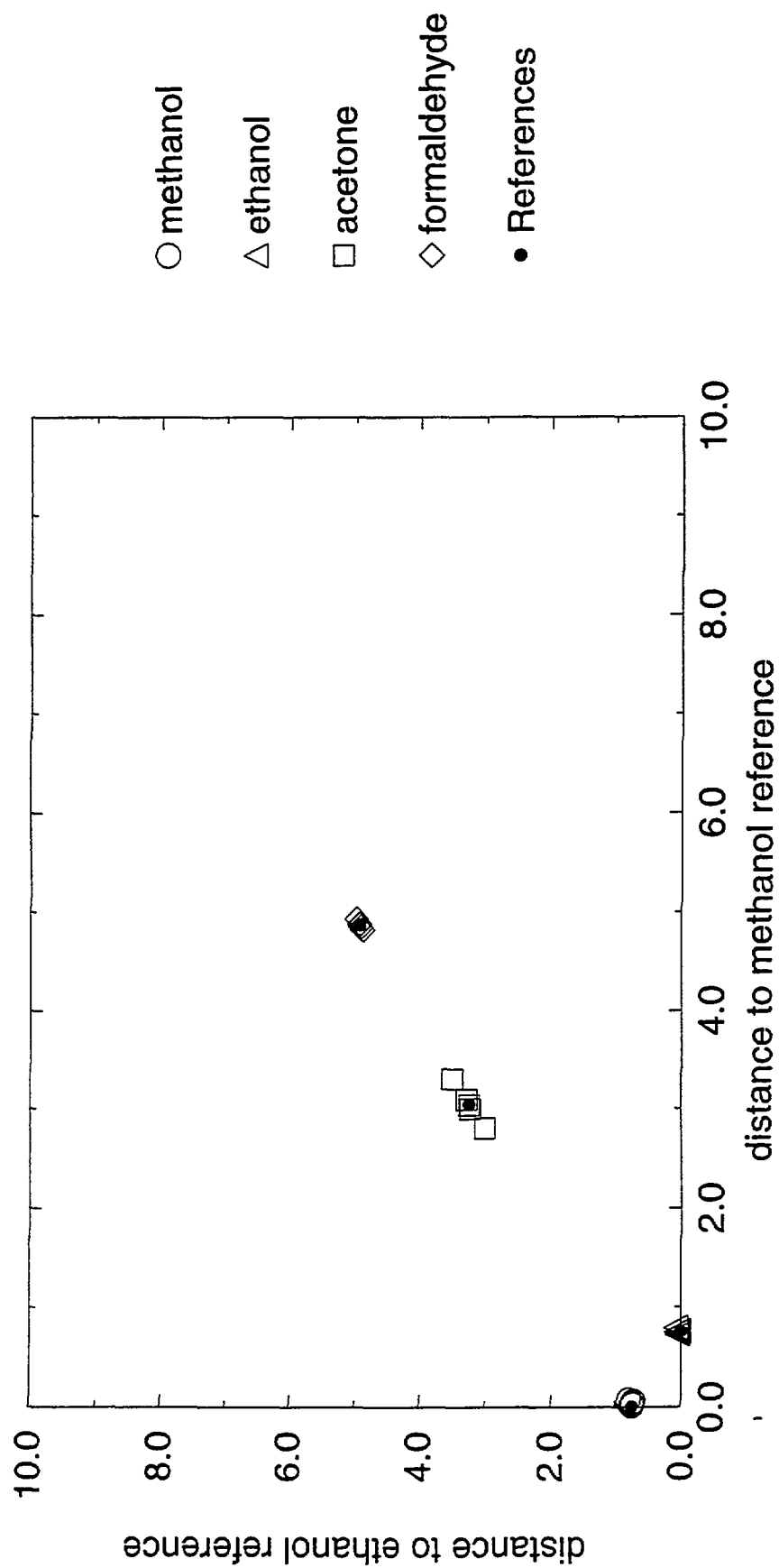


Figure 11b : FFT 8 coef. - original data - 5 cycles + ref.

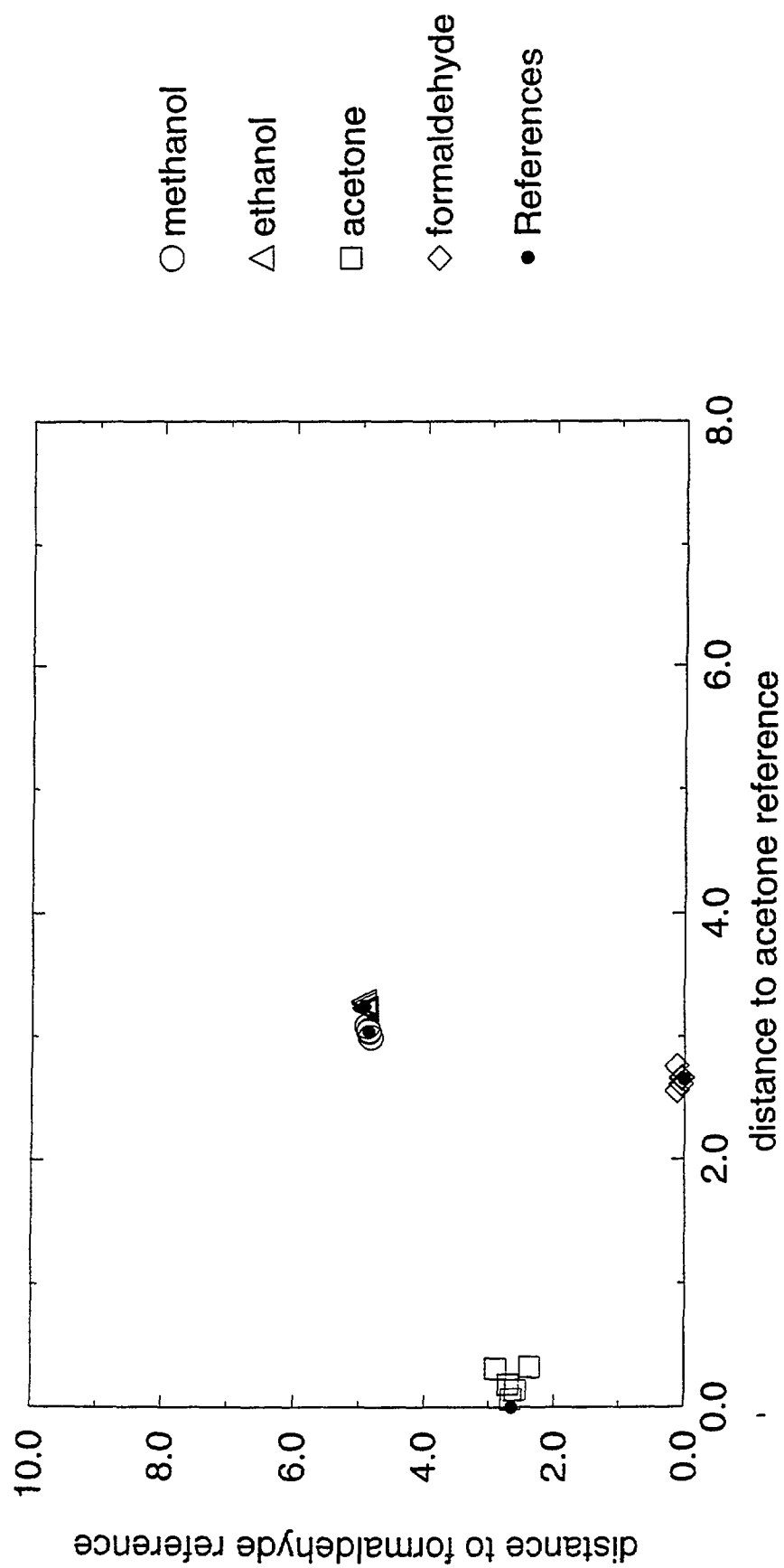


Figure 12a: FFT 8 coef. - 10% noisy data - 5 cycles + ref.

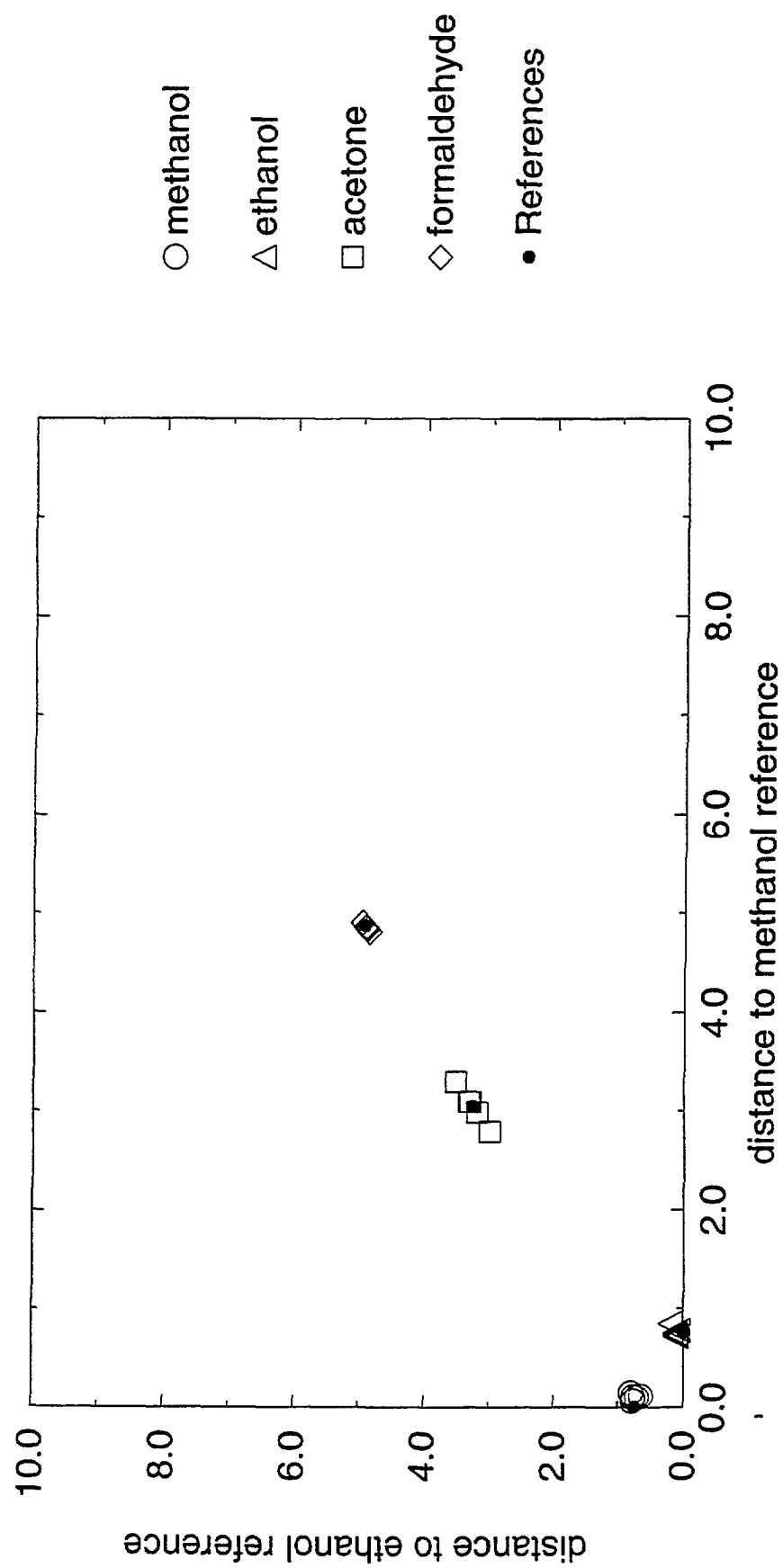


Figure 12b : FFT 8 coef. - 10% noisy data - 5 cycles + ref.

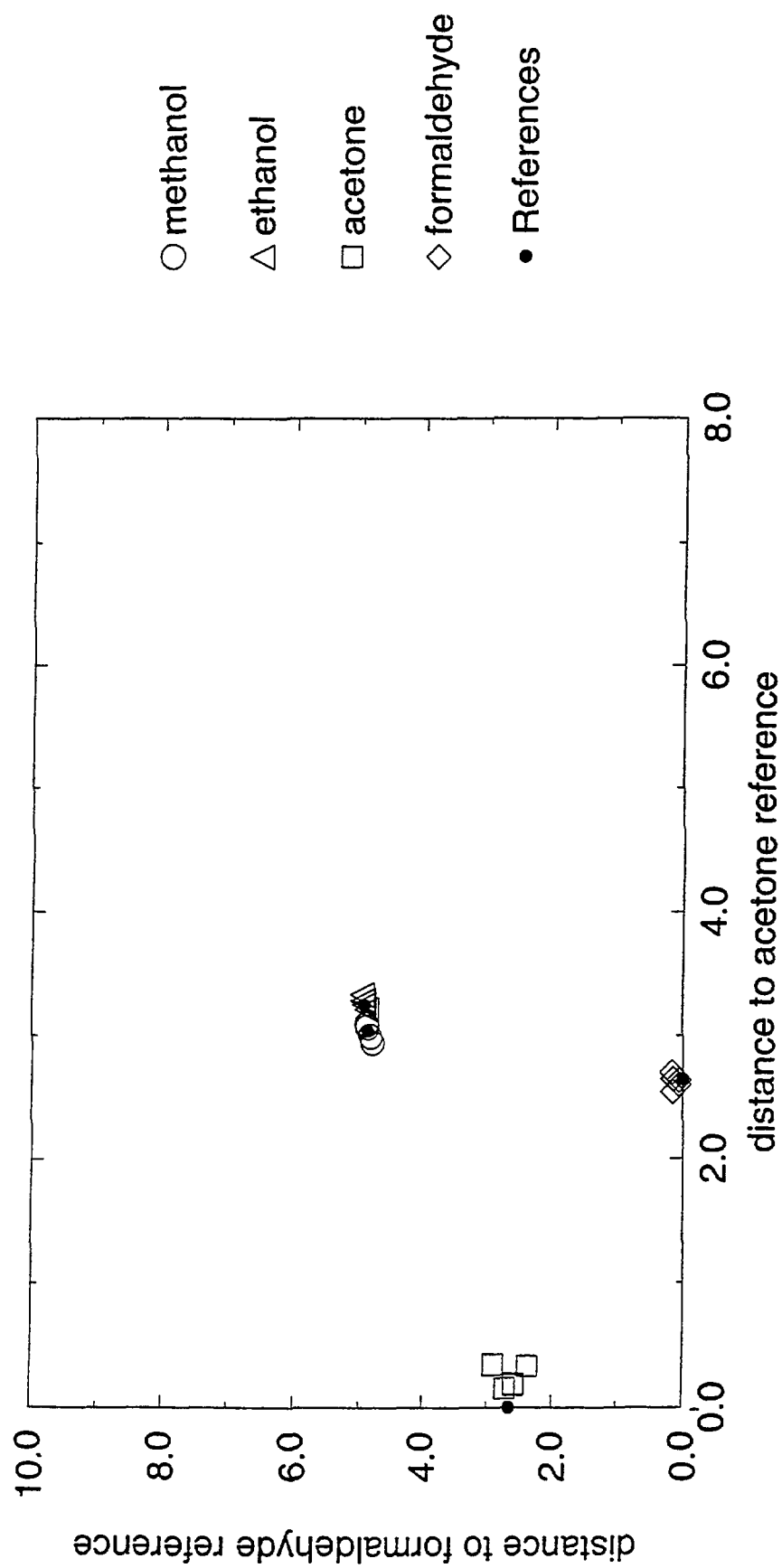


Figure 13a : FFT 8 coef. - drifting data - 5 cycles + ref.

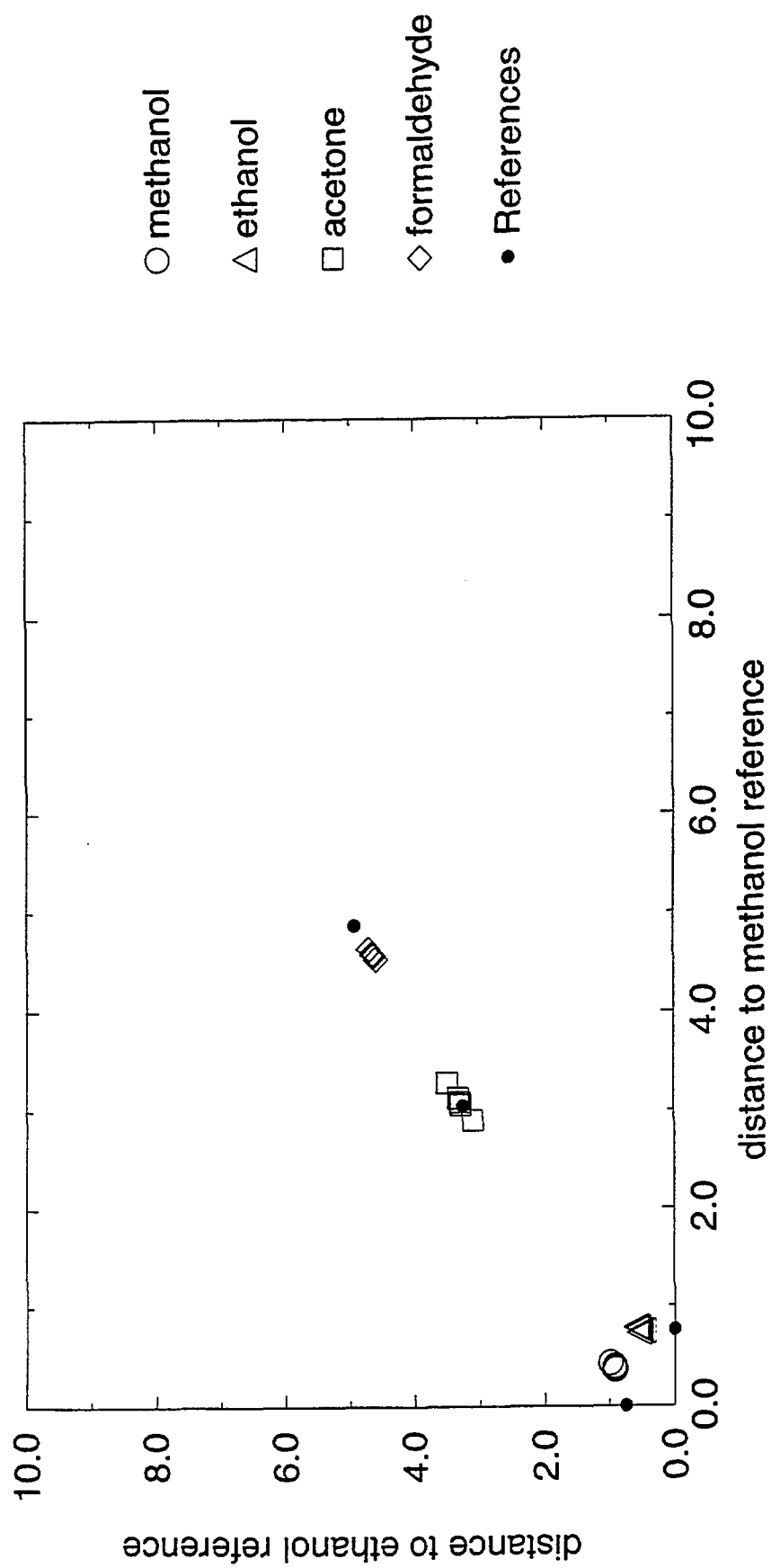


Figure 13b : FFT 8 coef. - drifting data - 5 cycles + ref.

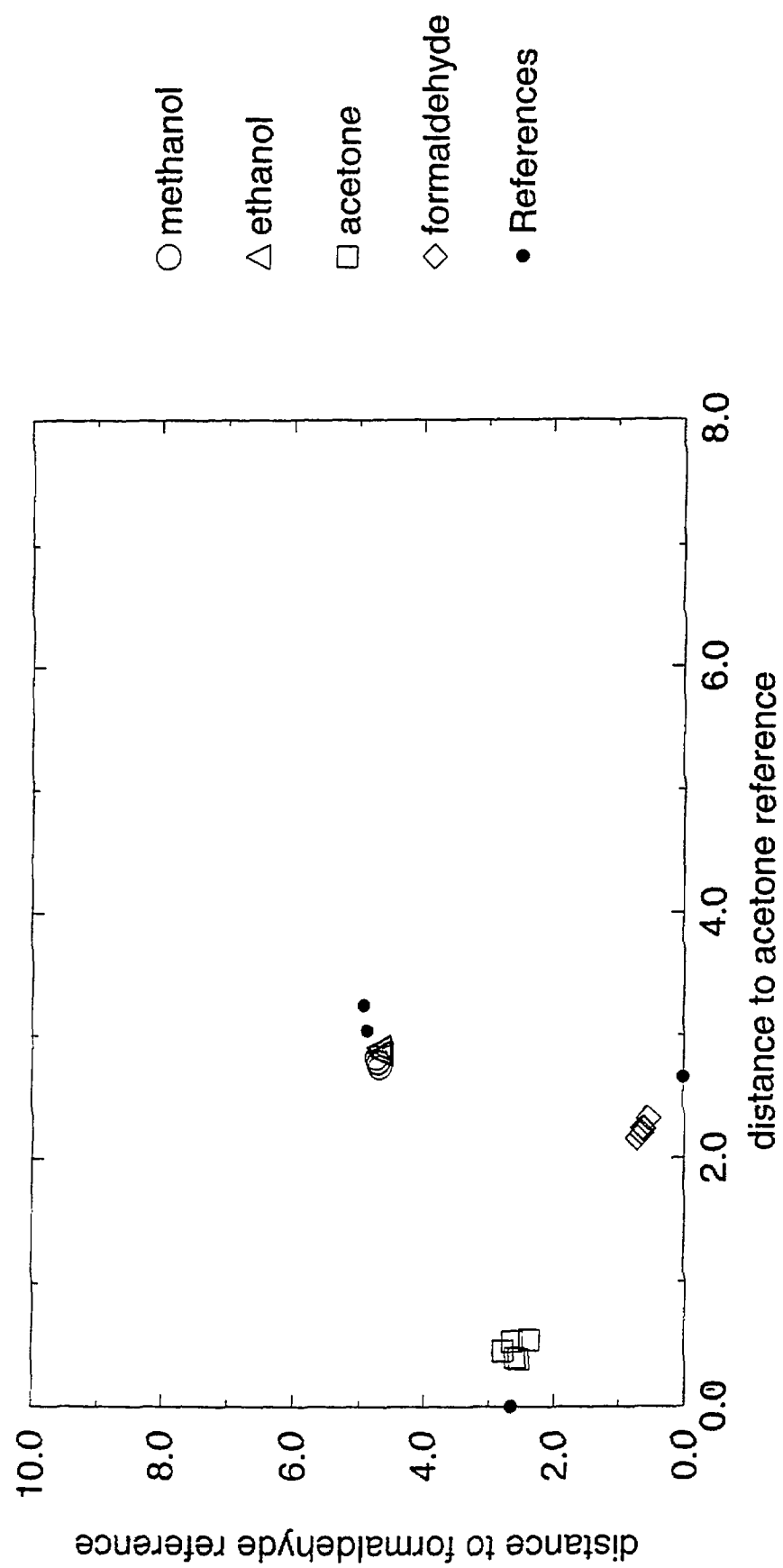


Figure 14 : Haar transform of the 4 references

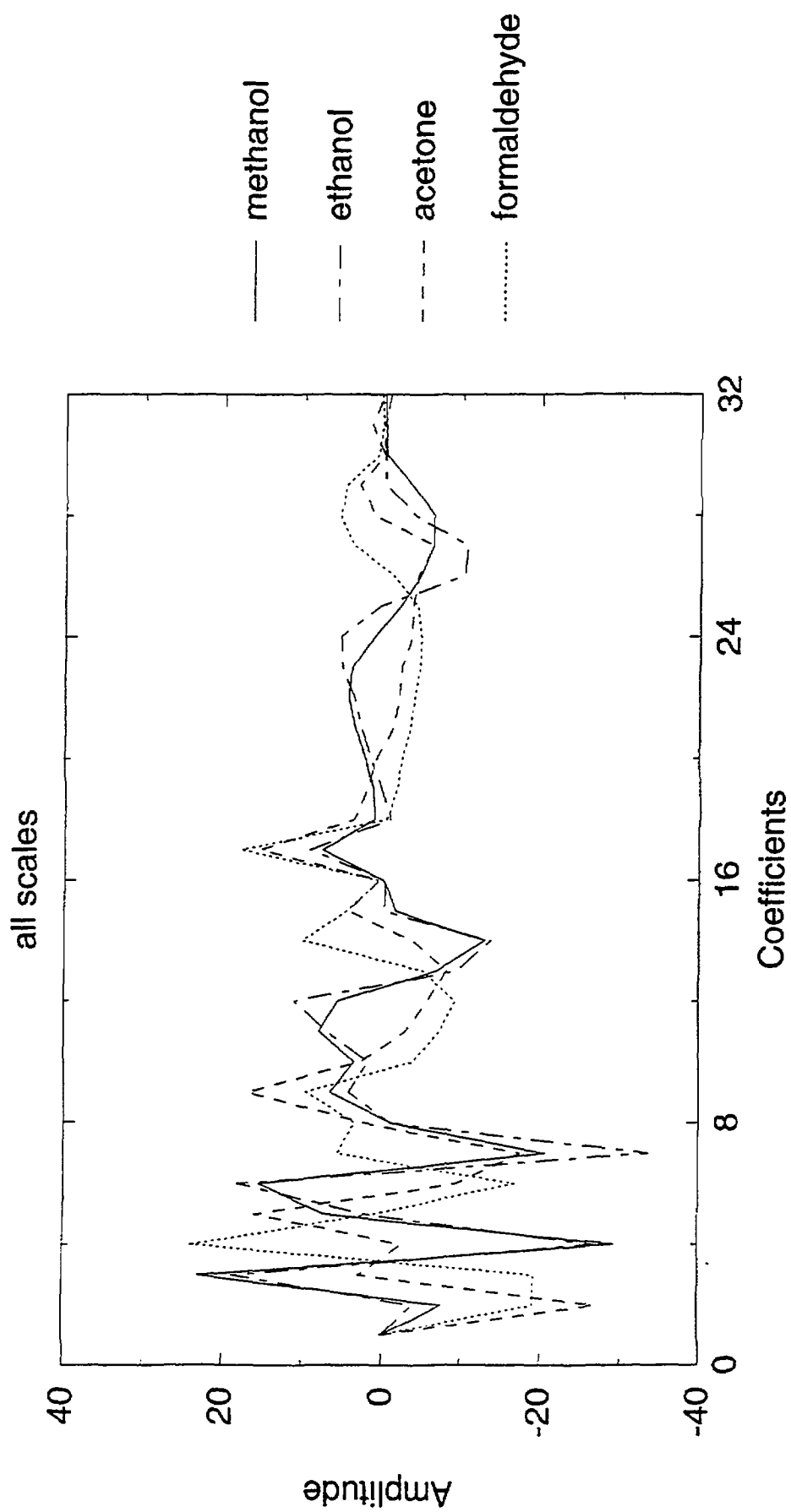


Figure 15 : Reconstructed signals from the Haar transform

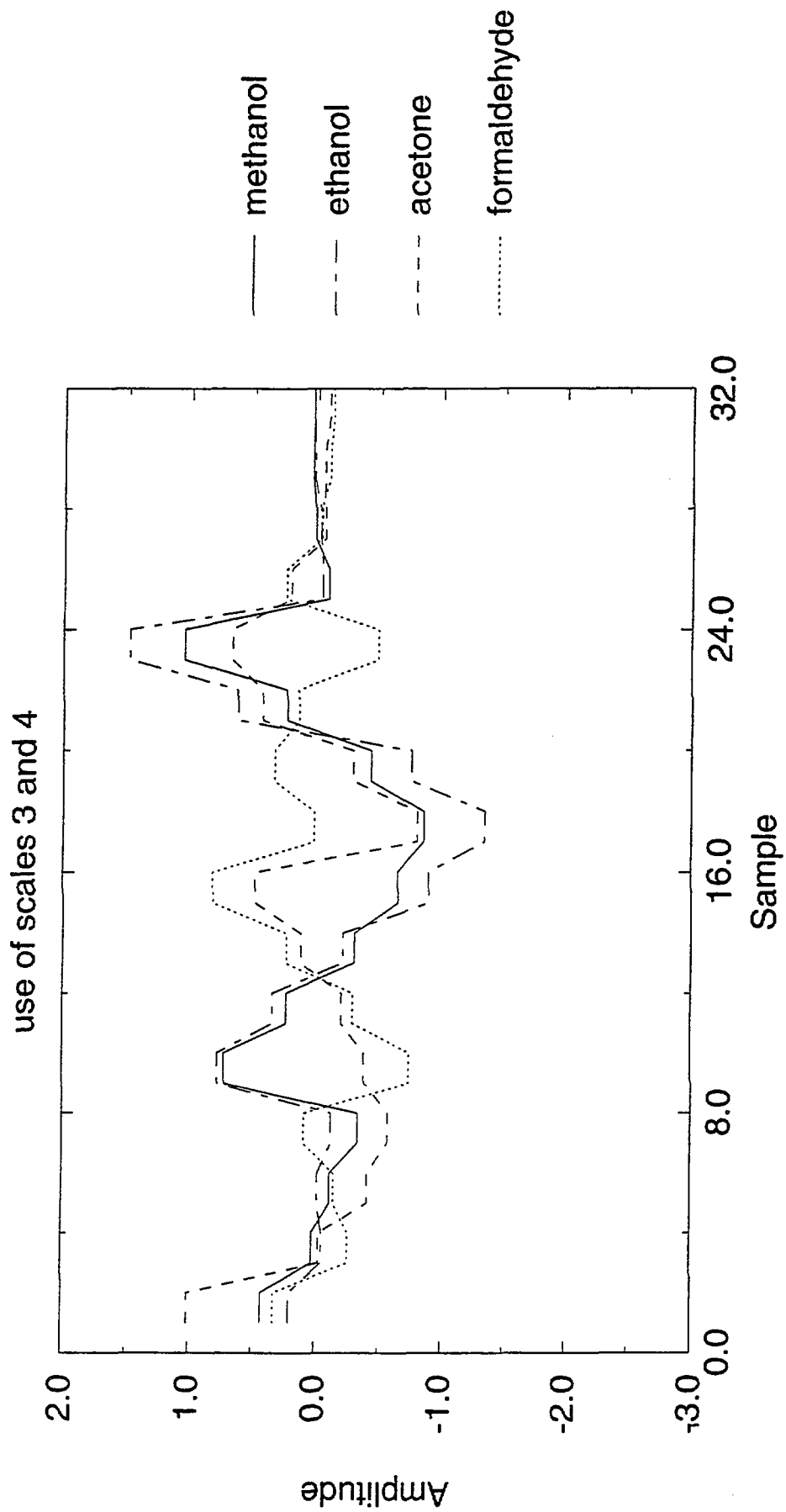


Figure 16 : Reconstructed signals from the Haar transform

use of scales 2, 3, and 4

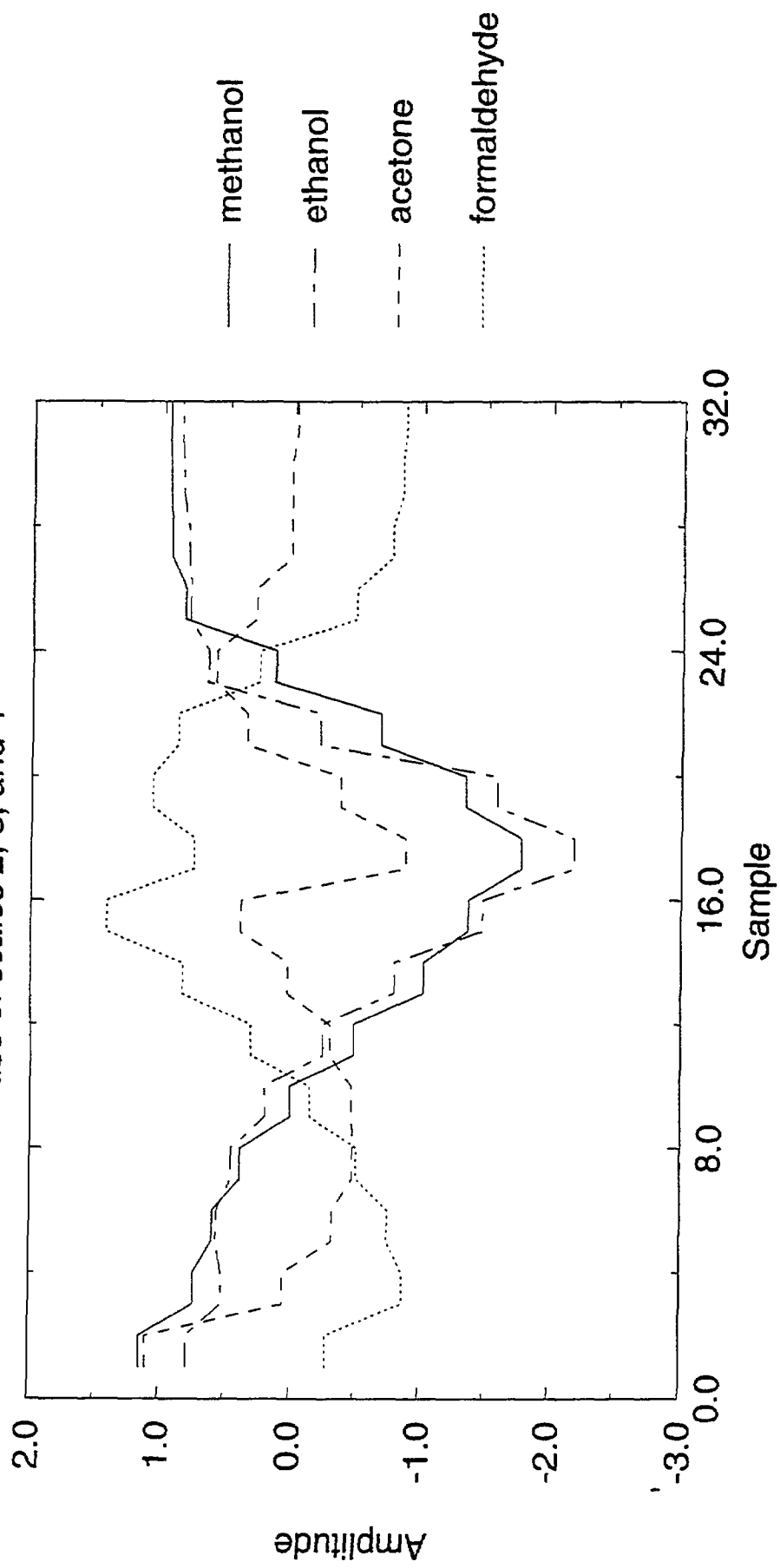


Figure 17 : Reconstructed signals from the Haar transform

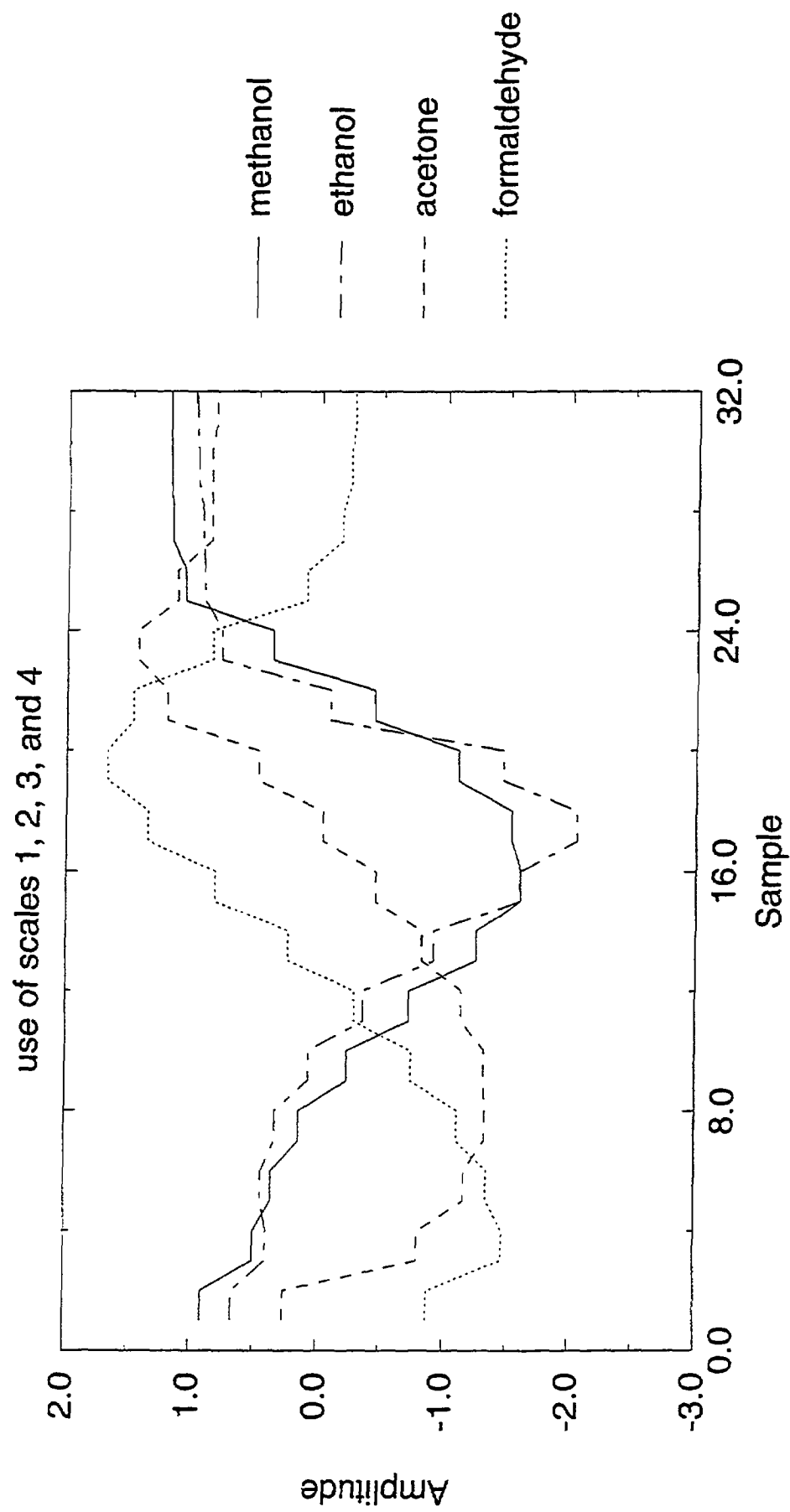


Figure 18a : Haar transform - original data - 5 cycles + ref.

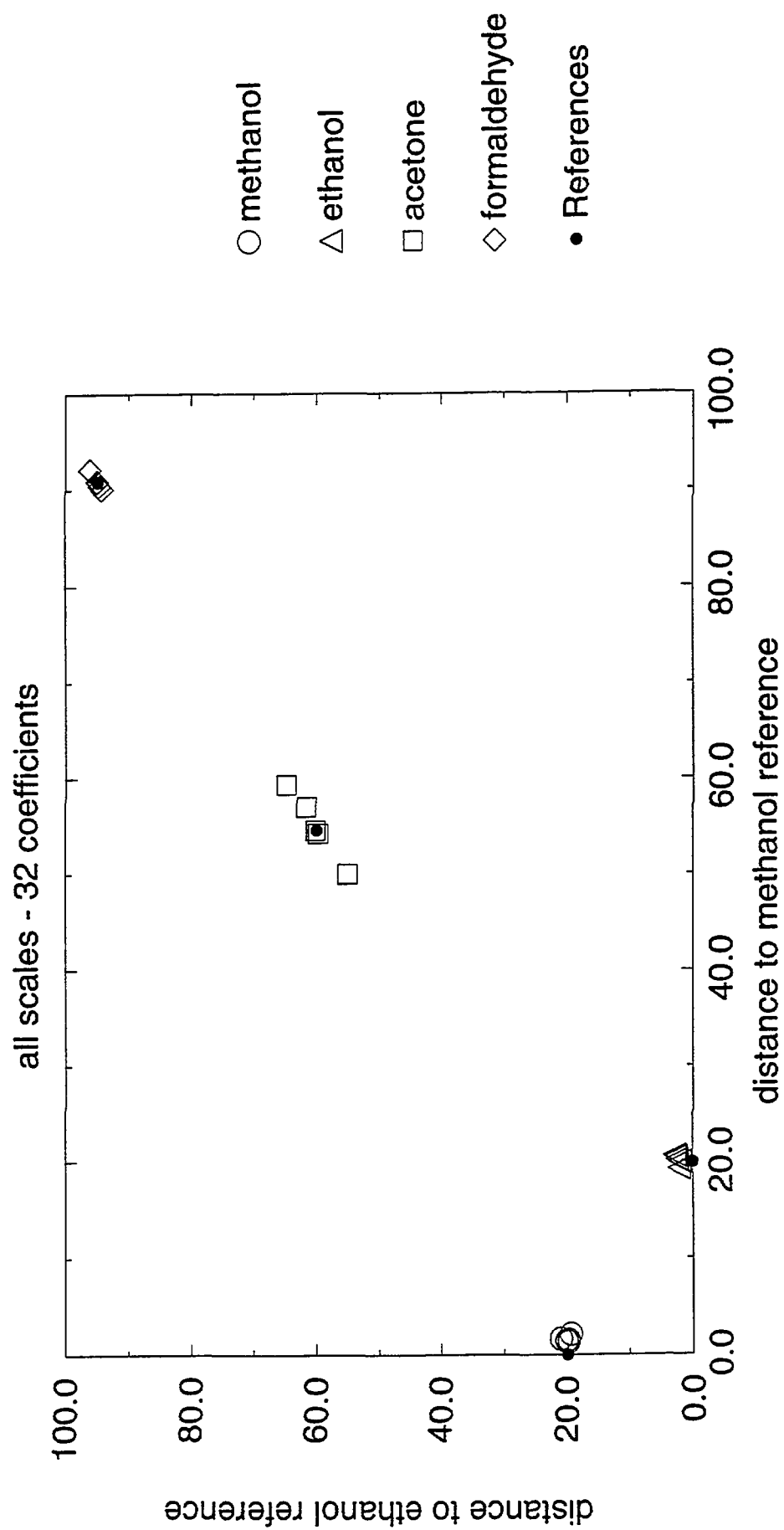


Figure 18b : Haar transform - original data - 5 cycles + ref.

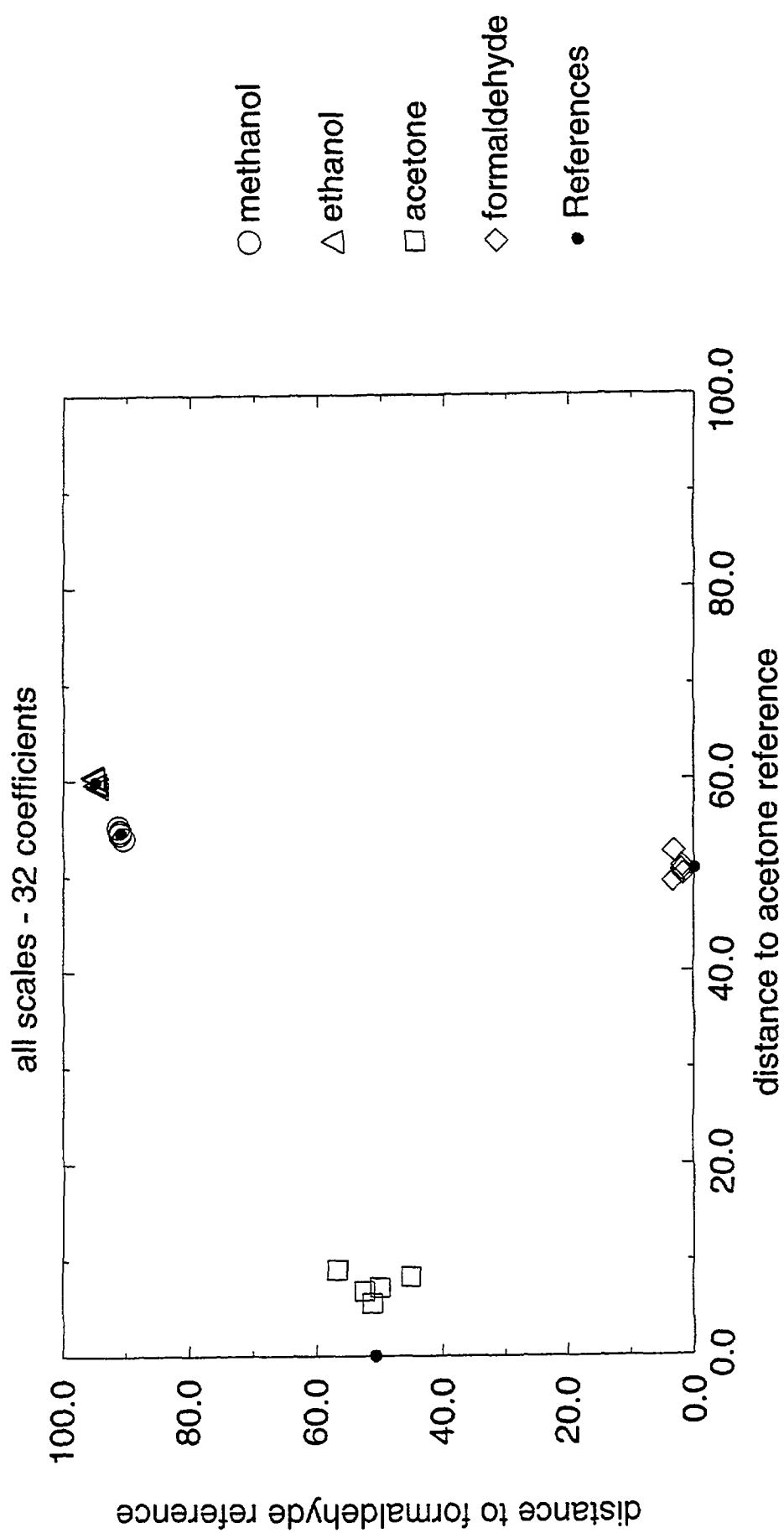


Figure 19a : Haar transform - original data - 5 cycles + ref.

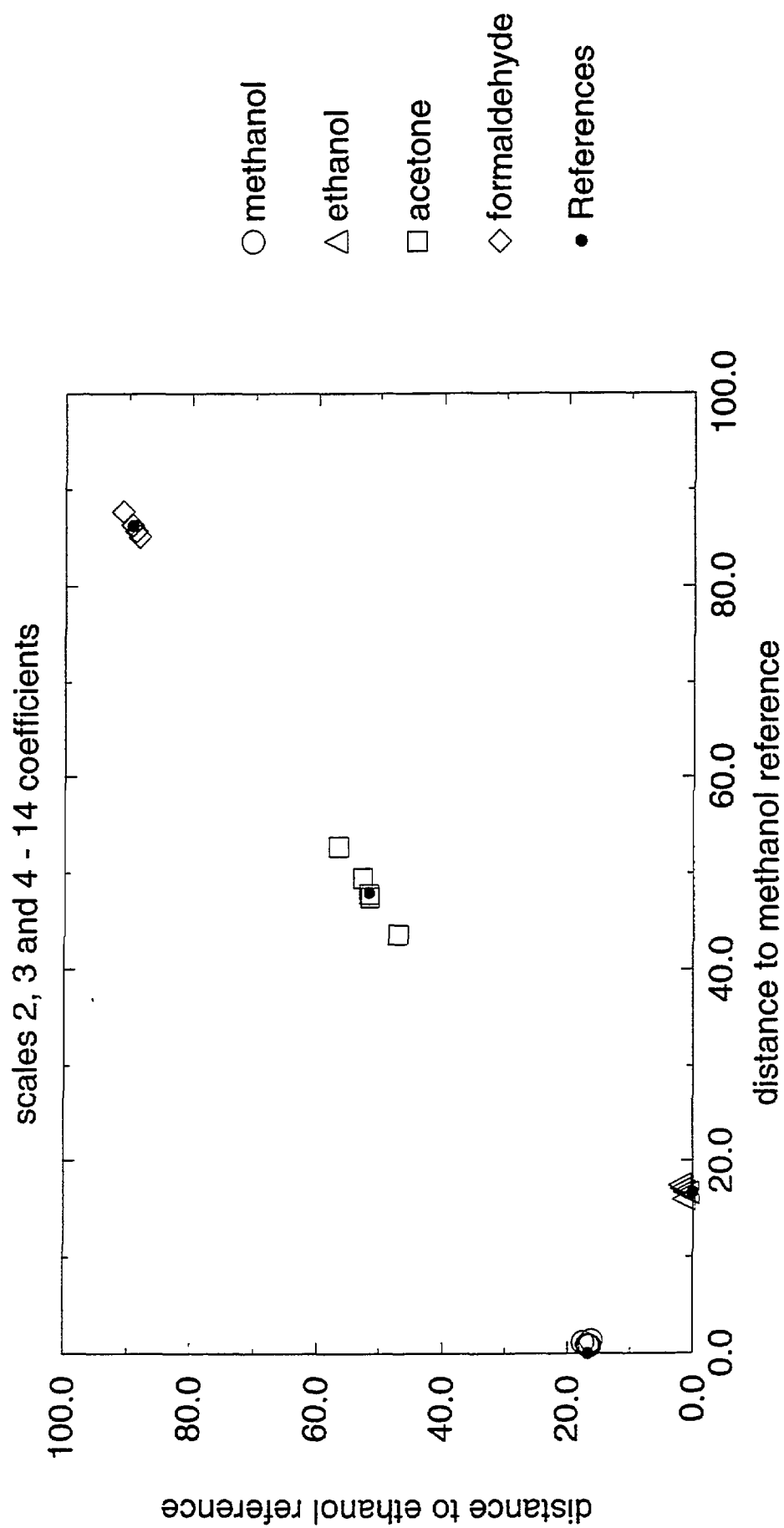


Figure 19b : Haar transform - original data - 5 cycles + ref.

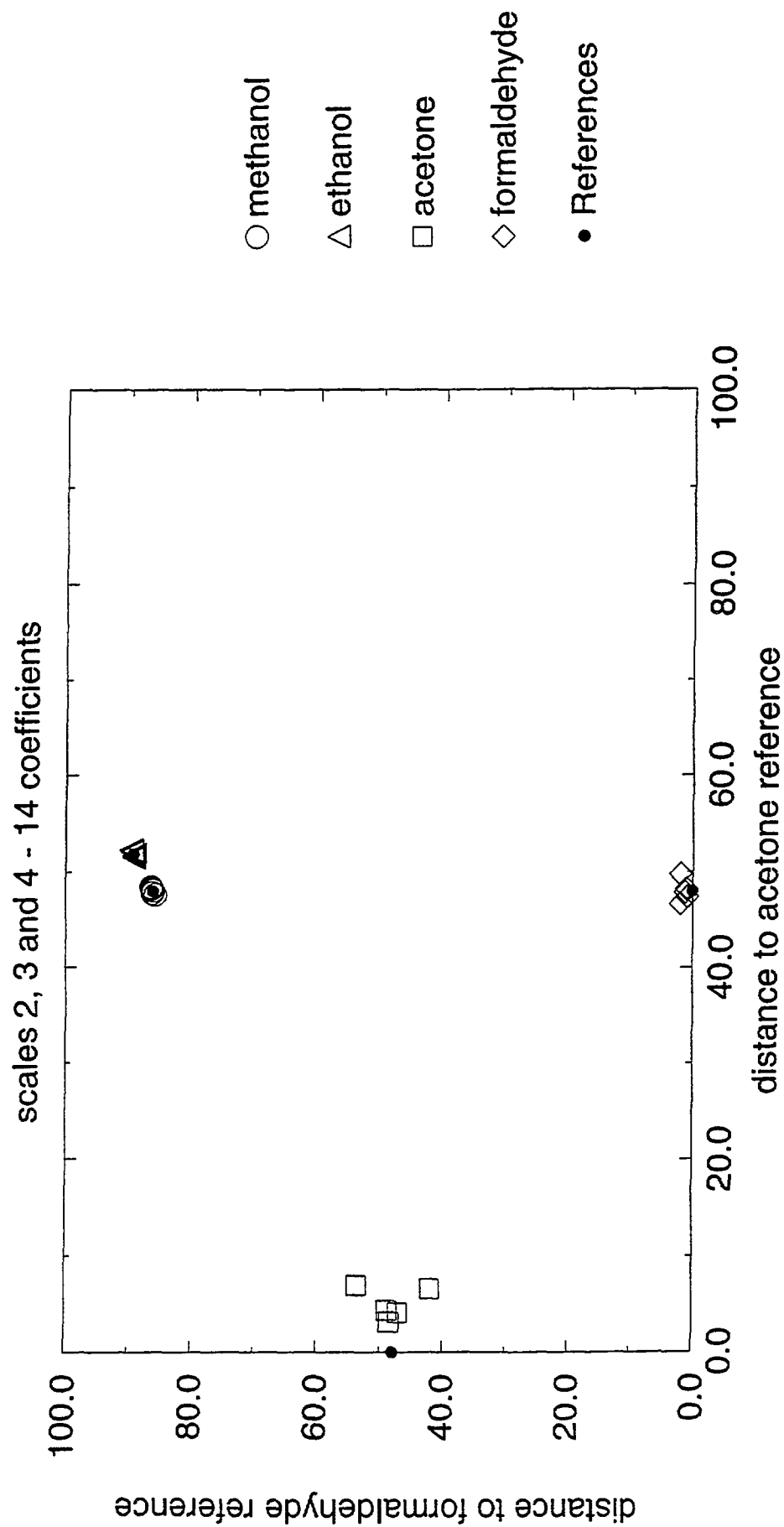


Figure 20a : Haar transform - original data - 5 cycles + ref.

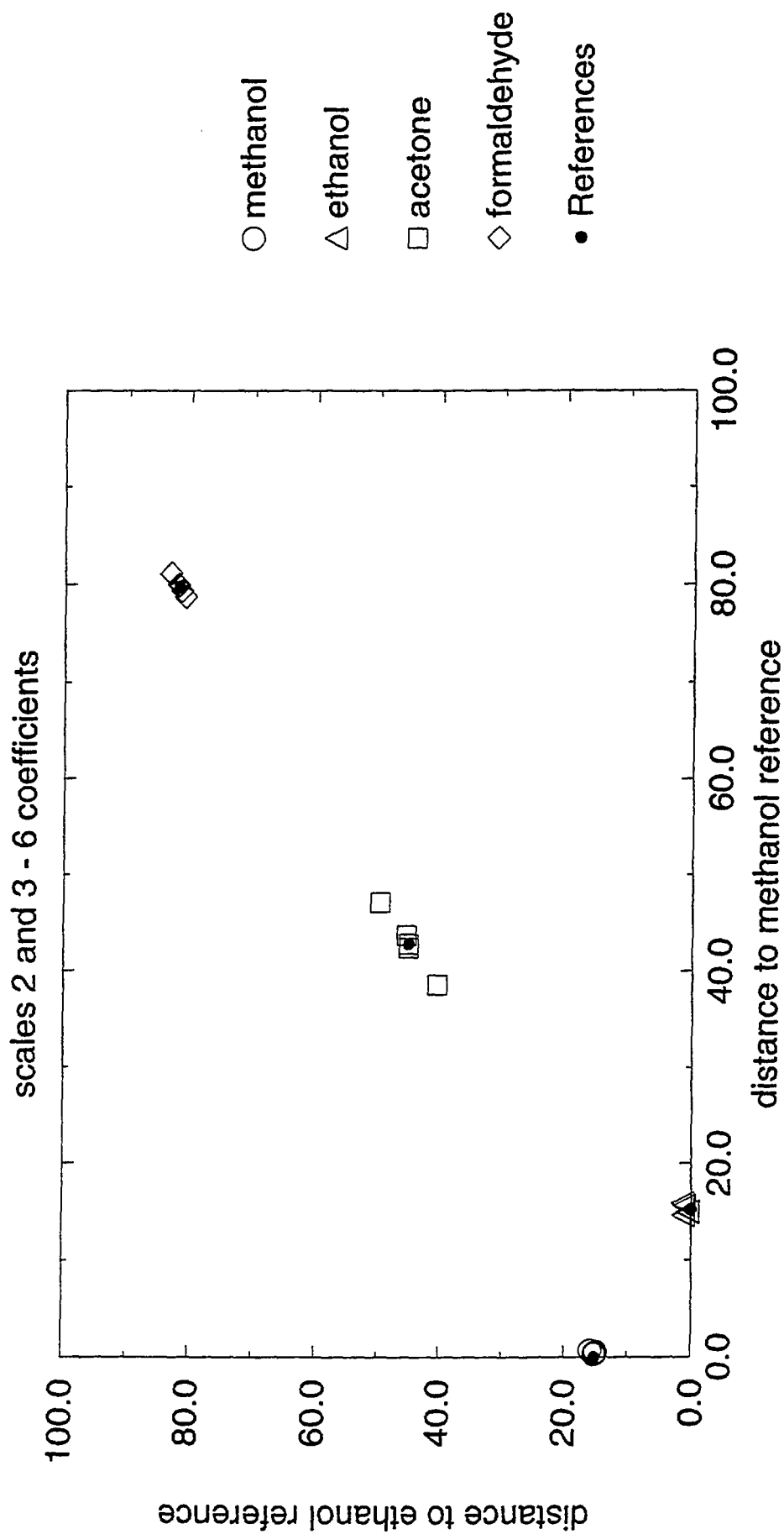


Figure 20b : Haar transform - original data - 5 cycles + ref.

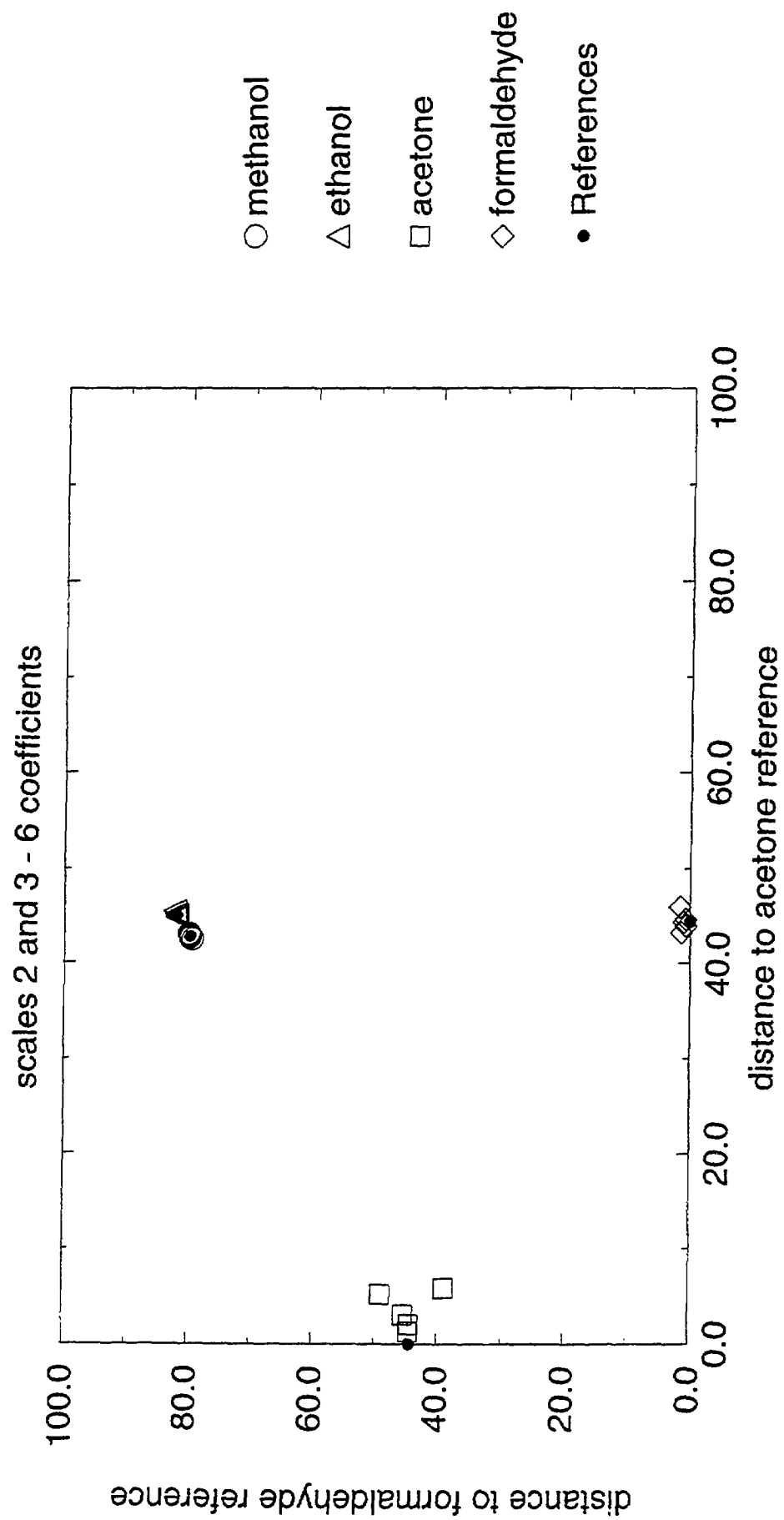


Figure 21a : Haar transform - original data - 5 cycles + ref.

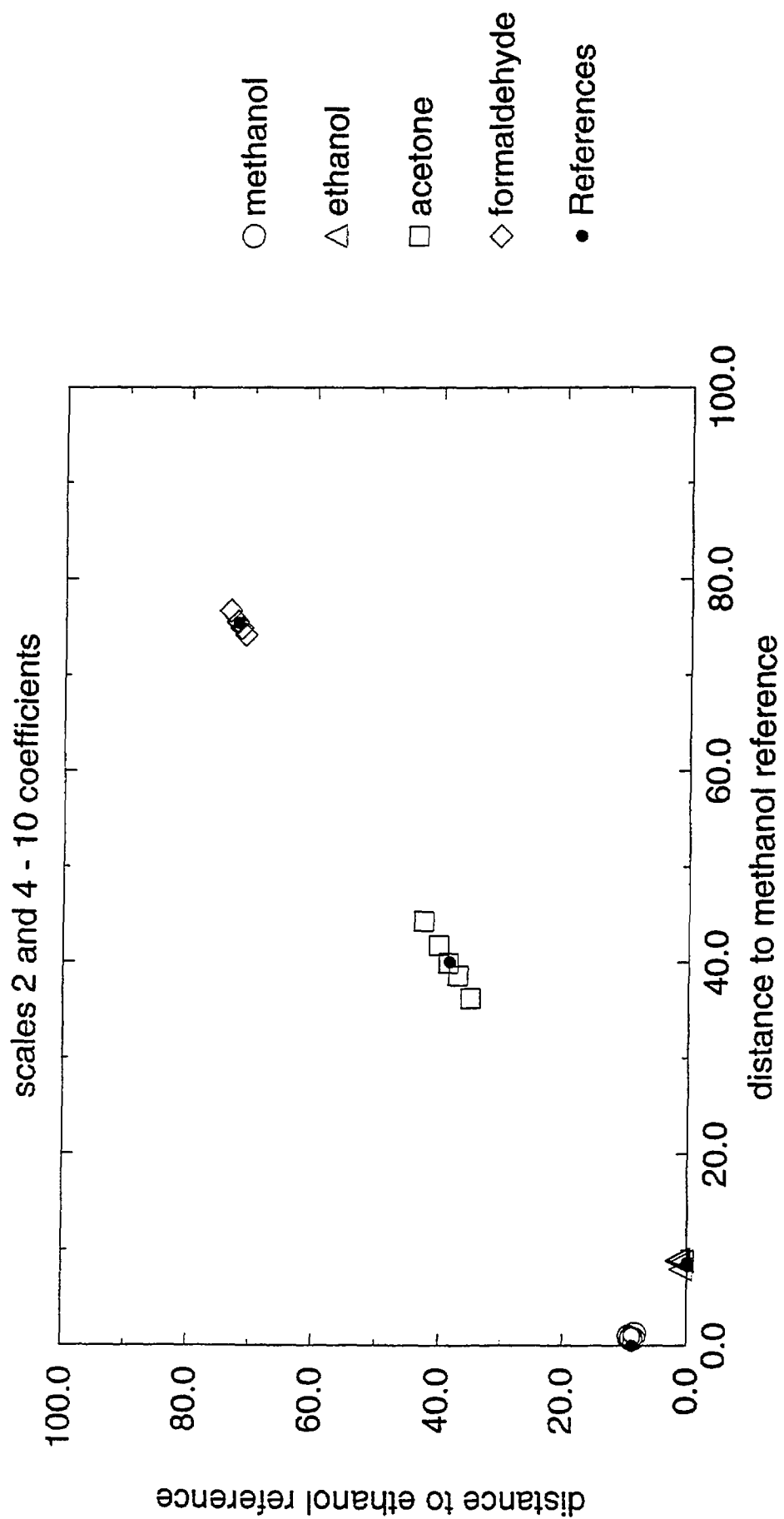
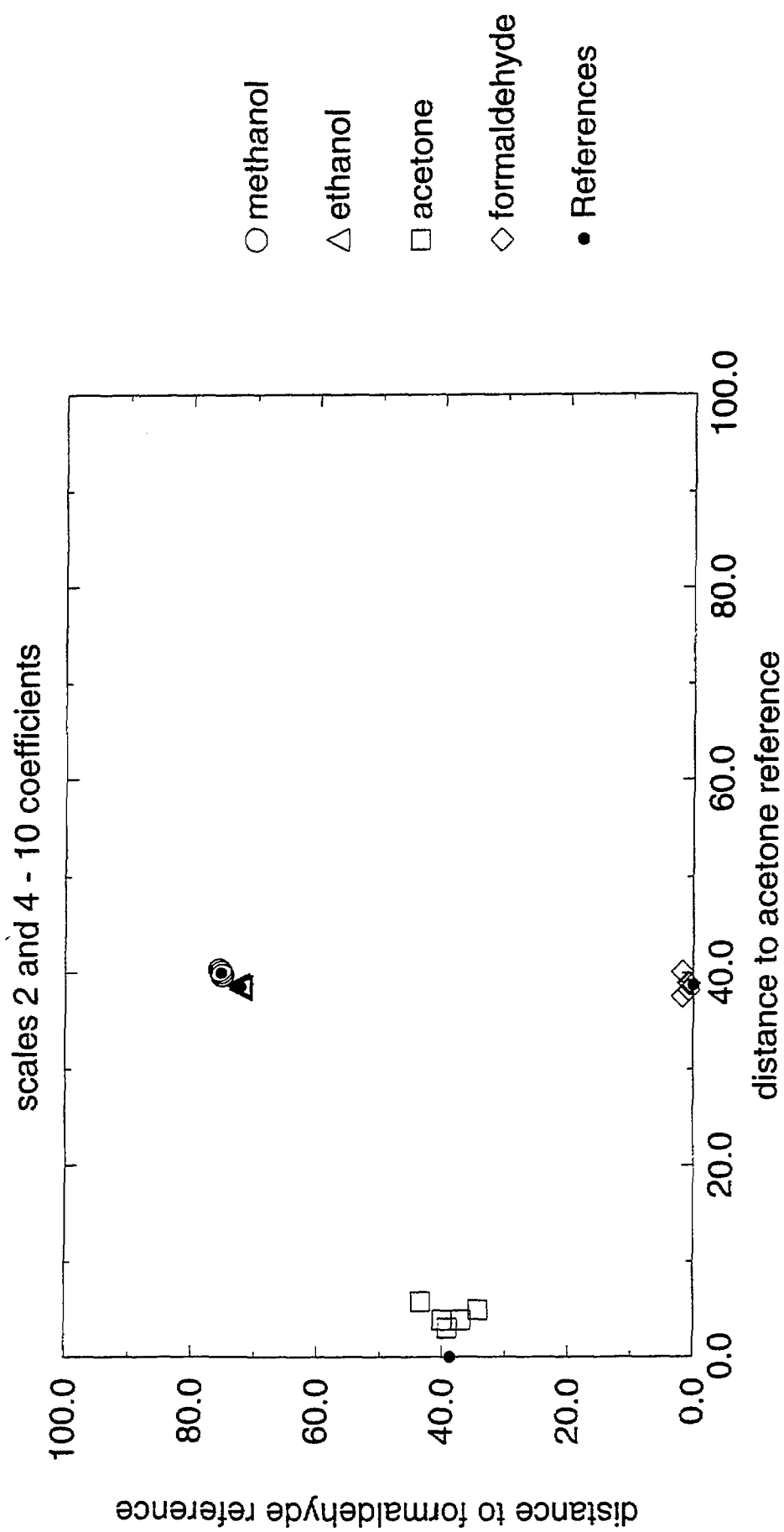


Figure 21b : Haar transform - original data - 5 cycles + ref.



	Thermometer 16	Gray 4
Alc/Non-Alc.	21.5 (4)	8 (0)
Met/Et	4.5 (2)	3 (2)
Acet/Form	13 (2.6)	7.75 (1.3)

Table 1 : Statistical results - mean (standard deviation) - on the distance between references obtained using the 16 level thermometer coding and the 4 bit Gray coding

	Thermometer 16	Gray 4
alcohol	100	100
non-alcohol	100	100
methanol	100	50
ethanol	87	87
acetone	100	100
formaldehyde	100	75

Table 2 : Statistical results (in percentage) on the gas classification using the 16 level thermometer coding and the 4 bit Gray coding on original data.

	Thermometer 16	Gray 4
alcohol	100	100
non-alcohol	100	100
methanol	50	62
ethanol	87	62
acetone	62	75
formaldehyde	100	75

Table 3 : Statistical results (in percentage) on the gas classification using the 16 level thermometer coding and the 4 bit Gray coding on noisy data.

	Thermometer 16	Gray 4
alcohol	100	100
non-alcohol	81	69
methanol	100	62
ethanol	75	62
acetone	50	50
formaldehyde	100	37

Table 4: Statistical results (in percentage) on the gas classification using the 16 level thermometer coding and the 4 bit Gray coding on drifting data.

Section III

Publications Associated with the Project

1. Milke, J.A., "Towards an Artificial Nose for Fire Detection," presented at the Annual Conference on Fire Research, Rockville, MD, October 19, 1993.
2. Milke, J.A., "Initial Application of Neural Networks to Discriminate Between Fire and Non-Fire Odors," presented at the Annual Conference on Fire Research, Rockville, MD, October 19, 1993.
3. Milke, J.A., and Denny, S., "Initial Application of Neural Networks to Discriminate Between Fire and Non-Fire Odors," Proceedings: Society of Fire Protection Engineers Engineering Seminar, San Francisco, May, 1994, 81-88.
4. Milke, J.A., "Large-scale Experiments of Fire Signatures to Develop a Discriminating Fire Detector," presented at the Annual Conference on Fire Research, Gaithersburg MD, October 19, 1994.
5. Milke, J.A., "Application of Neural Networks for Discriminating Fire Detectors," Proceedings: 10th International Conference on Fire Detection, AUBE '95, Duisburg, Germany, April, 1995, 213-222.
6. Milke, J.A. and McAvoy, T.J., "Analysis of Signature Patterns for Discriminating Fire Detection with Multiple Sensors," Fire Technology, 31, (3), 2nd Quarter 1995, 120-136 (received Harry C. Bigglestone Award).
7. Milke, J.A., McAvoy, T.J., Kunt, T. and Hopkins, M., "Using Multivariate Statistical Methods to Detect Fires," Proceedings: International Conference on Fire Research and Engineering, Orlando, FL, September, 1995, 301-306.
8. McAvoy, T.J., Milke, J.A., and Kunt, T., "Using Multivariate Statistical Methods to Detect Fires," Fire Technology, 32 (1) 1st Quarter 1996, 6-24.
9. Milke, J.A., "Multivariate Methods for Discriminating Fire Detection," 13th Meeting of the UJNR Panel on Fire Research and Safety, Gaithersburg, MD: March 20, 1996.
10. Dong, D., and McAvoy, T., "Nonlinear Principal Component Analysis - Based on Principal Curves and Neural Networks", Computers and Chemical Engineering, 20: 1996, 65-78.
11. Milke, J.A., "Analysis of Signature Patterns for Discriminating Fire Detection with Multiple Sensors," Harry C. Bigglestone Lecture, National Fire Protection Association Annual Meeting, Boston, MA, May 20, 1996.
12. Milke, J.A., and McAvoy, T.J., "Analysis of Fire and Non-fire Signatures for Discriminating Fire Detection," accepted for presentation at 5th International Symposium of IAFSS, Australia, March 1997.

NIST-114 (REV. 6-93) ADMAN 4.09		U.S. DEPARTMENT OF COMMERCE NATIONAL INSTITUTE OF STANDARDS AND TECHNOLOGY		(ERB USE ONLY)	
		ERB CONTROL NUMBER		DIVISION	
MANUSCRIPT REVIEW AND APPROVAL		PUBLICATION REPORT NUMBER NIST-GCR-96-699		CATEGORY CODE	
INSTRUCTIONS: ATTACH ORIGINAL OF THIS FORM TO ONE (1) COPY OF MANUSCRIPT AND SEND TO THE SECRETARY, APPROPRIATE EDITORIAL REVIEW BOARD		PUBLICATION DATE December 1996		NUMBER PRINTED PAGES	
TITLE AND SUBTITLE (CITE IN FULL) Neural Networks for Smart Fire Detection					
CONTRACT OR GRANT NUMBER 60NANB2D1300		TYPE OF REPORT AND/OR PERIOD COVERED Final Report, June 28, 1996			
AUTHOR(S) (LAST NAME, FIRST INITIAL, SECOND INITIAL) Milke, J. A. and McAvoy, T. J. Department of Fire Protection Engineering and Chemical Engineering University of Maryland, College Park, MD				PERFORMING ORGANIZATION (CHECK (X) ONE BOX) <input type="checkbox"/> NIST/GAITHERSBURG <input type="checkbox"/> NIST/BOULDER <input type="checkbox"/> JILA/BOULDER	
LABORATORY AND DIVISION NAMES (FIRST NIST AUTHOR ONLY)					
SPONSORING ORGANIZATION NAME AND COMPLETE ADDRESS (STREET, CITY, STATE, ZIP) U.S. Department of Commerce National Institute of Standards and Technology, Gaithersburg, MD 20899					
PROPOSED FOR NIST PUBLICATION					
<input type="checkbox"/> JOURNAL OF RESEARCH (NIST JRES) <input type="checkbox"/> J. PHYS. & CHEM. REF. DATA (JPCRD) <input type="checkbox"/> HANDBOOK (NIST HB) <input type="checkbox"/> SPECIAL PUBLICATION (NIST SP) <input type="checkbox"/> TECHNICAL NOTE (NIST TN)		<input type="checkbox"/> MONOGRAPH (NIST MN) <input type="checkbox"/> NATL. STD. REF. DATA SERIES (NIST NSRDS) <input type="checkbox"/> FEDERAL INF. PROCESS. STDS. (NIST FIPS) <input type="checkbox"/> LIST OF PUBLICATIONS (NIST LP) <input type="checkbox"/> NIST INTERAGENCY/INTERNAL REPORT (NISTIR)		<input type="checkbox"/> LETTER CIRCULAR <input type="checkbox"/> BUILDING SCIENCE SERIES <input type="checkbox"/> PRODUCT STANDARDS <input checked="" type="checkbox"/> OTHER <u>NIST-GCR</u>	
PROPOSED FOR NON-NIST PUBLICATION (CITE FULLY)		<input type="checkbox"/> U.S. <input type="checkbox"/> FOREIGN		PUBLISHING MEDIUM <input checked="" type="checkbox"/> PAPER <input type="checkbox"/> CD-ROM <input type="checkbox"/> DISKETTE (SPECIFY) _____ <input type="checkbox"/> OTHER (SPECIFY) _____	
SUPPLEMENTARY NOTES					
ABSTRACT (A 2000-CHARACTER OR LESS FACTUAL SUMMARY OF MOST SIGNIFICANT INFORMATION. IF DOCUMENT INCLUDES A SIGNIFICANT BIBLIOGRAPHY OR LITERATURE SURVEY, CITE IT HERE. SPELL OUT ACRONYMS ON FIRST REFERENCE.) (CONTINUE ON SEPARATE PAGE, IF NECESSARY.) Research was conducted using multiple sensors with algorithm to detect fires more quickly than currently available smoke detectors while also decreasing the susceptibility to unnecessary alarms. The effort involved the production of signatures from three types of sources; flaming fires, non-flaming fires and non-fire, nuisance sources, followed by analysis to recognize signature patterns for the three type of sources. The first phases of research consisted of establishing the feasibility of distinguishing between signatures from fire and non-fire sources using a small-scale apparatus. The second phase consisted of introducing the signatures in a 12 ft square room with a height of 8 ft. Measurements included CO, CO ₂ , and O ₂ concentrations, presence of oxidizable gases, light obscuration and temperature. The signatures measured could be associated with the three types of sources. Using a multivariate statistical analysis, the response time of a prototype detector was appreciably less than that of commercially available detectors, with a significant reduction in unnecessary alarm susceptibility. In the third phase, pairs of sources were provided simultaneously to determine if a nuisance source could mask the signature from a fire source and if two nuisance sources provide a signature similar to that from a fire. Results indicate that the ratio of the CO to CO ₂ concentrations is representative of flaming fire sources and to a limited extent for non-flaming fire sources, independent of the presence of a nuisance source.					
KEY WORDS (MAXIMUM OF 9; 28 CHARACTERS AND SPACES EACH; SEPARATE WITH SEMICOLONS; ALPHABETIC ORDER; CAPITALIZE ONLY PROPER NAMES) carbon dioxide; carbon monoxide; fire alarms; fire detection; fire detectors; fire research; light obscuration; neural networks; oxygen; response time; sensors; signature detection; smoke detectors					
AVAILABILITY <input checked="" type="checkbox"/> UNLIMITED <input type="checkbox"/> FOR OFFICIAL DISTRIBUTION - DO NOT RELEASE TO NTIS <input type="checkbox"/> ORDER FROM SUPERINTENDENT OF DOCUMENTS, U.S. GPO, WASHINGTON, DC 20402 <input checked="" type="checkbox"/> ORDER FROM NTIS, SPRINGFIELD, VA 22161				NOTE TO AUTHOR(S): IF YOU DO NOT WISH THIS MANUSCRIPT ANNOUNCED BEFORE PUBLICATION, PLEASE CHECK HERE. <input type="checkbox"/>	

